

# **Well-Controlled Synthesis and Applications of Polythiophene- based Mixed Ion-Electron Conductors**

## **DISSERTATION**

Von der Universität Bayreuth zur Erlangung des Grades  
eines Doktors der Naturwissenschaften (Dr. rer. nat.) genehmigte Abhandlung  
im Promotionsprogramm

*Photophysik synthetischer und biologischer multichromophorer Systeme*

der Graduiertenschule für Mathematik und Naturwissenschaften  
der Universität Bayreuth

von

**Philip Armin Schmode**

geboren in Augsburg/ Deutschland

Bayreuth, 2020



---

Die vorliegende Arbeit wurde in der Zeit vom April 2016 bis April 2020 in der Arbeitsgruppe Angewandte Funktionspolymere am Lehrstuhl für Makromolekulare Chemie I der Universität Bayreuth unter der Betreuung von Prof. Dr. Mukundan Thelakkat angefertigt.

Amtierender Direktor der Graduiertenschule: Prof. Dr. Markus Lippitz

Dissertation eingereicht am: 14.05.2020

Wissenschaftliches Kolloquium: 17.09.2020

Prüfungsausschuss:

Prof. Mukundan Thelakkat            (erster Gutachter)

Prof. Anna Köhler                    (zweite Gutachterin)

Prof. Markus Retsch                (Vorsitzender)

Prof. Georg Papastavrou            (Prüfer)



*„Ich habe fertig!“  
Giovanni Trapattoni*

---

## **Danksagung - Acknowledgement**

An dieser Stelle möchte ich mich ganz herzlich bei allen bedanken, die mich über die letzten Jahre begleitet haben und zum Gelingen dieser Arbeit beigetragen haben.

Mein erster und größter Dank gilt meinem Doktorvater Prof. Mukundan Thelakkat, welcher mir einerseits das Vertrauen schenkte und mir völlig freie Hand bei der Wahl des Themas ließ, andererseits für die immerwährende Bereitschaft zu sehr hilfreichen Diskussionen, persönliche Gespräche und Ratschläge. Herzlichen Dank auch für die Möglichkeit meines Auslandsaufenthalts in Saudi-Arabien und die Bereitstellung eines erstklassigen Arbeitsplatzes und Labors. Danke Muku!

Der gesamten MC1 möchte ich für die Unterstützung während der letzten Jahre danken. Besonders Petra und Christina für ihre zuvorkommende Art und die schnelle Hilfe bei sämtlichen Belangen, ohne euch würde der Lehrstuhl nicht funktionieren. Ein großes Dankeschön geht an Sandra Ganzleben und Jutta Failner für die Bereitstellung destillierter Lösungsmittel und das Teilen Ihres Erfahrungsschatzes. Vielen Dank an die gesamte AFuPo Gruppe, insbesondere an Paul Reichstein, David Heinrich und Florian Meichsner für das sehr angenehme Arbeitsklima und zahlreiche Diskussionen, es hat mich sehr gefreut mich euch im Labor/Büro zu arbeiten. Martina Fried möchte ich für ihre Unterstützung in der täglichen Laborarbeit, Synthese einiger Verbindungen und die Zusammenarbeit an der GPC danken. Bei Alexander Krimalowski gilt großer Dank für viele MALDI-ToF Messungen, Paul Reichstein für die Messungen von vielen SAXS/WAXS Proben. Meinen ehemaligen Praktikanten Florian Meichsner, Nicolas Mödl, Jan Kuliga, Melissa Cabrera und Teresa Menzel sei für ihren Einsatz im Labor gedankt.

Besonders meinen langjährigen Wegbegleitern an der Universität Bayreuth, Dominic Rosenbach, Gert Krauss, Basti Klose, Andi Frank, Eva Fürsattel, Simon Gumbel, Markus Stihl, Max Schnepf und Bernd Kopera möchte ich einen besonderen Dank aussprechen. Ohne Euch wäre die Zeit in Bayreuth nicht so schön geworden!

---

Auch zahlreiche Kooperationspartner haben direkt oder indirekt zum Gelingen dieser Arbeit beigetragen. Ein großer Dank hierbei geht nach Halle, an Prof. Thomas Thurn-Albrecht, Oleksandr Dolynchuk und Robert Kahl für die erfolgreiche Zusammenarbeit, die zahlreichen wertvollen Diskussionen und das damit verbundene erlangte Wissen über die Röntgenstreuung.

Weiterhin möchte ich mich bei Konstantin Schötz und Prof. Anna Köhler für die tolle Zusammenarbeit und der Durchführung vieler sehr interessanter Experimente bedanken.

A huge thank you to Prof. Sahika Inal for giving me possibility to join her research group at the King Abdullah University of Science and Technology in Thuwal Saudi-Arabia, for her hospitality and her support during this work. I am also very grateful to David Ohayon from the Inal group for all his support regarding microfabrication of OECTs and their characterization. Also big thanks to Achilleas Savva for his elaborate work on EQCM-D measurements with my polymers. Thanks to the whole BioEI group in KAUST for a really great and very productive time in KAUST, which helped to improve this thesis considerably.

Ein besonderer Dank geht an das Graduiertenkolleg 1640, welches mich sowohl finanziell als auch inhaltlich erheblich unterstützt hat.

Der größte Dank gebührt meiner großartigen Familie für die Unterstützung. Meiner lieben Yvonne danke ich für ihre überragende Unterstützung während der gesamten Doktorarbeit. Vielmehr bedanke ich mich bei meiner lieben Oma Sybille und meiner Tante Angela, meinen Schwiegereltern Heidelore und Werner, auf deren Unterstützung jederzeit blind verlassen konnte. Vielen Dank für all das Vertrauen und euren Glauben an mich. Ohne euren Rückhalt wären weder mein Studium noch diese Arbeit möglich gewesen.



---

	Summary / Zusammenfassung	1
<b>1</b>	Introduction – Bioelectronics and OECTs	9
<b>2</b>	Objective of the Thesis	47
<b>3</b>	Overview of the Thesis	51
	Individual Contributions to Joint Publications	60
<b>4</b>	Influence of $\omega$ -bromo Substitution on Structure and Opto-Electrical Properties of Homopolymers and Gradient Copolymers of 3-hexylthiophene	63
<b>5</b>	Favored Face-on Crystal Orientation in Thin Films of Poly(3-(6-bromohexyl)-thiophene) on Graphene as a Result of Modified Interfacial Interactions	105
<b>6</b>	High Performance Organic Electrochemical Transistors based on Conjugated Polyelectrolyte Copolymers	135
<b>7</b>	The Key Role of Side Chain Linkage in Structure Formation and Mixed Conduction of Ethylene Glycol Substituted Polythiophenes	177
<b>8</b>	A highly Soluble alkyl substituted PEDOT via Kumada Catalyst Transfer Polymerization	226
<b>9</b>	Appendix: Unpublished data: Materials Synthesis, Characterization and OECT Device Fabrication	256
	List of Publications	272
	Erklärung	273

## Summary

The majority of organic mixed ion-electron conductors (OMIEC) are polar/ionic semiconducting polymers, which are able to conduct both ions and electronic charges. This class of materials is highly attractive for bioelectronic applications in aqueous media, where such a mixed conduction is required. The aim of this thesis was on the one hand the controlled-synthesis and characterization of a new generation of water-compatible OMIECs based on the parent conjugated polyelectrolyte poly[6-(thiophen-3-yl) hexane-1-sulfonate tetraalkyl ammonium] (PTHS<sup>-</sup>M<sup>+</sup>), which is water soluble. On the other hand, the relevant properties like electronic charge carrier transport, volumetric capacitance, swelling and stability in aqueous solution were studied in detail and the interplay of these properties was elucidated.

The first two chapters of this thesis are dealing with the analysis of the crystal structure, the aggregation and the hole mobility of the precursor polymer, poly(3-(6-bromohexyl)-thiophene) P3BrHT, as well as copolymers consisting of both P3HT and P3BrHT. P3BrHT is the starting material for all  $\omega$ -functionalized polythiophenes; eg. PTHS<sup>-</sup>M<sup>+</sup>. Therefore, the copolymers P3HT-co-P3BrHT 1,2 and 3 with different copolymer compositions were studied using SAXS/WAXS, absorption spectroscopy and by testing as active materials in OFETs. In this study, we elucidate the tremendous impact of side chain functionalization of conjugated p-type polymers on aggregation, crystallinity and charge transport; all these properties increasing with the increasing content of 3HT. Additionally, we investigated crystal orientation of P3BrHT and P3HT on different substrates. Molecular orientation is an important aspect of improving the charge transport within organic electronic devices. The results evidence that P3HT films of various thicknesses on graphene show mixed edge-on and face-one crystal

orientation with edge-on crystals formed. In contrast, P3BrHT on graphene has solely face-on oriented crystals in thin films up to a particular film thickness.

In order to design new OMIECs, we used different strategies. The first concept involves copolymerization of functional comonomers, to improve the properties and the performance of PTHS<sup>-</sup>M<sup>+</sup> in bioelectronic devices. We incorporated 3-hexylthiophene (3HT) and THS-TMA<sup>+</sup> as comonomers, because of the excellent hole transport properties of P3HT and water compatibility as well as good ion transport of PTHS<sup>-</sup>TMA<sup>+</sup>. For this, we converted the above-described copolymers, P3HT-co-P3BrHT to PTHS<sup>-</sup>TMA<sup>+</sup>-co-P3HT using a post polymerization method. Upon testing the copolymers PTHS<sup>-</sup>TMA<sup>+</sup>-co-P3HT in OECTs, we observed several improvements like reduced threshold voltage, higher stability in contact with water, increased hole mobility and high ion transport properties, especially for the copolymer with 51:49 mol% ratio for 3HT: THS-TMA<sup>+</sup>.

In a second strategy, polar polythiophenes carrying polar groups as side chains, were synthesized in a well-controlled manner and investigated. Here, different diethylene glycol functionalized polythiophene derivatives were prepared, which differ only in the nature of side-chain linkage on 3-position of thiophene moiety. We investigated three such polythiophenes, equipped with diethylene glycol side chains, with no spacer (P3MEET), with a methyl (P3MEEMT) and an ethyl spacer (P3MEEET). Among the three, P3MEEET showed the highest crystallinity (~58 %), best hole transport mobility (0.005 cm<sup>2</sup>/Vs) and best performance in OECTs. Also, P3MEEET shows the highest reported water uptake (84 % swelling) in the oxidized state in p-type polymers, as determined with E-QCMD experiments.

In depletion-mode OECT devices, the most used p-type semiconductor is still PEDOT:PSS, due to the commercial availability and the extraordinary conductivity of

these doped systems. But PEDOT is insoluble in organic solvents and therefore the PSS-doped system is used as a dispersion in aqueous/alcohol medium. However, there is a need for a highly soluble, highly ion conducting, and easily oxidizable PEDOT polymer which can be used in accumulation mode devices. So, the eighth chapter of this thesis deals with the design and synthesis of a highly soluble EDOT monomer with a swallow-tail substituent and its controlled polymerization using KCTP. With this newly designed monomer, we achieved highly soluble PEDOT polymers up to a molecular weight of 10 kg/mol and low polydispersity. Furthermore, the polymer can be oxidized in presence of an aqueous electrolyte, which makes the polymer highly attractive for bioelectronic applications.

In summary, my research work gives fundamental inputs towards the understanding of what is necessary to design and tune new organic mixed ion-electron conductors. This necessitates the understanding of a complex interplay of different and often conflicting parameters in conjugated polymers which determine the mixed conductivity in general. Especially, this knowledge offers tools towards the application-related demands to realize high performance materials. Thus, these materials should show an optimum balance between high ionic and electronic charge transport. A compromise is needed since the ion conduction requires hydration and swelling of the polymer in aqueous media, whereas efficient electron transport is generally observed in highly crystalline hydrophobic conjugated polymers. Additionally, polymers for OECT applications should exhibit low ionization potentials and undergo oxidation in contact with the aqueous analyte at low applied voltages, because for the application as biosensors one must avoid the electrolysis of water at higher gate voltages ( $> 1$  V). Also, an optimum swelling of the oxidized polymer in contact with the aqueous analyte solutions is required. This is important, because a too poor water and ion uptake inhibit ion

transport through the polymer bulk, whereas a too high degree of swelling disrupts the intermolecular electronic hopping mechanism, thus lowering the effective electronic transport properties. I demonstrated that this complex demand can be fulfilled by the tool of copolymerization, the diligent choice of polar side chains and the copolymer composition. Thus, this work extends and improves the existing use of conjugated polyelectrolytes and polar polymers in OECTs.

## Zusammenfassung

Der Großteil organischer Ion-Elektron Mischleiter (MIEC) sind halbleitende polar/ionische Polymere, die sowohl Ionen als auch elektronische Ladungen leiten können. Diese Materialklasse ist sehr attraktiv für bioelektronische Anwendungen in wässrigem Medium, bei welchen eine solche gemischte Leitung erforderlich ist. Ziel dieser Arbeit bestand zum einen darin, die kontrollierte Synthese und Charakterisierung einer neuen Generation wasserkompatibler MIEC auf der Basis des bereits bekannten konjugierten Polyelektrolyten Poly[6-(thiophen-3-yl) hexan-1-sulfonat tetraalkyl ammonium] PTHS-M<sup>+</sup>, welcher wasserlöslich ist. Zum anderen wurden die relevanten Eigenschaften wie elektronischer Ladungsträgertransport, volumenspezifische Kapazität, gezielte Quellung und Stabilität des Polymers in wässriger Lösung im Detail untersucht und das Zusammenspiel dieser Eigenschaften erläutert.

Die ersten beiden Kapitel dieser Arbeit befassen sich mit der Analyse der Kristallstruktur, den Aggregationseigenschaften und der Lochmobilität des Ausgangspolymers Poly (3- (6-bromhexyl) -thiophen) P3BrHT sowie von Copolymeren, bestehend aus P3HT und P3BrHT. P3BrHT ist das Ausgangsmaterial für alle  $\omega$ -funktionalisierten Polythiophene, wie zum Beispiel PTHS-M<sup>+</sup>. Die Copolymere P3HT-co-P3BrHT 1,2 und 3 mit unterschiedlichen Copolymer Zusammensetzungen wurden unter Verwendung von SAXS/WAXS, Absorptionsspektroskopie und die Ladungsträgermobilität, durch Testen als aktive Materialien in organischen Feldeffekt Transistoren, untersucht. In dieser Studie wird der enorme Einfluss der Seitenkettenfunktionalisierung konjugierter p-Typ Polymere auf Aggregation, Kristallinität und Ladungstransport verdeutlicht, wobei sich mit einem erhöhten Gehalt an 3HT all diese Materialeigenschaften verbessern. Zusätzlich wurde

die Kristallorientierung von P3BrHT und P3HT auf verschiedenen Substraten untersucht. Die molekulare Orientierung ist ein wichtiger Aspekt bei der Verbesserung des Ladungstransports in organischen elektronischen Bauteilen. Die Ergebnisse belegen, dass P3HT-Filme mit verschiedenen Dicken auf Graphen eine gemischte Kristallorientierung von *edge-on* und *face-on* Kristallen aufweist. Im Gegensatz dazu, weist P3BrHT auf Graphen in dünnen Filmen bis zu einer gewissen Filmdicke ausschließlich *face-on* orientierte Kristalle auf.

Um neue OMIECs zu entwickeln, verfolgten wir verschiedene Strategien. Die erste Methode stellte die Copolymerisation von funktionellen Comonomeren dar, um somit die Eigenschaften und die Performance von PTHS<sup>-</sup>M<sup>+</sup> in bioelektronischen Bauelementen zu verbessern. Es wurde 3-Hexylthiophen (3HT) als Comonomer zusammen mit THS<sup>-</sup>TMA<sup>+</sup> verwendet, da P3HT über hervorragende Lochtransporteigenschaften verfügt und PTHS<sup>-</sup>TMA<sup>+</sup> eine hervorragende Wasserverträglichkeit und Ionenleitung aufweist. Dazu haben wir die oben beschriebenen Copolymere P3HT-co-P3BrHT polymeranalog in PTHS<sup>-</sup>TMA<sup>+</sup>-co-P3HT umgewandelt. Beim Einbau der Copolymere PTHS<sup>-</sup>TMA<sup>+</sup>-co-P3HT in OECTs beobachteten wir verschiedene Verbesserungen wie die Verringerung der Schwellenspannung, eine höhere Stabilität des Polymerfilms in Kontakt mit Wasser, verbesserte Lochtransporteigenschaften und einen hohen Ionentransport, besonders für das Copolymer mit der Zusammensetzung von 51:49 mol% 3HT/THS<sup>-</sup>TMA<sup>+</sup>.

In einem zweiten Ansatz wurden auch polare Polythiophene untersucht, welche polare Gruppen als Seitenketten tragen, welche ebenfalls kontrolliert polymerisiert wurden. Hier wurden verschiedene Diethylenglykol-funktionalisierte Polythiophenderivate untersucht., welche sich nur in der Art der Seitenkettenbindung an der 3-Position zur Thiopheneinheit unterscheiden. Wir untersuchten drei mit Diethylenglykolseitenketten

funktionalisierte Polythiophene ohne Spacer (P3MEET), mit einem Methyl- (P3MEEMT) und einem Ethyl-Spacer (P3MEEET). Unter diesen drei Polymeren, zeigte P3MEEET in dieser Studie die höchste Kristallinität (~58%), die beste Lochtransportmobilität ( $0,005 \text{ cm}^2/\text{Vs}$ ) und die beste Performance in OECTs. P3MEEET zeigt vielmehr die höchste berichtete Wasseraufnahme im oxidierten Zustand in p-Typ Polymeren, gemessen mit E-QCMD-Experimenten.

In *depletion-mode* OECTs ist PEDOT: PSS aufgrund der kommerziellen Verfügbarkeit und der hohen Leitfähigkeit immer noch der am häufigsten verwendete p-Typ Halbleiter. Die kurzen PEDOT Oligomere sind jedoch in organischen Lösungsmitteln unlöslich und das durch PSS dotierte System wird daher als wässrige Dispersion in wässrigem/alkoholischem Medium verwendet. Deshalb besteht grundsätzlich ein Bedarf an einem gut löslichen, gut ionenleitenden und leicht oxidierbaren PEDOT-Polymer, welches in *accumulation-mode* Transistoren verwendet werden kann. Das achte Kapitel dieser Arbeit befasst sich mit dem Design und der Synthese eines hochlöslichen Monomers für PEDOT-Derivate mit einem Schwalbenschwanzsubstituenten und seiner kontrollierten Polymerisation unter Verwendung von KCTP. Mit diesem neu entwickelten Monomer wurden hochlösliche PEDOT-Polymere mit einem Molekulargewicht von  $10 \text{ kg/mol}$  und einer geringen Polydispersität erzielt. Darüber hinaus kann das Polymer in Gegenwart eines wässrigen Elektrolyten oxidiert werden, was das Polymer für bioelektronische Anwendungen hoch attraktiv macht.

Zusammenfassend lässt sich sagen, dass meine Forschungsarbeit einen grundlegenden Beitrag zum Verständnis dessen liefert, was zum Design neuer organischer Ion-Elektron Mischleiter erforderlich ist. Dies erfordert das Verständnis eines komplexen Zusammenspiels verschiedener und häufig widersprüchlicher

Parameter in konjugierten Polymeren, welche hauptsächlich die gemischte Leitfähigkeit bestimmen. Insbesondere bieten diese neu erlangten Kenntnisse über OMIEC einen Wegweiser für die anwendungsbezogenen Anforderungen an Polymere zur Realisierung von Hochleistungsmaterialien. Die Materialien sollten ein perfektes Gleichgewicht zwischen ionischem und elektronischem Ladungstransport aufweisen. Ein Kompromiss ist notwendig, da die Ionenleitung eine Hydratisierung und ein Quellen des Polymers in wässrigen Medien erfordert, wohingegen ein effizienter elektronischer Transport im Allgemeinen in hochkristallinen hydrophoben konjugierten Polymeren beobachtet wird. Außerdem sollten Polymere für OECT Anwendungen bei niedrigen angelegten Spannungen (niedriges Ionisationspotential) in Kontakt mit dem wässrigen Analyten oxidieren, da bei der Anwendung in Biosensoren die Elektrolyse von Wasser bei höheren Gate-Spannungen ( $> 1$  V) vermieden werden muss. Weiterhin ist ein optimales Quellverhalten des oxidierten Polymers in Kontakt mit den wässrigen Analytlösungen erforderlich. Dies ist von großer Bedeutung, da eine zu geringe Wasser- und Ionenaufnahme den Ionentransport durch die Polymerstruktur hemmt, wohingegen ein zu hoher Quellungsgrad den intermolekularen Ladungstransportmechanismus stört und so die effektiven elektronischen Transporteigenschaften verschlechtert. Ich habe aufgezeigt, dass diese komplexen Anforderungen durch das Konzept der Copolymerisation und durch die gezielte Auswahl der polaren Seitenketten und der Copolymerzusammensetzung erfüllt werden kann. Somit erweitert und verbessert diese Arbeit das Verständnis über bestehende Verwendung von ionischen und polaren Polythiophenen in organisch elektrochemischen Transistoren.

## 1.Introduction – Organic Bioelectronics

Bioelectronics involve the development and studies of organic electronic devices which operate as translators between biology and human-made electronic systems.<sup>1</sup> Utilized in one translation direction, organic bioelectronics can be used to regulate the physiology and processes of cells, tissues, and organs in a chemically specific manner and at high resolution. Conversely, organic bioelectronics can also be applied to biological systems to selectively sense, record, and monitor different signals and physiological states, as well as convert relevant parameters into electronic readable signals, processing and decision making. This is schematically shown in **Figure 1**.

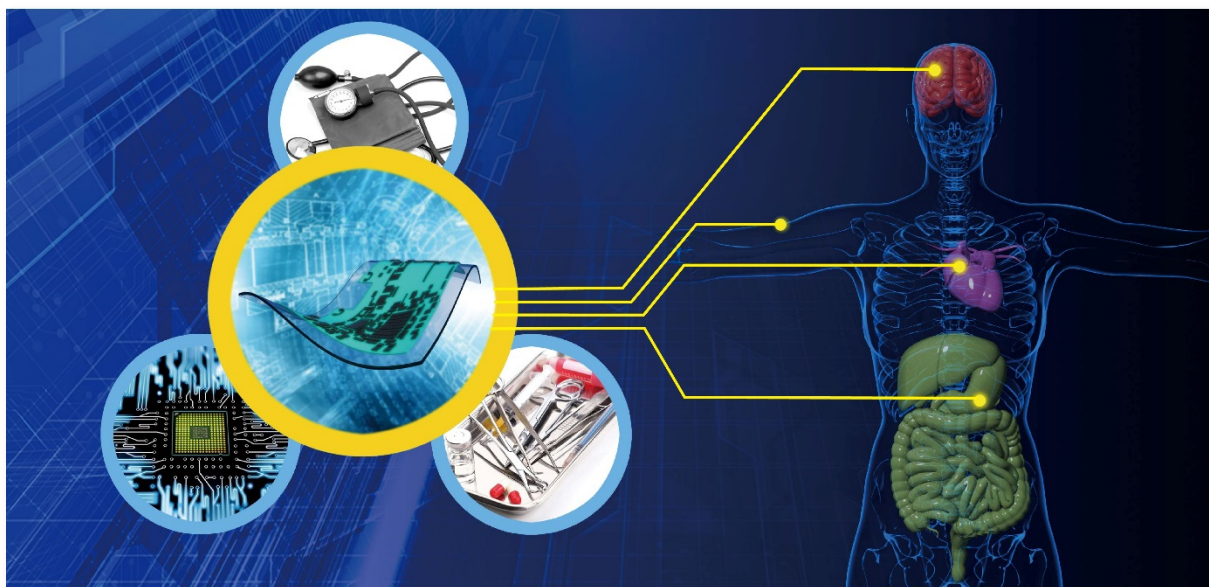


**Figure 1:** Schematic illustration of recently developed soft bioelectronic systems which have provided tremendous opportunities in personalized and self-administered healthcare. Figure 1 adapted from Ref.<sup>2</sup>.

This response of biosystems on electrical voltage dates back to the 18<sup>th</sup> century, when Luigi Galvani made his famous experiment.<sup>3</sup> In this experiment, he moved detached frog legs with low applied voltage.<sup>3</sup> However, the major activities in the present field of bioelectronics relate to the development of biosensors and materials that transduce biorecognition or biocatalytic processes in the form of readable electronic signals (**Figure 2**).<sup>4,5</sup> Such biosensors can be electrodes, ion pumps, piezoelectric crystals or transistors.

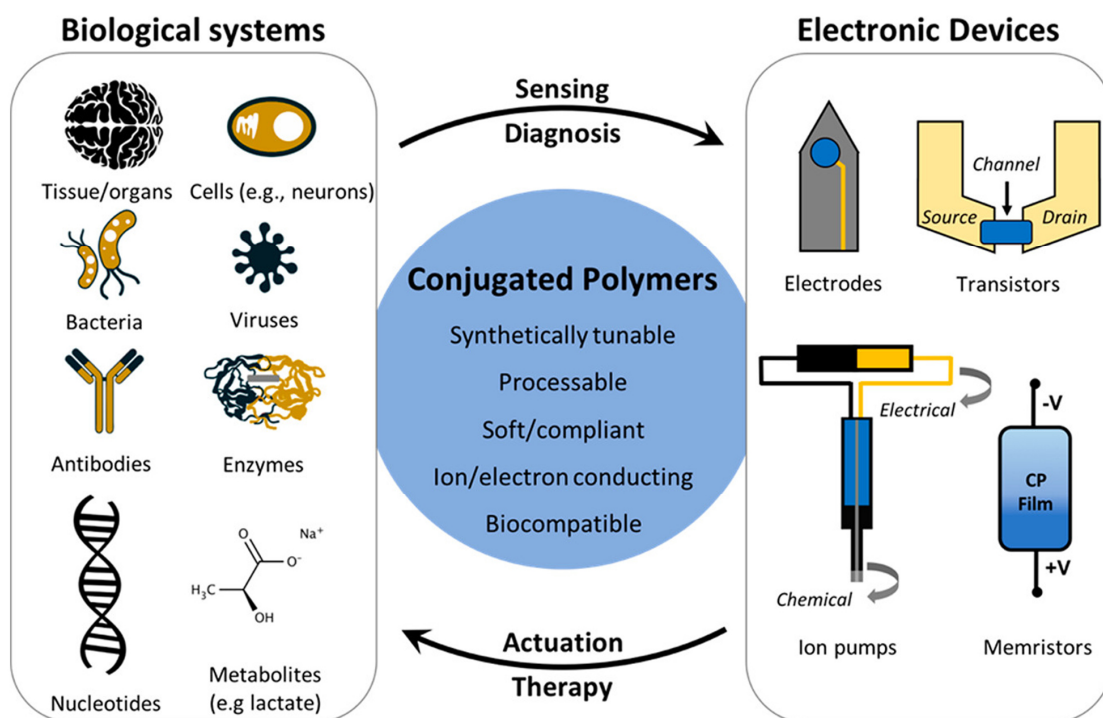


**Figure 2:** Schematic Illustration of different type of electronic devices (e.g. electrodes, ion pumps, piezoelectric crystals or transistors), which can record biological signals, produced from various biological systems. Furthermore, the advantages of conjugated polymers compared to inorganic materials are shown. (Figure adapted from Inal et. al. Ref. <sup>4</sup>)

Thus, bioelectronics devices can improve the therapy for patients, enhance clinical diagnostics and can be able to further understand complex biological processes. Such devices including biosensors as glucose monitors for diabetics, cardiac pacemakers and cochlear implants are already in daily clinical use.<sup>2,6</sup> All these available

bioelectronics devices are based on inorganic materials, such as silicon.<sup>3</sup> At the same time, the pharmaceutical industry is beginning to explore “bioelectronic medical devices”, aiming to replace systemic administration of certain drugs with electrical stimulation from implanted devices.<sup>1,4</sup> Further into the future, electronic tattoos will monitor our health on a continuous basis, providing a wealth of data that will revolutionize medicine and help personalize disease treatment.<sup>4</sup>

At present the field of bioelectronics is limited by the availability of materials, which can transduce signals across the biotic/abiotic interface. The key to new and improved organic bioelectronic devices is to improve the interface between tissue and electronics.<sup>4</sup> Currently used technologies are based on inorganic materials and ceramics, which exhibit major incompatibilities in terms of chemical structure (inorganics vs. organic), mechanical (low vs. high Young’s modulus) and electrical (ionic vs. electronic conduction) properties at the interface between tissue and electronics.<sup>4</sup> These incompatibilities limit the information transfer between biology and electronics, and also the lifetime of bioelectronics systems.<sup>4</sup> Conjugated polymers have been shown to overcome all the above mentioned problems.<sup>7</sup> They share similarities in their chemical nature with biological molecules and can be engineered in various forms, including hydrogels that have Young’s moduli similar to those of soft tissue and can conduct ions.<sup>4,8,9</sup> Additionally, the structure of organics can be tuned synthetically, and their properties can be controlled using a variety of functionalization strategies.<sup>4,8,9</sup> Finally, organic electronic materials can be integrated with a variety of mechanical supports, giving rise to devices with form factors (conformable, stretchable, fibrous, 3D porous) that enable integration with biological systems.<sup>4,8,9</sup> Inorganic materials consist of a network of covalent bonds, whereas polymers are bound only by relatively weak van-der-Waals forces. This allows the easy exchange of ions between

the biological media and the semiconductor.<sup>3</sup> Moreover, the whole polymer film can interact with the biological media, as opposed to inorganic materials, where only the surface of the film interacts. Another advantage of organic materials is the possibility to tune their opto-electronical, mechanical and biological properties. Also, organic semiconductors exhibit a good ion transport and are easily processable. **Figure 3** shows the above mentioned factors during the interaction of the doped organic *p*-type semiconductor poly(3,4-ethylenedioxythiophene) polystyrene sulfonate (PEDOT:PSS) and of silicon with biological media.<sup>10</sup> Taken all these aspects in account, a new generation of organic mixed ion-electron conductors addressing all these issues were developed, which will be discussed later in detail.

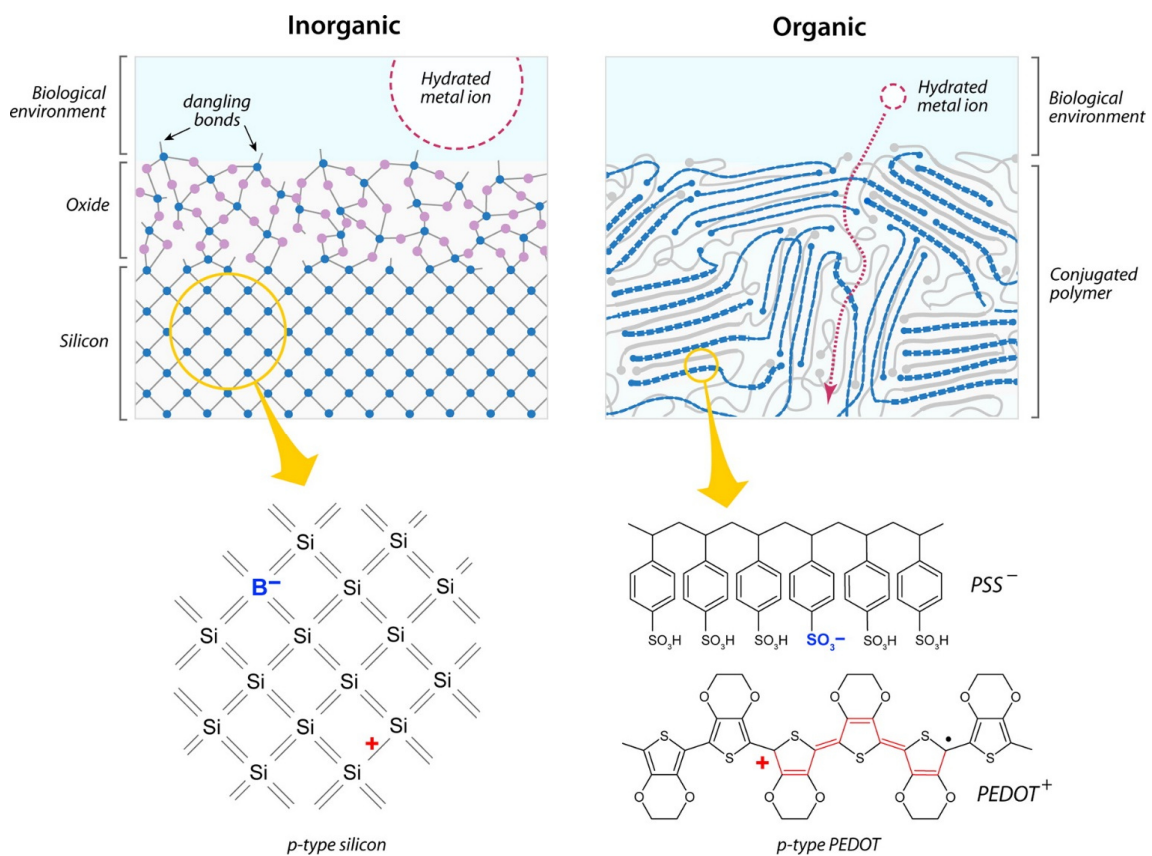


**Figure 3:** Schematic illustration of the diffusion of ions injected from a biological media through an inorganic and organic semiconductor. Inorganic *p*-type silicon and organic *p*-type PEDOT: PSS are used as examples. Figure adapted from Ref. <sup>11</sup>

## 1.1. Organic Semiconductors

The history of conjugated polymers was described in a recent review by Goel et. al.<sup>12</sup> The long success story of conjugated polymer started back in 1976, when *trans*-polyacetylene (Pac) was discovered.<sup>13</sup> After this breakthrough, many other different conjugated polymers were synthesized, e. g. the most popular early examples are polyaniline (PANI), poly(*p*-phenylene vinylene) (PPV) and polypyrrole (PPy, **Figure 4**).<sup>13,14</sup> Most of the initial work focused on achieving highly conductive polymers. Upon doping with potassium vapor, high conductivities of around  $\sigma = 10^4 \text{ S cm}^{-1}$  were reported.<sup>15</sup> PANI and PPy can be easily synthesized via electrochemical polymerization methods, for example using ferric chloride. Both polymers are reported to show high conductivities after doping of around  $500 - 2000 \text{ S cm}^{-1}$ .<sup>15-18</sup> The main disadvantage of the above mentioned polymers is that they suffer from poor solubility (also processability) and the lack of stability of the oxidized state.

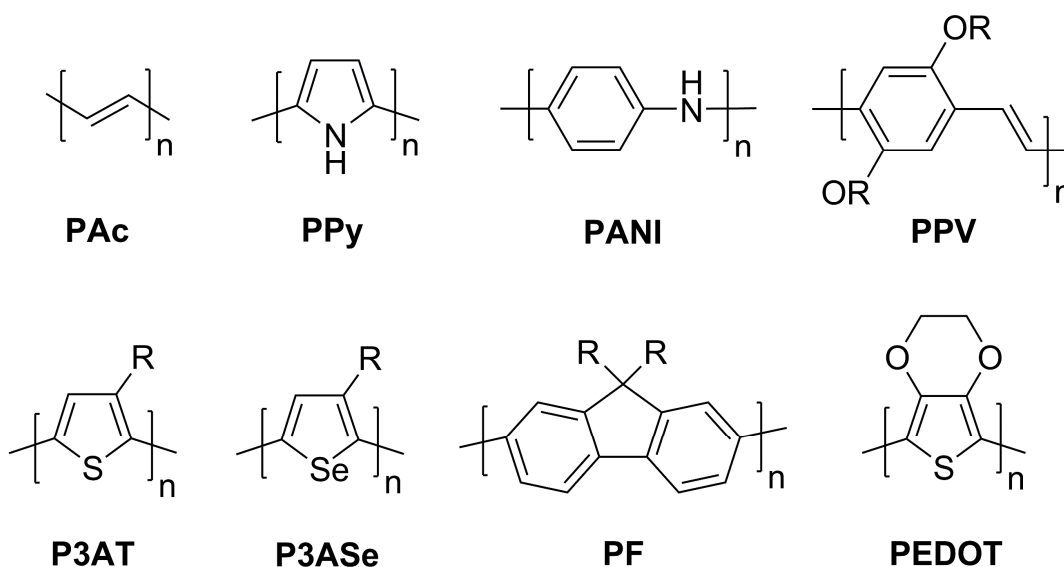


**Figure 4:** Selection of conjugated polymers: *trans*-polyacetylene (PAc), polypyrrole (PPy), polyaniline (PANI), poly(*p*-phenylenevinylene) (PPV), poly(3-alkylthiophene) (P3AT), poly(3-alkylselenophene) (P3Ase), polyfluorene (PF), poly(3,4-ethylenedioxythiophene) (PEDOT). (reproduced with permission from Goel et. al. Ref.<sup>12</sup>)

The scenario further changed with the development of doped PEDOT:PSS (poly(3,4-ethylenedioxythiophene):poly(styrene sulfonate)). In this polymer system, the doped PEDOT state is highly stabilized with the PSS chains of much higher molecular weight. Also other acidic dopants like p-toluene sulfonic acid (Tos) are well-studied.<sup>19</sup> The properties which make doped PEDOT:PSS interesting for almost all applications in organic devices are the intrinsic high conductivity (up to 6000 S/cm) and the good processability in the form of mostly aqueous dispersions.<sup>20–22</sup> After the discovery of the electroluminescence undoped conjugated polymers, a huge interest in creating new conjugated polymers with a particular emission wavelength arose. Famous examples are different derivatives of poly-(p-phenylenevinylene) (PPV), which have been studied especially for the application in OLEDs.<sup>23</sup> The activity in the field of conjugated polymers broadened with the observation of the photoinduced charge transfer and the combination of a polymer with an acceptor molecule paved the way for organic photovoltaics (OPV).<sup>24,25</sup> In OPV, poly(3-alkylthiophenes) (P3ATs) are the most studied conjugated polymers, because of their versatility regarding the structural design, desirable electrical and optical properties. Hole mobilities up to  $\mu_h \approx 0.1 \text{ cm}^2 \text{ V}^{-1} \text{ s}^{-1}$  in organic field-effect transistors (OFETs) have been reported for poly(3-hexylthiophene) (P3HT).<sup>26–28</sup> To obtain high performance P3HT, it is important to control the molecular weight, polydispersity and regioregularity of P3HT, which leads to well-defined polymers when synthesized via Kumada catalyst transfer polymerization (KCTP), a controlled polymerization technique suitable for polythiophene derivatives.<sup>29–31</sup> The controlled polymerization of conjugated polymers, especially of poly(3-alkylthiophenes) (P3ATs) are discussed in the following chapter.

## 1.2. Controlled Synthesis of Conjugated Polymers

The Kumada catalyst-transfer polycondensation (KCTP) is a polymerization method with great potential for the synthesis of electron-rich conjugated polymers and block copolymers. The scope of monomers is growing steadily in recent years now covering thiophene-, fluorene-, phenylene- and pyrrole-based conjugated polymers.<sup>32</sup> Further, all-conjugated block copolymers, gradient polymers and brush polymers prepared by KCTP have been reported. However, the extension of KCTP method to donor-acceptor low band gap systems is still not fully realized. The discovery of the chain-growth mechanism by Yokozawa and McCollough demonstrated the unique character of the Nickel-catalyzed KCTP among other transition-metal catalyzed polycondensations.<sup>29,31,33</sup> The preparation of poly(3-hexylthiophene) (P3HT) is the most prominent example for KCTP since it allows excellent control over regioregularity, molecular weight, narrow polydispersity and well-defined chain ends. Kumada catalyst transfer polymerization (KCTP) is also called Grignard metathesis polymerization (GRIM). **Figure 5** illustrates the mechanism of the polymerization. In this type of catalyst transfer polymerization an active Grignard monomer is formed *in situ* from a dihalide via a Grignard metathesis reaction. In general, there are two methods for the formation of the active Grignard reagent, the Yokozawa and the McCollough route.<sup>30,33</sup> The Yokozawa route uses 2-bromo-3-(6-bromohexyl)-iodothiophene (**1**) as monomer together with *i*-PrMgCl as Grignard reagent. Due to the higher reactivity of the iodine compared to the bromine-group, only one active Grignard monomer (**3a**) is formed. In contrast to the Yokozawa route, the McCollough route uses 2,5-dibromo-3-(6-bromohexyl) thiophene (**2**) with *t*-BuMgCl as starting reagent. This leads to two regioisomers (**3a**, **3b**) of the active Grignard monomer. The sterical hindrance of **3b** leads to a high percentage (ca. 75 %) of the desired monomer **3a**. After the addition of

the nickel aryl catalyst dichloro(1,3-bis(diphenylphosphino)propane)nickel ( $\text{Ni}(\text{dppp})\text{Cl}_2$ ) a nickel-inserted dimer **4** is formed in the sterically less hindered tail to tail conformation. After that, the initiating species **5** is built via an intermolecular transfer followed by an oxidative addition. Now the chain growth proceeds of multiple cycles of transmetalation, reductive elimination and intramolecular oxidative addition. As a result of the sterically hinderance of the monomer **3b** is not consumed during the polymerization. After the complete consumption of the monomers the chain end is still active which allows the introduction of an end-group. Also the diligent choice of the quenching agent is of great significance towards the final properties of the polymer.<sup>31,34</sup> It is important to mention that the KCTP is not solely based on a chain-growth mechanism but exhibits the characteristics of a living polymerization, because one equivalent of Ni-catalyst initiates one polymer chain. This highly controlled preparation method for P3HT paves the way for the design of new materials for optoelectronic applications with superior material properties and towards application in upcoming technologies.<sup>35,36</sup>

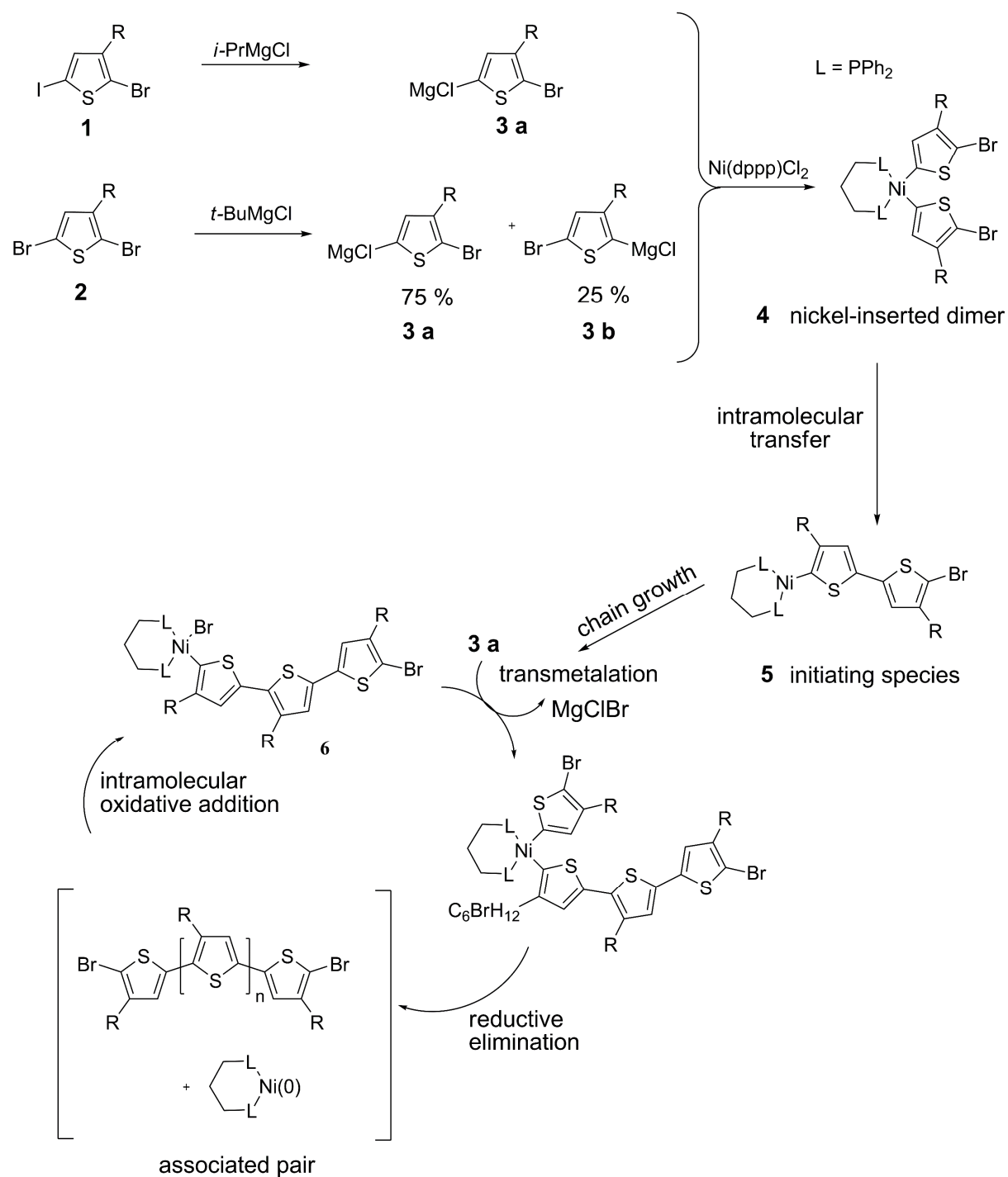


**Figure 5.** Grignard metathesis reaction for the formation of the active Grignard monomer and proposed mechanism of the Kumada catalyst-transfer polycondensation (KCTP) of polythiophene derivatives. Adapted from Lohwasser et al.<sup>31</sup>

### 1.4. Charge Transport in Conjugated Polymers

The charge transport of organic semiconductors and the characterization of these processes was described in detail by Köhler and Bässler in the book “*Electronic Processes in Organic Semiconductors: An Introduction (Wiley)*”;<sup>37</sup> Here the main points from this work are summarized. In general, the charge transport in organic semiconductors differs from that in inorganic semiconductors. In inorganic materials, the charge carrier mobility is independent of the charge carrier density, whereas in organic semiconductors the mobility strongly depends on the charge carrier density.<sup>38,39</sup> Organic semiconductors are disordered materials and, therefore, relatively low charge carrier mobilities are obtained in comparison to inorganic semiconductors.<sup>40</sup> Non-doped organic semiconductors are electric insulators, unless charge carriers are injected to the polymer from electrodes or charges generated by excitation by light. The key parameter that determines the motion of charge carriers in semiconductors is the mobility  $\mu$ , which is defined as drift velocity  $v$  divided by the electric field  $F$  (eq. 1).<sup>37</sup>

$$\mu = \frac{v}{F} \quad (1)$$

The drift velocity is not necessarily proportional to the electric field  $F$ , which leads to a field-dependence of the charge carrier mobility  $\mu$ . Given by Ohm’s law, the current density  $J$  is defined by the materials conductivity  $\sigma$  and the electrical field as<sup>37</sup>

$$J = \sigma \cdot F \quad (2)$$

The current can be also described as follows, where  $n$  is the number of charge carriers and  $e$  is the elementary charge.

$$J = e \cdot n \cdot v = e \cdot n \cdot \mu \cdot F \quad (3)$$

Therefore, for discrete charge carriers, the charge carrier mobility and the conductivity of organic materials can be expressed as

$$\sigma = e \cdot n \cdot \mu \quad (4)$$

The mechanism of charge carrier transport in organic semiconductors can be described by different models, such as hopping transport, polaronic transport and disorder-controlled transport for all individual transport regimes. The disorder in form of chemical or structural defects resulting in localized states in the organic semiconductor and the transport of charge carriers can only occur by a non-coherent transfer of electrons. This hopping process is thermally activated and the mobility  $\mu$  becomes dependent on the temperature  $T$  and the electrical field  $F$ .<sup>38</sup> All different types of the mechanism of charge transport are discussed in literature.<sup>37</sup>

The performance of organic semiconductors in electrical devices such as organic photovoltaics (OPV), organic light emitting diodes (OLEDs) or organic field effect transistors (OFETs) is mainly influenced by the efficiency of the charge carrier transport in such systems. There are several experimental techniques to measure the charge carrier mobility  $\mu$ , the most prominent methods are time of flight techniques (ToF), space-charge-limited currents (SCLC) method, the carrier extraction by linearly increasing voltage (CELIV) method and field effect transistors (FETs).<sup>37</sup> The application and analysis of organic semiconductors in field effect transistors will be discussed more in detail.

### *Organic Field Effect Transistors*

Extracting the charge carrier mobility of organic semiconductors using organic field effect transistors (OFETs) is one of the widely used methods in material science.<sup>41–43</sup> The obtained values may not be related to the bulk property of the materials (as in the case of methods such as SCLC), since charge transport in OFET is determined only at some few nanometers of the interface of the semiconductor with dielectric. Additionally, the charge carrier concentration in an OFET is much higher than in a SCLC device and therefore, the extracted OFET mobility values are usually higher than the respective bulk values. In OFETs charge transport is measured only in some nanometer thick layer directly at the interface between the dielectric. In an OFET, the gate electrode is separated by the dielectric from the organic semiconducting film. The dielectric usually consists of SiO<sub>2</sub> or Al<sub>2</sub>O<sub>3</sub>. Often a pre-surface treatment of the dielectric is necessary, to minimize charge traps at the surface.<sup>44</sup> The source and drain electrodes are separated by each other through the organic semiconductor. An illustration of a bottom-gate/bottom-contact OFET device is shown in **Figure 6**. An electrical current flow between the source and drain electrodes as a function of applied gate voltage, which enable the characterization of the semiconductor.

The operation principle and the different operation regimes are illustrated in **Figure 6**. When a gate voltage  $V_G$  higher than the threshold voltage  $V_{th}$  is applied, charges accumulate in a nanometer thick layer at the dielectric-semiconductor interface due to a generated electrical field (red, **Figure 6**). This accumulation layers form the channel for the charge transport. Depending on the polarity of the applied gate voltage either electrons ( $V_G > 0$  V in n-type materials) or holes ( $V_G < 0$  V in p-type materials) are induced. Due to the very small thickness of the accumulation layer, charge transport and device operation are sensitive to the properties of the dielectric-semiconductor

interface and surface orientation and alignment of the semiconductor at the interface.<sup>45,46</sup>

If a potential is applied at the drain electrode ( $V_d$ ) at a constant  $V_g$  above the threshold, the charges move between the source- and drain-electrode and a drain current  $I_d$  is measured. If  $V_d$  is increased the current  $I_d$  will also increase linearly with  $V_d$ . Upon increasing  $V_d$ , the pinch-off point is reached where the distribution of induced charge carriers is characterized by a linear decrease from the maximum value at the source electrode to 0 at the drain electrode. At higher voltages a saturation current  $I_{D,sat}$  flows across the channel and the pinch-off point moves towards the source electrode, creating a depletion zone close to the drain electrode. Typical output and transfer curve ( $I$ - $V$  curve) are shown in **Figure 6**. The charge carrier mobility can be extracted out of the  $I_D^{-0.5}$ - $V_G$  plot using **equation 5**, when the transistor is operated in the saturation regime.<sup>37</sup>

$$I_D = \frac{W}{2L} C \cdot \mu (V_G - V_{Th})^2 \quad (5)$$

In this equation,  $W$  is the channel width,  $L$  is the channel length and  $C$  the capacitance of the dielectric.

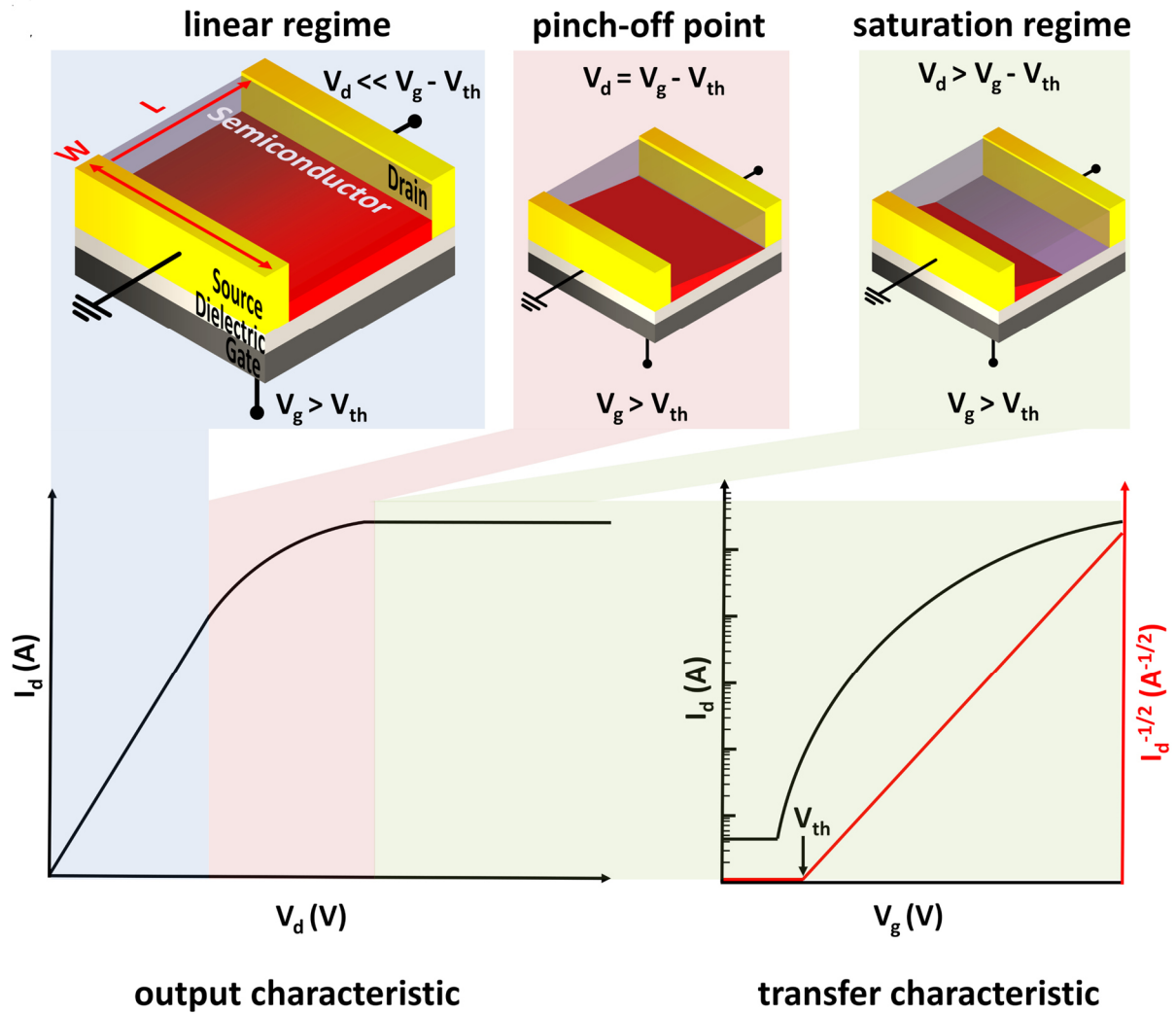


**Figure 6:** Schematic illustration of the operation principle of an OFET. At low potentials applied at the drain current, a linear increase of the drain current  $I_d$  with the drain voltage  $V_d$  is observed. At the pinch-off point, a saturation of the drain current can be observed, because for higher applied voltages  $V_d$  the accumulated charges at the interface are depleted. (reproduced with permission from Goel et. al. Ref.<sup>12</sup>)

## 1.5. Analysis of the Structure Formation of Conjugated Polymers with X-ray Diffraction

The structure formation of conjugated polymers has a huge impact on the performance of electronics devices based on these materials.<sup>47,48</sup> X-ray scattering is a technique for analyzing the structural features of materials based on the interaction of electromagnetic radiation with condensed matter.<sup>49</sup> Compared to other methods which only give information about the material surface (atomic force microscopy, XPS/UPS) or thin films of materials (transmission electron microscopy), X-ray scattering methods provide structural information both in bulk (SAXS/WAXS) and thin films (GIWAXS).

The X-rays can interact with the electrons of the materials. This leads to an excitation of the electrons in the shell and scattering of the X-ray beam. This scattering occurs at multiple positions in an ordered lattice, so the scattered wave will form destructive and constructive interferences, which depends on the distance of the lattice plane  $d$  and results in distinct diffraction patterns. According to the Bragg equation, the conditions for the constructive interference are defined as follows:<sup>50</sup>

$$n \cdot \lambda = 2d \cdot \sin \theta \quad (6)$$

where  $\lambda$  is the wavelength of the X-ray radiation and  $\theta$  is the angle of incidence. Nanoscale dimensions are huge (5 – 100 nm) compared to the X-ray wavelength (e.g.  $\text{CuK}\alpha = 0.154 \text{ nm}$ ), the corresponding angular range of the observed scattering pattern is thus very small and, therefore, known as small-angle X-ray scattering (SAXS). Vice versa, periodic structures on the atomic or intermolecular scale (5 – 0.2 nm) generate a scattering pattern at higher angles, known as wide-angle X-ray scattering (WAXS). Thus the crystalline lattice and  $\pi$ - $\pi$  distance in conjugated polymers can be analyzed in WAXS regime.<sup>51</sup> At smaller incident angles, structures up to 100 nm can be analyzed

in SAXS. This is very useful to monitor microphase separations in block copolymers and also lamellar long periods in crystals (**Figure 7**).<sup>52</sup> Additionally, grazing incidence small-angle X-ray scattering (GISAXS) and wide-angle X-ray scattering (GIWAXS) are advanced scattering techniques based on synchrotron radiation for the analysis of thin film structures.<sup>53,54</sup> By measuring at a very low angle of incidence (grazing) the probe volume can be increased large enough to measure thin films of only  $\sim 100$  nm thickness. Grazing-incidence scattering gives information about the orientation of structures relative to the substrate or film-air interface, the orientation of nanoscale microdomains in block copolymers films by GISAXS or crystallites by GIWAXS. Both methods are established tools to create a general understanding of materials properties like charge transport and the orientation of structures in thin film.<sup>47,48</sup>

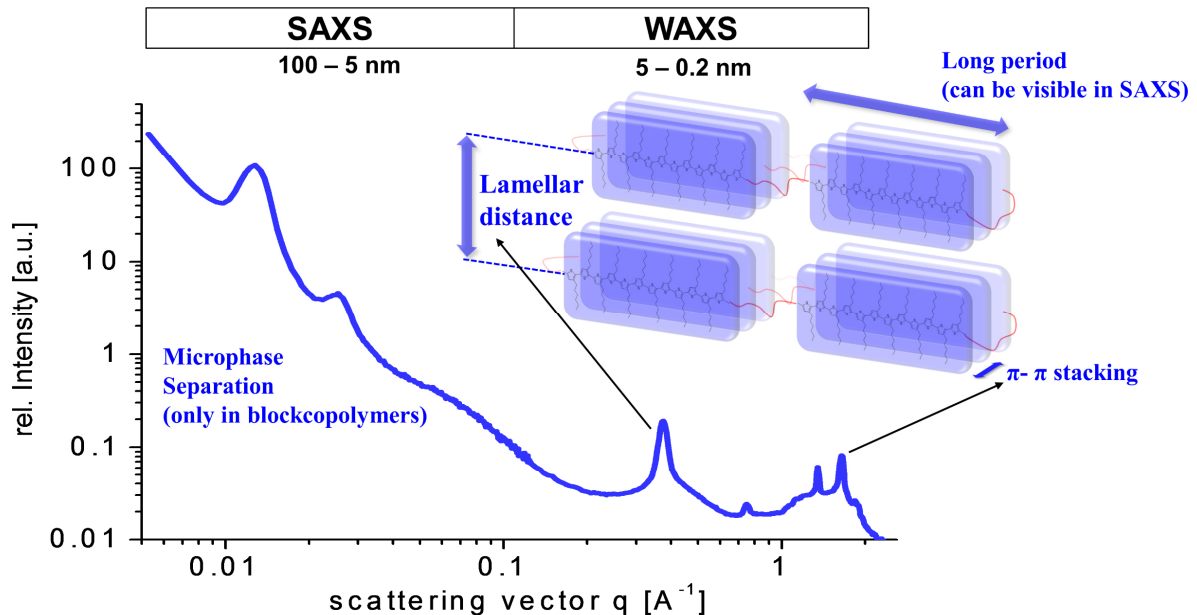


**Figure 7:** Length scales accessible by X-ray scattering experiments in different angular regions. Small angle X-ray-scattering (SAXS) for periodic structures on the nanoscale (5 – 100 nm) and wide-angle X-ray scattering (WAXS) to unravel crystalline features of semiconducting polymers (5 – 0.2 nm).

## 1.6. Organic Electrochemical Transistors and Organic Mixed Conductors

### *Organic Electrochemical Transistors (OECTs)*

Organic electrochemical transistors (OECTs) are a rapidly developing device structure and is the most widely used device configuration in bioelectronic applications. OECTs are characterized by the interplay of both ionic and electronic inputs to modulate the transistor channel conductance.<sup>55,56</sup> This characteristic renders OECTs suitable for interfacing electronics with biological systems, which make use of ionic and biochemical currents and gradients for signaling.<sup>9,57</sup> To date, OECTs have demonstrated their potential for molecular sensing<sup>58–60</sup>, cell culture analysis<sup>61–64</sup>, medical diagnostics<sup>65,66</sup>, neuromorphic computing<sup>67,68</sup>, digital logic circuits<sup>69</sup> and printed electronics<sup>70–72</sup> on several soft, cheap, transparent substrates.

The first reported OECT dates back to 1984 reported by Wrighton et. al.<sup>73</sup> In this device geometry, a three-electrode transistor setup was used with polypyrrole as active material. Biasing was achieved through an electrolyte using a gate electrode immersed in the electrolyte.<sup>73,74</sup> Similarly, based on polyaniline and poly(3-methylthiophene), the OECT setup was used for sensing of redox reagents and the detection of the pH value. Many other materials were tested in OECTs, which will be discussed in the section on organic mixed ionic-electronic conductors (OMIECs).

As discussed above (**Section 1.4.**) a typical OFET comprises a solid dielectric between a channel semiconductor material and a gate electrode. In such an OFET device, a charge buildup at the semiconductor-dielectric interface is induced by a gate voltage and leads to a modulation of the channel conductance at the interface (**Figure 8A**).<sup>42</sup> If the solid gate dielectric is replaced by an electrolyte solution, initiated by an electric field, ions move towards the organic semiconductor interface. This leads to the formation of an electric double layer (EDL) along the electrolyte-semiconductor

interface, if the semiconductor is not permeable to ions from the electrolyte. This special type of OFET is also called electrolyte gated OFET (EGOFET, **Figure 8B**). This type of transistors has the advantage of exhibiting a relatively higher capacitance (typically of  $1\text{--}10\ \mu\text{Fcm}^{-2}$ ), which allows the device operation at lower gate voltages, usually below 2 V.<sup>75,76</sup>

If ions can diffuse into the semiconducting material, the charge accumulation is no longer limited to the semiconductor-electrolyte interface, and the device now is called organic electrochemical transistor (OECT, **Figure 8C**). So, the main difference in an OECT is that ions from the electrolyte can penetrate into the MIEC polymer film and simultaneously change the capacitance throughout the entire volume of the MIEC.

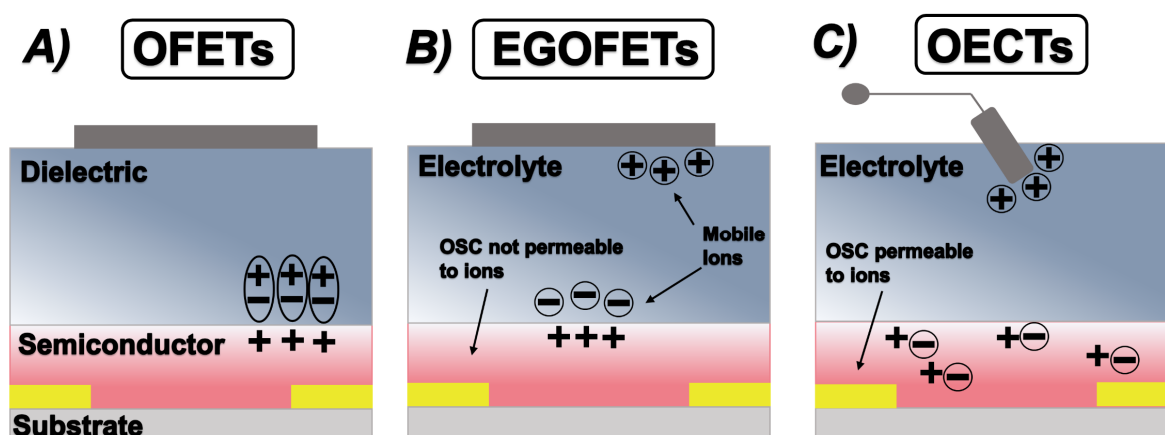


**Figure 8:** Schematic cross-section showing the working principles of A) OFETs, B) EGOFETs and C) OECTs (reproduced from Ref.<sup>56</sup>)

In this configuration, individual polymer chains provide a capacitive interface, thus leading to a volumetric capacitance which can be orders of magnitude larger than the electrical double layer capacitance residing along the interface between an electrolyte and an organic semiconductor layer, which is not permeable to ions.<sup>77</sup> Due to the high volumetric capacitance, a traditional metal gate electrode may not provide enough charges to dope the OECT channel, necessitating the use of redox gate electrodes,

most commonly Ag/AgCl, or electrodes with a much larger specific surface area.<sup>78</sup> It is important to mention, that since OECT operation requires ion migration through a solid medium, the switching speeds of OECTs tend to be slow. Typical OECTs can operate only below the kHz frequency range, much lower than the MHz range achieved by OFETs.<sup>78–80</sup> The device configuration of a typical OECT is again shown in **Figure 9**.

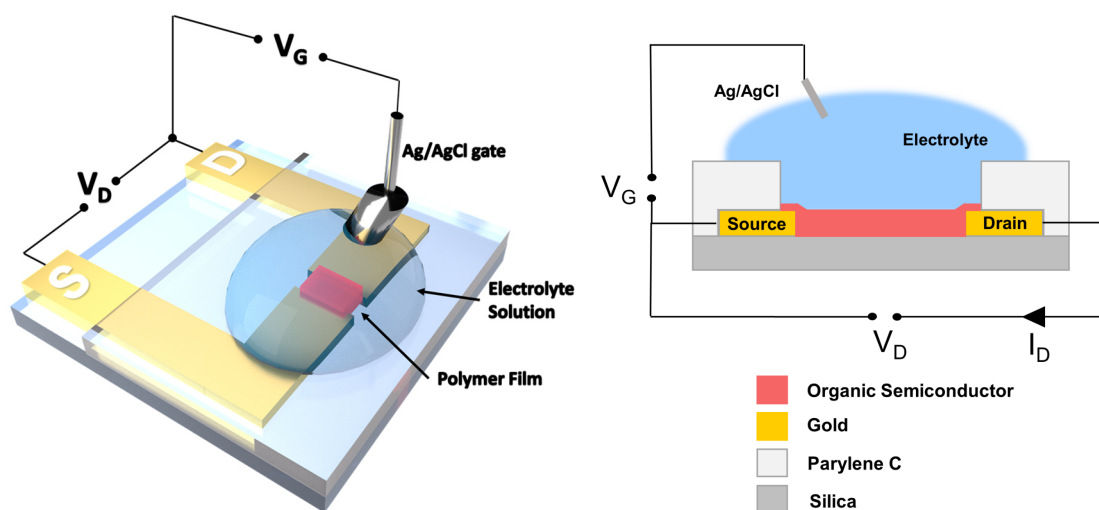


**Figure 9:** 3D (left) and cross-section (right) illustration of the a typical OECT device configuration with Ag/AgCl as gate electrode. (reproduced with permission from Schmode et. al. Ref.<sup>81</sup>)

An OECT relies on ion diffusion from the electrolyte into the organic film at applied gate potential thereby changing its doping state and hence its conductivity.<sup>82</sup> The operation is controlled by a potential applied at the gate (gate voltage,  $V_G$ ) and at the drain (drain voltage,  $V_D$ ), which are referenced with respect to the source electrode. The gate voltage dopes the semiconductor and controls the injection of ions into the semiconductor and therefore the capacitance (redox state in the language of electrochemistry) of the organic film. The drain voltage induces a current (drain current,  $I_D$ ), which is proportional to the quantity of mobile charges (holes or electrons and ions) in the channel.<sup>57</sup> The most important figure of merit for OECT devices is the transconductance  $g_m$ , which is a direct measure of the extent to which an OECT device

can amplify input signals and can be extracted from the first derivative of the transfer curve (**Equation 7**).<sup>9,57,83</sup>

$$g_m = \frac{\partial I_D}{\partial V_G} \quad (7)$$

The transconductance depends on the device geometry like the channel length  $L$ , channel width  $W$ , thickness of film and the biasing conditions of measurement. The transconductance of an OECT in the saturation regime was experimentally observed to depend on the thickness of the semiconductor (not valid in OFET) and is proportional to  $Wd/L$ . This led to the following equation for OECT<sup>77</sup>, expressed as

$$g_m = \frac{d \cdot W}{L} \mu \cdot C^* (V_G - V_{Th}) \quad (8)$$

where  $\mu$  is the charge carrier mobility in an OECT,  $C^*$  is considered as the volumetric capacitance and  $V_{Th}$  the threshold voltage. While in OEFT and EGOFET devices the charge carrier mobility  $\mu$  is the main figure of merit to characterize the performance of organic semiconductors, in OECTs the  $\mu C^*$  product describes the mixed conducting properties of organic semiconductors, i.e. the ability of an effective ion and electron or hole transport depending on the thickness of the film.<sup>11</sup>

The usual model used to describe the transconductance in depletion mode operation of an OECTs is the Bernards model.<sup>82</sup> This model assumes that ions from the electrolyte enter the doped semiconductor in the channel and change the capacitance throughout its volume, capturing the steady-state and transient response.<sup>57,82</sup> According to this model, the device operation is divided into two circuits: an ionic circuit, which describes the flow of ions in the gate–electrolyte–channel (polymer) structure,

and an electronic circuit, which describes the flow of electronic charges in the source–channel–drain structure.

However, OECT research is at present limited to the availability of materials, which exhibit low oxidation potential in aqueous media, stability in contact with water, moderate swelling and a compromise between high charge carrier transport and good ion transport. A compromise is needed since the ion conduction requires hydration and swelling of the polymer in aqueous media, whereas efficient electron transport is generally observed in highly crystalline hydrophobic conjugated polymers. Thus, designing a conjugated polymer with balanced ion and electron transport, working at very low gate voltages ( $< 1\text{V}$  vs. Ag/AgCl) is one of the biggest challenges in polymer science.<sup>7,84</sup> The materials which were investigated in OECTs are discussed in the following chapter.

As explained above, the OECT device operation can be divided into depletion mode (using doped materials) or accumulation mode (with pristine undoped semiconductors). The semiconducting nature of the channel material in the pristine state (without any applied gate voltage) dictates the operation mode of the OECT. In the so-called accumulation mode operation, the MIEC is poorly conductive in the unbiased state, the OFF state. Application of a negative gate voltage causes injection of holes (in p-type) and diffusion of anions (for charge neutralization) into the channel and a corresponding accumulation of holes (electrochemical doping in the language of electrochemistry), leading to the ON state (**Figure 10a**).<sup>85</sup>

In contrast to accumulation mode OECTs, in depletion mode OECTs the organic semiconductor is conductive and is doped in the unbiased device and the application of a gate potential leads to an electrochemical dedoping (decrease the electronic charges on polymer chain) of the semiconductor.

The operating principle of a depletion mode OECT using poly(3,4-ethylenedioxythiophene):poly(styrenesulfonate) (PEDOT:PSS) is illustrated in **Figure 10b**. A typical material for OECTs working in depletion mode is the conducting polymer poly(3,4-ethylenedioxythiophene) p-type doped by poly(styrene sulfonate) (PEDOT:PSS) of much higher molecular weight.

As the PEDOT backbone is partially oxidized, with sulfonate groups in PSS providing high stability of the oxidized state, it operates in depletion mode. By applying a negative potential at the drain electrode ( $V_D$ ) while maintaining zero potential at the source and gate electrodes, the holes located along the PEDOT backbone are transported across the channel. Increasing  $V_G$  causes anions in the electrolyte to migrate toward the gate electrode, forming an electrical double layer. Concomitantly, cations are injected from the electrolyte into the channel material thereby progressively charge balancing the PSS anions and dedoping the PEDOT backbone, thereby depressing the source–drain current and turning the device “OFF”.

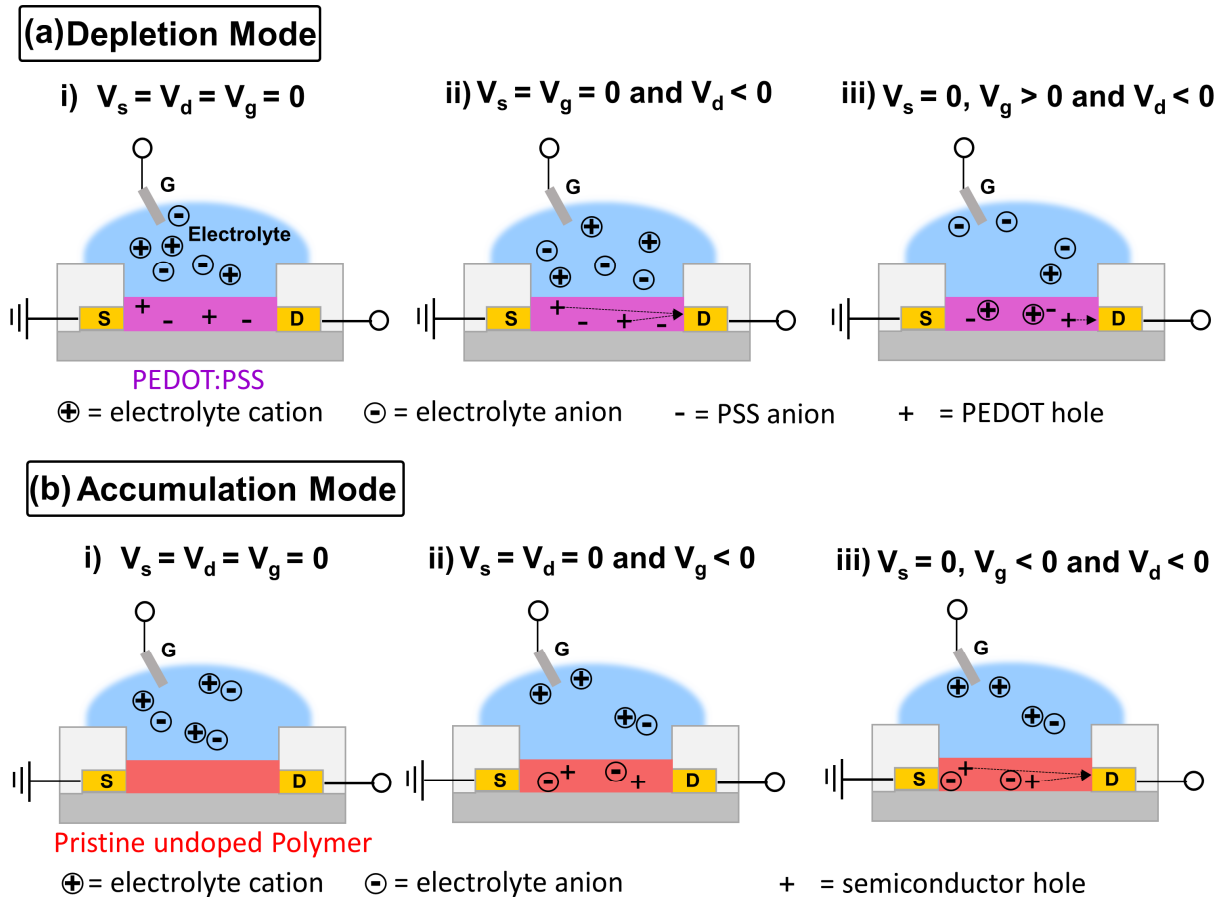


**Figure 10:** Operating principles for a depletion mode based OEET using PEDOT:PSS (a) and for an accumulation mode based OEET using non-doped and non-polyelectrolyte p-type semiconductor (b).

### Organic Mixed Ion-Electron Conductors

Organic MIECs are semiconductors, which can transport holes (or electrons) and ions efficiently. OEET channel materials can be subdivided into basically two categories, electron rich (p-type operation) and electron-deficient (n-type operation). As mentioned, PEDOT:PSS is the most widely used doped p-type organic semiconductor for depletion mode OEET applications. It consists of very short and insoluble PEDOT segments, which are p-type doped by the water soluble PSS chains of much higher molecular weight.<sup>4,11</sup> The insoluble nature of the PEDOT as homopolymer makes it difficult to modify it synthetically and therefore investigating a structure property relationship. PEDOT:PSS exhibits a very high OEET hole mobility  $\mu_{\text{OEET}}$  and a medium

volumetric capacitance  $C^*$ , measured with bandwidth experiments estimating the electronic transit time and electrochemical impedance spectroscopy.<sup>11</sup> But there are several drawbacks using PEDOT:PSS. PSS is highly acidic which negatively influences the long term stability of the devices.<sup>86,87</sup> Furthermore PEDOT:PSS requires the use of an external cross-linker to improve the adhesion on the gold electrodes, as well as the stability in aqueous environment.<sup>86–88</sup> Many other dopants (TOS, PSTFSILi 100, PMATFSILi 80, dextran sulfate) were used to improve the performance of PEDOT, usually resulting in decreased charge carrier mobilities without having a huge effect on the volumetric capacitance.<sup>11,84,89–91</sup> Only upon using tosylate as dopant, the resulting PEDOT:TOS shows an increased ion transport, while maintaining the high charge carrier mobility of PEDOT:PSS in OECTs.<sup>90</sup> All PEDOT derivatives used in OECTs are shown in **Figure 11** regarding their mixed conducting properties.

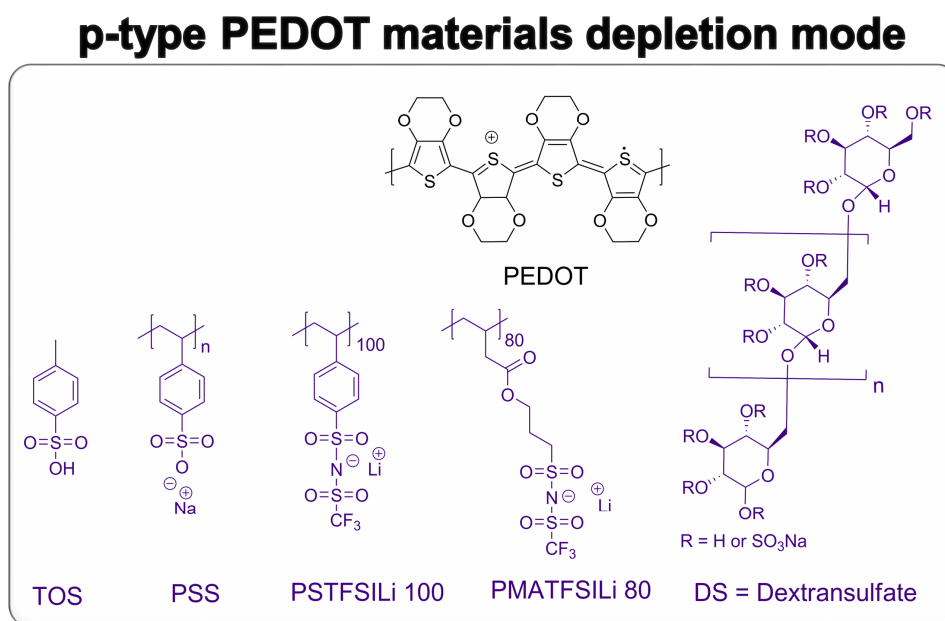


**Figure 11:** Schematic illustration of the different p-type PEDOT derivatives with various molecular, polymeric and biological dopants, namely tosylate, poly(styrene sulfonate), (trifluoromethylsulfonyl)sulfonylimide (styrenic or methacrylic backbone, and Li<sup>+</sup> as the counter ion), and dextran sulfate.<sup>11,84,89–91</sup>

Beside the research on integrating PEDOT:PSS into depletion mode OECTs, recent research mainly focuses on non-doped organic semiconductors, which are suitable for accumulation mode OECTs. There are only a few reports on the application of undoped soluble PEDOT derivatives used in accumulation mode OECTs. Most of the research on soluble poly-3,4-dialkoxy thiophenes (PProDOT) is done on 3,4-propylenedioxythiophene derivatives, because they are synthetically much more easily accessible.<sup>92,93</sup> Recently, OECTs based on the PProDOT derivative, ProDOT(OE)-DMP are reported. The polymer showed promising performance in accumulation mode OECTs and towards ion and charge transport.<sup>94</sup>

The chemical structures of p-type polymers reported for accumulation mode operation are shown in **Figure 12**. The benchmark materials for accumulation mode OECTs are polythiophene based polymers, functionalized with polar ethylene glycol side chains to promote ion transport. A series of ethylene glycol functionalized polythiophene polymers were tested in OECTs by Nielsen et al.<sup>85</sup> Compared to OECTs based on PEDOT:PSS, no additional external cross-linker is needed to stabilize these MIEC polymers in contact with water. Different types of copolymers were tested based on benzodithiophene (BDT), thieno-thiophene (TT) and thiophenes with triethylene glycol side chains. The influence on the device performance of the sidechain orientation and density was also investigated. A higher density of side chains increased the  $\pi$ - $\pi$  stacking distance of the polymer which is detrimental for the electronic transport but provided the ability of swelling which is required for good ionic transport.<sup>85</sup> The best performing polymers in this study, p(g2T-T) and p(gBDT-g2T), showed a higher volumetric capacitance but at the same time a reduced hole transport compared to PEDOT:PSS. Changing the comonomer to a thieno-thiophene unit (TT), increased the hole mobility drastically. This polymer is called p(2gT-TT), it exhibits  $\mu C^*$  product of

around  $240 \text{ F cm}^{-1} \text{ V}^{-1} \text{ s}^{-1}$  and is at the moment the benchmark accumulation p-type materials for OECTs at present.<sup>95</sup> The very good OECT performance of this material is a consequence of the perfect balance of good ion transport, a low oxidation potential and high tendency of swelling (ethylene glycol thiophene units) and the high electronic charge transport properties of thieno-thiophene. Savva et. al. extended the series of ethylene glycol substituted polythiophenes by studying OECT performance and the bulk charging behavior polymer series with varying amounts of EG side chains attached to a dialkoxybithiophene-co-thienothiophene (2T-TT) backbone (i.e., p(g2T-TT) analogues) in aqueous electrolytes.<sup>96</sup> For the polymer series investigated in this work, incorporating EG side chains caused the  $g_m$  of the OECTs to increase by five orders of magnitude due to an increase in  $C^*$  and  $\mu_{h\text{-OECT}}$  and a shift in  $V_{th}$  toward 0 V, compared to the more non-polar polymer g-0 %. Furthermore, the polymer with hexakis ethylene glycol side (2g) chain show lower  $g_m$  and ON current, although an excessive water uptake compared to the benchmark polymer p(2gT-TT)/g-100%.

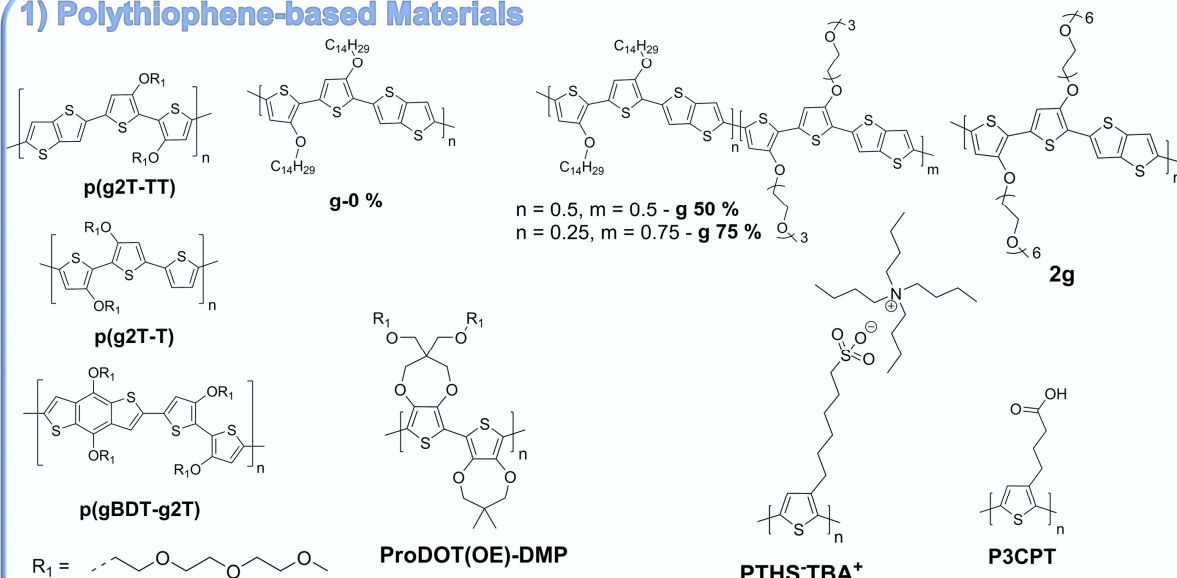
A recent example of a solvent-resistant polythiophene derivative was presented by Khau et al.<sup>97</sup> The presented, that the carboxylic acid functionalized polythiophene derivative poly [3-(4-carboxypropyl)-thiophene] (P3CPT) can be easily processed from water and thus does not require additional cross-linkers to stabilize the polymer film in contact with the electrolyte. OECT devices fabricated with this polymer show high transconductances  $g_m$  ( $26 \pm 0.2 \text{ mS}$ ) and competitive volumetric capacitance  $C^*$  of around  $150 \text{ F cm}^{-3}$ .

Another class of non-doped polar semiconductors suitable for accumulation mode OECTs comprises conjugated polyelectrolytes. Brendel et. al. from our research group reported poly[6-(thiophen-3-yl) hexane-1-sulfonate tetraalkyl ammonium], PTHS<sup>-</sup>TBA<sup>+</sup> for the first time in 2014, where the thiophene is carrying extremely polar, ionic alkyl

sulfonate groups as side chains.<sup>98</sup> PTHS-M<sup>+</sup> was obtained by post polymerization reaction of a precursor polymer, which was polymerized in a well-controlled manner using KCTP. It showed good results towards a high ON current and high transconductance,  $g_m$ .<sup>99</sup> Also, the importance of a controlled polymerization for this kind of conjugated polyelectrolytes was shown towards high charge transport.<sup>98</sup> Moreover, the influence of different M<sup>+</sup> cations on OECT properties was evaluated and we found the smallest tetramethyl ammonium (TMA<sup>+</sup>) to be the most suitable counter ion.<sup>100</sup> However, the high solubility of the various PTHS-M<sup>+</sup> polyelectrolytes in polar or aqueous solvents entails difficulties (similar to PEDOT:PSS) during the OECT operation, because films delaminate upon exposure to water, necessitating the use of an external cross-linker.<sup>98,99</sup> However, this electrically insulating cross-linker dilutes the active material in the transistor channel and was shown, in the case of PEDOT:PSS, to enhance the water-stability of the film at the expense of its mixed (ionic and electronic) conductivity.<sup>86,101</sup> The drop in electrical conductivity upon inclusion of such crosslinkers stems from the changes in the film morphology.<sup>87</sup> Further, all the PTHS-M<sup>+</sup> polyelectrolytes display a threshold voltage ( $V_{th}$ ) of around  $-0.5$  V in an OECT. For biosensing applications where the recognition events lead to doping of the channel (that is, switching the transistor ON), materials with low  $V_{th}$  are desirable as at low external voltages applied, the devices consume less power, but also avoid possible Faradaic reactions that can take place in complex biological media rich with electroactive species and interfere with the device output.

## p-type Accumulation mode OECTs Materials

### 1) Polythiophene-based Materials



### 2) Diketopyrrolopyrrole-based Materials

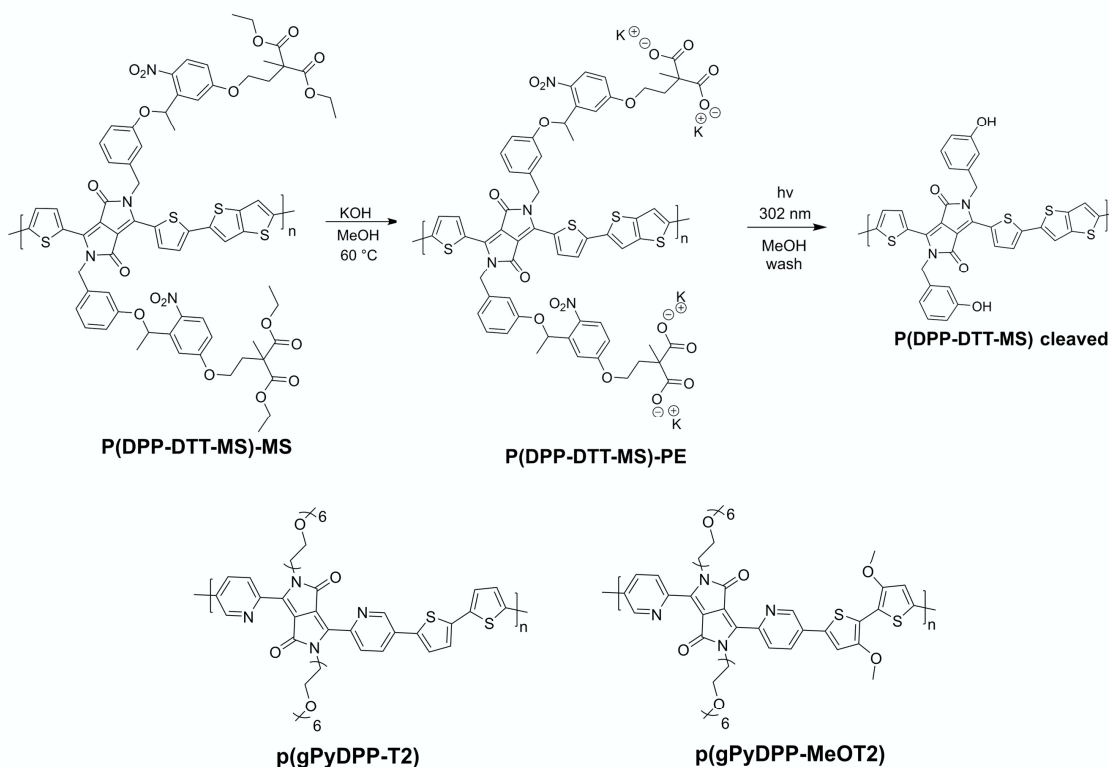


**Figure 12:** Chemical structures of selected and recent examples of p-type polymers used in accumulation mode OECTs. 1) Polythiophene-based polymers: p(g2T-TT), g-0% (reproduced from Ref. <sup>95</sup>), p(g2T-T) and p(gBDT-g2T) (reproduced from Ref. <sup>85</sup>), g-50%, g-75 % and 2g (reproduced from Ref. <sup>96</sup>), ProDOT(OE)-DMP (reproduced from Ref. <sup>94</sup>), PTHS<sup>-</sup>TBA<sup>+</sup> and P3CPT (reproduced from Ref. <sup>97,99</sup>) 2) Diketopyrrolo pyrrole-based OMIEC: P(DPP-DTT-MS)<sup>102</sup>, p(gPyDPP-T2) and p(gPyDPP-MeOT2)<sup>103</sup>.

## p-type Accumulation mode OECTs Materials

### 3) Isoindigo-based Materials

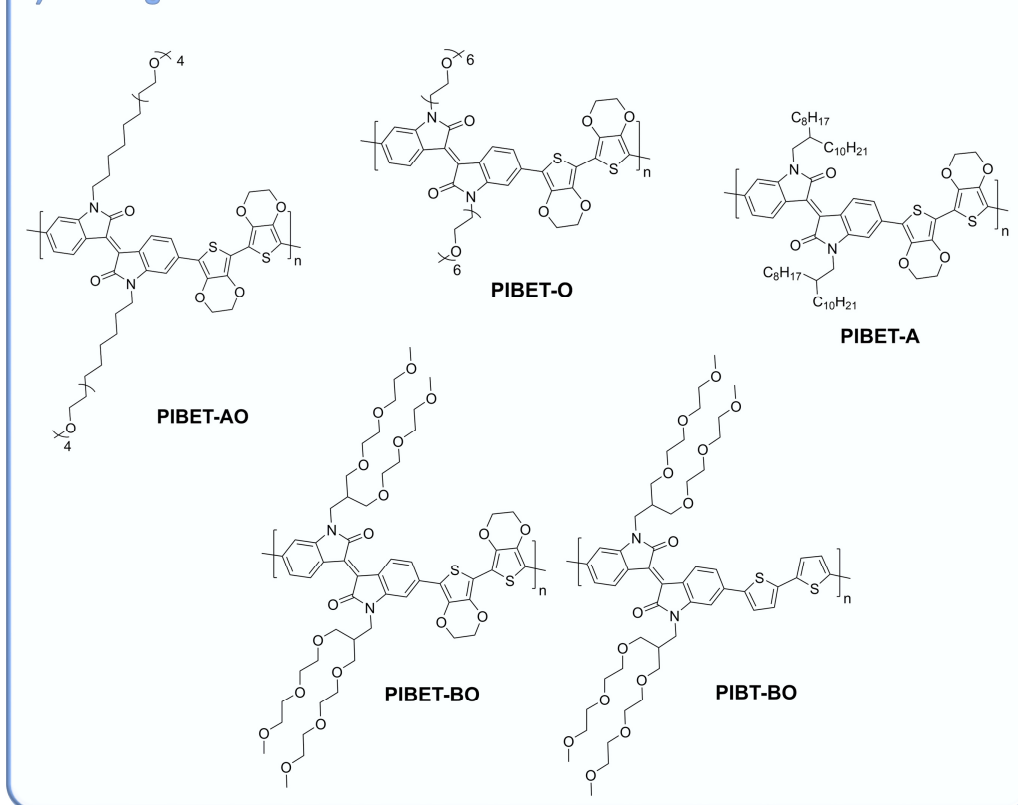


**Figure 13:** Chemical structures of selected and recent examples of p-type polymers based on an isoindigo backbone for accumulation mode OECTs. Chemical Structures were reproduced from Ref.<sup>104</sup>

The first example of a fully solution printed OECT was presented by Schmatz and co-workers.<sup>102</sup> They realized this fully printed OECT by a multistage cleavable side chain process, using a diketopyrrolo pyrrole polymer (DPP) backbone. P(DPP-DTT-MS) was converted to the polyelectrolyte P(DPP-DTT-MS)-PE through a postpolymerization hydrolysis of the side chain terminal ester groups using KOH in methanol. After hydrolysis, the resulting polyelectrolyte P(DPP-DTT-MS)-PE exhibited water solubility. After coating and drying, films were irradiated to initiate side chain cleavage through an intramolecular rearrangement of the *o*-nitrobenzyl unit. The polymer became solvent resistant after side chain cleavage, allowing for films of P(DPP-DTT-MS cleaved) to be submerged in water without dissolving. The polymer showed a relative

high threshold voltage  $V_{th}$  of around -0.5 V and a medium transconductance of 1.1 mS at -1 V, when operating in OECTs.

One strategy to prevent oxygen reduction reactions (ORR) of OMIEC under OECT preparation, is described by Giovannitti et. al.<sup>103</sup> Formation of  $H_2O_2$  during device operation is a concern when operating in biological environments since corrosive damage to the device materials, or lipid peroxidation can occur.<sup>103</sup> They developed two donor-acceptor polymers based on DPP [p(gPyDPP-T2) and p(gPyDPP-MeOT2)], which exhibit large differences in the ionization potential  $I_P$ , thus no ORR in ambient conditions in pH neutral aqueous electrolytes was observed for p(gPyDPP-MeOT2)]. Although p(gPyDPP-MeOT2)] displays a lower electronic charge carrier mobility in OECTs compared to state-of-the-art polymers, the chemical design strategy is a viable for avoiding hazardous side-products during OECT operation and achieving low OFF currents devices.

Donor-acceptor copolymers, beside DPPs, were recently reported by Wang et. al.<sup>104</sup>, consisting of electron-deficient isoindigo units and electron-rich EDOT groups. The chemical structures of the copolymers used in this study are shown in **Figure 13**. The investigated four different types of side chains: hybrid alkyl-EG chains (PIBET-AO), linear hydrophilic EG chains (PIBET-O), branched hydrophilic EG chains (PIBET-BO and PIBT-BO), and branched hydrophobic alkyl chains (PIBET-A). Out of OECT operation it can be concluded, that with increasing the number of EG side chains from linear in PIBET-O to branched in PIBET-BO comes hand in hand with a decrease in transconductance as well as device stability over time. In contrast, PIBET-AO leads to devices having a similar transconductance with respect to PIBET-O but enhanced operational stability and substrate adhesion.

The development of efficient high-performance n-type molecules or polymers for as OECT channel materials is usually lagging behind their p-type counterparts. Theory and experiments have proven, that this delay in development is not due to the different charge transport mechanism of holes and electrons, but rather due to the stability issues of electron conducting materials, especially in their doped state.<sup>105</sup> This instability arises from the instability of the  $\pi$ -radical anions towards water and oxygen.<sup>106</sup> Especially in OECT devices this instability is crucial and therefore it demands for the development of new polar n-type materials. All known n-type materials for accumulation mode transistors are shown in **Figure 14**.

### n-type Accumulation mode OECTs Materials

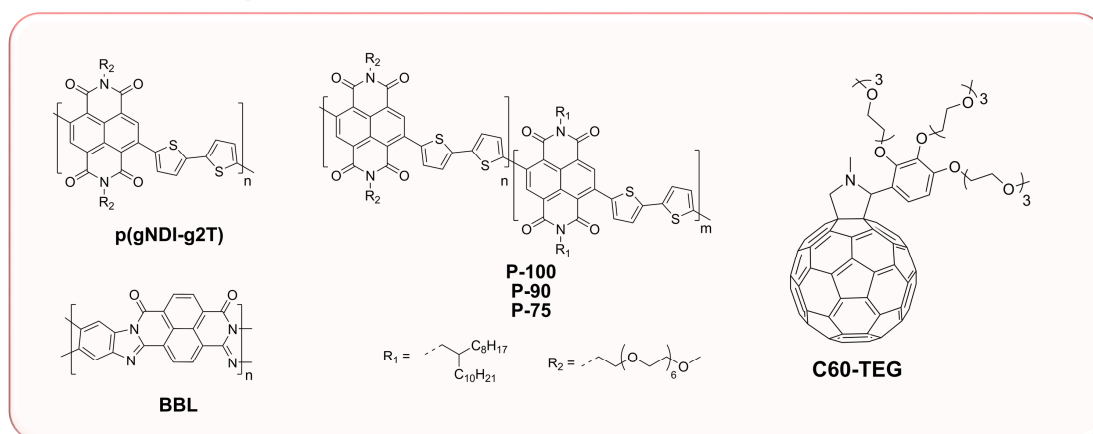


**Figure 14:** Chemical structures of the tested n-type accumulation mode OECT materials: p(gNDI-g2T) (reproduced from Ref.<sup>55</sup>), P-100, P-90 and P-75 (reproduced from Ref.<sup>107</sup>), BBL (reproduced from Ref.<sup>108</sup>) and C60-TEG (reproduced from Ref.<sup>109</sup>).

Nevertheless, the first reported n-type polymer in 2016 for accumulation mode OECTs was p(gNDI-gT2).<sup>55</sup> This is an alternating polymer based on naphthalene-1,4,5,8-tetracarboxylic diimide (NDI) and bithiophene (T2) polymer backbone, where the NDI unit is functionalized with a polar ethylene glycol side chain. With this polymer stable OECTs could be fabricated, because the interaction of the ethylene glycol side chain leads to the formation of stable p- and n-doped states. Recently, the impact of the side

chains was studied in detail by copolymerizing either alkyl or glycol chains containing NDI monomers in different ratios.<sup>107</sup> While a higher content of the glycol monomer has a negative influence on the electron mobility, the volumetric capacitance is, as well as the tendency of water uptake is increased (P100 is the copolymer with 100 % glycol monomer, P50 with 50% glycol, respectively). Also ladder type n-type polymers showed great potential, due to their very high capacitance. BBL shows an impressive volumetric capacitance of around  $900 \text{ Fcm}^{-3}$ , This value exceeded that of the best NDI-based OECTs by more than 2-fold.<sup>108</sup> However, the devices based on BBL suffered from a slow response time due to the limited ion diffusion throughout the BBL morphology. Bischak and coworkers reported as first the application of polar fullerenes as active materials in OECTs.<sup>109</sup> They synthesized 2-(2,3,4-tris(methoxytriglycol)phenyl)[60]fulleropyrrolidine (C60-TEG), and observed high volumetric capacitance  $C^*$  of  $220 \pm 50 \text{ Fcm}^{-3}$  and a hole mobility  $\mu_{\text{OECT}}$  of  $3 \cdot 10^{-2} \text{ cm}^2\text{V}^{-1}$  under n-type OECT operation. This study represents the first step towards small-molecule application in OECTs.

## 1. Introduction

---

- (1) Simon, D. T.; Gabrielsson, E. O.; Tybrandt, K.; Berggren, M. Organic Bioelectronics: Bridging the Signaling Gap between Biology and Technology. *Chem. Rev.* **2016**, *116* (21), 13009–13041.
- (2) Wu, H.; Gao, W.; Yin, Z. Materials, Devices and Systems of Soft Bioelectronics for Precision Therapy. *Adv. Healthc. Mater.* **2017**, *6* (10), 1700017.
- (3) Rivnay, J.; Owens, R. M.; Malliaras, G. G. The Rise of Organic Bioelectronics. *Chem. Mater.* **2014**, *26* (1), 679–685.
- (4) Inal, S.; Rivnay, J.; Suiu, A.-O.; Malliaras, G. G.; McCulloch, I. Conjugated Polymers in Bioelectronics. *Acc. Chem. Res.* **2018**, *51* (6), 1368–1376.
- (5) *Bioelectronics: From Theory to Applications*; Wilner, I., Ed.; WILEY-VCH: Weinheim, 2005.
- (6) Wilson, B. S.; Dorman, M. F. Cochlear Implants: A Remarkable Past and a Brilliant Future. *Hear. Res.* **2008**, *242* (1–2), 3–21.
- (7) Moser, M.; Ponder, J. F.; Wadsworth, A.; Giovannitti, A.; McCulloch, I. Materials in Organic Electrochemical Transistors for Bioelectronic Applications: Past, Present, and Future. *Adv. Funct. Mater.* **2018**, 1807033.
- (8) Du, J.; Catania, C.; Bazan, G. C. Modification of Abiotic–Biotic Interfaces with Small Molecules and Nanomaterials for Improved Bioelectronics. *Chem. Mater.* **2014**, *26* (1), 686–697.
- (9) Berggren, M.; Richter-Dahlfors, A. Organic Bioelectronics. *Adv. Mater.* **2007**, *19* (20), 3201–3213.
- (10) Savva, A.; Wustoni, S.; Inal, S. Ionic-to-Electronic Coupling Efficiency in PEDOT:PSS Films Operated in Aqueous Electrolytes. *J. Mater. Chem. C* **2018**, *6* (44), 12023–12030.
- (11) Inal, S.; Malliaras, G. G.; Rivnay, J. Benchmarking Organic Mixed Conductors for Transistors. *Nat. Commun.* **2017**, *8* (1).
- (12) Goel, M.; Heinrich, C. D.; Krauss, G.; Thelakkat, M. Principles of Structural Design of Conjugated Polymers Showing Excellent Charge Transport toward Thermoelectrics and Bioelectronics Applications. *Macromol. Rapid Commun.* **2019**, 1800915.
- (13) Shirakawa, H.; Louis, E. J.; MacDiarmid, A. G.; Chiang, C. K.; Heeger, A. J. Synthesis of Electrically Conducting Organic Polymers: Halogen Derivatives of Polyacetylene, (CH)<sub>x</sub>. *J. Chem. Soc. Chem. Commun.* **1977**, No. 16, 578.
- (14) Mateeva, N.; Niculescu, H.; Schlenoff, J.; Testardi, L. R. Correlation of Seebeck Coefficient and Electric Conductivity in Polyaniline and Polypyrrole. *J. Appl. Phys.* **1998**, *83* (6), 3111–3117.
- (15) Chiang, J.-C.; MacDiarmid, A. G. ‘Polyaniline’: Protonic Acid Doping of the Emeraldine Form to the Metallic Regime. *Synth. Met.* **1986**, *13* (1–3), 193–205.
- (16) Li, J.; Tang, X.; Li, H.; Yan, Y.; Zhang, Q. Synthesis and Thermoelectric Properties of Hydrochloric Acid-Doped Polyaniline. *Synth. Met.* **2010**, *160* (11–12), 1153–1158.
- (17) Lowen, S. V.; Van Dyke, J. D. Mechanistic Studies of the Electrochemical Polymerization of Pyrrole: Deuterium Isotope Effects and Radical Trapping Studies. *J. Polym. Sci. Part Polym. Chem.* **1990**, *28* (3), 451–464.
- (18) Qi, G.; Huang, L.; Wang, H. Highly Conductive Free Standing Polypyrrole Films Prepared by Freezing Interfacial Polymerization. *Chem. Commun.* **2012**, *48* (66), 8246.
- (19) Groenendaal, L.; Jonas, F.; Freitag, D.; Pielartzik, H.; Reynolds, J. R. Poly(3,4-Ethylenedioxythiophene) and Its Derivatives: Past, Present, and Future. *Adv. Mater.* **2000**, *12* (7), 481–494.
- (20) Yu, Z.; Xia, Y.; Du, D.; Ouyang, J. PEDOT:PSS Films with Metallic Conductivity through a Treatment with Common Organic Solutions of Organic Salts and Their Application as a Transparent Electrode of Polymer Solar Cells. *ACS Appl. Mater. Interfaces* **2016**, *8* (18), 11629–11638.
- (21) Fan, Z.; Li, P.; Du, D.; Ouyang, J. Significantly Enhanced Thermoelectric Properties of PEDOT:PSS Films through Sequential Post-Treatments with Common Acids and Bases. *Adv. Energy Mater.* **2017**, *7* (8), 1602116.

- (22) Wang, X.; Zhang, X.; Sun, L.; Lee, D.; Lee, S.; Wang, M.; Zhao, J.; Shao-Horn, Y.; Dincă, M.; Palacios, T.; Gleason, K. K. High Electrical Conductivity and Carrier Mobility in OCVD PEDOT Thin Films by Engineered Crystallization and Acid Treatment. *Sci. Adv.* **2018**, *4* (9), eaat5780.
- (23) Braun, D.; Heeger, A. J. Visible Light Emission from Semiconducting Polymer Diodes. *Appl. Phys. Lett.* **1991**, *58* (18), 1982–1984.
- (24) Sariciftci, N. S.; Braun, D.; Zhang, C.; Srdanov, V. I.; Heeger, A. J.; Stucky, G.; Wudl, F. Semiconducting Polymer-buckminsterfullerene Heterojunctions: Diodes, Photodiodes, and Photovoltaic Cells. *Appl. Phys. Lett.* **1993**, *62* (6), 585–587.
- (25) Sariciftci, N. S.; Smilowitz, L.; Heeger, A. J.; Wudl, F. Photoinduced Electron Transfer from a Conducting Polymer to Buckminsterfullerene. *Science* **1992**, *258* (5087), 1474–1476.
- (26) Bao, Z.; Dodabalapur, A.; Lovinger, A. J. Soluble and Processable Regioregular Poly(3-hexylthiophene) for Thin Film Field-effect Transistor Applications with High Mobility. *Appl. Phys. Lett.* **1996**, *69* (26), 4108–4110.
- (27) Siringhaus, H. Integrated Optoelectronic Devices Based on Conjugated Polymers. *Science* **1998**, *280* (5370), 1741–1744.
- (28) Chang, J.-F.; Sun, B.; Breiby, D. W.; Nielsen, M. M.; Sölling, T. I.; Giles, M.; McCulloch, I.; Siringhaus, H. Enhanced Mobility of Poly(3-Hexylthiophene) Transistors by Spin-Coating from High-Boiling-Point Solvents. *Chem. Mater.* **2004**, *16* (23), 4772–4776.
- (29) Yokoyama, A.; Miyakoshi, R.; Yokozawa, T. Chain-Growth Polymerization for Poly(3-Hexylthiophene) with a Defined Molecular Weight and a Low Polydispersity. *Macromolecules* **2004**, *37* (4), 1169–1171.
- (30) Sheina, E. E.; Liu, J.; Iovu, M. C.; Laird, D. W.; McCullough, R. D. Chain Growth Mechanism for Regioregular Nickel-Initiated Cross-Coupling Polymerizations. *Macromolecules* **2004**, *37* (10), 3526–3528.
- (31) Lohwasser, R. H.; Thelakkat, M. Toward Perfect Control of End Groups and Polydispersity in Poly(3-Hexylthiophene) via Catalyst Transfer Polymerization. *Macromolecules* **2011**, *44* (9), 3388–3397.
- (32) Kiriya, A.; Senkovskyy, V.; Sommer, M. Kumada Catalyst-Transfer Polycondensation: Mechanism, Opportunities, and Challenges. *Macromol. Rapid Commun.* **2011**, *32* (19), 1503–1517.
- (33) Miyakoshi, R.; Yokoyama, A.; Yokozawa, T. Catalyst-Transfer Polycondensation. Mechanism of Ni-Catalyzed Chain-Growth Polymerization Leading to Well-Defined Poly(3-Hexylthiophene). *J. Am. Chem. Soc.* **2005**, *127* (49), 17542–17547.
- (34) Lohwasser, R. H.; Thelakkat, M. Synthesis and Characterization of Monocarboxylated Poly(3-Hexylthiophene)s via Quantitative End-Group Functionalization. *Macromolecules* **2010**, *43* (18), 7611–7616.
- (35) *P3HT Revisited - from Molecular Scale to Solar Cell Devices*; Ludwigs, S., Andrienko, D., Eds.; Advances in polymer science; Springer: Berlin, 2014.
- (36) Higashihara, T.; Ueda, M. Precision Synthesis of Tailor-Made Polythiophene-Based Materials and Their Application to Organic Solar Cells. *Macromol. Res.* **2013**, *21* (3), 257–271.
- (37) Köhler, A.; Bäessler, H. *Electronic Processes in Organic Semiconductors: An Introduction*; Wiley-VCH Verlag GmbH & Co. KGaA: Weinheim, Germany, 2015. h
- (38) Tanase, C.; Blom, P. W. M.; de Leeuw, D. M. Origin of the Enhanced Space-Charge-Limited Current in Poly(p-Phenylene Vinylene). *Phys. Rev. B* **2004**, *70* (19), 193202.
- (39) Tanase, C.; Meijer, E. J.; Blom, P. W. M.; de Leeuw, D. M. Unification of the Hole Transport in Polymeric Field-Effect Transistors and Light-Emitting Diodes. *Phys. Rev. Lett.* **2003**, *91* (21), 216601.
- (40) Laquai, F.; Wegner, G.; Bäessler, H. What Determines the Mobility of Charge Carriers in Conjugated Polymers? *Philos. Trans. R. Soc. Math. Phys. Eng. Sci.* **2007**, *365* (1855), 1473–1487.
- (41) Horowitz, G. Organic Thin Film Transistors: From Theory to Real Devices. *J. Mater. Res.* **2004**, *19* (7), 1946–1962.

- (42) Brown, A. R.; Jarrett, C. P.; de Leeuw, D. M.; Matters, M. Field-Effect Transistors Made from Solution-Processed Organic Semiconductors. *Synth. Met.* **1997**, *88* (1), 37–55. ht
- (43) Sze, S. M.; Ng, K. K. *Physics of Semiconductor Devices*, 3rd ed.; Wiley-Interscience: Hoboken, N.J, 2007.
- (44) Kobayashi, S.; Nishikawa, T.; Takenobu, T.; Mori, S.; Shimoda, T.; Mitani, T.; Shimotani, H.; Yoshimoto, N.; Ogawa, S.; Iwasa, Y. Control of Carrier Density by Self-Assembled Monolayers in Organic Field-Effect Transistors. *Nat. Mater.* **2004**, *3* (5), 317–322.
- (45) Zaumseil, J.; Sirringhaus, H. Electron and Ambipolar Transport in Organic Field-Effect Transistors. *Chem. Rev.* **2007**, *107* (4), 1296–1323.
- (46) Sirringhaus, H.; Brown, P. J.; Friend, R. H.; Nielsen, M. M.; Bechgaard, K.; Langeveld-Voss, B. M. W.; Spiering, A. J. H.; Janssen, R. A. J.; Meijer, E. W.; Herwig, P.; de Leeuw, D. M. Two-Dimensional Charge Transport in Self-Organized, High-Mobility Conjugated Polymers. *Nature* **1999**, *401* (6754), 685–688.
- (47) Botiz, I.; Stingelin, N. Influence of Molecular Conformations and Microstructure on the Optoelectronic Properties of Conjugated Polymers. *Materials* **2014**, *7* (3), 2273–2300.
- (48) Noriega, R.; Rivnay, J.; Vandewal, K.; Koch, F. P. V.; Stingelin, N.; Smith, P.; Toney, M. F.; Salleo, A. A General Relationship between Disorder, Aggregation and Charge Transport in Conjugated Polymers. *Nat. Mater.* **2013**, *12*, 1038.
- (49) Roe, R. J. *Methods of X-Ray and Neutron Scattering in Polymer Science*; Topics in polymer science; Oxford University Press: New York, 2000.
- (50) Bragg, W. H.; Bragg, W. L. The Reflection of X-Rays by Crystals. *Proc. R. Soc. Math. Phys. Eng. Sci.* **1913**, *88* (605), 428–438.
- (51) Reiter, G.; Strobl, G. R. *Progress in Understanding of Polymer Crystallization*; 2007.
- (52) Chu, B.; Hsiao, B. S. Small-Angle X-Ray Scattering of Polymers. *Chem. Rev.* **2001**, *101* (6), 1727–1762.
- (53) Müller-Buschbaum, P. Grazing Incidence Small-Angle X-Ray Scattering: An Advanced Scattering Technique for the Investigation of Nanostructured Polymer Films. *Anal. Bioanal. Chem.* **2003**, *376* (1), 3–10.
- (54) Ree, M. Probing the Self-Assembled Nanostructures of Functional Polymers with Synchrotron Grazing Incidence X-Ray Scattering. *Macromol. Rapid Commun.* **2014**, *35* (10), 930–959.
- (55) Giovannitti, A.; Nielsen, C. B.; Sbircea, D.-T.; Inal, S.; Donahue, M.; Niazi, M. R.; Hanifi, D. A.; Amassian, A.; Malliaras, G. G.; Rivnay, J.; McCulloch, I. N-Type Organic Electrochemical Transistors with Stability in Water. *Nat. Commun.* **2016**, *7* (1), 13066.
- (56) Sun, H.; Gerasimov, J.; Berggren, M.; Fabiano, S. N-Type Organic Electrochemical Transistors: Materials and Challenges. *J. Mater. Chem. C* **2018**, *6* (44), 11778–11784.
- (57) Rivnay, J.; Inal, S.; Salleo, A.; Owens, R. M.; Berggren, M.; Malliaras, G. G. Organic Electrochemical Transistors. *Nat. Rev. Mater.* **2018**, *3* (2), 17086.
- (58) Lin, P.; Yan, F.; Yu, J.; Chan, H. L. W.; Yang, M. The Application of Organic Electrochemical Transistors in Cell-Based Biosensors. *Adv. Mater.* **2010**, *22* (33), 3655–3660.
- (59) Lin, P.; Luo, X.; Hsing, I.-M.; Yan, F. Organic Electrochemical Transistors Integrated in Flexible Microfluidic Systems and Used for Label-Free DNA Sensing. *Adv. Mater.* **2011**, *23* (35), 4035–4040.
- (60) Khodagholy, D.; Curto, V. F.; Fraser, K. J.; Gurfinkel, M.; Byrne, R.; Diamond, D.; Malliaras, G. G.; Benito-Lopez, F.; Owens, R. M. Organic Electrochemical Transistor Incorporating an Ionogel as a Solid State Electrolyte for Lactate Sensing. *J. Mater. Chem.* **2012**, *22* (10), 4440.
- (61) Jimison, L. H.; Tria, S. A.; Khodagholy, D.; Gurfinkel, M.; Lanzarini, E.; Hama, A.; Malliaras, G. G.; Owens, R. M. Measurement of Barrier Tissue Integrity with an Organic Electrochemical Transistor. *Adv. Mater.* **2012**, *24* (44), 5919–5923.
- (62) Tarabella, G.; D'Angelo, P.; Cifarelli, A.; Dimonte, A.; Romeo, A.; Berzina, T.; Erokhin, V.; Iannotta, S. A Hybrid Living/Organic Electrochemical Transistor Based on the Physarum Polycephalum Cell Endowed with Both Sensing and Memristive Properties. *Chem. Sci.* **2015**, *6* (5), 2859–2868.

- (63) Hempel, F.; Law, J. K.-Y.; Nguyen, T. C.; Munief, W.; Lu, X.; Pachauri, V.; Susloparova, A.; Vu, X. T.; Ingebrandt, S. PEDOT:PSS Organic Electrochemical Transistor Arrays for Extracellular Electrophysiological Sensing of Cardiac Cells. *Biosens. Bioelectron.* **2017**, *93*, 132–138.
- (64) Salyk, O.; Víteček, J.; Omasta, L.; Šafaříková, E.; Stříteský, S.; Vala, M.; Weiter, M. Organic Electrochemical Transistor Microplate for Real-Time Cell Culture Monitoring. *Appl. Sci.* **2017**, *7* (10), 998.
- (65) Campana, A.; Cramer, T.; Simon, D. T.; Berggren, M.; Biscarini, F. Electrocardiographic Recording with Conformable Organic Electrochemical Transistor Fabricated on Resorbable Bioscaffold. *Adv. Mater.* **2014**, *26* (23), 3874–3878.
- (66) Leleux, P.; Johnson, C.; Strakosas, X.; Rivnay, J.; Hervé, T.; Owens, R. M.; Malliaras, G. G. Ionic Liquid Gel-Assisted Electrodes for Long-Term Cutaneous Recordings. *Adv. Healthc. Mater.* **2014**, *3* (9), 1377–1380.
- (67) van de Burgt, Y.; Lubberman, E.; Fuller, E. J.; Keene, S. T.; Faria, G. C.; Agarwal, S.; Marinella, M. J.; Alec Talin, A.; Salleo, A. A Non-Volatile Organic Electrochemical Device as a Low-Voltage Artificial Synapse for Neuromorphic Computing. *Nat. Mater.* **2017**, *16* (4), 414–418.
- (68) Gkoupidenis, P.; Koutsouras, D. A.; Malliaras, G. G. Neuromorphic Device Architectures with Global Connectivity through Electrolyte Gating. *Nat. Commun.* **2017**, *8* (1), 15448.
- (69) Nilsson, D.; Robinson, N.; Berggren, M.; Forchheimer, R. Electrochemical Logic Circuits. *Adv. Mater.* **2005**, *17* (3), 353–358.
- (70) Zeglio, E.; Schmidt, M. M.; Thelakkat, M.; Gabrielsson, R.; Solin, N.; Inganäs, O. Conjugated Polyelectrolyte Blends for Highly Stable Accumulation-Mode Electrochemical Transistors. *Chem. Mater.* **2017**, *29*, 10, 4293–4300
- (71) Fabiano, S.; Sani, N.; Kawahara, J.; Kergoat, L.; Nissa, J.; Engquist, I.; Crispin, X.; Berggren, M. Ferroelectric Polarization Induces Electronic Nonlinearity in Ion-Doped Conducting Polymers. *Sci. Adv.* **2017**, *3* (6), e1700345.
- (72) Hamedi, M.; Forchheimer, R.; Inganäs, O. Towards Woven Logic from Organic Electronic Fibres. *Nat. Mater.* **2007**, *6* (5), 357–362.
- (73) Kittlesen, G. P.; White, H. S.; Wrighton, M. S. Chemical Derivatization of Microelectrode Arrays by Oxidation of Pyrrole and N-Methylpyrrole: Fabrication of Molecule-Based Electronic Devices. *J. Am. Chem. Soc.* **1984**, *106* (24), 7389–7396.
- (74) Kergoat, L.; Piro, B.; Berggren, M.; Horowitz, G.; Pham, M.-C. Advances in Organic Transistor-Based Biosensors: From Organic Electrochemical Transistors to Electrolyte-Gated Organic Field-Effect Transistors. *Anal. Bioanal. Chem.* **2012**, *402* (5), 1813–1826.
- (75) Zhao, D.; Fabiano, S.; Berggren, M.; Crispin, X. Ionic Thermoelectric Gating Organic Transistors. *Nat. Commun.* **2017**, *8* (1), 14214.
- (76) Xia, Y.; Zhang, W.; Ha, M.; Cho, J. H.; Renn, M. J.; Kim, C. H.; Frisbie, C. D. Printed Sub-2 V Gel-Electrolyte-Gated Polymer Transistors and Circuits. *Adv. Funct. Mater.* **2010**, *20* (4), 587–594.
- (77) Rivnay, J.; Leleux, P.; Ferro, M.; Sessolo, M.; Williamson, A.; Koutsouras, D. A.; Khodagholy, D.; Ramuz, M.; Strakosas, X.; Owens, R. M.; Benar, C.; Badier, J.-M.; Bernard, C.; Malliaras, G. G. High-Performance Transistors for Bioelectronics through Tuning of Channel Thickness. *Sci. Adv.* **2015**, *1* (4), e1400251.
- (78) Laiho, A.; Herlogsson, L.; Forchheimer, R.; Crispin, X.; Berggren, M. Controlling the Dimensionality of Charge Transport in Organic Thin-Film Transistors. *Proc. Natl. Acad. Sci.* **2011**, *108* (37), 15069–15073.
- (79) Khodagholy, D.; Rivnay, J.; Sessolo, M.; Gurfinkel, M.; Leleux, P.; Jimison, L. H.; Stavriniidou, E.; Herve, T.; Sanaur, S.; Owens, R. M.; Malliaras, G. G. High Transconductance Organic Electrochemical Transistors. *Nat. Commun.* **2013**, *4* (1), 2133.
- (80) Bucella, S. G.; Luzio, A.; Gann, E.; Thomsen, L.; McNeill, C. R.; Pace, G.; Perinot, A.; Chen, Z.; Facchetti, A.; Caironi, M. Macroscopic and High-Throughput Printing of Aligned

- Nanostructured Polymer Semiconductors for MHz Large-Area Electronics. *Nat. Commun.* **2015**, *6* (1), 8394.
- (81) Schmode, P.; Ohayon, D.; Reichstein, P. M.; Savva, A.; Inal, S.; Thelakkat, M. High-Performance Organic Electrochemical Transistors Based on Conjugated Polyelectrolyte Copolymers. *Chem. Mater.* **2019**, *31* (14), 5286–5295.
- (82) Bernards, D. A.; Malliaras, G. G. Steady-State and Transient Behavior of Organic Electrochemical Transistors. *Adv. Funct. Mater.* **2007**, *17* (17), 3538–3544.
- (83) Zeglio, E.; Inganäs, O. Active Materials for Organic Electrochemical Transistors. *Adv. Mater.* **2018**, *30* (44), 1800941.
- (84) Rivnay, J.; Inal, S.; Collins, B. A.; Sessolo, M.; Stavrinidou, E.; Strakosas, X.; Tassone, C.; Delongchamp, D. M.; Malliaras, G. G. Structural Control of Mixed Ionic and Electronic Transport in Conducting Polymers. *Nat. Commun.* **2016**, *7* (1).
- (85) Nielsen, C. B.; Giovannitti, A.; Sbircea, D.-T.; Bandiello, E.; Niazi, M. R.; Hanifi, D. A.; Sessolo, M.; Amassian, A.; Malliaras, G. G.; Rivnay, J.; McCulloch, I. Molecular Design of Semiconducting Polymers for High-Performance Organic Electrochemical Transistors. *J. Am. Chem. Soc.* **2016**, *138* (32), 10252–10259.
- (86) Håkansson, A.; Han, S.; Wang, S.; Lu, J.; Braun, S.; Fahlman, M.; Berggren, M.; Crispin, X.; Fabiano, S. Effect of (3-Glycidioxypropyl)Trimethoxysilane (GOPS) on the Electrical Properties of PEDOT:PSS Films. *J. Polym. Sci. Part B Polym. Phys.* **2017**, *55* (10), 814–820.
- (87) ElMahmoudy, M.; Inal, S.; Charrier, A.; Uguz, I.; Malliaras, G. G.; Sanaur, S. Tailoring the Electrochemical and Mechanical Properties of PEDOT:PSS Films for Bioelectronics. *Macromol. Mater. Eng.* **2017**, *302* (5), 1600497.
- (88) Mantione, D.; del Agua, I.; Schaafsma, W.; ElMahmoudy, M.; Uguz, I.; Sanchez-Sanchez, A.; Sardon, H.; Castro, B.; Malliaras, G. G.; Mecerreyes, D. Low-Temperature Cross-Linking of PEDOT:PSS Films Using Divinylsulfone. *ACS Appl. Mater. Interfaces* **2017**, *9* (21), 18254–18262.
- (89) Inal, S.; Rivnay, J.; Hofmann, A. I.; Uguz, I.; Mumtaz, M.; Katsigiannopoulos, D.; Brochon, C.; Cloutet, E.; Hadziioannou, G.; Malliaras, G. G. Organic Electrochemical Transistors Based on PEDOT with Different Anionic Polyelectrolyte Dopants. *J. Polym. Sci. Part B Polym. Phys.* **2016**, *54* (2), 147–151.
- (90) Winther-Jensen, B.; West, K. Vapor-Phase Polymerization of 3,4-Ethylenedioxythiophene: A Route to Highly Conducting Polymer Surface Layers. *Macromolecules* **2004**, *37* (12), 4538–4543.
- (91) Harman, D. G.; Gorkin, R.; Stevens, L.; Thompson, B.; Wagner, K.; Weng, B.; Chung, J. H. Y.; in het Panhuis, M.; Wallace, G. G. Poly(3,4-Ethylenedioxythiophene):Dextran Sulfate (PEDOT:DS) – A Highly Processable Conductive Organic Biopolymer. *Acta Biomater.* **2015**, *14*, 33–42.
- (92) Österholm, A. M.; Ponder, J. F.; De Keersmaecker, M.; Shen, D. E.; Reynolds, J. R. Disentangling Redox Properties and Capacitance in Solution-Processed Conjugated Polymers. *Chem. Mater.* **2019**, *31* (8), 2971–2982.
- (93) Ponder, J. F.; Pittelli, S. L.; Reynolds, J. R. Heteroatom Role in Polymeric Dioxyselenophene/Dioxythiophene Systems for Color and Redox Control. *ACS Macro Lett.* **2016**, *5* (6), 714–717.
- (94) Savagian, L. R.; Österholm, A. M.; Ponder, J. F.; Barth, K. J.; Rivnay, J.; Reynolds, J. R. Balancing Charge Storage and Mobility in an Oligo(Ether) Functionalized Dioxythiophene Copolymer for Organic- and Aqueous- Based Electrochemical Devices and Transistors. *Adv. Mater.* **2018**, *30* (50), 1804647.
- (95) Giovannitti, A.; Sbircea, D.-T.; Inal, S.; Nielsen, C. B.; Bandiello, E.; Hanifi, D. A.; Sessolo, M.; Malliaras, G. G.; McCulloch, I.; Rivnay, J. Controlling the Mode of Operation of Organic Transistors through Side-Chain Engineering. *Proc. Natl. Acad. Sci.* **2016**, *113* (43), 12017–12022.
- (96) Savva, A.; Hallani, R.; Cendra, C.; Surgailis, J.; Hidalgo, T. C.; Wustoni, S.; Sheelamanthula, R.; Chen, X.; Kirkus, M.; Giovannitti, A.; Salleo, A.; McCulloch, I.; Inal, S. Balancing Ionic and

- Electronic Conduction for High-Performance Organic Electrochemical Transistors. *Adv. Funct. Mater.* **2020**, *30* (11), 1907657.
- (97) Khau, B. V.; Savagian, L. R.; De Keersmaecker, M.; Gonzalez, M. A.; Reichmanis, E. Carboxylic Acid Functionalization Yields Solvent-Resistant Organic Electrochemical Transistors. *ACS Mater. Lett.* **2019**, *1* (6), 599–605.
- (98) Brendel, J. C.; Schmidt, M. M.; Hagen, G.; Moos, R.; Thelakkat, M. Controlled Synthesis of Water-Soluble Conjugated Polyelectrolytes Leading to Excellent Hole Transport Mobility. *Chem. Mater.* **2014**, *26* (6), 1992–1998.
- (99) Inal, S.; Rivnay, J.; Leleux, P.; Ferro, M.; Ramuz, M.; Brendel, J. C.; Schmidt, M. M.; Thelakkat, M.; Malliaras, G. G. A High Transconductance Accumulation Mode Electrochemical Transistor. *Adv. Mater.* **2014**, *26* (44), 7450–7455.
- (100) Schmidt, M. M.; ElMahmoudy, M.; Malliaras, G. G.; Inal, S.; Thelakkat, M. Smaller Counter Cation for Higher Transconductance in Anionic Conjugated Polyelectrolytes. *Macromol. Chem. Phys.* **2018**, *219* (2), 1700374.
- (101) Zhang, S.; Kumar, P.; Nouas, A. S.; Fontaine, L.; Tang, H.; Cicoira, F. Solvent-Induced Changes in PEDOT:PSS Films for Organic Electrochemical Transistors. *APL Mater.* **2015**, *3* (1), 014911.
- (102) Schmatz, B.; Lang, A. W.; Reynolds, J. R. Fully Printed Organic Electrochemical Transistors from Green Solvents. *Adv. Funct. Mater.* **2019**, *29* (44), 1905266.
- (103) Giovannitti, A.; Rashid, R. B.; Thiburce, Q.; Paulsen, B. D.; Cendra, C.; Thorley, K.; Moia, D.; Mefford, J. T.; Hanifi, D.; Weiyuan, D.; Moser, M.; Salleo, A.; Nelson, J.; McCulloch, I.; Rivnay, J. Energetic Control of Redox-Active Polymers toward Safe Organic Bioelectronic Materials. *Adv. Mater.* **2020**, 1908047.
- (104) Wang, Y.; Zeglio, E.; Liao, H.; Xu, J.; Liu, F.; Li, Z.; Maria, I. P.; Mawad, D.; Herland, A.; McCulloch, I.; Yue, W. Hybrid Alkyl–Ethylene Glycol Side Chains Enhance Substrate Adhesion and Operational Stability in Accumulation Mode Organic Electrochemical Transistors. *Chem. Mater.* **2019**, *31* (23), 9797–9806.
- (105) Facchetti, A.  $\pi$ -Conjugated Polymers for Organic Electronics and Photovoltaic Cell Applications †. *Chem. Mater.* **2011**, *23* (3), 733–758.
- (106) de Leeuw, D. M.; Simenon, M. M. J.; Brown, A. R.; Einerhand, R. E. F. Stability of N-Type Doped Conducting Polymers and Consequences for Polymeric Microelectronic Devices. *Synth. Met.* **1997**, *87* (1), 53–59.
- (107) Giovannitti, A.; Maria, I. P.; Hanifi, D.; Donahue, M. J.; Bryant, D.; Barth, K. J.; Makdah, B. E.; Savva, A.; Moia, D.; Zetek, M.; Barnes, P. R. F.; Reid, O. G.; Inal, S.; Rumbles, G.; Malliaras, G. G.; Nelson, J.; Rivnay, J.; McCulloch, I. The Role of the Side Chain on the Performance of N-Type Conjugated Polymers in Aqueous Electrolytes. *Chem. Mater.* **2018**, *30* (9), 2945–2953.
- (108) Sun, H.; Vagin, M.; Wang, S.; Crispin, X.; Forchheimer, R.; Berggren, M.; Fabiano, S. Complementary Logic Circuits Based on High-Performance n-Type Organic Electrochemical Transistors. *Adv. Mater.* **2018**, *30* (9), 1704916.
- (109) Bischak, C. G.; Flagg, L. Q.; Yan, K.; Li, C.-Z.; Ginger, D. S. Fullerene Active Layers for N-Type Organic Electrochemical Transistors. *ACS Appl. Mater. Interfaces* **2019**, *11* (31), 28138–28144.

### **2.Objective of the Thesis**

Organic mixed ion-electron conductors (OMIEC) are mainly polar/ionic semiconducting polymers, which are able to conduct both ions and electronic charges. This class of materials is highly attractive for bioelectronic applications using organic electrochemical transistors (OECTs), where such a mixed conduction is required. State of the art bioelectronic devices are based on inorganic materials (metals and ceramics), such as glucose sensors or cochlear implants. The key to new and improved technologies is to improve the interface between the tissue and electronic materials. Polar conjugated polymers are highly suitable for this type of application, because they are synthetically tunable, easily processable, soft/ compliant, can be both ion and electron conducting, and biocompatible. Our research group reported for the first time in 2014, the controlled polymerization of a conjugated polyelectrolyte, poly[6-(thiophen-3-yl) hexane-1-sulfonate tetra alkyl ammonium], PTHS·M<sup>+</sup> and their application in OECTs. PTHS·M<sup>+</sup> was obtained by post polymerization reaction of a precursor polymer P3BrHT, which was polymerized in a well-controlled manner using KCTP. It showed promising results in terms of a high ON current and high transconductance,  $g_m$ . We could also show the importance of a controlled polymerization for this kind of application of a conjugated polyelectrolyte. Moreover, the influence of different M<sup>+</sup> cations on OECT properties was evaluated and we found the smallest tetramethyl ammonium (TMA<sup>+</sup>) to be the most suitable counter ion for obtaining high transconductance. However, the high solubility of the various PTHS·M<sup>+</sup> polyelectrolytes in aqueous solvents entails difficulties during the OECT operation, because films delaminate upon exposure to water. This necessitates the use of an external cross-linker. However, this electrically insulating cross-linker dilutes the active material in the transistor channel and was shown, for the case of PEDOT:PSS, to

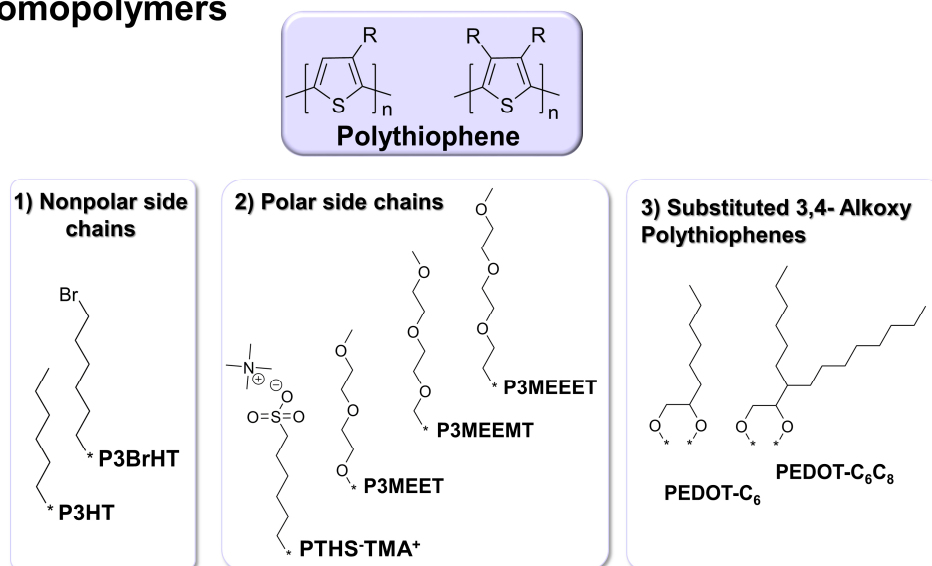
enhance the water-stability of the film at the expense of its mixed (ionic and electronic) conductivity. Furthermore, PTHS·M<sup>+</sup> exhibits a relatively poor hole mobility  $\mu_{\text{OECT}}$  in OECT operation and a high threshold voltage of around -0.5 V. For biosensing applications where the recognition events lead to doping of the channel (that is, switching the transistor ON), materials with low  $V_{\text{th}}$  are desirable as at low external voltages applied, the devices consume less power, but also avoid possible Faradaic reactions that can take place in complex biological media rich with electro-active species and interfere with the device output.

In this thesis first we studied the properties of the precursor homopolymer P3BrHT and its copolymers, P3BrHT-co-P3HT. The hydrophobic 3HT was selected as a comonomer to decrease the solubility of the final polyelectrolyte copolymers in water. The aggregation properties, crystallinity, charge transport and the alignment on various substrates must be studied, to obtain a better understanding of a  $\omega$ -side chain functionalization on the final polymer properties. Finally, the P3BrHT segment in P3BrHT-co-P3HT copolymers will be converted in a post polymerization reaction to result in polyelectrolyte copolymers, PTHS·M<sup>+</sup>-co-P3HT. The idea here is to fine tune the composition and improve the properties of the known conjugated polyelectrolyte PTHS·M<sup>+</sup> with respect to its mixed conduction properties as well as to reduce the solubility in water without sacrificing the swelling behavior. The idea is to exploit the hydrophobic character of P3HT to tune the water solubility of the final copolymer by varying the composition. Additionally, the beneficial properties of P3HT like the excellent hole transport properties should be maintained.

Another strategy to design new OMIECs is to avoid all ionic groups (as present in PTHS·M<sup>+</sup>) and to introduce polar side chains in polythiophene derivatives. In this respect, polythiophenes functionalized with ethylene glycol (EG) side chains are of

great interest, because they have been reported to enable enhanced swelling and facilitates ion transport in addition to electronic transport in such systems.

### A) Homopolymers



### B) Copolymers

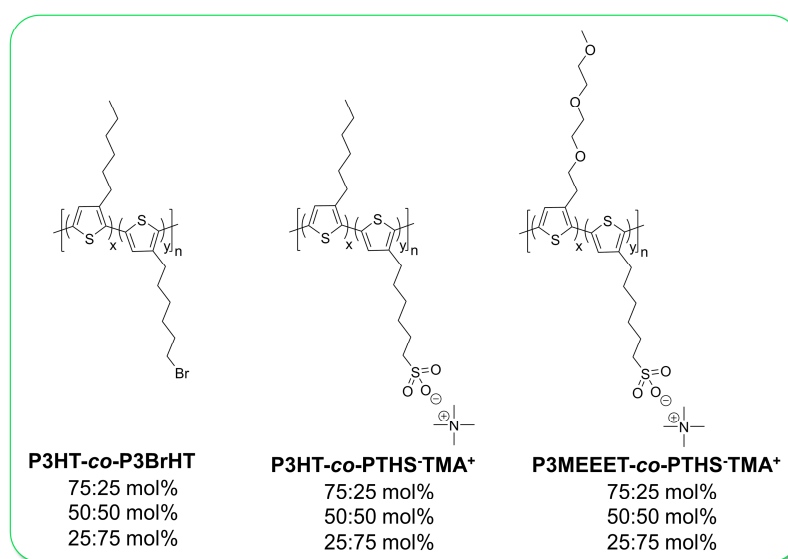


**Figure 1:** Overview over the synthetic strategy of the thesis. Different homopolymers are planned with non-polar side chains (**A1**), polar side chains (**A2**) and different substituted PEDOT derivatives to tailor the solubility (**A3**). Furthermore, copolymers are planned to tune the polymer dependent properties like solubility and mixed-conduction properties (**B**).

Here, the nature of binding of an EG side chain on mixed conduction properties need to be tested in a series of such polymers where the EG group will be attached without, using a methyl or ethyl spacer group. We expect that these differences of attachment can have a profound influence on ionic and electronic conduction properties.

In bioelectronic devices the most used p-type semiconductor is highly doped PEDOT:PSS, which is used in depletion mode OECTs. Moreover, the PEDOT present in PEDOT/PSS are made up of insoluble oligomers and they are prepared in a non-controlled fashion and the doped form is stabilized using PSS in a dispersion. Thus, the last synthetic strategy for novel OMIECs is for obtaining a highly soluble, well-controlled and processable PEDOT homopolymer using controlled polymerization techniques such as KCTP. Here the open question is if a suitable monomer with sufficient solubility can be designed and polymerized using KCTP and if the final material is an interesting candidate for mixed conduction.

All the polymers need to be characterized using diverse methods (GPC, DSC, X-ray scattering, etc.). The performance as a mixed conductor will be evaluated by incorporating the suitable candidates in accumulation mode OECTs. The accumulation mode OECTs will be fabricated and characterized in joint research work. This involves current-voltage measurements in transistor mode, impedance spectroscopy, swelling experiments using QCM.

Further, for future OECT research at Bayreuth, the detailed preparation of OECT microelectrodes involving coating and etching of multiple layers will be jointly established with service providers having advanced photolithography facilities.

### 3. Overview over the Thesis

This thesis focuses on the synthesis of diverse novel polythiophene-based organic mixed conductors and the influence of the polymer architecture and composition on structure formation and in their application in OECTs. The key theme within this thesis is how to understand the interplay of ionic and electronic charge transport in mixed conductors, keeping the basic moiety of thiophene and varying the side chains and composition in copolymers.

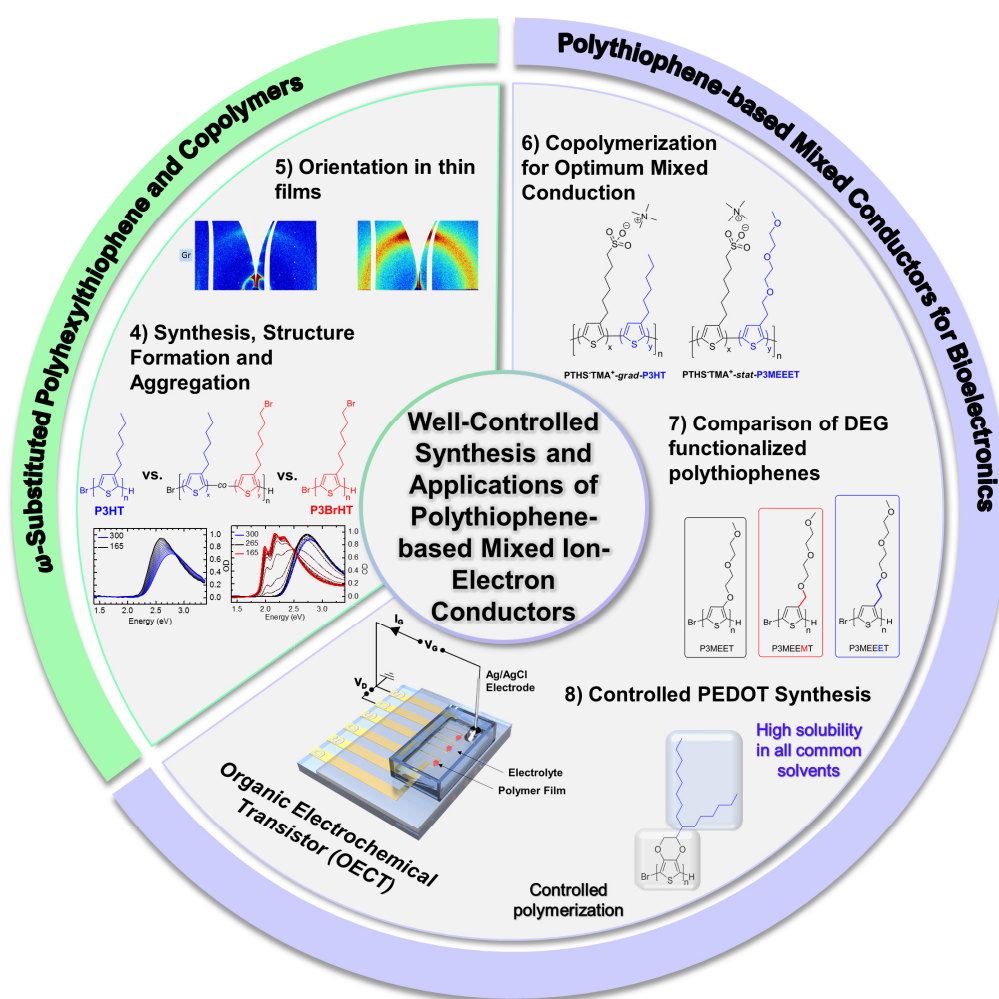


**Figure 1:** Overview over the thesis including the five chapters: influence of  $\omega$ -bromo substitution on structure and opto-electrical properties of homopolymers and gradient copolymers of 3-hexylthiophene (4), favored face-on crystal orientation in thin films of poly(3-(6-bromohexyl)-thiophene) on graphene as a result of modified interfacial interactions (5), high performance organic electrochemical transistors based on conjugated polyelectrolyte copolymers (6), the key role of side chain linkage in structure formation and mixed conduction of ethylene glycol substituted polythiophenes (7) A highly Soluble alkyl substituted PEDOT via Kumada Catalyst Transfer Polymerization' (8).

Since the basic concept involves the variation of side chains, first the properties of P3BrHT, the starting polymer of all  $\omega$ -functionalized polythiophenes, was evaluated compared to the benchmark polythiophene P3HT, as well as in copolymers consisting of both. A one-pot reaction of the two monomers 3BrHT and 3HT resulted in a series of gradient copolymers. The opto-electronic properties, as well as the crystal structure of these copolymers were characterized and compared (**Chapter 4**). Molecular orientation is a crucial aspect in influencing the charge transport within organic electronic devices. Therefore, additionally, the orientation of P3BrHT was compared to P3HT on various substrates. (**Chapter 5**). In order to study the influence of composition on the relevant properties such as hole mobility, stability of the polymer film in contact with water, high threshold voltage, ion transport), I used the tool of copolymerization of THS<sup>+</sup>M<sup>+</sup> with 3-hexylthiophene (3HT), due to the good electronic charge transport properties and the hydrophobicity of P3HT (**Chapter 6**). Further, a series of polythiophenes functionalized with diethylene glycol side chains were synthesized and characterized, differing in the side chain connection to the thiophene backbone (**Chapter 7**). Doped PEDOT:PSS dispersions is the most used material used in depletion mode OECTs. Because of this, a new highly soluble PEDOT derivative with well-controlled molecular weight was designed and polymerized via KCTP in a controlled fashion. (**Chapter 8**).

## Chapter 4: Influence of $\omega$ -bromo Substitution on Structure and Opto-Electrical Properties of Homopolymers and Gradient Copolymers of 3-Hexylthiophene

The nature of side chains in conjugated polymers exhibit a huge influence on the resulting polymer properties like solubility, aggregation in solution and crystallinity. These properties affect the charge transport in conjugated polymers to a very large extent. In this work, the influence of a  $\omega$ -bromo substituent on the state-of-the-art p-type semiconductor poly-3-hexylthiophene (P3HT) is systematically studied in a series of gradient copolymers, P3HT-co-P3BrHT 1,2 and 3. These three copolymers were synthesized using controlled Kumada catalyst transfer polymerization (KCTP).

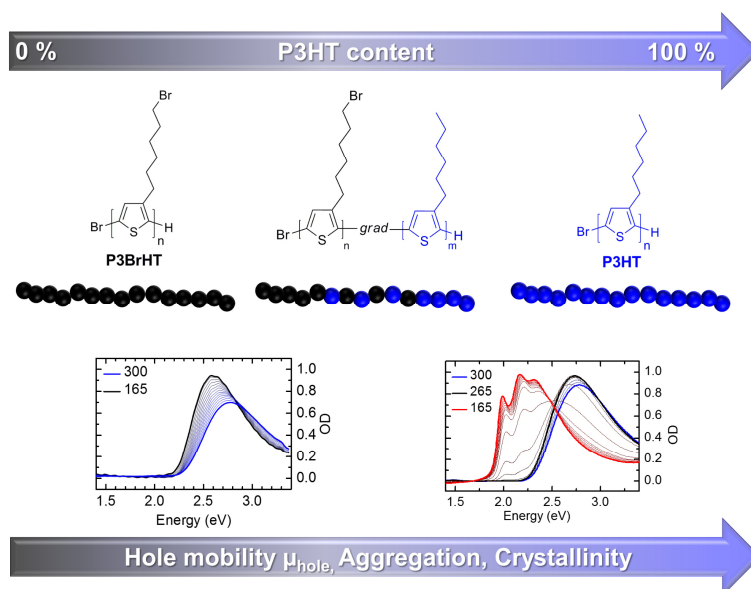


**Figure 2:** Overview over the investigated polymers P3BrHT, P3HT and the copolymers P3HT-co-P3BrHT 1,2 and 3 with compositions of 30/70, 51/49 and 77/23 mol% respectively in this study (Copyright 2020 American Chemical Society).

A comparison with both homopolymers, poly[3-(6-bromohexyl)-thiophene (P3BrHT) and P3HT gives insights into the changes in aggregation, crystal structure, crystallinity, and charge transport properties. We found that the melting point as well as the melting enthalpy increases concomitantly with increasing amount of 3HT in the copolymers; the melting point increasing from 135 °C (P3BrHT) to 237 °C (P3HT) and melting

enthalpy from 6 J/g to 23 J/g. In aggregation studies using temperature dependent absorption and emission spectroscopy in solution we show that the low crystalline P3BrHT does not show any measurable aggregation up to 165 K in THF, whereas with increasing 3HT content, the aggregation clearly sets in and critical transition temperature  $T_c$  increases from about 180 K for P3HT-co-P3BrHT 1 (25 mol% 3HT) to 250 K for P3HT. This is accompanied by an increase of the overall fraction of aggregates. The crystal structure and crystallinity of the samples were further studied with wide angle X-ray scattering. Here also we observe a large increase in the crystallinity in the copolymers and a gradual monotonic decrease of the a and b crystal lattice parameters in the polymers with decreasing 3BrHT content that evidences co-crystallization of 3HT and 3BrHT units. This trend is also displayed in the increasing hole mobility extracted out of OEFT experiments. Based on our detailed study, we elucidate the drastic influence of an  $\omega$ -bromo substituent in P3HT towards structure formation and diverse opto-electronic properties.

### **Chapter 5: Favored Face-on Crystal Orientation in Thin Films of Poly(3-(6-bromohexyl)-thiophene) on Graphene as a Result of Modified Interfacial Interactions**

Molecular orientation is an important aspect in improving the efficiency of organic electronic devices. In many ordered materials, orientation can be achieved by directional crystallization on a substrate. However, despite a face-on orientation in monolayers of poly(3-hexylthiophene) (P3HT) on graphite, fully face-on oriented crystals with vertically layered  $\pi$ - $\pi$  stacks in thicker P3HT films has not been realized to date. This finding is assumed to be a result of two competing interfacial interactions of P3HT chains with graphite and vacuum, which result in face-on and edge-on crystal orientations, respectively.

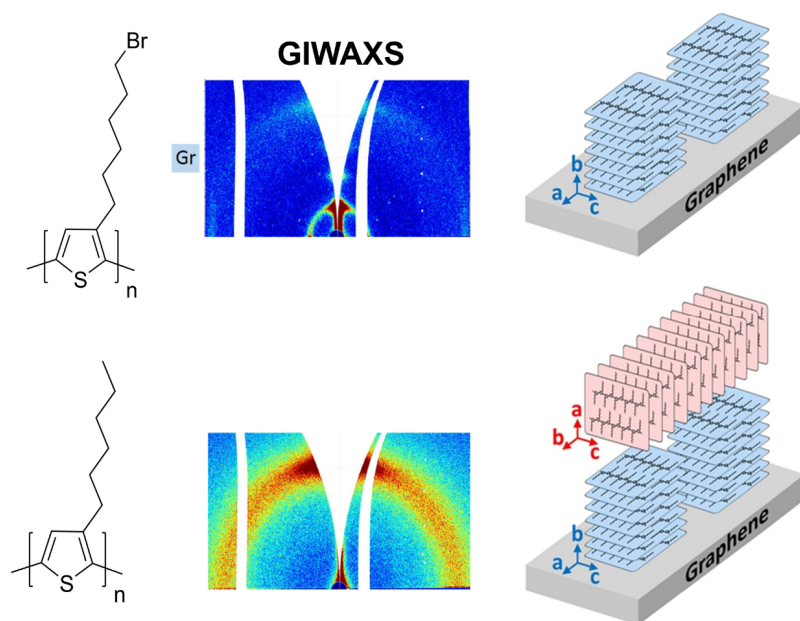


**Figure 3:** Schematic illustration of the different orientations of P3HT (mixed edge/face-on orientation) and P3BrHT (solely face-on orientation) on graphene.

Here it is shown that modification of the chemical structure of P3HT side chains can alter the interfacial interactions and result in a complete face-on alignment. Specifically, we present a comparative study of the substrate induced crystal orientation in P3HT and poly(3-(6-bromohexyl)-thiophene) (P3BrHT). The orientation in thin films of both polymers crystallized on a single-layer graphene was explored by grazing incidence X-ray diffraction. The results evidence that P3HT films of various thickness on graphene show mixed edge-on and face-one crystal orientation with edge-on crystals formed at the top surface, even in films as thin as 5 nm. In contrast, P3BrHT on graphene has solely face-on oriented crystals in films with thickness up to about 26 nm and shifts to the mixed crystal orientation with increasing film thickness. The surface morphology of the films investigated by atomic-force microscopy supports these results. It is concluded that the formation of edge-on crystals in P3BrHT was suppressed but not eliminated completely.

## Chapter 6: High Performance Organic Electrochemical Transistors based on Conjugated Polyelectrolyte Copolymers

A new generation of polythiophene-based polyelectrolytes are reported to address fundamental issues in an organic electrochemical transistor (OECT). In such devices, the semiconductor must be able to transport and store ions and to possess simultaneously a very high electronic mobility. For this, the ion-conducting 6-(thiophen-3-yl) hexane-1-sulfonate tetramethyl ammonium monomer (THS-TMA<sup>+</sup>) is copolymerized with the hole-conducting 3-hexylthiophene (3HT) to obtain copolymers, PTHS-TMA<sup>+</sup>-co-P3HT 1-3 with a gradient architecture.

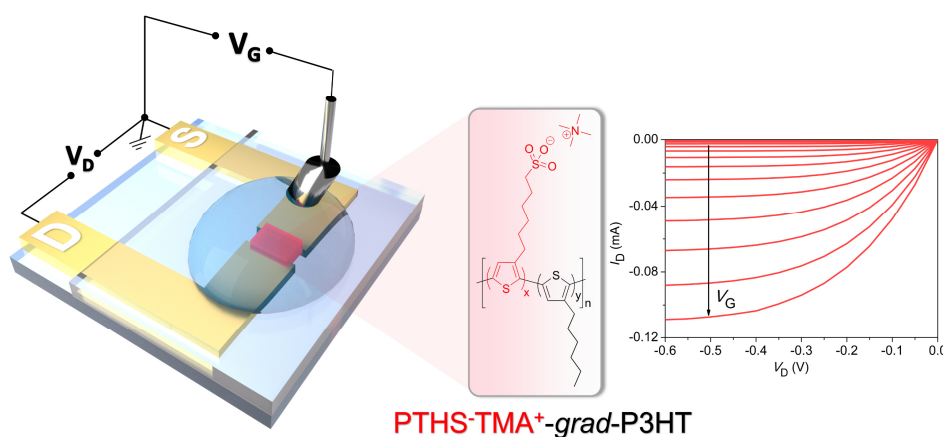


**Figure 4:** Illustration of an organic electrochemical transistor (OECT) and the structure of the best performing conjugated copolyelectrolyte P3HT-co-PTHS-TMA<sup>+</sup> with a composition of 51:49 mol% used in this device. The corresponding output curve is also shown for P3HT-co-PTHS-TMA<sup>+</sup> with gate voltages ranging from 0 V to -0.60 V ( $\Delta V = -0.05$  V, Copyright 2019 American Chemical Society).

The copolymers having up to 50 mol% 3HT content are easily oxidizable and are crystalline. Consequently, for the copolymers, a higher stability in water is achieved, thus reducing the amount of cross-linker needed to stabilize the film. Furthermore, OECTs using copolymers with 75 and 50 mol% of PTHS-TMA<sup>+</sup> content exhibit 2-3 orders of magnitude higher ON/OFF ratio and an extremely lower threshold voltage (-

0.15 V) compared to PTHS<sup>-</sup> TMA<sup>+</sup>. Additionally, high volumetric capacitance ( $C^* > 100 \text{ F/cm}^3$ ) is achieved, indicating that the ion transport is not hampered by the hydrophobic 3HT up to 50 mol%, for which a very high OECT hole mobility of  $0.017 \text{ cm}^2/\text{Vs}$  is also achieved. Thus, the concept of copolymerization to combine both ionic and electronic charge transport in an organic mixed conductor offers an elegant approach to obtain high performance OECT materials.

## **Chapter 7: The Key Role of Side Chain Linkage in Structure Formation and Mixed Conduction of Ethylene Glycol Substituted Polythiophenes**

Functionalizing conjugated polymers with polar ethylene glycol side chains enables enhanced swelling and facilitates ion transport in addition to electronic transport in such systems. Here we investigate three polythiophene homopolymers (P3MEET, P3MEEMT and P3MEEET), having differently linked (without, methyl and ethyl spacer, respectively) diethylene glycol side chains. All the polymers were tested in organic electrochemical transistors (OECTs). They show drastic differences in the device performance. The highest  $\mu_{\text{OECT}} C^*$  product of  $11.5 \text{ F/cmVs}$  was obtained for ethyl spaced P3MEEET. How the injection and transport of ions is influenced by the side-chain linkage was studied with electrochemical impedance spectroscopy (EIS), which shows a dramatic increase in volumetric capacitance from  $80 \pm 9$  up to  $242 \pm 17 \text{ F/cm}^3$  on going from P3MEET to P3MEEET. Thus, ethyl-spaced P3MEEET exhibits one of the highest reported volumetric capacitance values among p-type polymers. Moreover,

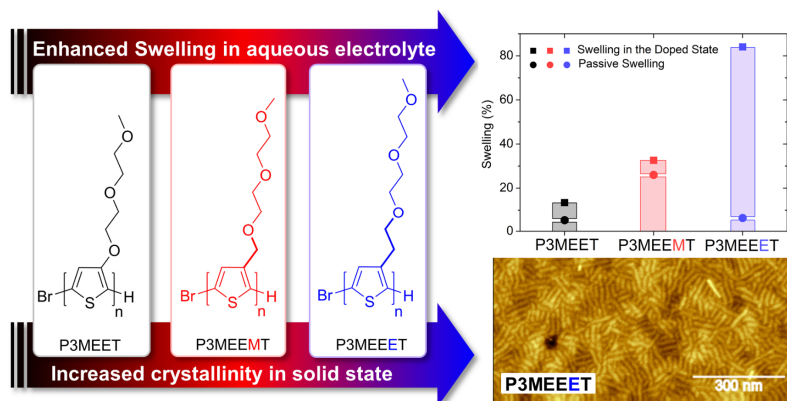


**Figure 4:** Chemical Structures of P3MEET, P3MEEMT and P3MEEET. Also, the enhanced swelling (EQCMD-D) and the increased lamellar order (AFM) of P3MEEET compared to the other two polythiophenes is shown (Copyright 2020 American Chemical Society).

P3MEEET exhibits in dry thin films an OFET hole mobility of  $0.005 \text{ cm}^2/\text{Vs}$ , highest among the three, which is one order of magnitude higher than for P3MEEMT. The extracted hole mobility from OECT (oxidized swollen state) and the hole mobility in solid state thin films (OFET) show contradictory trends for P3MEEMT and P3MEEET. In order to understand exactly the properties in the hydrated and dry states, the crystal structure of the polymers was investigated with WAXS and GIWAXS and the water uptake under applied potential was monitored using E-QCMD. These measurements reveal an amorphous state for P3MEET, whereas and a semicrystalline state for P3MEEMT and P3MEEET. On the other hand, E-QCMD confirms that P3MEEET swells ten times more than P3MEEMT in the oxidized state. Thus, the importance of the ethyl spacer towards crystallinity and mixed-conduction properties was clearly demonstrated, emphasizing the impact of side chain-linkage of diethylene glycol. This detailed study offers a better understanding how to design high performance organic mixed conductors.

## Chapter 8: A highly Soluble alkyl substituted PEDOT via Kumada Catalyst Transfer Polymerization

PEDOT:PSS [poly(3,4-ethylenedioxythiophene) polystyrene sulfonate] is the most used hole conductor in the field of materials science. In this work, a new synthetic strategy is presented to create new highly soluble, highly oxidizable and highly aggregating PEDOT homopolymers.

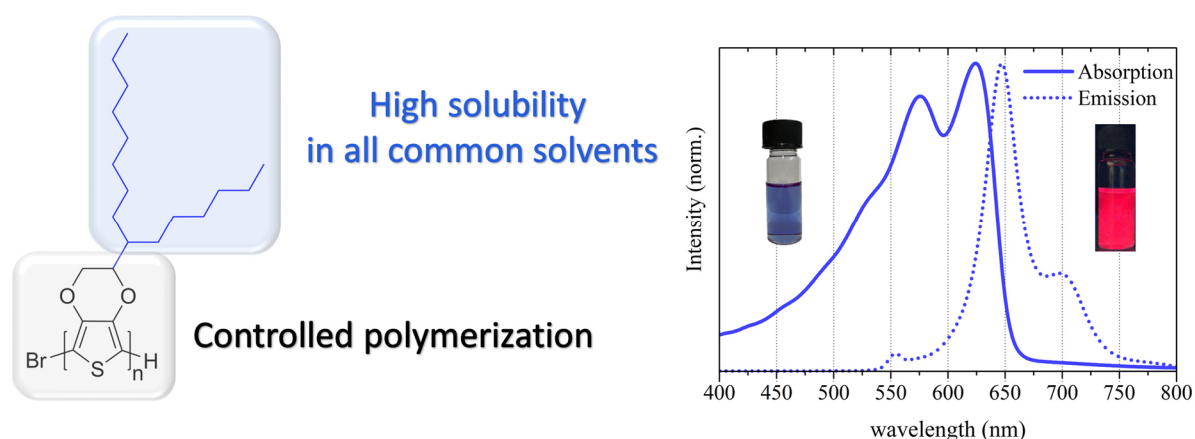


**Figure 5:** New developed PEDOT homopolymer with a solubilizing C<sub>6</sub>/C<sub>8</sub> side chain. Absorption and emission spectra of PEDOT C<sub>6</sub>/C<sub>8</sub> 2.

The new developed EDOT monomer can be polymerized via Kumada catalyst transfer polymerization in a well-controlled fashion, resulting in defined polymers PEDOT-C<sub>6</sub>C<sub>8</sub> 1 and 2, with two different molecular weights as desired and low dispersity. Through functionalization with a branched alkyl side chain, the polymers exhibit excellent solubility in all common solvents such as hexane or THF. These highly aggregating polymers are easily oxidizable in thin films, and they show a promising hole mobility ( $\mu_{\text{hole}} = 5 \cdot 10^4 \text{ cm}^2\text{V}^{-1}\text{s}^{-1}$ ) in organic field effect transistors. Also, compared to the pristine samples, the conductivity improves to  $10^{-3} \text{ S/cm}^{-1}$ , even when doped with low amounts (10 mol%) of Spiro-TFSI<sub>2</sub>. This new design concept of soluble PEDOT homopolymers will lead to a new generation of PEDOT polymers.

## Individual Contributions to Joint Publications

The following section specifies the individual contributions of the authors:

### Chapter 4

*„ Influence of  $\omega$ -bromo Substitution on Structure and Opto-Electrical Properties of Homopolymers and Gradient Copolymers of 3-hexylthiophene” published as *Macromolecules* **2020**, 53, 7, 2474-2484.*

by Philip Schmode, Konstantin Schötz, Oleksandr Dolynchuk, Fabian Panzer, Anna Köhler, Thomas Thurn-Albrecht and Mukundan Thelakkat.

I synthesized and characterized the homopolymer P3BrHT and the copolymers P3HT-co-P3BrHT 1-3. Konstantin Schötz performed the temperature dependent emission and absorption spectroscopy. Oleksandr Dolynchuk analyzed the crystal structure of the homopolymers and the copolymers. Anna Köhler, Thomas Thurn-Albrecht and Mukundan Thelakkat supervised the project and corrected the final manuscript.

### Chapter 5

*„ Favored Face-on Crystal Orientation in Thin Films of Poly(3-(6-bromohexyl)-thiophene) on Graphene as a Result of Modified Interfacial Interactions”*

Oleksandr Dolynchuk, Philip Schmode, Matthias Fischer, Mukundan Thelakkat, Thomas Thurn-Albrecht.

Prepared for submission.

Oleksandr Dolynchuk performed all WAXS orientation experiments. I synthesized and characterized the homopolymer P3BrHT and purified the commercial P3HT. Thomas Thurn-Albrecht and Mukundan Thelakkat supervised the project and corrected the final manuscript.

## Chapter 6

*„High Performance Organic Electrochemical Transistors based on Conjugated Polyelectrolyte Copolymers”*

by Philip Schmode, David Ohayon, Paul M. Reichstein, Achilleas Savva, Sahika Inal and Mukundan Thelakkat.

*Published as Chem. Mater.* **2019**, *31 (14)*, 5286–5295.

I designed, synthesized and characterized the conjugated copolyelectrolytes. I wrote the manuscript. Paul M. Reichstein helped with the x-ray measurements. The OECT measurements were carried out during my research stay at KAUST. David Ohayon (KAUST) assisted during OECT fabrication, measurements and analysis. Together with Achilleas Savva (KAUST) QCM-D measurements were performed. Mukundan Thelakkat and Sahika Inal (KAUST) supervised the project and corrected the final manuscript.

## Chapter 7

*„The Key Role of Side Chain Linkage in Structure Formation and Mixed Conduction of Ethylene Glycol Substituted Polythiophenes”*

by Philip Schmode, Achilleas Savva, Robert Kahl, David Ohayon, Florian Meichsner, Oleksandr Dolynchuk, Thomas Thurn-Albrecht, Sahika Inal and Mukundan Thelakkat.

*Published as ACS Applied Materials & Interfaces*, **2020**, *12 (11)*, 13029-13039

I designed, synthesized and characterized the diethylenglycol functionalized polythiophenes. Furthermore, I wrote the manuscript. Florian Meichsner performed the

OFET measurements. Robert Kahl and Oleksandr Dolynchuk (from Halle) performed WAXS and AFM measurements. David Ohayon (KAUST) assisted during OECT fabrication, measurements and analysis. Achilleas Savva performed the viscoelastic modeling of the EQCM-D data. Thomas Thurn-Albrecht, Sahika Inal and Mukundan Thelakkat supervised the project and corrected the final manuscript.

## **Chapter 8**

*„A highly Soluble alkyl substituted PEDOT via Kumada Catalyst Transfer Polymerization”*

by Philip Schmode, Mahima Goel, Florian Meichsner, and Mukundan Thelakkat.

Prepared for submission.

I designed, synthesized and characterized the PEDOT polymers. I wrote the manuscript. Florian Meichsner performed the OFET measurements. Mahima Goel measured the conductivity of the pristine and doped polymers. Mukundan Thelakkat supervised the project and corrected the final manuscript.

# Chapter 4:

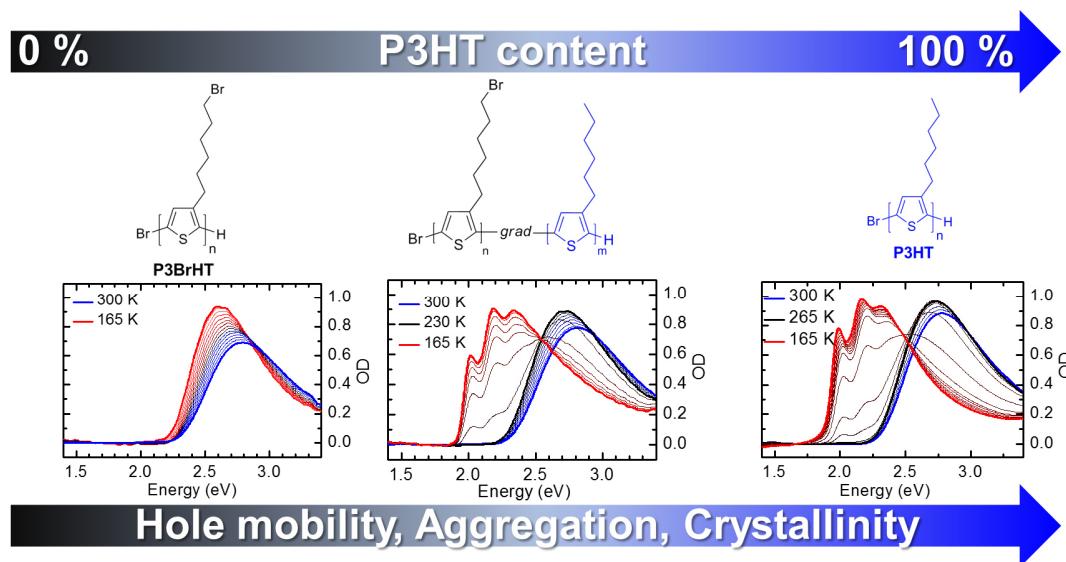
## Influence of $\omega$ -bromo substitution on structure and opto-electronic properties of homopolymers and gradient copolymers of 3-hexylthiophene

Philip Schmode<sup>†</sup>, Konstantin Schötz<sup>§</sup>, Oleksandr Dolynchuk<sup>\* ‡</sup>, Fabian Panzer<sup>§</sup>, Anna Köhler<sup>§</sup>, Thomas Thurn-Albrecht<sup>‡</sup> and Mukundan Thelakkat<sup>\* †</sup>

<sup>†</sup>Applied Functional Polymers, Department of Macromolecular Chemistry I, University of Bayreuth, Universitätsstr. 30, 95440 Bayreuth, Germany

<sup>§</sup> Experimental Physics II, University of Bayreuth, 95440 Bayreuth, Germany

<sup>‡</sup> Experimental Polymer Physics, Martin Luther University Halle-Wittenberg, Von-Danckelmann-Platz 3, 06120 Halle, Germany



Reproduced with permission from *Macromolecules* **2020**, *53*, 7, 2474-2484.

Copyright 2020 American Chemical Society

## ABSTRACT

The nature of side chains and substituents influence the resulting electronic and structural properties of conjugated polymers. Here, we report fundamental studies on the influence of a  $\omega$ -bromohexyl sidechain in polythiophene (resulting in P3BrHT) as well as in a series of gradient copolymers using 3-hexylthiophene (3HT) comonomer. The rate of polymerization of 3BrHT is slower compared to 3HT. Temperature dependent absorption and emission show that with increasing content of 3BrHT, aggregation, critical transition temperature and the fraction of aggregates decrease. Wide angle X-ray scattering shows that P3BrHT has a triclinic crystal lattice; the crystallinity being almost half of P3HT and an increase in the crystallinity and a gradual monotonic decrease of the  $a$  and  $b$  crystal lattice parameters with decreasing 3BrHT content in copolymers. Finally, the consequences of change in aggregation and crystallinity on charge transport are elucidated using OFET, giving a general explanation for the influence of a  $\omega$ -bromo substituent in polythiophene copolymers.

## INTRODUCTION

$\pi$ -conjugated semiconducting polymers are of great interest in the field of organic field effect transistors<sup>1</sup> (OFETs), organic photovoltaics<sup>2</sup> (OPV), and in organic bioelectronic devices.<sup>3</sup> The most studied hole transport material in such devices is poly(3-hexylthiophene) (P3HT) due to its high solubility in organic solvents and good charge transport properties.<sup>1,4</sup> Moreover, charge transport properties of polythiophenes strongly depend on the morphology, chain orientation on the substrate, and the strength of the interchain interactions.<sup>5</sup> Selecting the side chains is as essential as selecting the conjugated backbones when designing conjugated polymers.<sup>6</sup> Solution-processable conjugated polymers generally consist of two parts:  $\pi$ -conjugated backbones determining the optoelectronic properties and the side chains influencing the aggregation in solution and orientation in thin films.<sup>7</sup> To tune the relevant structural and electronic properties of conjugated polymers for specific applications, side-chain engineering has emerged as a powerful tool in recent years. Many attempts were made to improve the performance of thiophene-based polymers, mainly by introducing different side chains to the thiophene core, in order to optimize properties like energy levels, charge transport and crystallinity.<sup>8-13</sup> An additional use of side-chain modification is for increasing thermal stability via cross-linking reactions.<sup>14-16</sup> Additionally, with the development of the controlled chain growth mechanism of different polythiophenes by Yokozawa and McCullough,  $\omega$ -side chain substituted polythiophenes can be synthesized with controlled molecular weight, low dispersity, high regioregularity, and defined end groups.<sup>17-21</sup> One of the facile  $\omega$ -side chain modification in polythiophenes involves bromine end group, which can further be transformed into diverse functional groups by a post-polymerization reaction.<sup>22</sup> Using this approach, the solubility can be tailored, e.g. anionic and cationic

conjugated polyelectrolytes can be synthesized.<sup>23–25</sup> Thus, the starting polymer for such side chain modifications is poly[3-(6-bromohexyl)] thiophene (P3BrHT). However, P3BrHT is not well studied for its aggregation in solution, structure formation in bulk as well as charge transport properties. Moreover, polymer architectures such as random, gradient or block copolymers derived from P3BrHT are interesting precursor polymers for further functionalization.<sup>26,27</sup> Here also a detailed study of aggregation of such copolymers in solution, as well as structure formation in bulk can be very helpful to understand the role of side chain functionalization.

With the above questions in mind we synthesized comparable homopolymers, P3HT and P3BrHT and gradient copolymers involving 3-(6-bromohexyl) thiophene 3BrHT and 3-hexylthiophene 3HT as monomers to elucidate structure–property relationship. Here, we investigate directly the impact of the bromine functionalization of the side chains by comparing P3BrHT vs. P3HT as well as a series of gradient copolymers P3HT-co-P3BrHT 1,2 and 3 with different 3HT content. These gradient copolymers were obtained by a copolymerization of these two monomers using Ni(dppp)Cl<sub>2</sub> in a one pot synthesis. This is possible because of the higher reactivity of the 3-hexylthiophene monomer compared to 3-(6-bromohexyl) thiophene.<sup>28</sup> The aggregation of the P3HT, P3BrHT, and the copolymers P3HT-co-P3BrHT 1,2 and 3 was investigated for the first time using temperature-dependent absorption and emission spectroscopy. The differences in the crystallinity as well as the crystal structure of the investigated polythiophene polymers were studied with differential scanning calorimetry (DSC) and wide-angle X-ray scattering (WAXS). Finally, the polymers were tested in organic field effect transistors (OEFTs) to evaluate their charge carrier mobility. Based on our detailed study of the two polythiophene

derivatives P3HT and P3BrHT, and their gradient copolymers, we have demonstrated the tremendous impact of a small variation in the side chain functionalization of conjugated p-type polymers.

## RESULTS AND DISCUSSION

The Kumada catalyst transfer polymerization is a powerful method to generate well-defined polythiophenes with high regioregularity, low dispersity, and controlled molecular weight.<sup>17–19,21,23</sup> In this type of catalyst transfer polymerization, an active Grignard monomer is formed in situ from the dihalide monomers via a Grignard exchange reaction. The polymerization is started by the addition of the nickel catalyst dichloro[1,3-bis(diphenylphosphino)propane] nickel Ni(dppp)Cl<sub>2</sub>. In these experiments, a catalyst to monomer ratio of 1:100 was used and all polymerizations were quenched with hydrochloric acid.<sup>21</sup> To compare the homopolymerization rates, the molecular weights were normalized to the maximum molecular weight, that can be reached at almost full conversion, which is given by the monomer to catalyst ratio (**Figure S1**).<sup>21</sup> In comparison to the homopolymerization of P3HT, the homopolymerization of P3BrHT proceeds slower under our experimental conditions. To quantify the difference in rate of polymerization, the slope in the linear regime of both curves was measured and the polymerization of P3HT was observed to be 17 % faster than the polymerization of P3BrHT (**Figure S1**). Utilizing this fact, we prepared three gradient copolymers P3HT-co-P3BrHT 1-3 with monomer feed-in ratios (0.25:0.75, 0.5:0.5, and 0.75:0.25 molar respectively; **Figure 1**).<sup>28</sup> A typical example for molecular weight and dispersity evolution during copolymerization is given in **Figure S2c**. Here we like to point out that Palermo et al.<sup>26</sup> reported the synthesis of

random, block, and gradient copolymers of (3-hexyl)thiophene (3HT) and 3-(6-bromohexyl)-thiophene (3BrHT) by using a tolyl-functionalized Ni(dppe)Br catalyst instead of Ni(dppp)Cl<sub>2</sub>. They also provided strong evidence for rate-determining reductive elimination and identified Ni<sup>II</sup>-bithiophene complexes as the catalyst resting states on using Ni(dppe)Cl<sub>2</sub> as catalyst.<sup>29</sup> These results, combined with the previously reported data for Ni(dppp)Cl<sub>2</sub>-catalyzed polymerization, suggest that the ligand structure has a strong influence on the polymerization mechanism and probably on reaction rates of different monomers.<sup>20</sup> The built-in ratios of the monomers were determined via <sup>1</sup>H-NMR, by comparing the signal of the methyl group of the 3-hexylthiophene repeating unit to the methylene group next to the bromine. Slightly different built-in ratios (3HT:3BrHT = 0.3:0.7, 0.51:0.49 and 0.77:0.23) compared to feed-in ratios were obtained.

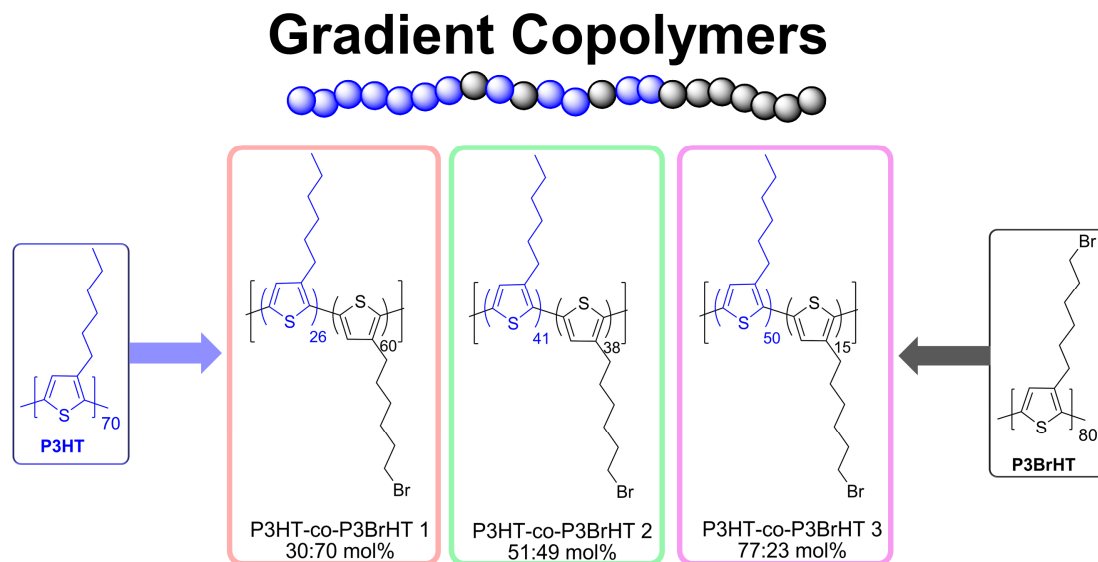


**Figure 1:** Polymer structures of P3HT and P3BrHT and the copolymers poly[3-(hexylthiophene)-co-3-(6-bromohexyl) thiophene] copolymers (P3HT-co-P3BrHT 1,2 and 3) with different monomer feed ratios via Kumada catalyst transfer polymerization using Ni(dppp)Cl<sub>2</sub> as catalyst.

The molecular weights and dispersity of polymers were characterized via SEC with polystyrene calibration and MALDI-ToF-MS (**Figure S2a**) with dithranol as matrix material. The polymer and copolymer properties are summarized in **Table 1**. The typical MALDI-ToF-MS spectra for the copolymers are given in **Figure S2b**. Copolymers with a molecular weight of 15-17 kg/mol (SEC), low polydispersities of 1.18 to 1.20 and high regioregularity >97 % were obtained. MALDI-ToF-MS measurements deliver absolute molecular weights of  $M_n$  = of 13, 16 and 19 kg/mol for copolymers P3HT-co-P3BrHT 1-3 respectively. Furthermore, the number of repeating units was determined by the built-in ratio and the absolute molecular weight measured by MALDI-ToF-MS are given in **Table 1**. We like to point out here, that the molecular weight of P3HT determined with SEC (using polystyrene calibration) is usually overestimated by a factor of 1.6 compared to absolute molecular weight obtained from MALDI-ToF, whereas P3BrHT shows comparable values with a factor of 1.01 (see **Figure S2d**).

**Table 1:** Characteristics of the three synthesized copolymers, P3HT-co-P3BrHT 1-3 and the homopolymers P3HT and P3BrHT as reference polymers.

	Feed-in ratio 3HT/3BrHT T <sup>a</sup> [mol%]	Built-in ratio 3HT/3BrHT <sup>c</sup> [mol%]	Repeating units 3-HT/3-BrHT <sup>d</sup>	M <sub>n</sub> , MALDi-T oF-MS [kg/mol]	M <sub>n</sub> (Đ) SEC <sup>b</sup> [kg/mol]
P3BrHT	0/100-	-	0/65	20	19.8 (1.10)
P3HT-co-P3BrHT 1	25/75	30/70	26/60	19.2	16.5 (1.19)
P3HT-co-P3BrHT 2	50/50	51/49	41/38	16.4	17 (1.18)
P3HT-co-P3BrHT 3	75/25	77/23	50/15	12.8	15 (1.20)
P3HT	100/0	-	80/0	11.6	18.3 (1.06)

a: Determined by the weight of the monomers.

b: SEC with polystyrene calibration and THF as eluent.

c: Measured with <sup>1</sup>H-NMR from the corresponding characteristic signals.

d: Identified with the absolute molecular weight from MALDI-ToF-MS and <sup>1</sup>H-NMR.

To further analyze the impact of an  $\omega$ -bromine side chain functionalization, we conducted temperature-dependent absorption and emission spectroscopy. **Figure 2** shows the temperature-dependent photoluminescence (PL) and absorption spectra of P3HT, the three copolymers, P3HT-co-P3BrHT 1-3 and neat P3BrHT solved in THF with a concentration of 0.2 mg/ml.

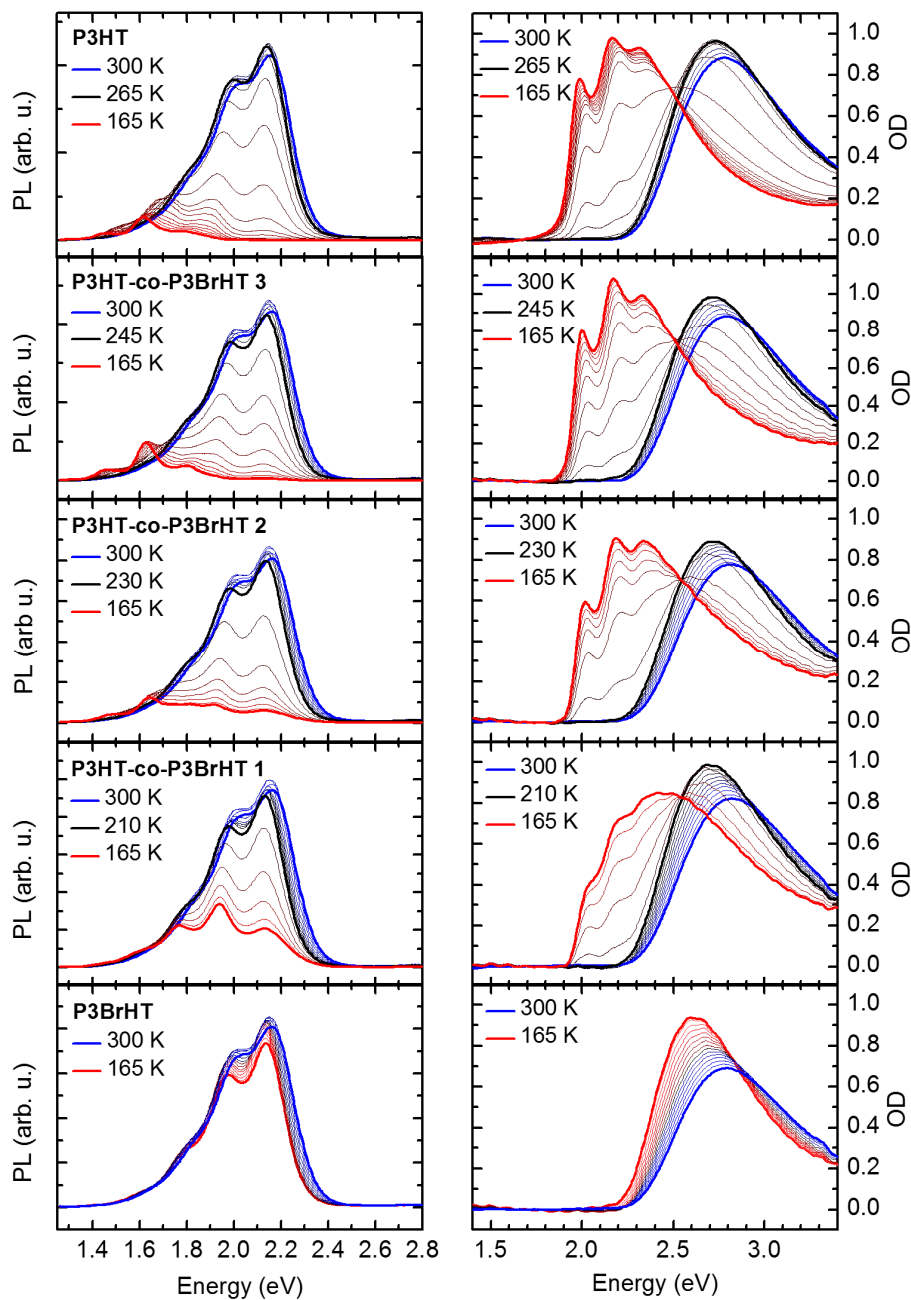


**Figure 2:** Temperature-dependent photoluminescence (left) and absorption spectra (right) of neat P3HT, the three copolymers, P3HT-co-P3BrHT 1-3 and neat P3BrHT, dissolved in THF with a concentration of 0.2 mg/ml in the range of 165 (red) to 300K (blue). Temperature steps are 10K in general and 5K close to  $T_c$ . The 3BrHT-content in the compounds increases from top to bottom.

With increasing content of 3BrHT, and thus concomitantly reducing fraction of 3HT, we observe a decrease in aggregation properties, an evolution similar to what is

observed for neat P3HT with reducing molecular weight.<sup>30,31</sup> For all five compounds, the absorption at 300 K, (blue, thick line) is broad and unstructured, with a maximum around 2.80 eV. This absorption is the signature of the disordered phase of the polymer.<sup>32</sup> Upon cooling, the maximum shifts by about 100 meV (for P3HT) to 200 meV (for P3BrHT) towards red and becomes more intense. This increase in oscillator strength is attributed to an elongation of the conjugation length due to conformational changes of the backbone.<sup>31,33</sup> Except for neat P3BrHT, the increase and redshift of the absorption stops at a certain compound-dependent temperature (black, thick line). A new, structured absorption feature at lower energy arises upon further cooling, while the intensity of the disordered phase decreases, leading to an isosbestic point at around 2.52 eV. The occurrence of an isosbestic point implies a direct transformation of one phase to another phase.<sup>34</sup> For P3HT, as well as for other polymers, this low temperature phase has been identified as an aggregated or ordered phase of the compound.<sup>35–37</sup> The critical temperature for this transitions decreases with increasing 3BrHT content. Neat P3BrHT solutions show no aggregation under these measurement conditions down to 165K. The temperature dependent formation of aggregate fraction with increasing 3BrHT content is detailed in **Figure 3**. Upon aggregation, the oscillator strength changes by some factor  $F$ . This factor can be obtained by comparing the temperature-induced absorption decrease below  $T_c$  in the disordered phase with the absorption increase in the amorphous phase as demonstrated by Clark et al.<sup>38</sup> After correction for the change in oscillator strength, the increase in aggregate absorption indicates the actual fraction of aggregates formed in the solution. This is shown in **Figure 3a** as a function of temperature. The derivative of this curve with respect to temperature, shown in **Figure 3b**, gives the transition temperature  $T_c$  as peak value, as well as the width of

the transition.<sup>39</sup> We see that, with increasing 3BrHT content,  $T_c$  decreases from about 250 K for P3HT to 180 K for P3HT-co-P3BrHT 1, hand in hand with a decrease of the overall fraction of aggregates from 0.65 for P3HT to 0.34 for P3HT-co-P3BrHT 1. Concomitantly, the width of the phase transition increases from 14K to 41K. These observations indicate that increasing the amount of 3BrHT in the copolymer diminishes the ability of the polymer to form aggregates.

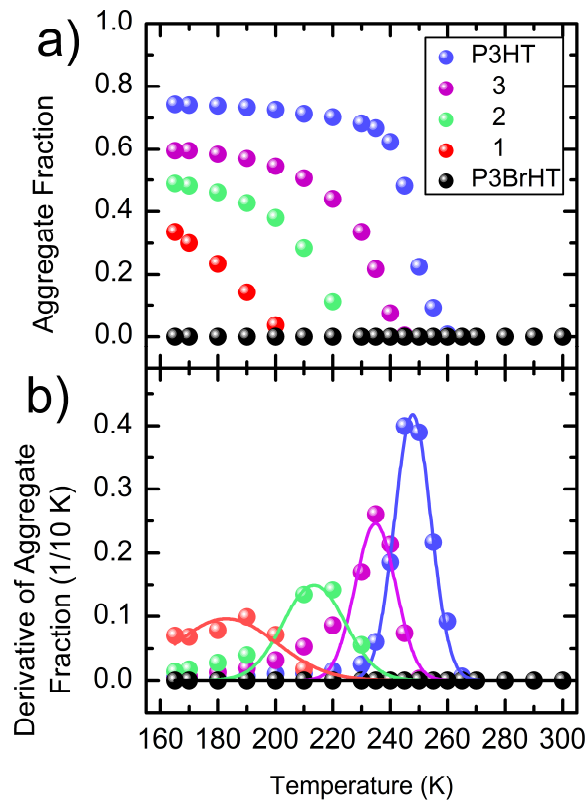


**Figure 3:** (a) Aggregate fraction of the polymers as a function of temperature, extracted from the temperature-dependent solution absorption spectra. 3, 2 and 1 stand for P3HT-P3BrHT 3, P3HT-P3BrHT 2 and P3HT-P3BrHT 1, respectively. (b) Derivative of the aggregate fraction (symbols) together Gaussian fits to the data points (solid lines).

This is also manifested in the PL spectra. The overall evolution of the PL with reducing temperature in the three copolymers is similar to P3HT. At 300 K, the PL shows one peak at 2.15 eV and shoulders at 2.00 eV and 1.81 eV, which are associated with the 0-0, 0-1 and 0-2 vibronic transitions of the disordered phase.<sup>31</sup> Upon cooling, these features undergo only a slight red-shift since emission occurs

from more planar chromophores than the absorption. Below  $T_c$ , the peaks lose intensity and new spectral features occur at lower energies. The PL spectrum of P3HT-co-P3BrHT 3 (with 77 mol% P3HT) at 165 K closely resembles the one of neat P3HT at low temperatures, with vibrational peaks at about 1.80 eV (0-0), 1.65 eV (0-1) and 1.45 eV (0-1).<sup>40</sup> This spectrum is characteristic for a weakly-interacting H-aggregate of P3HT. In contrast to P3HT and P3HT-co-P3BrHT 3, the PL of the other two copolymers differs insofar, that near 165 K vibrational features at about 2.1 and 1.9 eV remain, while the ones at 1.80 eV, 1.65 eV and 1.45 eV reduce in intensity compared to P3HT-co-P3BrHT 3. No aggregation is observed in the PL of P3BrHT.

To analyze these PL spectra, we fitted the spectrum of the copolymer with the highest 3BrHT content, P3HT-co-P3BrHT 1 at 210 K, i.e. just above the phase transition. At that temperature, it displays only emission from the disordered phase and the spectral shape can readily be reproduced by a Franck-Condon-Progression using one effective mode at 175 meV with a Huang-Rhys factor of 1 and a disorder parameter of 70 meV (**Figure 4a**, displayed in blue). These values are characteristic for the amorphous phase of P3HT. To evaluate the additional features that form upon cooling P3HT-co-P3BrHT 1 below the  $T_c$ , we considered the PL spectrum at 165 K. This spectrum can be very well reproduced by a superposition of the same Franck-Condon-Progression that was used at 210 K and a second, similar progression at 220 meV lower energy with a reduced disorder parameter of 47 meV (**Figure 4b**). Such a feature has previously also been observed for P3HT, yet only within a small temperature range below the  $T_c$ .

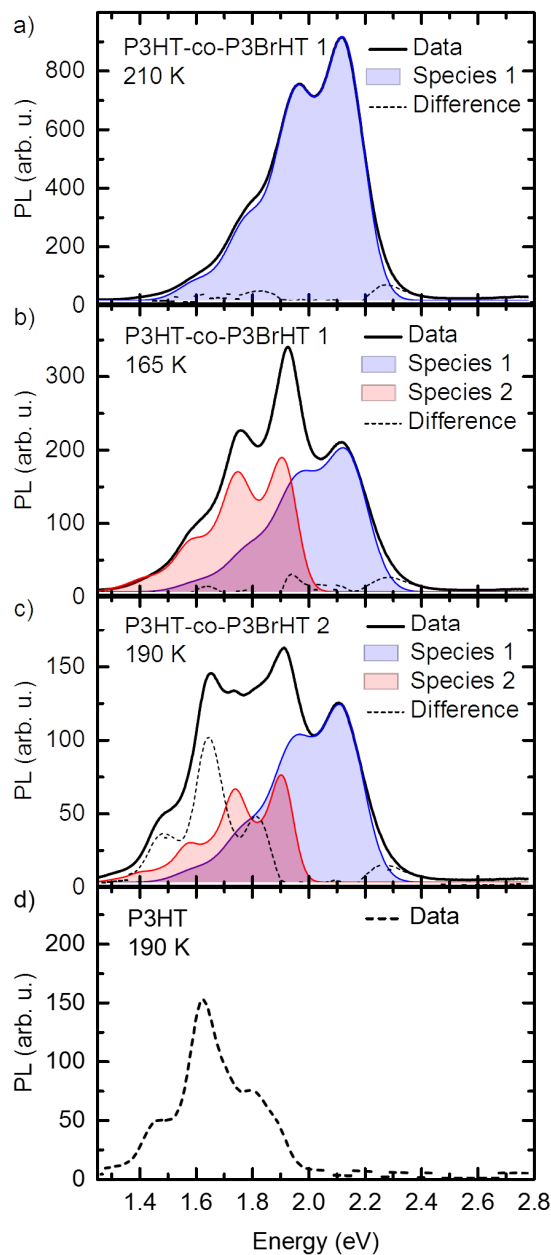


**Figure 4:** a) Solution PL spectrum of P3HT-co-P3BrHT 1 at 210 K (black solid line) together with a Franck-Condon-fit to the spectrum (Species 1, blue filled curve). (b) PL spectrum of the same solution at 165 K (black solid line) and decomposition into 2 species and a residue as described in the text. (c) Solution PL spectrum of P3HT-co-P3BrHT 2 at 190 K (black solid line) and decomposition into 2 species and a residue as described in the text (d) PL of neat P3HT in solution at 190 K.

These values are characteristic for the amorphous phase of P3HT. To evaluate the additional features that form upon cooling P3HT-co-P3BrHT 1 below the  $T_c$ , we

considered the PL spectrum at 165 K. This spectrum can be very well reproduced by a superposition of the same Franck-Condon-Progression that was used at 210 K and a second, similar progression at 220 meV lower energy with a reduced disorder parameter of 47 meV (**Figure 4b**). Such a feature has previously also been observed for P3HT, yet only within a small temperature range below the  $T_c$ . By comparison with X-ray data, it was identified as a phase of P3HT in which the backbones of adjacent chains already assemble on top of each other while still being somewhat conformationally disordered rather than fully planarized. In this state, there is no noticeable electronic interaction of the  $\pi$ -systems between adjacent chains. The energy shift of about 200 meV between the two species was mainly attributed to the increased local dielectric constant a backbone experiences due to the pi-system of the chains above and below, compared to the amorphous environment where adjacent aliphatic chains predominate.<sup>40</sup>

As detailed in ref. 39, for P3HT, these chains are loosely assembled so that their weak electrostatic interaction already allows for van-de-Walls (dispersion) effects, yet without significant resonance interaction. They evolve into what is referred to as weakly interacting H-aggregates upon further cooling with their characteristically suppressed 0-0 peak, as displayed in **Figure 4d**. In Figure 4b it seems that the inclusion of a high content of P3BrHT (70 mol%) in the copolymer induces substantial structural disorder. As a result, the remaining P3HT segments can no longer form H-aggregates but only assemble loosely, so that their spectrum looks like that of a disordered ensemble yet shifted in energy due to the dispersion effects.

This changes when the content of P3BrHT is reduced to 49 mol%, as in P3HT-co-P3BrHT 2 (**Figure 4c**). At 190 K, we observe a spectral form that can be reproduced as superposition of emission from amorphous chains (blue colour), non-interacting yet assembled chains (red colour) and H-aggregates, as evidenced by the residue that closely resembles the H-aggregate emission of P3HT at the same temperature, and that can be reproduced with the same parameters in a Franck-Condon progression with suppressed 0-0 (**Figure 4d**). Full details of the Franck-Condon progressions are given in the supporting information.

Reducing the temperature is an alternative way to induce aggregation, which can also be achieved by reducing the quality of a solvent. We therefore observe similar features when we use a poor solvent for these compounds. In chloroform, all our polymers dissolve well and show identical spectra that are characteristic for amorphous P3HT chains (**see Figure S6b**). In contrast, when a solvent mixture of chloroform:ethylacetate (10:90) is used, the absorption and PL spectra all show spectral signatures for aggregation, yet their intensity reduces with increasing content of P3BrHT, as shown in **Figure S7**. In absorption, the relative amount of disordered to H-aggregated chains can be assessed from comparing the intensity of absorption at 2.8 eV, i.e. at the peak of the absorption from disordered chains, to that around 2 eV, where the H-aggregates absorb. Even without explicitly separating the spectra into the two contributions and correcting for the change in oscillator strength, as would be required for a quantitative analysis, it is evident that a higher P3BrHT content increases the fraction of disordered chains. Similarly, with increasing P3BrHT content the PL peak at 2.15 eV reduces, indicative of emission from disordered chains. Concomitantly, the peak at 1.7 eV, associated with H-aggregates, increases. The aggregation behavior of the P3BrHT compared to P3HT-co-P3BrHT 1-3 in thin

film shows no noticeable difference when spun from chloroform, where all polymers dissolve well, solely the absorption maximum of the copolymers shows a bathochromic shift of about 50 nm. (**Figure S5**).

To investigate the thermal stability of the copolymers, P3HT-co-P3BrHT 1 was representatively analyzed by thermogravimetric analysis (TGA) and compared with those of P3BrHT and P3HT (**Figure S3**). The 3BrHT section starts to degrade at temperatures about 280 °C, presumably due to cleavage of the bromine. The 3HT part is stable up to 400 °C, which is in agreement with the TGA of P3HT. Interesting findings were obtained by analyzing the copolymers and the corresponding homopolymers via differential scanning calorimetry (DSC) under nitrogen atmosphere with a heating and cooling rates of 10 K/min (**Figure 5**). All DSC data are given in **Table 2**. The homopolymer P3BrHT shows a low melting point ( $T_{m,Peak} = 136$  °C) compared to the melting point of P3HT ( $T_{m,Peak} = 231$  °C). Also, the lower recrystallization temperature  $T_{c,peak}$  and the low melting enthalpy  $\Delta H_m$  of P3BrHT compared to P3HT is noteworthy. The melting points as well as  $\Delta H_m$  for the copolymers are clearly influenced by the volume composition. The higher the content of the 3HT in copolymer, the higher the values of  $T_m$  and  $\Delta H_m$  (**Table 2**). None of the copolymers shows two different crystallization points; only a single recrystallization point being observed for each indicating a possible co-crystallization of 3HT and 3BrHT units. This is a clear indication of lack of any phase separation between P3HT and P3BrHT parts in the studied systems. It is to be noted that a phase separation in a gradient copolymer depends on the composition profile, molecular weights of the individual blocks, and the effective degree of incompatibility  $\chi N$  involved.<sup>41</sup>

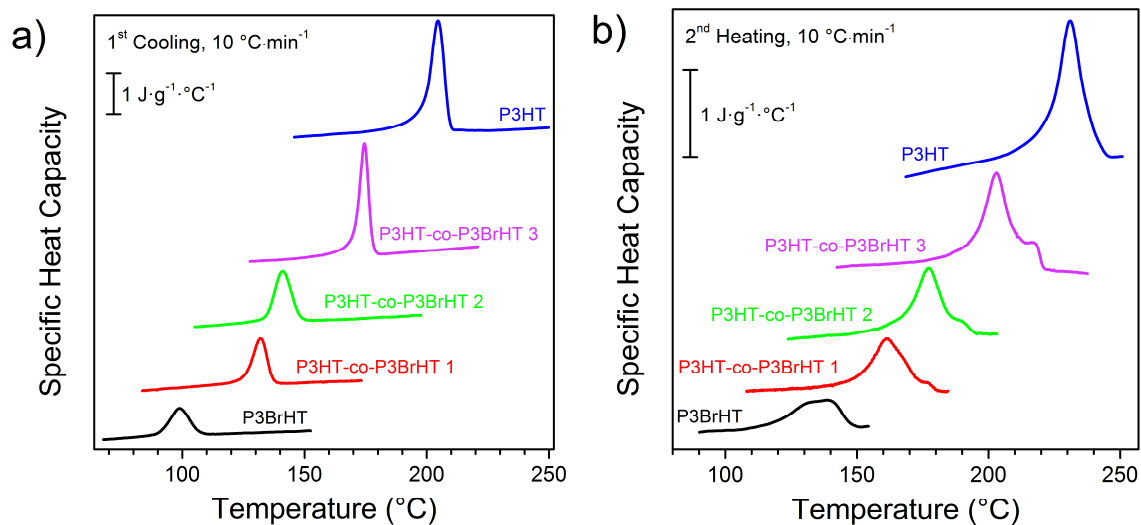


**Figure 5:** DSC cooling (a) and heating (b) curves of the homopolymers P3HT, P3BrHT, and copolymers P3HT-co-P3BrHT 1-3 measured with a rate of 10 K/min under nitrogen atmosphere. The curves were vertically shifted by a constant for better visibility.

**Table 2:** Thermal properties of P3BrHT, P3HT, and the copolymers P3HT-co-P3BrHT 1-3 measured via DSC and the crystallinity value calculated from WAXS.

	$T_{m,peak}$	$\Delta H_m$	$T_{c,peak}$	Crystallinity (WAXS)
	(°C)	(J·g <sup>-1</sup> )	(°C)	(%)
P3BrHT	136	7.1	99	43
P3HT-co-P3BrHT 1	161	10	132	42
P3HT-co-P3BrHT 2	177	11.5	141	43
P3HT-co-P3BrHT 3	203	17.5	175	46
P3HT	231	24.6	205	81

For a detailed understanding on the crystal structure of the homopolymers and copolymers of P3HT and P3BrHT, we performed temperature dependent WAXS measurements. **Figures 6a,b** show the WAXS curves of bulk P3HT and P3BrHT measured at 20°C and above the corresponding melting points of the homopolymers (250 and 155°C). According to the previous studies, we took the assumption of a monoclinic unit cell for P3HT and the lattice parameters calculated from the WAXS peaks in Figure 6a yielded  $a = 1.677 \text{ nm}$ ,  $b = 0.757 \text{ nm}$ ,  $c = 0.788 \text{ nm}$ , and  $\gamma = 92.7^\circ$ .<sup>42,43</sup> Using the determined lattice parameters, the crystal peaks in the corresponding WAXS curve were indexed as depicted in **Figure 6a**. Note that in contrast to the previous studies of P3HT crystal structure, the peaks (300) and (1 $\bar{1}$ 1) have different  $q$  values as a result of the non-equal lattice parameters  $b$  and  $c$ .<sup>42,43</sup> The WAXS curve of P3BrHT in **Figure 6b** appears to be quite different from that of P3HT, thus the crystal lattice determination cannot be performed based on this single scattering curve of the powder sample. Therefore, to get an oriented sample, we spin-coated the solution of P3BrHT in chloroform on a single-layer graphene substrate and crystallized it from the melt in a vacuum oven. The reciprocal space maps of the WAXS patterns of about 50 nm thin P3BrHT film on graphene measured at incident angles of 0.22° and 10° are shown in **Figures 6c and 6d**, respectively. All reflections in **Figures 6c,d** along with the distinct peaks in **Figure 6b** are numbered ascending with the increasing  $q$  value. As can be seen in **Figure 6c**, peaks 2 and 6 are located both parallel and normal to the substrate surface indicating a mixed edge-on and face-on crystal orientation in the film.<sup>44</sup> It is worth mentioning that the molecular orientation in thin films of semiconducting polymers is of a particular interest for the organic photovoltaic applications.

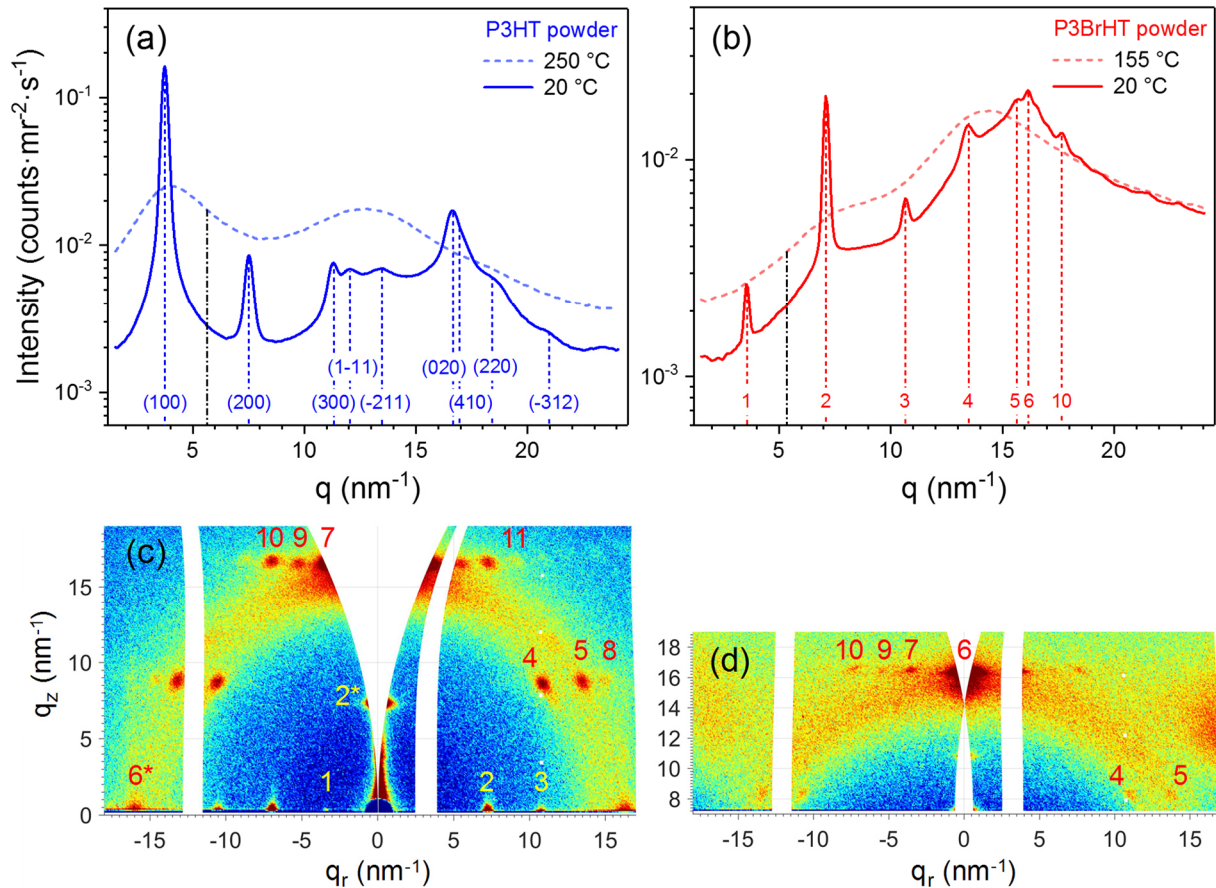


**Figure 6:** WAXS of bulk P3HT (a) and P3BrHT (b) measured in semicrystalline state at 20°C and amorphous state above the melting temperatures of the corresponding polymers, at 250°C (for P3HT) and 155°C (for P3BrHT). Figures (c,d) represent the reciprocal space maps of the WAXS patterns of about 50 nm thin P3BrHT on a single layer graphene measured at incident angles of 0.22° (c) and 10° (d).

However, a thorough study of the P3BrHT crystal orientation on graphene goes beyond the framework of this work and will be addressed in our upcoming publication. By comparing the chemical structure and the WAXS curves of P3HT and P3BrHT, we assume that the equidistant peaks 1, 2, 3, and the peak 6 are reflections from (100), (200), (300), and (020) crystal planes of the face-on oriented crystals, respectively. Consequently, the peaks 4, 7, 10 represent (310), (120), and (220) crystal planes of the face-on oriented crystals. As the twins of these reflections from the edge-on oriented crystals are not seen in Figure 6c, it can be concluded that the amount of the edge-on crystals is smaller than that of the face-on crystals and only

peaks 2\* and 6\* belong to the edge-on crystals. If we assume now that the lattice parameter  $c$  has same value as in case of P3HT all lattice constants can be calculated under no further assumptions. Hereinafter, this assumption is designated as Scenario 1 and the resultant lattice constant are given in **Table 3**. Using the values for Scenario 1, we could index the peaks in **Figures 6c,d** as well as calculate the crystal peak positions along with the angle  $\varphi_{6,i}$  between the reflection 6, which is the  $\pi$ -stacking direction, and all other reflections from the face-on oriented crystals in **Figure 6c,d**. **Table 3** summarizes our findings on both calculated and measured peak positions. However, as it is seen from **Table 3**, peaks 8 and 9 indexed for Scenario 1 do not coincide in both  $q$  and  $\varphi_{6,i}$  values with their measured counterparts. Moreover, the corresponding Miller indices are incorrect according to the symmetry of WAXS pattern in **Figure 6c**. A better solution could only be found after withdrawing the limitation imposed on the value of parameter  $c$ . As such, the recalculated lattice constants were designated as Scenario 2 and are listed in **Table 3**. Analogously to Scenario 1, we indexed the peaks in **Figures 6c,d** according to Scenario 2 as well as calculated the crystal peak positions and the angles  $\varphi_{6,i}$ . The corresponding outcome presented in **Table 3** evidences that both  $q$  and  $\varphi_{6,i}$  values for all peaks indexed for Scenario 2 are in well accordance with the measured quantities. Thereby, we deduce that the P3BrHT crystal lattice parameters calculated for Scenario 2 are reasonable and consistent with the experimental WAXS data. It must be noted that the resultant large value for lattice constant  $c$  is quite surprising. Excluding the unlike possibility of chemical bonds stretching, we have to assume that the obtained  $c$  value reflects significant changes of polymer chain conformation caused by the Br-substitution.

**Table 3:** The measured and calculated crystal peak positions of the face-on oriented P3BrHT crystals along with the angle  $\varphi_{6,i}$  between the reflection 6 and other reflections from the face-on oriented crystals in Figure 6c.

Pea k	Measured		Calculated by Scenario 1: $a = 1.774 \text{ nm}$ , $b = 0.772 \text{ nm}$ , $c = 0.788 \text{ nm}$ , $\alpha = 91.2^\circ$ , $\beta =$ $87.9^\circ$ , $\gamma = 91.8^\circ$			Calculated by Scenario 2: $a = 1.778 \text{ nm}$ , $b = 0.773 \text{ nm}$ , $c = 1.153 \text{ nm}$ , $\alpha = 91.1^\circ$ , $\beta =$ $91.1^\circ$ , $\gamma = 91.8^\circ$		
	$q$ [ $\text{nm}^{-1}$ ]	$\varphi_{6,i}$ [ $^\circ$ ]	Miller indices	$q$ [ $\text{nm}^{-1}$ ]	$\varphi_{6,i}$ [ $^\circ$ ]	Miller indices	$q$ [ $\text{nm}^{-1}$ ]	$\varphi_{6,i}$ [ $^\circ$ ]
1	3.56	$\approx 90$	(100)	3.55	88.2	(100)	3.54	88.1
2	7.12	$\approx 90$	(200)	7.09	88.2	(200)	7.08	88.1
3	10.69	$\approx 90$	(300)	10.64	88.2	(300)	10.62	88.1
4	13.53	51.6	(310)	13.59	51.5	(310)	13.57	51.3
5	15.65	56.9	(311)	15.65	56.5	(212)	15.66	56.7
6	16.25	0	(020)	16.28	0	(020)	16.27	0
7	16.83	12.7	(120)	16.77	12.2	(120)	16.77	12.2
8	16.91	60.2	( $\bar{1}20$ )	16.56	12.4	( $4\bar{1}\bar{1}$ )	16.95	62.6
9	17.26	18.5	( $\bar{2}20$ )	17.56	23.8	(021)	17.26	18.4
10	17.93	23.3	(220)	17.96	23.2	(220)	17.95	23.2
11	18.68	28.2	(121)	18.65	27.5	( $22\bar{1}$ )	18.63	28.3

An analogous situation is well known for poly(tetrafluoroethylene), which in the crystalline state forms a 13/6-helix with increased  $c$  lattice constant as compared to a planar zig-zag structure of polyethylene crystal chains.<sup>45</sup> In addition, the larger size of the P3BrHT unit cell along the  $a$  crystal axis is quite explicable taking into account that P3BrHT side chains are more voluminous in comparison with P3HT hexyl side chains.

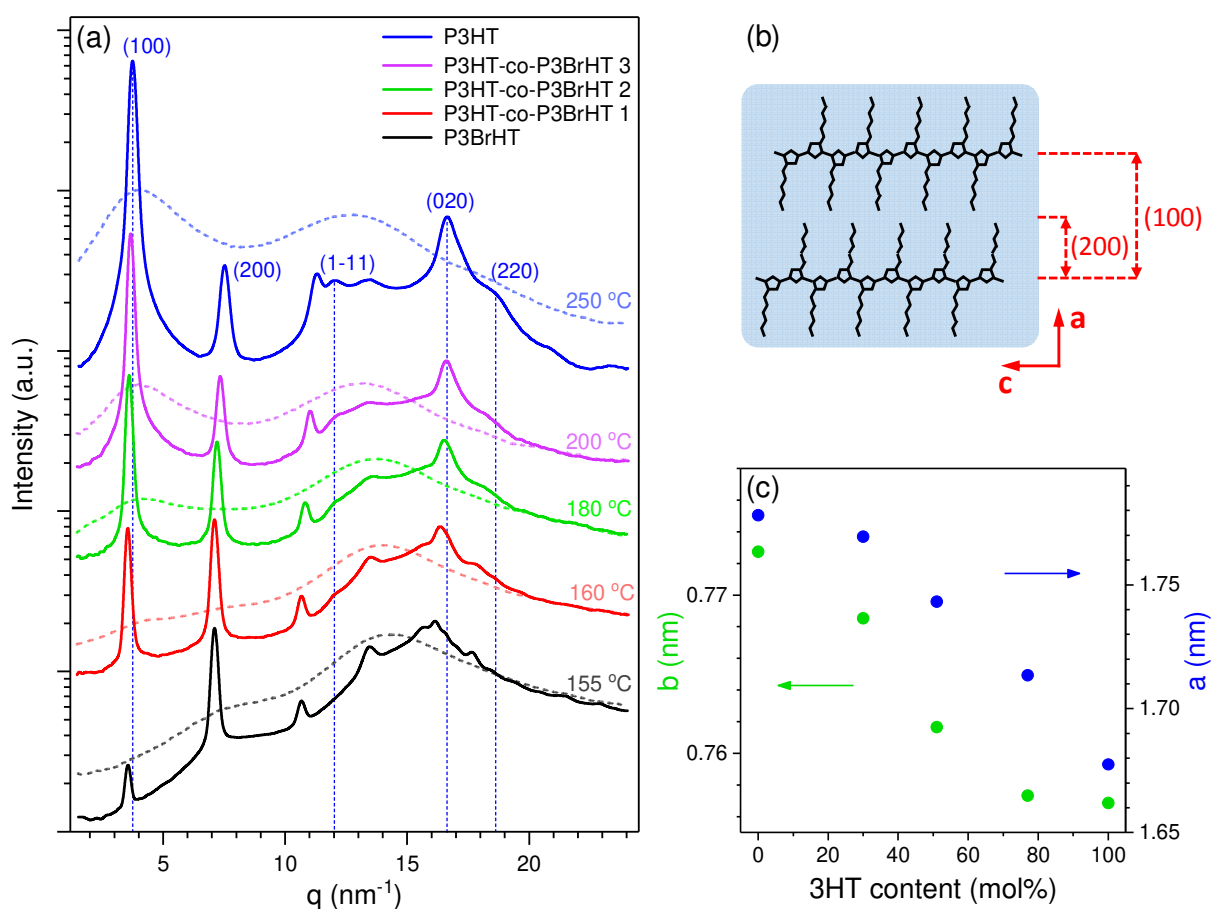


**Figure 7:** (a) WAXS of bulk P3HT, P3BrHT, and their copolymers measured in semicrystalline state at 20°C (solid lines) and amorphous state (dashed lines) at temperatures (shown near each WAXS curve) above the melting points of the corresponding polymers; (b) schematic illustration of the (ac) crystal plane of P3HT/P3BrHT; (c) the dependence of the lattice parameters  $a$  and  $b$  determined from WAXS on the 3HT content.

The WAXS curves of P3HT-co-P3BrHT along with WAXS of the respective homopolymers measured at room temperature and in the melt are shown in **Figure 7a**. Based on the qualitative similarity of WAXS curves of P3HT and the copolymers, we assumed that the latter possess the same monoclinic symmetry of their crystals as P3HT. Thus, the  $q$  values of peaks (100), ( $1\bar{1}1$ ), (020), and (220) (see **Figure 7a**) are sufficient to determine the crystal lattice parameters for all copolymers under study. As found, the lattice constant  $c$  remains nearly unchanged for all copolymers and has a value between 0.785 and 0.789 nm, being basically same as for P3HT. On the contrary, the lattice parameters  $a$  and  $b$  differ for the copolymers and their dependence on the 3HT content is given in **Figure 7c**. As it is clearly visible in **Figure 7c**, the lattice constants  $a$  and  $b$  monotonically decrease with increasing 3HT content in the copolymers. Such a behavior unambiguously points to co-crystallization of 3HT and 3BrHT units. Furthermore, the ratio of the intensities of (100) and (200) peaks (**Figure 7a**) changes gradually and monotonically with increasing 3HT content as well. Note that the intensity of (200) peak in P3BrHT is higher than that of the (100) peak due to a high electron density of Br atoms allocated in the middle between two successive backbones along the  $a$  crystal axis, as sketched in the **Figure 7b**. Consequently, the monotonic change of the (100)/(200) intensity ratio with rising 3HT content reflects the increasing amount of 3HT units built in the crystal lattice and as such, co-crystallization of 3HT and 3BrHT units in the copolymers becomes evident. Additionally, based on the approach used by Balko et al.<sup>43</sup> we estimated the crystallinity of bulk P3HT, P3BrHT, and their copolymers.

The black dashed-dotted lines in **Figures 6 a,b** indicate the  $q$  value in-between the (100) and (200) crystal peaks, at which the intensity of the amorphous halo was taken to compute the crystallinity as follows:

$$\chi_c = \left(1 - \frac{I_{am,cr}}{I_{am,m}}\right) \cdot 100\%, \quad (1)$$

where  $I_{am,cr}$  and  $I_{am,m}$  are intensities of the amorphous halo in the crystalline and molten states, respectively. The obtained crystallinity values are listed in **Table 2**. First of all, it is worth noticing that the crystallinity of P3BrHT estimated according to Eq 2 yields  $\chi_c \approx 43\%$ , which is almost twice lower than that in P3HT. Moreover, it is quite surprising that the crystallinity of all copolymers under study show only a slight increase from copolymer 1 to 3 and remains nearly same as that of P3BrHT. We hypothesize that the reason for this could be lower intracrystalline chain dynamics in P3BrHT and the gradient copolymers, as revealed by the recent fundamental experimental studies.<sup>46</sup> The lower heat capacity  $C_p(T)$  values of P3BrHT measured by DSC (**Figure S4**) can support this hypothesis.

To further reveal the influence of the  $\omega$ -bromine side chain functionalization on the homopolymers, as well as on the copolymers, the hole mobility in organic field effect transistors was determined. Halogens atoms in organic semiconductors can act as a charge trap and also are able to quench the luminescence, resulting in decreased charge carrier mobilities.<sup>47</sup> The devices were prepared in a bottom gate/bottom contact geometry. Typical output and transfer characteristics are given in **Figure S8**. A detailed description of the device preparation, as well as the transfer and output curves of P3BrHT and the copolymers can be found in the supporting information. The hole mobilities of P3BrHT compared to P3HT-co-P3BrHT 1-3 were calculated from the slope transfer curves in the linear regime. From the poor crystallinity and

weak aggregation properties of P3BrHT, it can be expected that P3BrHT will exhibit poorer charge transport compared to P3HT. This is also confirmed by the OFET measurements: P3BrHT shows a lower hole mobility  $\mu_{\text{hole}} = 7.9 \cdot 10^{-5} \text{ cm}^2 \text{ V}^{-1} \text{ s}^{-1}$  in contrast to P3HT ( $\mu_{\text{hole}} = 4.9 \cdot 10^{-2} \text{ cm}^2 \text{ V}^{-1} \text{ s}^{-1}$ ).<sup>29</sup> By incorporating 30 mol% of 3HT as comonomer, the hole mobility of P3HT-co-P3BrHT 1 does not change drastically, but slightly increases to  $\mu_{\text{hole}} = 9.7 \cdot 10^{-5} \text{ cm}^2 \text{ V}^{-1} \text{ s}^{-1}$ . However, the hole mobility increases one order of magnitude by incorporating 51 mol% of 3HT to  $\mu_{\text{hole}} = 2.3 \cdot 10^{-4} \text{ cm}^2 \text{ V}^{-1} \text{ s}^{-1}$  and even two orders of magnitude with 77 mol% of 3HT as comonomer ( $\mu_{\text{hole}} = 7.1 \cdot 10^{-3} \text{ cm}^2 \text{ V}^{-1} \text{ s}^{-1}$ ). (Figure 8). Thus, we clearly detect an increase in the hole mobility with increasing amount of 3HT in the copolymers. This is in line with the higher aggregation tendency observed in emission experiments and also observed in the thermal properties, where increased 3HT content results in a higher melting enthalpy. Note that the bulk crystallinity results obtained from WAXS do not exactly correlate with the charge transport as measured in OFETs. However, a monotonic decrease of  $\pi$ - $\pi$  distance reflected in the decreasing lattice constant  $b$  with increasing 3HT content in the copolymers do correlate with the increasing hole mobility. Additionally, it has to be taken into account that OFET mobility gives only a measure of interface charge carrier properties in some 5-10 nm of the film close to a Si/SiO<sub>2</sub> substrate used in OFET and possible additional influences of orientation and crystallization in thin films are to be considered.

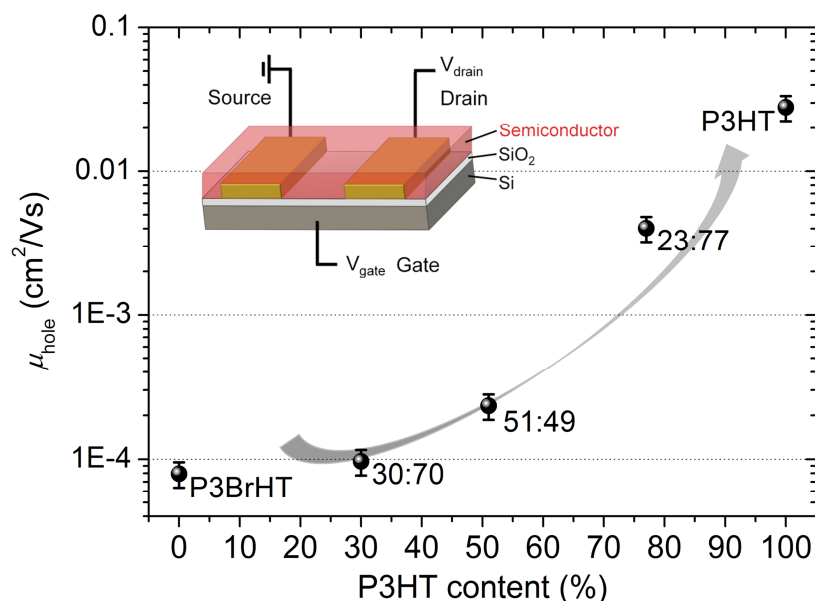


**Figure 8:** Dependence of the hole mobility on the content of 3-hexylthiophene for the different homopolymers and copolymers, P3HT-co-P3BrHT 1-3.

## CONCLUSION

In this study we presented a detailed and fundamental analysis of the aggregation, thermal and charge transport properties of poly(3-hexyl) thiophene (P3HT) and poly-3-(6-bromohexyl)-thiophene (P3BrHT) and a series of gradient copolymers of different compositions, P3HT-co-P3BrHT 1-3. First, we demonstrated that the rate of polymerization of 3BrHT is 17 % slower compared to 3HT using  $\text{Ni}(\text{dppp})\text{Cl}_2$  as catalyst and therefore a one-pot reaction results in a gradient rather than a random copolymer. Three different copolymers, P3HT-co-P3BrHT 1-3. with different built-in monomer ratios (30:70, 51:49 and 77:23) with controlled molecular weights, low dispersity and high regioregularity were synthesized. By introducing a  $\omega$ -bromine group into the side chain, aggregation behavior, crystallinity and hole mobility were drastically altered. To understand the aggregation properties, temperature-dependent emission and absorption spectroscopy were conducted. With increasing content of 3BrHT, and thus simultaneous reducing content of 3HT, we observe a decreasing

tendency of aggregation. We also observe that with increasing 3BrHT content, the critical transition temperature  $T_c$  from amorphous to ordered state decreases from about 250 K for P3HT to 180 K for P3HT-co-P3BrHT 1, hand in hand with a decrease of the overall fraction of aggregates from 0.65 for P3HT to 0.34 for P3HT-co-P3BrHT 1. The melting point and the melting enthalpy of the copolymers increased with increasing content of 3-hexylthiophene, compared to the homopolymer P3BrHT. In the analysis of temperature dependent WAXS measured in bulk and GIWAXS of thin films of P3BrHT spin coated on spin coated on single-layer graphene substrate, we determined that P3BrHT has a triclinic crystal lattice and crystallinity being almost twice less as compared to P3HT. We also observed a large reduction in crystallinity and a monotonic increase of the lattice constants  $a$  and  $b$ , when incorporating 3BrHT into the polymer structure. Here the reduction of crystallinity and distortion of the crystal lattice can explain the lower tendency of aggregation. Moreover, the monotonic increase of the constants  $a$  and  $b$  with increasing 3BrHT content in the copolymers points to a co-crystallization of 3HT and 3BrHT units in this gradient type of copolymers. The hole mobility was extracted with OFET measurements. Here with increasing content of 3HT, the hole mobility increased by almost three orders of magnitude, which is in line with the higher aggregation tendency. In summary, these studies demonstrate that the copolymer monomer composition can dramatically influence the optical, electronic, and thermal properties of the material. All in all, this study gives insights into a better understanding of the influence of  $\omega$ -side chain modifications of polythiophenes on aggregation, thermal properties, crystal structure, crystallinity and charge transport properties.

## REFERENCES

- (1) Sirringhaus, H. Integrated Optoelectronic Devices Based on Conjugated Polymers. *Science* **1998**, *280* (5370), 1741–1744.
- (2) Ma, W.; Yang, C.; Gong, X.; Lee, K.; Heeger, A. J. Thermally Stable, Efficient Polymer Solar Cells with Nanoscale Control of the Interpenetrating Network Morphology. *Advanced Functional Materials* **2005**, *15* (10), 1617–1622.
- (3) Simon, D. T.; Gabrielsson, E. O.; Tybrandt, K.; Berggren, M. Organic Bioelectronics: Bridging the Signaling Gap between Biology and Technology. *Chemical Reviews* **2016**, *116* (21), 13009–13041.
- (4) Elsenbaumer, R. L.; Jen, K. Y.; Oboodi, R. Processible and Environmentally Stable Conducting Polymers. *Synthetic Metals* **1986**, *15* (2–3), 169–174.
- (5) Noriega, R.; Rivnay, J.; Vandewal, K.; Koch, F. P. V.; Stingelin, N.; Smith, P.; Toney, M. F.; Salleo, A. A General Relationship between Disorder, Aggregation and Charge Transport in Conjugated Polymers. *Nature Mater* **2013**, *12* (11), 1038–1044.
- (6) Mei, J.; Bao, Z. Side Chain Engineering in Solution-Processable Conjugated Polymers. *Chemistry of Materials* **2014**, *26* (1), 604–615
- (7) Raithel, D.; Simine, L.; Pickel, S.; Schötz, K.; Panzer, F.; Baderschneider, S.; Schiefer, D.; Lohwasser, R.; Köhler, J.; Thelakkat, M.; et al. Direct Observation of Backbone Planarization via Side-Chain Alignment in Single Bulky-Substituted Polythiophenes. *Proc Natl Acad Sci USA* **2018**, *115* (11), 2699–2704.
- (8) Lévesque, I.; Bazinet, P.; Roovers, J. Optical Properties and Dual Electrical and Ionic Conductivity in Poly(3-Methylhexa(Oxyethylene)Oxy-4-Methylthiophene). *Macromolecules* **2000**, *33* (8), 2952–2957.
- (9) Sheina, E. E.; Khersonsky, S. M.; Jones, E. G.; McCullough, R. D. Highly Conductive, Regioregular Alkoxy-Functionalized Polythiophenes: A New Class of Stable, Low Band Gap Materials. *Chemistry of Materials* **2005**, *17* (13), 3317–3319.
- (10) Wu, X.; Chen, T.-A.; Rieke, R. D. Synthesis of Regioregular Head-to-Tail Poly[3-(Alkylthio)Thiophenes]. A Highly Electroconductive Polymer. *Macromolecules* **1995**, *28* (6), 2101–2102.
- (11) Wu, X.; Chen, T.-A.; Rieke, R. D. A Study of Small Band Gap Polymers: Head-to-Tail Regioregular Poly[3-(Alkylthio)Thiophenes] Prepared by Regioselective Synthesis Using Active Zinc. *Macromolecules* **1996**, *29* (24), 7671–7677.
- (12) Ogawa, Katsu.; Stafford, Jenny. A.; Rothstein, Scoot. D.; Tallman, Dennis. E.; Rasmussen, Seth. C. Nitrogen-Functionalized Polythiophenes: Potential Routes to New Low Band Gap Materials. *Synthetic Metals* **2005**, *152* (1–3), 137–140.
- (13) Groenendaal, L.; Jonas, F.; Freitag, D.; Pielartzik, H.; Reynolds, J. R. Poly(3,4-Ethylenedioxythiophene) and Its Derivatives: Past, Present, and Future. *Advanced Materials* **2000**, *12* (7), 481–494.
- (14) Miyanishi, S.; Tajima, K.; Hashimoto, K. Morphological Stabilization of Polymer Photovoltaic Cells by Using Cross-Linkable Poly(3-(5-Hexenyl)Thiophene). *Macromolecules* **2009**, *42* (5), 1610–1618.

- (15) Mueller, C. J.; Klein, T.; Gann, E.; McNeill, C. R.; Thelakkat, M. Azido-Functionalized Thiophene as a Versatile Building Block To Cross-Link Low-Bandgap Polymers. *Macromolecules* **2016**, *49* (10), 3749–3760.
- (16) Kim, B. J.; Miyamoto, Y.; Ma, B.; Fréchet, J. M. J. Photocrosslinkable Polythiophenes for Efficient, Thermally Stable, Organic Photovoltaics. *Adv. Funct. Mater.* **2009**, *19* (14), 2273–2281.
- (17) Yokoyama, A.; Miyakoshi, R.; Yokozawa, T. Chain-Growth Polymerization for Poly(3-Hexylthiophene) with a Defined Molecular Weight and a Low Polydispersity. *Macromolecules* **2004**, *37* (4), 1169–1171.
- (18) Miyakoshi, R.; Yokoyama, A.; Yokozawa, T. Catalyst-Transfer Polycondensation. Mechanism of Ni-Catalyzed Chain-Growth Polymerization Leading to Well-Defined Poly(3-Hexylthiophene). *Journal of the American Chemical Society* **2005**, *127* (49), 17542–17547.
- (19) Sheina, E. E.; Liu, J.; Iovu, M. C.; Laird, D. W.; McCullough, R. D. Chain Growth Mechanism for Regioregular Nickel-Initiated Cross-Coupling Polymerizations. *Macromolecules* **2004**, *37* (10), 3526–3528.
- (20) Iovu, M. C.; Sheina, E. E.; Gil, R. R.; McCullough, R. D. Experimental Evidence for the Quasi-“Living” Nature of the Grignard Metathesis Method for the Synthesis of Regioregular Poly(3-Alkylthiophenes). *Macromolecules* **2005**, *38* (21), 8649–8656.
- (21) Lohwasser, R. H.; Thelakkat, M. Toward Perfect Control of End Groups and Polydispersity in Poly(3-Hexylthiophene) via Catalyst Transfer Polymerization. *Macromolecules* **2011**, *44* (9), 3388–3397.
- (22) Pomerantz, M.; Cheng, Y.; Kasim, R. K.; Elsenbaumer, R. L. Poly(Alkyl Thiophene-3-Carboxylates). Synthesis, Properties and Electroluminescence Studies of Polythiophenes Containing a Carbonyl Group Directly Attached to the Ring. *Journal of Materials Chemistry* **1999**, *9* (9), 2155–2163.
- (23) Zhai, L.; Pilston, R. L.; Zaiger, K. L.; Stokes, K. K.; McCullough, R. D. A Simple Method to Generate Side-Chain Derivatives of Regioregular Polythiophene via the GRIM Metathesis and Post-Polymerization Functionalization. *Macromolecules* **2003**, *36* (1), 61–64.
- (24) Brendel, J. C.; Schmidt, M. M.; Hagen, G.; Moos, R.; Thelakkat, M. Controlled Synthesis of Water-Soluble Conjugated Polyelectrolytes Leading to Excellent Hole Transport Mobility. *Chemistry of Materials* **2014**, *26* (6), 1992–1998.
- (25) Kraft, M.; Adamczyk, S.; Polywka, A.; Zilberberg, K.; Weijtens, C.; Meyer, J.; Görrn, P.; Riedl, T.; Scherf, U. Polyanionic, Alkylthiosulfate-Based Thiol Precursors for Conjugated Polymer Self-Assembly onto Gold and Silver. *ACS Applied Materials & Interfaces* **2014**, *6* (14), 11758–11765.
- (26) Palermo, E. F.; van der Laan, H. L.; McNeil, A. J. Impact of  $\pi$ -Conjugated Gradient Sequence Copolymers on Polymer Blend Morphology. *Polymer Chemistry* **2013**, *4* (17), 4606.
- (27) Palermo, E. F.; Darling, S. B.; McNeil, A. J.  $\pi$ -Conjugated Gradient Copolymers Suppress Phase Separation and Improve Stability in Bulk Heterojunction Solar Cells. *J. Mater. Chem. C* **2014**, *2* (17), 3401.
- (28) Schmode, P.; Ohayon, D.; Reichstein, P. M.; Savva, A.; Inal, S.; Thelakkat, M. High Performance Organic Electrochemical Transistors Based on Conjugated Polyelectrolyte Copolymers. *Chem. Mater.* **2019**, *31* (14), 5286–5295.
- (29) Lanni, E. L.; McNeil, A. J. Mechanistic Studies on Ni(Dppe)Cl<sub>2</sub>-Catalyzed Chain-Growth Polymerizations: Evidence for Rate-Determining Reductive Elimination. *Journal of the American Chemical Society* **2009**, *131* (45), 16573–16579.

- (30) Scharsich, C.; Lohwasser, R. H.; Sommer, M.; Asawapirom, U.; Scherf, U.; Thelakkat, M.; Neher, D.; Köhler, A. Control of Aggregate Formation in Poly(3-Hexylthiophene) by Solvent, Molecular Weight, and Synthetic Method. *Journal of Polymer Science Part B: Polymer Physics* **2012**, *50* (6), 442–453.
- (31) Panzer, F.; Bäessler, H.; Lohwasser, R.; Thelakkat, M.; Köhler, A. The Impact of Polydispersity and Molecular Weight on the Order–Disorder Transition in Poly(3-Hexylthiophene). *The Journal of Physical Chemistry Letters* **2014**, *5* (15), 2742–2747.
- (32) Brown, P. J.; Thomas, D. S.; Köhler, A.; Wilson, J. S.; Kim, J.-S.; Ramsdale, C. M.; Siringhaus, H.; Friend, R. H. Effect of Interchain Interactions on the Absorption and Emission of Poly(3-Hexylthiophene). *Physical Review B* **2003**, *67* (6).
- (33) Hoffmann, S. T.; Bäessler, H.; Köhler, A. What Determines Inhomogeneous Broadening of Electronic Transitions in Conjugated Polymers? *The Journal of Physical Chemistry B* **2010**, *114* (51), 17037–17048.
- (34) Cohen, M. D.; Fischer, E. 588. Isosbestic Points. *Journal of the Chemical Society (Resumed)* **1962**, 3044.
- (35) Köhler, A.; Hoffmann, S. T.; Bäessler, H. An Order–Disorder Transition in the Conjugated Polymer MEH-PPV. *Journal of the American Chemical Society* **2012**, *134* (28), 11594–11601.
- (36) Clark, J.; Silva, C.; Friend, R. H.; Spano, F. C. Role of Intermolecular Coupling in the Photophysics of Disordered Organic Semiconductors: Aggregate Emission in Regioregular Polythiophene. *Physical Review Letters* **2007**, *98* (20).
- (37) Park, Y. D.; Lee, H. S.; Choi, Y. J.; Kwak, D.; Cho, J. H.; Lee, S.; Cho, K. Solubility-Induced Ordered Polythiophene Precursors for High-Performance Organic Thin-Film Transistors. *Advanced Functional Materials* **2009**, *19* (8), 1200–1206.
- (38) Clark, J.; Chang, J.-F.; Spano, F. C.; Friend, R. H.; Silva, C. Determining Exciton Bandwidth and Film Microstructure in Polythiophene Films Using Linear Absorption Spectroscopy. *Applied Physics Letters* **2009**, *94* (16), 163306.
- (39) Panzer, F.; Bäessler, H.; Köhler, A. Temperature Induced Order–Disorder Transition in Solutions of Conjugated Polymers Probed by Optical Spectroscopy. *The Journal of Physical Chemistry Letters* **2017**, *8* (1), 114–125.
- (40) Panzer, F.; Sommer, M.; Bäessler, H.; Thelakkat, M.; Köhler, A. Spectroscopic Signature of Two Distinct H-Aggregate Species in Poly(3-Hexylthiophene). *Macromolecules* **2015**, *48* (5), 1543–1553.
- (41) Lefebvre, M. D.; Olvera de la Cruz, M.; Shull, K. R. Phase Segregation in Gradient Copolymer Melts. *Macromolecules* **2004**, *37* (3), 1118–1123.
- (42) Balko, J.; Portale, G.; Lohwasser, R. H.; Thelakkat, M.; Thurn-Albrecht, T. Surface Induced Orientation and Vertically Layered Morphology in Thin Films of Poly(3-Hexylthiophene) Crystallized from the Melt. *J. Mater. Res.* **2017**, *32* (10), 1957–1968.
- (43) Balko, J.; Lohwasser, R. H.; Sommer, M.; Thelakkat, M.; Thurn-Albrecht, T. Determination of the Crystallinity of Semicrystalline Poly(3-Hexylthiophene) by Means of Wide-Angle X-Ray Scattering. *Macromolecules* **2013**, *46* (24), 9642–9651.
- (44) Skrypnichuk, V.; Boulanger, N.; Yu, V.; Hilke, M.; Mannsfeld, S. C. B.; Toney, M. F.; Barbero, D. R. Enhanced Vertical Charge Transport in a Semiconducting P3HT Thin Film on Single Layer Graphene. *Adv. Funct. Mater.* **2015**, *25* (5), 664–670.

(45) Strobl, G. R. *The Physics of Polymers Concepts for Understanding Their Structures and Behavior*; Springer: Berlin; New York, 2007.

(46) Fritzsching, K. J.; Mao, K.; Schmidt-Rohr, K. Avoidance of Density Anomalies as a Structural Principle for Semicrystalline Polymers: The Importance of Chain Ends and Chain Tilt. *Macromolecules* **2017**, *50* (4), 1521–1540.

(47) Köhler, A.; Bässler, H. *Electronic Processes in Organic Semiconductors: An Introduction*; Wiley-VCH: Weinheim, 2015.

## Supporting Information

### Instrumentation

$^1\text{H-NMR}$  spectra were recorded in deuterated chloroform  $\text{CDCl}_3$  on a Bruker Avance 250 spectrometer at 300 MHz at room temperature. Chemical shifts are noted in ppm and coupling constants in Hz. All spectra were calibrated according to the residual solvent peaks ( $\text{CHCl}_3$   $\delta=7.26$  ppm). Size exclusion chromatography (SEC) was performed utilizing a Waters 510 HPLC pump and THF with 0.25 wt% tetrabutylammonium bromide (TBAB) as eluent at a flow rate of 0.5 mL/min. A volume of 100  $\mu\text{L}$  of polymer solution (1-2 mg/mL) was injected into a column setup comprising a guard column (PSS, 5  $\times$  0.8 cm, SDV gel, particle size 5  $\mu\text{m}$ , pore size 100  $\text{\AA}$  respectively) and two separation columns (Varian, 30  $\times$  0.8 cm, mixed C gel, particle size 5  $\mu\text{m}$ ). Polymer size distributions were monitored with a WATERS 486 tunable UV detector at 254 nm and a Waters 410 differential RI detector. Polystyrene standards were used for calibration and 1,2-dichlorobenzene as an internal reference. Matrix assisted laser desorption ionization spectroscopy with time of flight detection mass spectroscopy measurements (MALDI-TOF) were performed on a Bruker Reflex III. For Polythiophene Polymers 1,8- dihydroxy-9,10-dihydroanthracen-9-one (dithranol) was used as matrix. The ratio of the mixture was 1000: 1 (Matrix: Polymer). Thermogravimetric analysis (TGA) of polymers was conducted using a Mettler Toledo TGA/SDTA 851e instrument under nitrogen atmosphere (20 mL/min) at a heating rate of 10 K/min and in the temperature range of 30-600°C. UV-Vis spectra were recorded on a Jasco V-670 spectrophotometer. All polymer solutions were measured in a concentration of 0.02 mg/ml. The spectra were recorded in quartz cuvettes with an internal diameter of 10 mm. Fluorescence spectroscopy was

performed on a Jasco FP-8600 spectrofluorometer in quartz cuvettes with an internal diameter of 10 mm.

For the temperature-dependent absorption and emission spectra, we used a home-build setup consisting of a wolfram lamp as light source for absorption measurements, a 405 nm (3.06 eV) continuous-wave diode laser from Coherent for excitation in emission measurements, and a spectrograph Shamrock SR303i with an Andor iDus CCD-camera for detection. All solutions were measured in a 1 mm fused silica cuvette that was placed in a temperature-controlled continuous flow helium cryostat from Oxford Instruments. We waited for 15 min after reaching a new temperature for the temperature to be fully equilibrated before taking the measurement. The spectra were measured in THF with a polymer concentration of 0.2 mg/ml.

Wide angle x-ray scattering (WAXS): Microfocus: A SAXSLAB laboratory Setup (Retro-F) (Copenhagen, Denmark) was used. As x-ray source, an AXO microfocus was used, with an AXO multilayer monochromator (Cu-K $\alpha$  radiation  $\lambda=0.15418$  nm, ASTIX) purchased from X-ray optics. For 2D Scattering patterns, a Dectris PILATUS R 300K detector (Daettwil, Switzerland) was used. SAXSGUI v2.19.02 was used for data reduction of the WAXS and SAXS patterns. All measurements were conducted in under vacuo and WAXS in transmission, GIWAXS in reflection. Sample to Detector distance is ca. 89 mm. All samples measured in ordered temperature region and in melt. A Perkin Elmer DSC 7 was used with a heating/cooling rate of 10 K/min under nitrogen atmosphere. All samples 1st cooling and 2nd heating is shown. Bottom gate/bottom contact organic field effect transistors (OFET Gen4) were purchased from Fraunhofer IPMS. N-doped silicon (doping at the surface  $n \sim 3 \times 10^{17}$  cm $^{-3}$ ) was used as the surface and gate electrode. The dielectric consists of a  $230 \pm 10$  nm layer of silicon oxide. Each substrate consisted of 16 devices with a constant channel width of 10 mm and varying channel length of 10 and 20  $\mu$ m. The source and drain electrodes were a 30 nm thick gold layer on a 10 nm ITO adhesion layer. The devices were prepared by cleaning in acetone and subsequently in iso-propanol in an ultrasonic bath for 10 min, followed by 15 min treatment in an ozone oven at 50 °C and subsequent silanization by 45 min treatment in a bath of 1 wt% octadecyltrichlorosilane (ODTS) in toluene at 60 °C. The devices were rinsed with toluene and *i*-propanol and dried. Thin polymer films were spin cast from 6 mg/mL

chloroform solutions at a spinning speed of 5000 rpm under ambient conditions. All devices were stored and measured under a nitrogen atmosphere. The IV-characteristics were measured using an Agilent B1500 semiconductor parameter analyzer. Using eqn (1) the charge carrier mobilities were calculated from the slope of the  $(I_d)^{0.5} - V_g$  plots.

$$I_d = \frac{W}{2L} C_i \mu (V_g - V_t)^2 \quad (1)$$

## Materials

3-bromothiophene (97 %), *t*-butylmagnesiumchloride (1.7 M in THF), tetrahydrofuran (99.5 %, extra dry, over molecular sieves, stabilized, AcroSeal®), 1,6-dibromohexane (96 %), *n*-butyllithium (1.6 M in hexane), hexane (97 %, extra dry, over molecular sieves, AcroSeal®), were purchased from Acros-Organics. dichloro[1,3-bis(diphenylphosphino)propane]nickel and 2,5-dibromo(3-hexyl)thiophene were synthesized according to literature.<sup>1-3</sup>

## Synthesis of 3-bromothiophene

30 g 3-bromothiophene (184 mmol, 1 equ.) was dissolved in dry hexane (250 ml) under argon atmosphere. Then, the solution was cooled down to  $-40\text{ }^\circ\text{C}$  to  $-50\text{ }^\circ\text{C}$ . 73,64 ml *n*-butyllithium (1.6 M in hexane, 184 mmol, 1 equ.) was added dropwise, and the solution was stirred for 10 min. Then, dry THF was added via syringe ( $\sim 15\text{ mL}$ ) until the white 3-lithiothiophene salt precipitated. The solution was then stirred for 1 h, after which the solution was allowed to warm to  $-10\text{ }^\circ\text{C}$ . Again, dry THF was added (30 ml) and 111.53 ml 1,6-dibromohexane (736.02 mmol, 4 equ.) was added. This solution was stirred for 2 h at room temperature and then extracted with diethylether and washed with water. The organic phase was dried over anhydrous  $\text{MgSO}_4$ , filtered and concentrated. Vacuum distillation at  $90 - 100\text{ }^\circ\text{C}$  at  $2 \times 10^{-3}$  mbar gave the product as colorless oil.

$^1\text{H-NMR}$ :  $\delta_{\text{H}}$  (300 MHz; ppm,  $\text{CDCl}_3$ ) 7.28 (m, 1 H), 6.94 (m, 2 H), 3.43 (t, 2 H), 2.65 (t, 2 H), 1.86 (t, 2 H), 1.7 – 1.2 (m, 6 H). Yield: 57 %

## Synthesis of 2,5-dibromo-3-(6-bromohexyl)-thiophene

26.05 g 3-(6-bromohexyl)thiophene (105.46 mmol, 1 equ.) and 43.17 g N-bromosuccinimide (242.55 mmol, 2,3 equ.) were dissolved under argon atmosphere and under the exclusion of light at RT in a mixture of dry THF and acetic acid (130 ml/ 130 ml). The solution was stirred for two hours and then extracted with diethylether and washed with water, saturated solution of sodium bicarbonate and 1 molar solution of sodium hydroxide. The organic phase was dried over anhydrous  $\text{MgSO}_4$ , filtered and concentrated. The raw product was purified by column chromatography with hexane as eluent. Vacuum distillation at 145 °C at  $2 \times 10^{-3}$  mbar gave the product as colorless oil.

$^1\text{H-NMR}$ :  $\delta_{\text{H}}$  (300 MHz; ppm,  $\text{CDCl}_3$ ) 6.94 (m, 1 H), 3.43 (t, 2 H), 2.65 (t, 2 H), 1.86 (t, 2 H), 1.7 – 1.2 (m, 6 H). Yield: 88 %

### **Synthesis of P3HT, P3BrHT and Poly[3-(hexylthiophene)-co-3-(6-bromohexyl)thiophene] copolymers**

2,5-dibromo-3-(6-bromohexyl)-thiophene (1 eq. or 0.75 eq. or 0.50 eq. or 0.25 eq. or 0 eq) and 2,5-dibromo-3-hexylthiophene (0 eq. or 0.25 eq. or 0.50 eq. or 0.75 eq. 1 eq) were added to a dry flask under argon and the vessel was evacuated once again and flushed with nitrogen. Then the concentration was set with dry THF to 0.5 mol/l and *t*-butylmagnesiumchloride (1.18 M in THF, 0.96 eq.) was added dropwise. The reaction mixture was stirred for 20 h under the exclusion of light. Then the reaction mixture was diluted with dry THF to 0.1 mol/l. The respective amount of  $\text{Ni}(\text{dppp})\text{Cl}_2$  (0.01 eq. suspension in 2-3 ml dry THF) was added in one portion to start the polymerization. After 2 h the polymerization was quenched with 1 ml 1 M HCl per gram monomer. The mixture was concentrated, and the polymer was precipitated in methanol. Furthermore, the polymer was purified by Soxhlet extraction with methanol and hexane and dried under vacuum.

$^1\text{H-NMR}$ :  $\delta_{\text{H}}$  (300 MHz; ppm,  $\text{CDCl}_3$ ): *P3BrHT*: 6.94 (m, 1  $\text{H}_a$ ), 3.43 (t, 2 H), 2.65 (t, 2 H), 1.86 (t, 2 H), 1.7 – 1.2 (m, 6 H). *P3HT*: 6,98 (s, 1  $\text{H}_{\text{arom.}}$ ), 2.80 (t, 2 H), 1.71 (tt, 2 H), 1.5-1.25 (m, 6 H), 0.91 (t, 3 H).

*SEC*: *P3HT-co-P3BrHT* 1:  $M_n = 16500$  g/mol,  $\text{Đ} = 1.19$ , *P3HT-co-P3BrHT* 2:  $M_n = 17000$  g/mol,  $\text{Đ} = 1.18$ , *P3HT-co-P3BrHT* 3:  $M_n = 15000$  g/mol,  $\text{Đ} = 1.20$ .

MALDI-ToF: P3HT-co-P3BrHT 1:  $M_n = 19200$  g/mol, P3HT-co-P3BrHT 2:  $M_n = 16400$  g/mol, P3HT-co-P3BrHT 3:  $M_n = 12800$  g/mol.

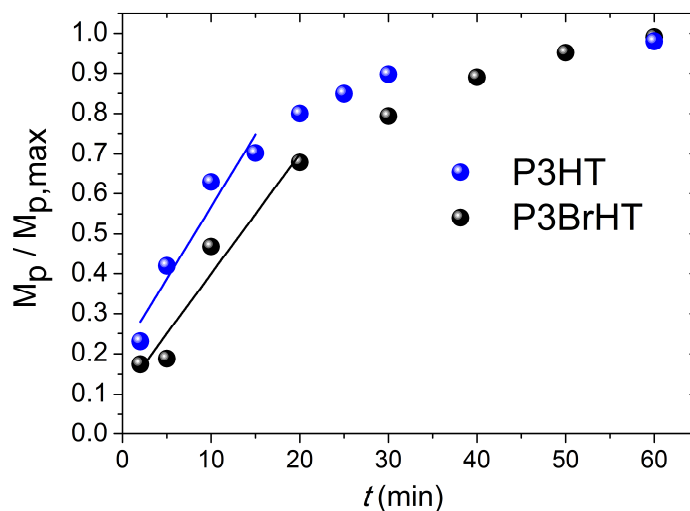


**Figure S1:** Comparison of the polymerization rates of P3HT and P3BrHT using Ni(dppp)Cl<sub>2</sub> as catalyst.

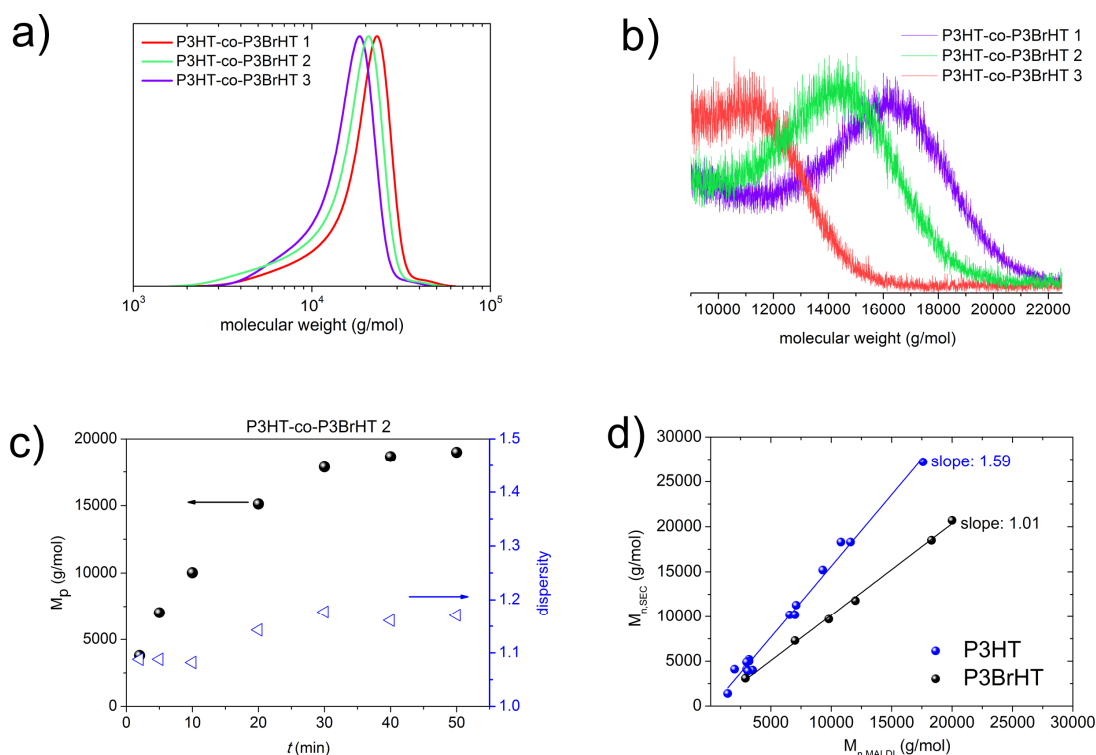


**Figure S2:** a) Molecular weight distributions of the copolymers P3HT-co-P3BrHT 1, 2 and 3 measured by THF SEC with polystyrene standard a) MALDI-ToF spectra of P3HT-co-P3BrHT 1, 2 and 3. Measured with dithranol as matrix with a concentration of polymer: matrix 1:1000. c) Representative kinetic plot for the copolymerization of 3HT and 3BrHT to get P3HT-co-P3BrHT 2 and the evolution of dispersity ( $\bar{D}$ ), Peak molecular weight and dispersities depending on the polymerization time are shown. d) Comparison of the

measured molecular weights of different P3HT with H/Br end group and P3BrHT with Br/H end group compared to the absolute molecular weight measured by MALDI-ToF. All listed polymers were synthesized in our group.

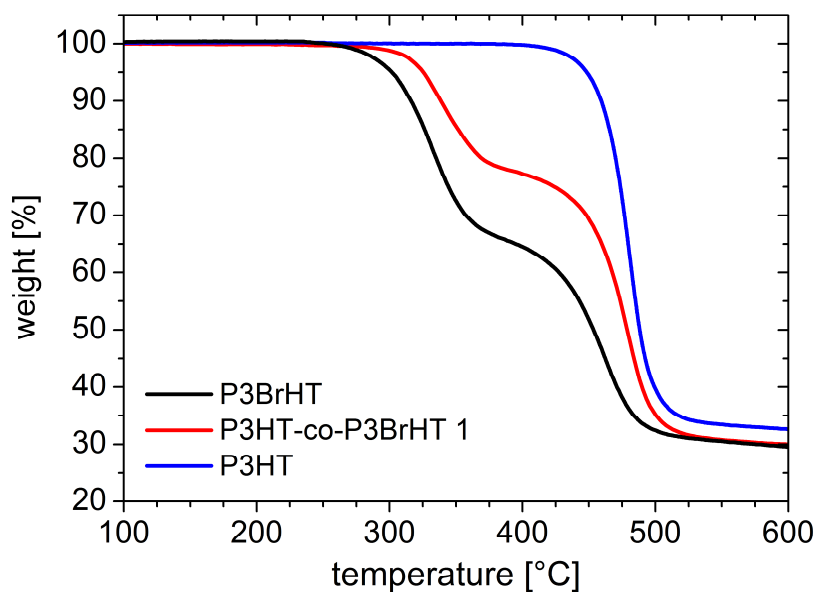


**Figure S3:** TGA measurement of P3BrHT, P3HT and P3HT-co-P3BrHT 1 under nitrogen atmosphere with a heating rate of 10 K/min.

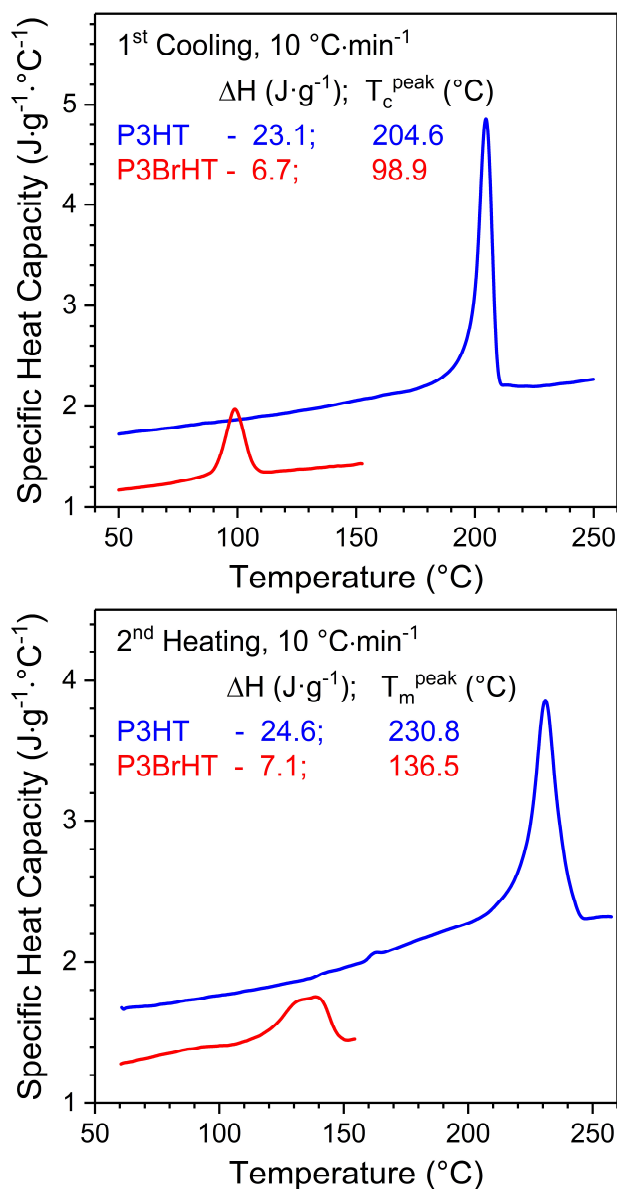


**Figure S4:** DSC cooling (left) and heating (right) curves of the homopolymers P3HT and P3BrHT measured with a rate of 10 K/min under nitrogen atmosphere. The curves were not shifted, in contrast to the data in Figure 4 in the main manuscript, and as such, allow discussing the absolute values of the specific heat capacity of the homopolymers. The corresponding discussion appears during the crystal structure analysis in the main text.

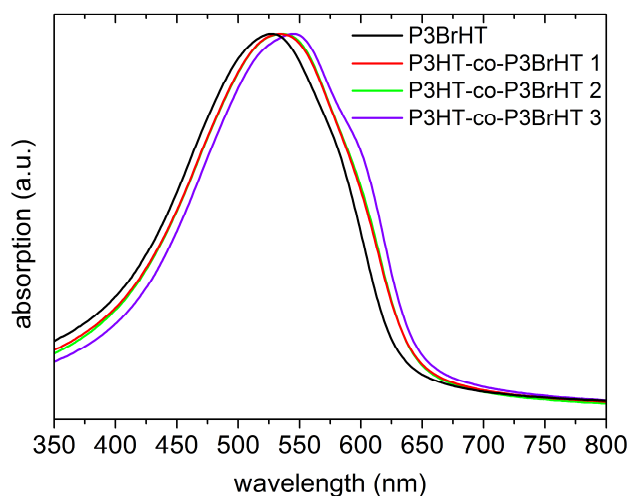


**Figure S5:** Absorption spectra of P3BrHT-H/Br, P3HT-co-P3BrHT 1, 2 and 3 in thin film. Films were prepared by spin-coating of 6 mg/ml chloroform solution.

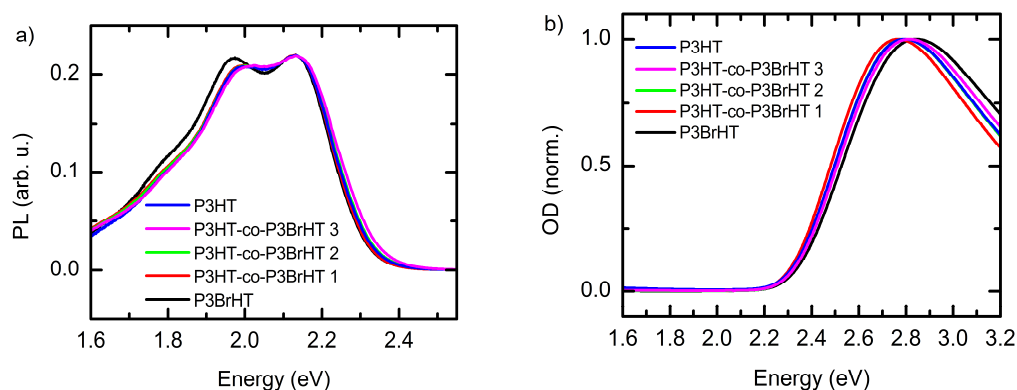


**Figure S6:** (a) Room temperature photoluminescence and (b) absorption spectra of the five polymers in chloroform solution.

### Franck-Condon-Analysis

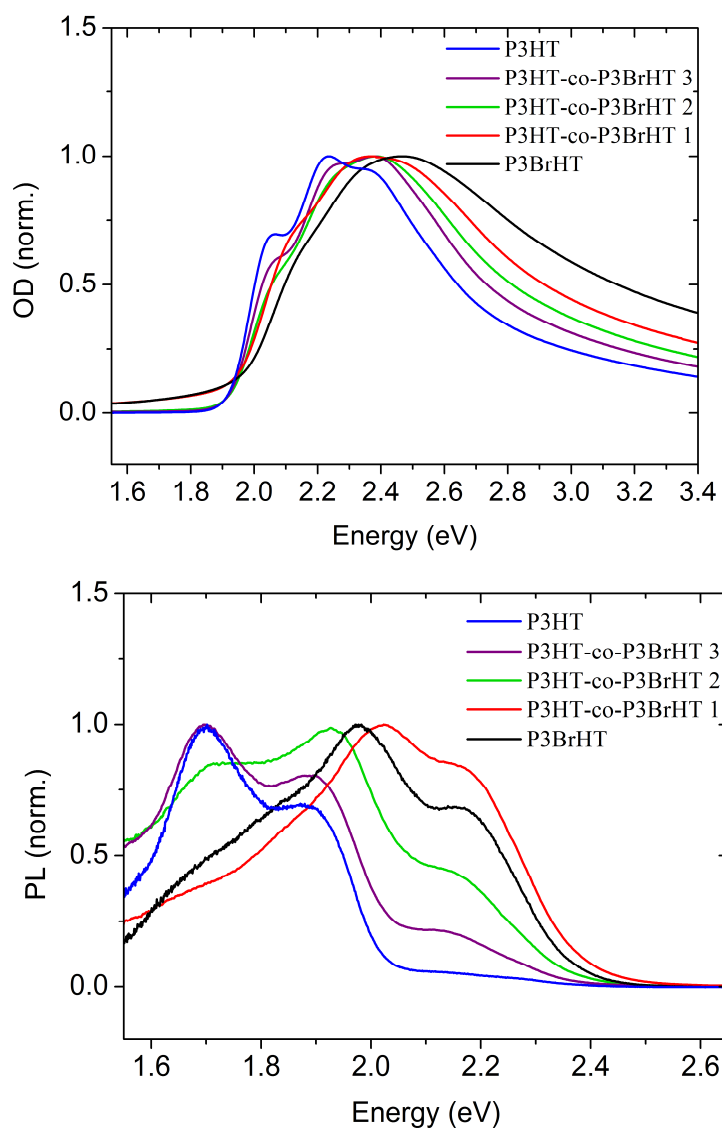
We fitted the PL spectra with a modified Franck-Condon-Progression accounting for interchain interaction, resulting in a suppression of the 0-0 peak with respect to a normal Franck-Condon-Progression.<sup>4</sup> The results of the analysis are listed in **Table S1**.  $E_{0-0}$  is the position of the 0-0 peak,  $E_{\text{vib}}$  the energy of the considered vibrational modes,  $S$  the dimensionless Huang-Rhys-Parameter,  $\sigma$  the Gaussian linewidth of the vibronic peaks, and  $\alpha$  the suppression of the 0-0-peak, where  $\alpha = 1$  means no suppression and  $\alpha = 0$  full suppression.

Except for species 3 and the low temperature PL of P3HT, no suppression of the 0-0 peak was necessary. The fit parameters of species 3 and P3HT match very closely. **Figure S2** shows the Franck-Condon-Fit to the PL spectrum of P3HT-co-P3BrHT 2 in THF at 190 K.

**Table S1:** Parameters derived from the Franck-Condon-Analysis of the PL spectra of **figure 4** in the main text.

Compound/ Species	Temperature in K	$E_{0-0}$ in eV	$E_{\text{vib}}$ meV	$\ln S$	$\sigma$ in meV	$\alpha$
1/1	210	2.134	175	1.016	70	1
1/1	165	2.141	175	1.016	76	1
1/2		1.922	170	1.004	47	1
			85	0.445		
2/1	190	2.127	175	1.016	77	1
2/2		1.916	170	1.004	40	1
			85	0.445		
2/3		1.808	170	0.877	50	0.271
P3HT/LEP*	190	1.800	170	0.818	50	0.288

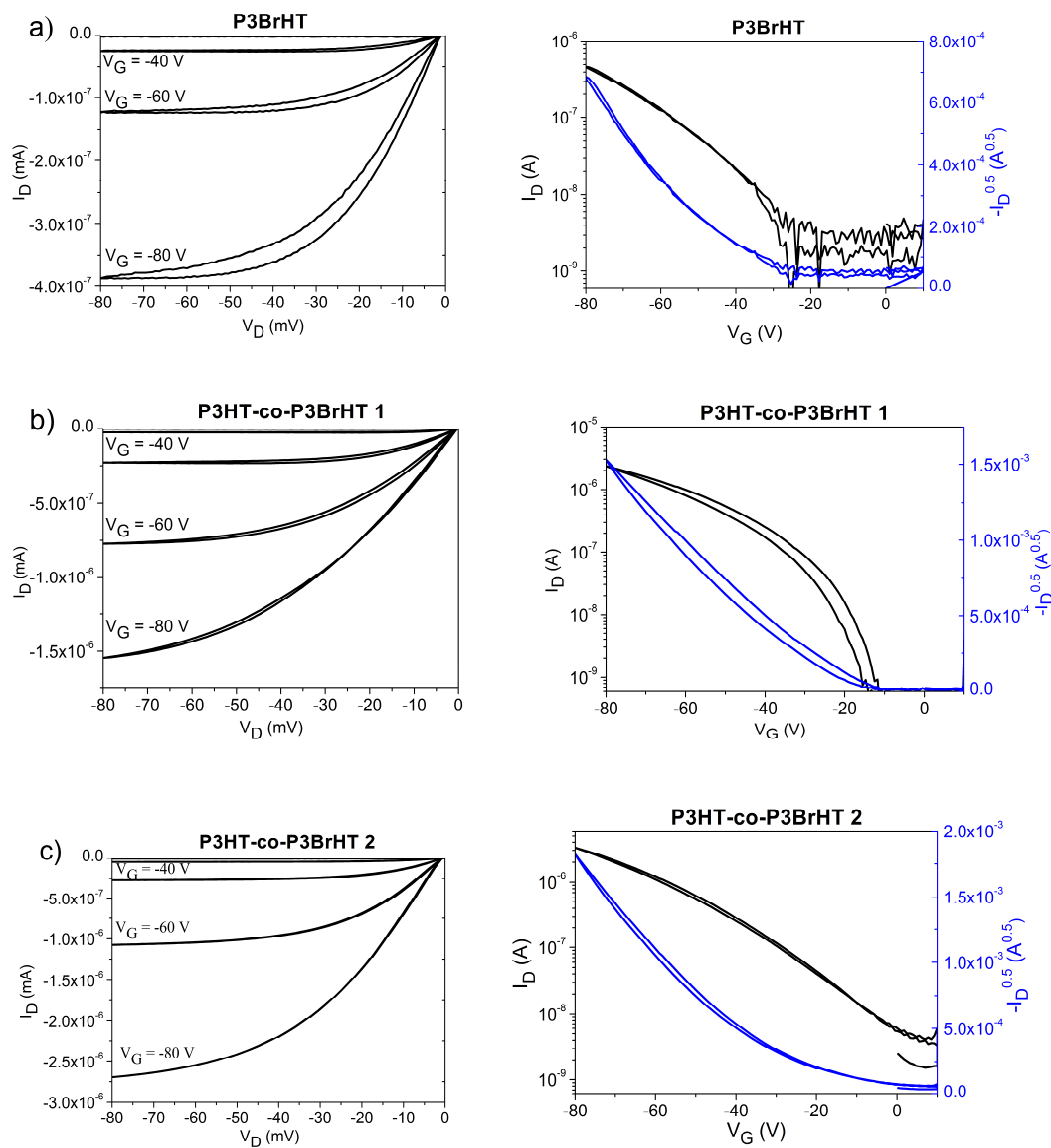
\* Low Energy Progression refer to Panzer et. al.<sup>5</sup> The High Energy Progression was ignored for deriving the presented fit parameters.



**Figure S7:** Absorption spectra (left) and photoluminescence spectra (right) of the homopolymers P3HT and P3BrHT and the copolymers P3HT-co-P3BrHT 1, 2 and 3 in a solvent mixture of chloroform/ethyl acetate 10/90%, measured at a polymer concentration of 0.02 mg/ml.

**Table S2:** The parameters of P3BrHT crystal lattice calculated from the WAXS pattern in Figures 6c, d for two different scenarios of the lattice parameter  $c$ .

	$a$	$b$	$c$	$\alpha$	$\beta$	$\gamma$
	[nm]	[nm]	[nm]	[°]	[°]	[°]
Scenario 1	1.774	0.772	0.788	91.2	87.9	91.8
Scenario 2	1.778	0.773	1.153	91.1	91.05	91.84



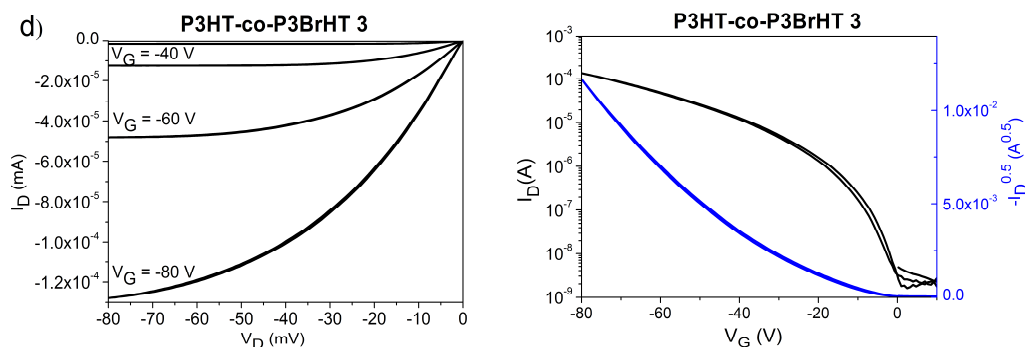


**Figure S8:** OFET Transfer and output curves of the polymers.

- (1) Zhai, L.; Pilston, R. L.; Zaiger, K. L.; Stokes, K. K.; McCullough, R. D. A Simple Method to Generate Side-Chain Derivatives of Regioregular Polythiophene via the GRIM Metathesis and Post-Polymerization Functionalization. *Macromolecules* **2003**, *36* (1), 61–64.
- (2) Iovu, M. C.; Sheina, E. E.; Gil, R. R.; McCullough, R. D. Experimental Evidence for the Quasi-“Living” Nature of the Grignard Metathesis Method for the Synthesis of Regioregular Poly(3-Alkylthiophenes). *Macromolecules* **2005**, *38* (21), 8649–8656.
- (3) Kergoat, L.; Piro, B.; Berggren, M.; Horowitz, G.; Pham, M.-C. Advances in Organic Transistor-Based Biosensors: From Organic Electrochemical Transistors to Electrolyte-Gated Organic Field-Effect Transistors. *Analytical and Bioanalytical Chemistry* **2012**, *402* (5), 1813–1826.
- (4) Clark, J.; Silva, C.; Friend, R. H.; Spano, F. C. Role of Intermolecular Coupling in the Photophysics of Disordered Organic Semiconductors: Aggregate Emission in Regioregular Polythiophene. *Physical Review Letters* **2007**, *98* (20).
- (5) Panzer, F.; Sommer, M.; Bäessler, H.; Thelakkat, M.; Köhler, A. Spectroscopic Signature of Two Distinct H-Aggregate Species in Poly(3-Hexylthiophene). *Macromolecules* **2015**, *48* (5), 1543–1553.

## Chapter 5:

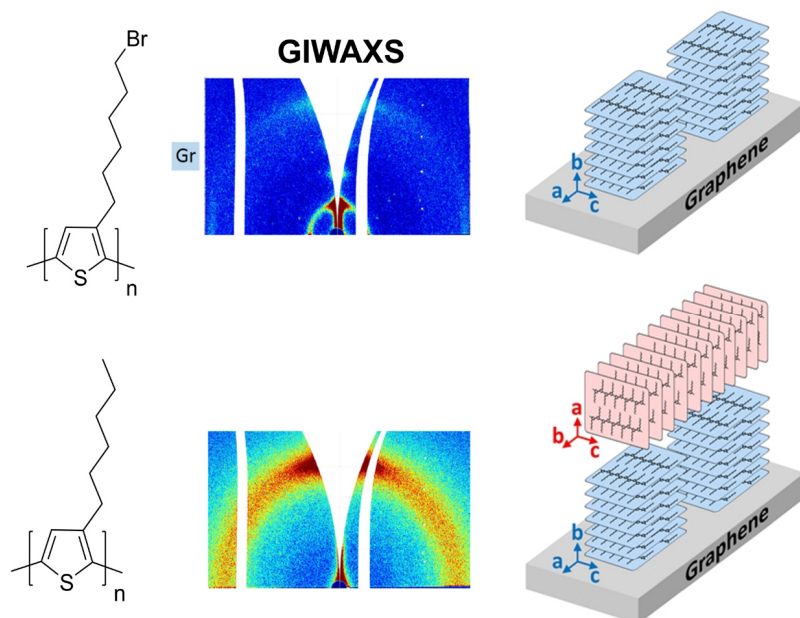
# Elucidating the effect of interfacial interactions on crystal orientations in thin films of polythiophenes

Oleksandr Dolynchuk<sup>†</sup>, Philip Schmode<sup>‡</sup>, Matthias Fischer<sup>†</sup>, Mukundan Thelakkat<sup>‡§</sup>, Thomas Thurn-Albrecht<sup>†\*</sup>

<sup>†</sup>Experimental Polymer Physics, Institute of Physics, Martin Luther University Halle-Wittenberg, Von-Danckelmann-Platz 3, D-06120 Halle, Germany

<sup>‡</sup>Applied Functional Polymers, Macromolecular Chemistry I, University of Bayreuth, Universitätsstraße 30, D-95447 Bayreuth, Germany

<sup>§</sup>Bavarian Polymer Institute, University of Bayreuth, Universitätsstraße 30, D-95447 Bayreuth, Germany



*Intended for Submission to Nat. Comm.*

**ABSTRACT:** Molecular orientation is an important aspect in improving the efficiency of organic electronic devices. In many ordered materials, orientation can be achieved by directional crystallization on a substrate. However, a full face-on molecular alignment of poly(3-hexylthiophene) (P3HT) on a substrate has never been realized so far. Here it is found that P3HT films crystallized on graphene exhibit the double-layered edge-on and face-on crystal orientation with edge-on crystals formed at the top surface. We assume this finding as the result of two competing interfacial interactions of P3HT chains with graphene and vacuum. By modifying the side chain chemical composition, it is shown that poly(3-(6-bromohexyl)-thiophene) on graphene, unlike P3HT, has solely face-on oriented crystals in films with thickness up to 26 nm. As such, we demonstrate that modification of the chemical structure of polythiophene side chains can alter the interfacial interactions and result in a drastic change of the molecular alignment.

## INTRODUCTION

Semicrystalline conjugated polymers attract great attention as organic materials for various electronic devices due to a striking combination of semiconducting, thermal, solution, and mechanical properties.<sup>1–5</sup> In particular, semiconducting polymers are promising candidates for organic photovoltaics applications. One of the key requirements for efficient polymer-based photovoltaic devices is an enhanced vertical charge transport and subsequent charge collection at the top and bottom electrodes. The charge transport properties of semicrystalline conjugated polymers are anisotropic and strongly depend on morphology and orientation of polymer crystals.<sup>6,7</sup> Thus, a controlled molecular orientation in nanostructured conjugated polymers opens a potential pathway for a much more efficient exploitation of their anisotropic properties. In this regard, a physics mechanism enabling such a control over the orientation would be highly important for fundamental study of the material anisotropic properties as well as for numerous applications in organic electronics and beyond.

Recently, it was shown that crystallization of non-semiconductor polymers at the interface to a solid substrate can proceed via a process called prefreezing and result in strongly oriented vertically layered morphology of polymer crystals.<sup>8,9</sup> Prefreezing is the formation of a mesoscopically thick crystalline layer at a transition temperature  $T_{max}$  above the bulk melting point  $T_m$  and, in contrast to heterogeneous nucleation, is an equilibrium phenomenon. After emergence, the prefrozen crystalline layer grows with decreasing temperature and diverges upon approaching  $T_m$ . Thus, crystallization via prefreezing entails the formation of highly oriented crystals of above 100 nm thickness.<sup>8</sup> The latest theoretical results demonstrated that the difference of the

interfacial energies between a liquid, crystal, and a substrate  $\Delta\gamma_{prefr} = \gamma_{sub,liq} - (\gamma_{sub,cry} + \gamma_{cry,liq})$  plays a dominant role and acts as a driving force for prefreezing.<sup>10</sup> Thereby, the crystal orientation emerging during prefreezing in the direction normal to the substrate surface is the result of the minimization of the crystal-substrate interaction energy  $\gamma_{sub,cry}$  and, therefore, can be tuned by modifying one or both components of the system, keeping the necessary precondition for prefreezing  $\Delta\gamma_{prefr} > 0$ .

Several attempts have been made to investigate experimentally and theoretically the orientation of poly(3-hexylthiophene) (P3HT), a widely studied semiconducting p-type polymer, and other oligothiophenes on graphite.<sup>11–19</sup> As it was shown, the monolayers of P3HT and  $\beta$ -alkylated oligothiophenes have the so-called face-on orientation with both thiophene rings and alkyl side chains lying parallel to the graphite surface. Such an orientation of polythiophene chains in thicker films would be highly advantageous for photovoltaic applications because of the high charge carrier mobility along the  $\pi$ - $\pi$  stacks of thiophene rings.<sup>5</sup> However, subsequent endeavors to induce the face-on orientation of P3HT crystals with the vertically layered  $\pi$ - $\pi$  stacks on graphite or graphene were only partly successful.<sup>20–25</sup> In the works by Skrypnichuk et al.,<sup>21–23</sup> thin P3HT films crystallized on a single layer graphene showed the mixed face-on and edge-on crystal orientation with the hexyl side chains parallel and perpendicular to the graphene surface, respectively. A reason for the appearance of edge-on P3HT crystals as well as physical phenomena underlying the formation of both crystal orientations remained unclear. Most recently, Balko et al.<sup>26</sup> presented a systematic study of the crystal orientation of P3HT films of various thickness on SiO<sub>2</sub>/Si substrates. The results suggested that the vacuum-polymer interface induces edge-on crystal orientation in P3HT that, hence, is

substrate independent. It was assumed that the observed orientation is related to surface freezing,<sup>27–32</sup> a phenomenon well known for alkanes and analogous to the aforementioned prefreezing transition at the liquid-solid interface,

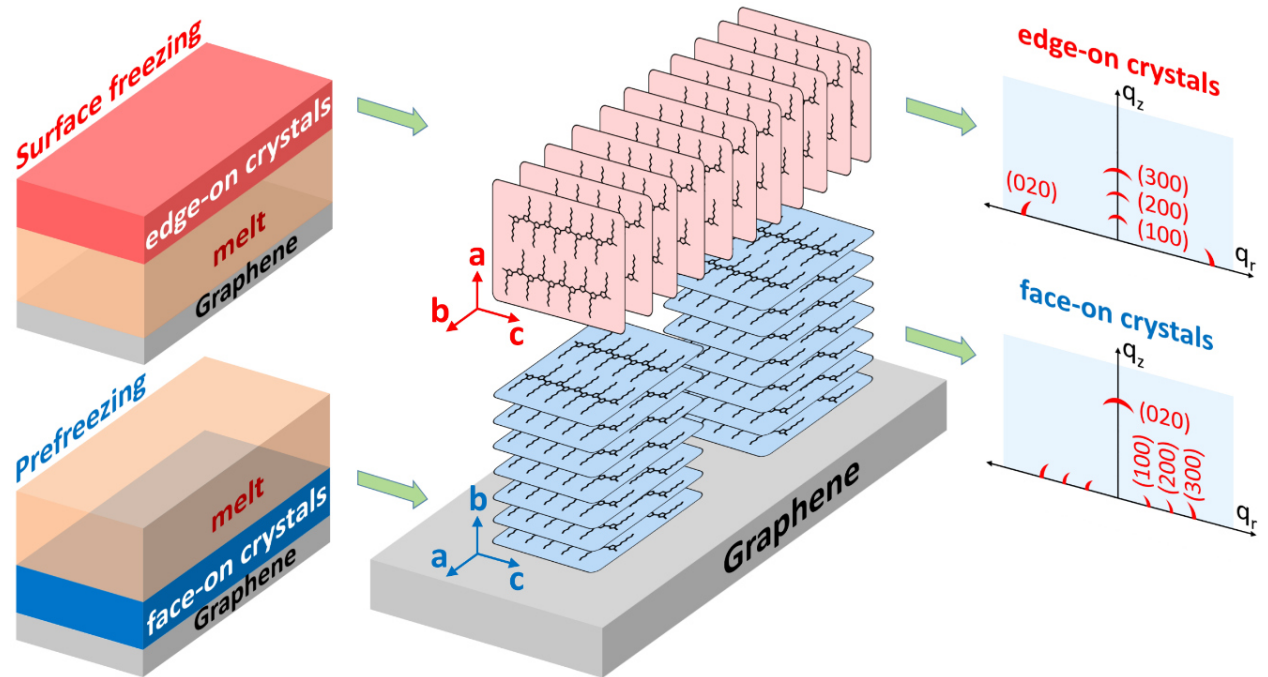


**Figure 1.** Schematic illustration of crystallization of thin P3HT films on graphene with face-on oriented crystals formed at the interface to graphene and edge-on oriented crystals formed at the interface to vacuum. The reciprocal space maps on the right schematically show the X-ray scattering patterns of edge-on (top) and face-on (bottom) crystals given that their orientation along the graphene surface is isotropic.

as it also occurs above the bulk melting temperature and is also driven by the orientation-dependent interfacial energy difference  $\Delta\gamma_{s,fr} = \gamma_{liq,vac} - (\gamma_{cry,vac} + \gamma_{cry,liq})$ , which however is distinct from that responsible for prefreezing.

In view of the discussed experimental outcomes, we assume that the mixed crystal orientation in thin P3HT films on graphene is the result of competing interactions of P3HT chains with graphene and vacuum, whereby these two interfaces induce via surface freezing and prefreezing two different orientations of the polymer crystals. The summary of our hypothesis of P3HT crystallization on graphene is given in

**Figure 1.** Based on the current knowledge on surface induced crystallization reviewed above, it is suggested here that modification of the chemical structure of P3HT chains can change the interfacial energies and eventually result in suppression of the unfavorable edge-on molecular orientation. In particular, since it is hexyl side chains of P3HT that form the interface to vacuum in case of edge-on orientation (see Figure 1), the substitution of methyl end groups with more polar atoms can decrease the interfacial energy difference  $\Delta\gamma_{s,fr}$  and, as such, affect the crystallization of polythiophene chains at this interface. To test this assumption, we here present a comparative study of the crystal orientation in films of P3HT and poly[3-(6-bromohexyl)-thiophene] (P3BrHT) of various thickness on a single layer graphene by using surface-sensitive grazing incidence wide-angle X-ray scattering (WAXS). The validation of the structural model of P3HT presented in Figure 1 forms another important goal of this work and is addressed accordingly. To further test our hypothesis and to complement the WAXS results, the top surface morphology of P3HT and P3BrHT films as well as possible morphological changes for varied film thickness are also investigated by the atomic force microscopy.

## RESULTS

Comparative study of crystal orientation in thin films of P3HT and P3BrHT on graphene. The WAXS patterns of 31 nm (a typical intermediate thickness) P3HT film on graphene recorded at incident angles of  $0.18^\circ$  and  $10^\circ$  are shown in **Figures 2c** and **2e**, respectively. It is worth noticing that while a small angle of incidence can be utilized for surface-sensitive WAXS and for visualizing Bragg reflections parallel to sample surface, higher incident angles allow accessing regions of higher  $q_z$  on the meridian. The (100) reflection of a monoclinic P3HT crystal lattice,<sup>26,33,34</sup> which is parallel to the a crystal axis (Figure 1), is clearly seen both parallel and perpendicular to the graphene surface and implies the mixed edge-on and face-on crystal orientation in the sample. Figure 2e demonstrates that the (020) reflection around  $q_z = 16.7 \text{ nm}^{-1}$  pointing towards the b crystal axis lies normal to the graphene surface and confirms the existence of the face-on oriented crystals. As such, the results in Figure 2c, e are in line with the previous studies of P3HT thin film crystal orientation on graphene reported by Skrypnichuk et al.<sup>21–23</sup> In contrast, the grazing incidence WAXS pattern of 21 nm thin P3BrHT on graphene in **Figure 2d** shows the most intense (200) reflection of the triclinic P3BrHT crystal lattice<sup>35</sup> located only parallel to the sample surface. An additional measurement (see Figure S1 in Supplementary Information) at an incident angle of  $4.5^\circ$ , which is close to Bragg's condition for (200) reflection, indicates no (200) reflection on meridian and along with the results in Figure 2f proves the complete face-on crystal orientation in this sample.

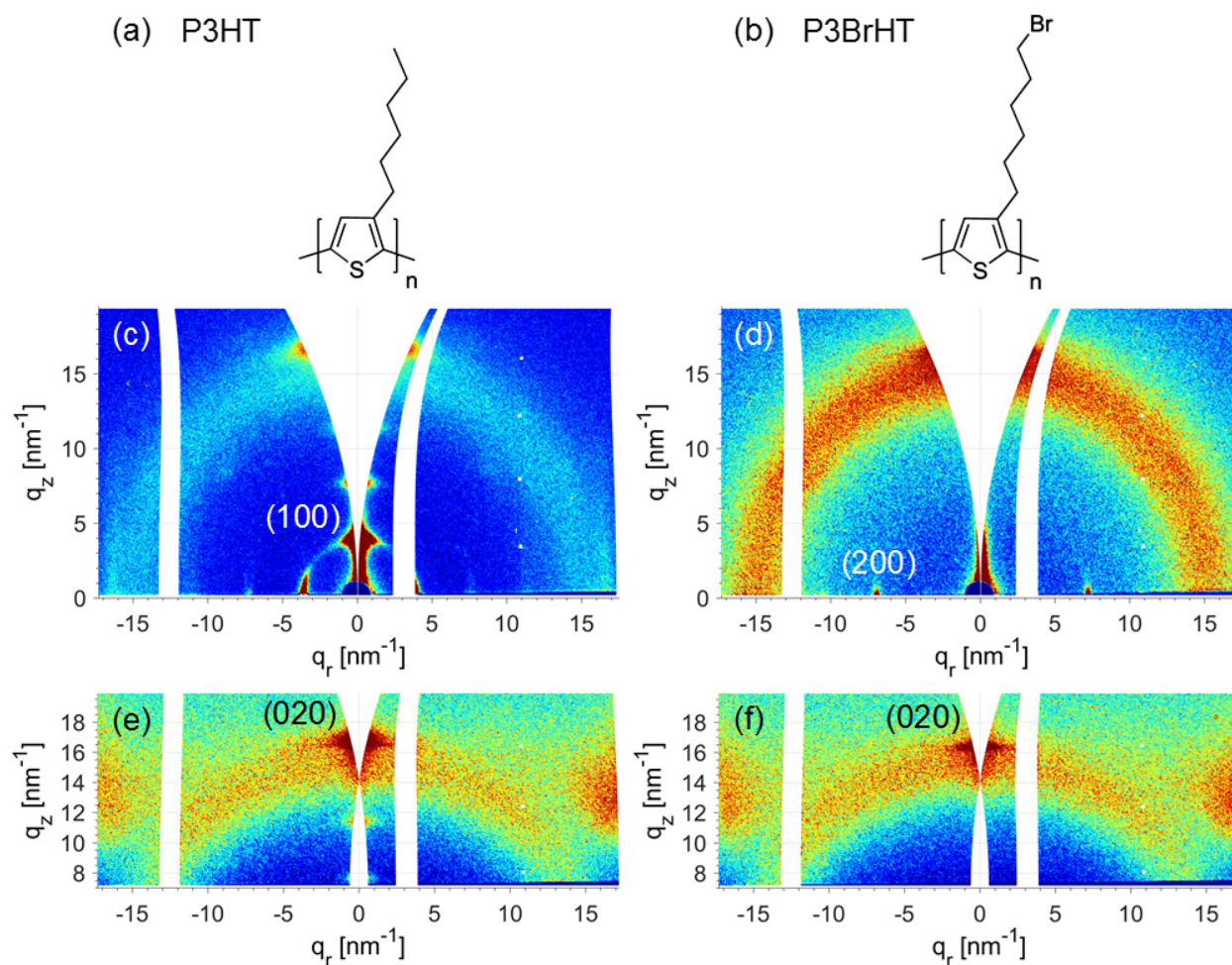


**Figure 2.** Chemical structures of P3HT (a) and P3BrHT (b) as well as reciprocal space maps of the WAXS patterns of 31 nm thin P3HT (c,e) and 21 nm thin P3BrHT (d,f) on graphene measured at incident angles of 0.18° (c), 0.2° (d) and 10° (e,f). Logarithmic color scale was adjusted for each image to make the less intense peaks visible.

Thereby, we are able to conclude that Br-substitution of methyl end group on side chains suppresses edge-on crystal orientation in 21 nm thin P3BrHT and indeed leads to the favoured face-on molecular alignment induced by the underlying graphene. The subsequent investigation is then devoted to the questions if our understanding of P3HT crystallization depicted in Figure 1 is correct and, secondly, if the complete face-on orientation of P3BrHT can be retained in thicker films.

### **Thickness dependent crystal orientation in P3HT films on graphene.**

**Figure 3** shows the WAXS images of P3HT films of various thickness (4-5, 45, and 100 nm) crystallized on graphene. As can be seen in Figures 3a,c,e, the (100) reflection of P3HT is allocated along both equator and meridian of the WAXS images and, therefore, evidences the mixed edge-on and face-on oriented crystals in all P3HT films under study. The corresponding WAXS patterns measured at an incident angle of  $10^\circ$  (Figure 3b,d,f) proves that the face-on oriented crystals are present in all investigated films. It is noteworthy to mention that the mixed alignment of P3HT chains is seen in the film as thin as 4-5 nm and, thus, suggests no dominating crystal orientation even in such a thin film. Furthermore, the intensity of the azimuthally distributed ( $90^\circ < \varphi_{100} < 180^\circ$ ) out-plane (100) reflection increases with increasing film thickness as visible in **Figure S2** in Supplementary Information. Hence, we ascertain that the amount of randomly oriented crystals increases with rising film thickness that presumably hints at the limited correlation length of crystal orientation. To test the assumption about the two layer model in Figure 1, we carried out a series of surface-sensitive grazing incidence WAXS measurements at various incident angles in the range  $\alpha_i = 0.11 - 0.22^\circ$  that results in the varied penetration depth of X-rays<sup>26,36,37</sup> (see Methods). Characterization of the crystal orientation distribution was performed on the basis of pole figures of the (100) reflection. The corresponding pole figures (see Figure S3 in Supplementary Information) were extracted directly from the measured scattering patterns by integrating the intensity over the range  $q = 3.2 - 4.4 \text{ nm}^{-1}$  of the (100) reflection schematically illustrated in Figure 3c.

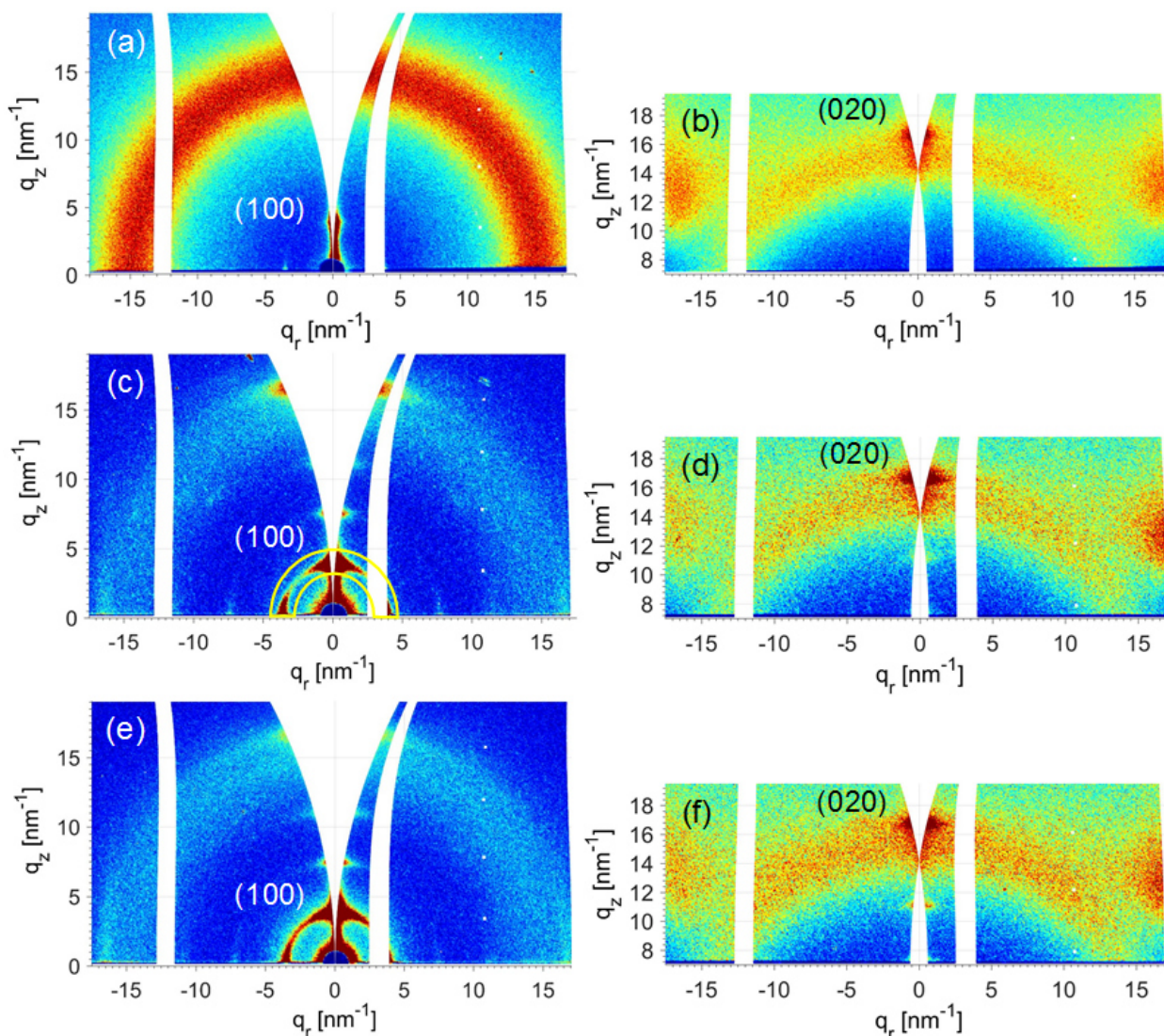


**Figure 3.** Reciprocal space maps of the WAXS patterns of P3HT films of thickness 4-5 nm (a,b), 45 nm (c,d), and 100 nm (e,f) on graphene measured at an incident angle of  $0.18^\circ$  (a,c,e) and  $10^\circ$  (b,d,f). The yellow semicircular lines around the (100) reflection in (c) illustrate the range of azimuthal angle  $\varphi$  used to create the polar figures (see Figures S2, S3 in Supplementary Information). Logarithmic color scale was adjusted for each image to make the less intense peaks visible.

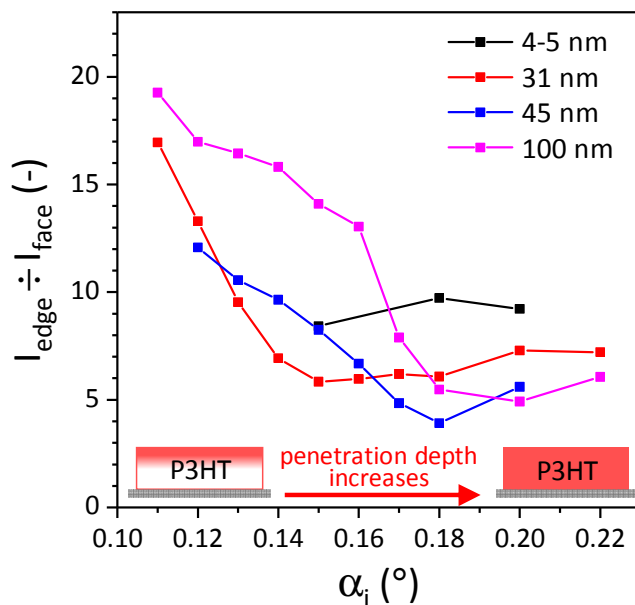


**Figure 4.** Ratio of intensities  $I_{edge}/I_{face}$  of the (100) reflection scattered from edge-on and face-on P3HT crystals on graphene as a function of incident angle  $\alpha_i$ . The connecting lines are a guide to the eye. The ratio  $I_{edge}/I_{face}$  was calculated from the corresponding pole figures (see Figure S3 in Supplementary Information) of (100) reflection of P3HT thin films of different thicknesses.

In this method, we neglected the refraction effects leading to an enhanced intensity of reflections close to  $\alpha_i = \alpha_c$  and excluded a small blank range of the reciprocal space around the  $q_z$  axis. Subsequently, we compared the maximum integrated intensities  $I_{edge}$  and  $I_{face}$  of the (100) reflection corresponding to edge-on ( $\varphi = 90^\circ$  in Figure S3 in Supplementary Information) and face-on ( $\varphi \approx 176^\circ$  in Figure S3 in Supplementary Information) crystal orientations, respectively. The ratio  $I_{edge}/I_{face}$  of these intensities taken as a relative measure of the orientation distribution within the film thickness is plotted in **Figure 4** as a function of incident angle  $\alpha_i$ . The results in Figure 4 indicate that the fraction of the edge-on oriented crystals in P3HT films of thickness 31–100 nm increases in the top layer of the films. Thereby we can deduce that edge-on crystals form at the interface of P3HT to vacuum, in line with our assumption illustrated in Figure 1. This observation is also in accordance with the previous study of the crystal orientation of thin P3HT films crystallized on SiO<sub>2</sub>/Si

substrates.<sup>26</sup> As discussed in the Introduction, the reason for edge-on crystal orientation can be surface freezing of P3HT chains to vacuum. Although there is no direct evidence for P3HT surface freezing, the substrate and film thickness independence of the appearance of edge-on crystal orientation suggests that surface freezing in P3HT is a plausible cause for the phenomenon. Note that the P3HT film of thickness 4-5 nm shows almost no change of crystal orientation with decreasing incident angle. This is expected due to the small film thickness and limitations of the method used.

**Thickness dependent crystal orientation in P3BrHT films on graphene.** In the following, we address the question if the complete face-on crystal orientation observed for 21 nm thin P3BrHT can be realized for thicker films. The WAXS patterns of 26 nm thin P3BrHT film on graphene shown in **Figure 5a,b** confirm the face-on orientation of the crystals. Figure S4 in Supplementary Information measured at an incident angle of 4° near the position of (200) crystal peak indicates no (200) reflection on meridian and evidences that only face-on aligned crystals are present in this sample. However, as it is visible in Figures 5c–f, the mixed edge-on and face-on crystal alignment arises in films with thickness of 35 and 46 nm.

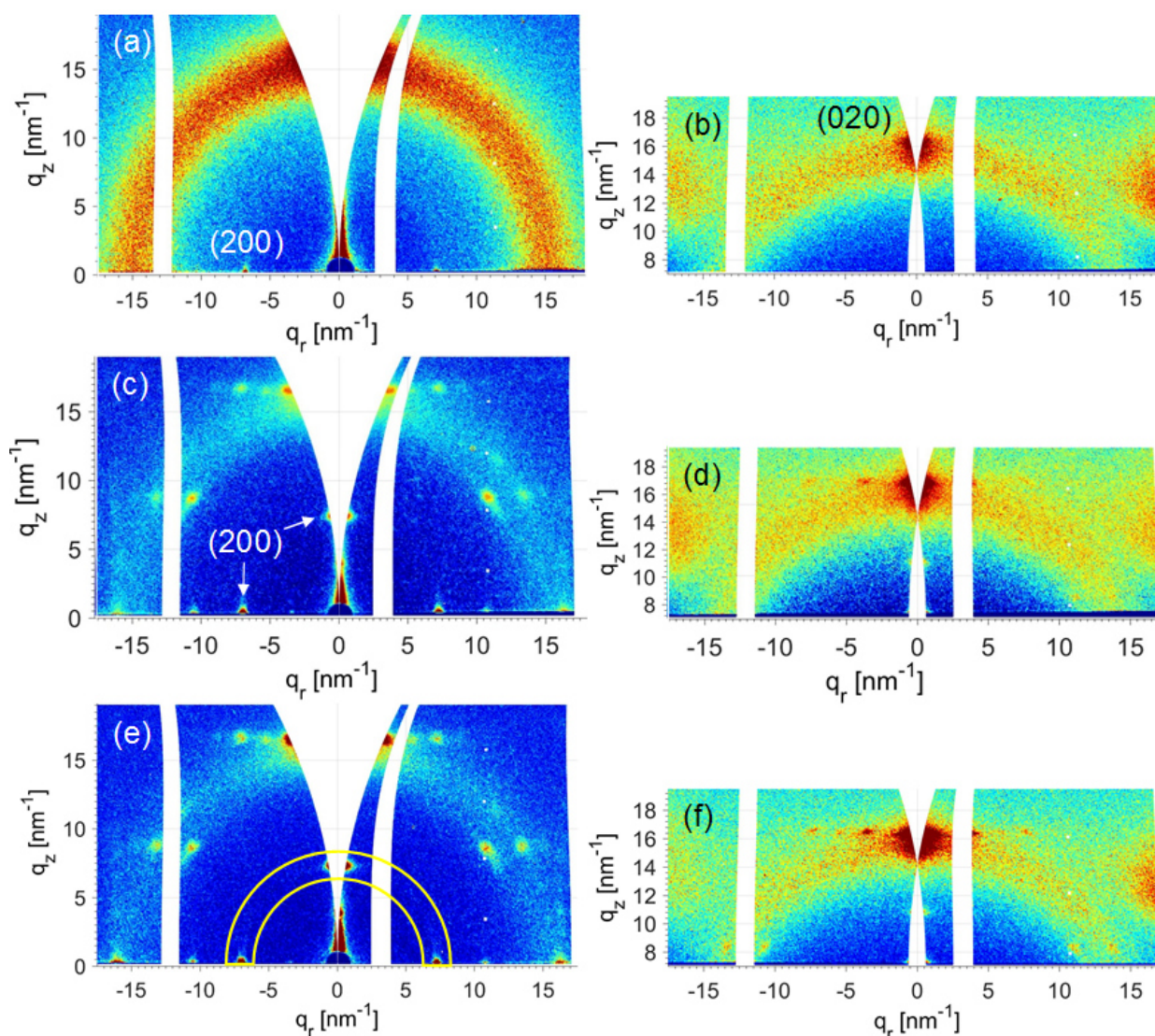


**Figure 5.** Reciprocal space maps of the WAXS patterns of P3BrHT films of thickness 26 nm (a,b), 35 nm (c,d), and 46 nm (e,f) on graphene measured at an incident angle of  $0.2^\circ$  (a,c,e) and  $10^\circ$  (b,d,f). The yellow semicircular lines around (200) reflection in (e) depict the range of azimuthal angle  $\varphi$  used to create the polar figures (see Figure S5 in Supplementary Information). Logarithmic color scale was adjusted for each image to make the less intense peaks visible.

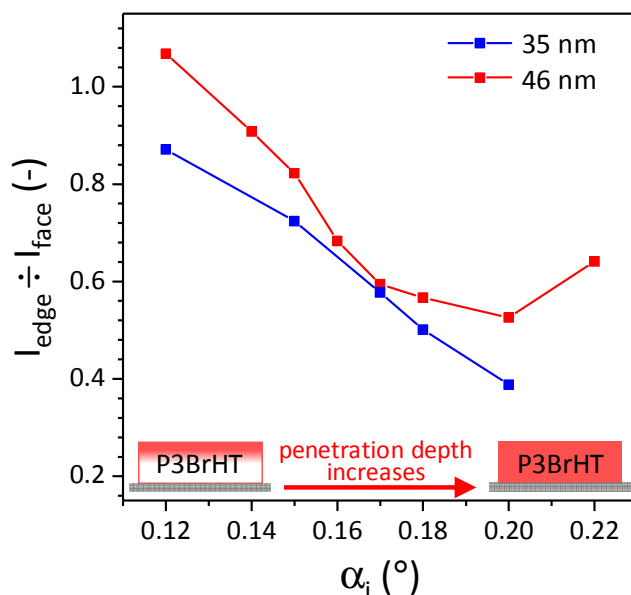


**Figure 6.** Ratio of intensities  $I_{edge}/I_{face}$  of the (200) reflection scattered from edge-on and face-on crystals in 35 nm (blue squares) and 46 nm (red squares) thin P3BrHT on graphene as a function of angle of incidence  $\alpha_i$ . The blue and red connecting lines are a guide to the eye. The ratio  $I_{edge}/I_{face}$  was calculated from the corresponding pole figures (see Figure S5 in Supplementary Information) of (200) reflection of 35 and 46 nm thin P3BrHT on graphene.

The determination of the crystal lattice of P3BrHT and subsequent indexing of crystal peaks was performed in our previous publication.<sup>35</sup> Here we would just like to note that according to the previous analysis, only (200) reflection on meridian and (020) reflection on equator belong to edge-on crystals, whereas all other crystal reflections are scattered from the well-ordered face-on oriented crystal structure. To confirm that the edge-on oriented crystals in thicker P3BrHT films originate also from the top surface, we carried out the analogous to P3HT surface-sensitive WAXS measurements on 35 and 46 nm thin P3BrHT films at various incident angles. The analysis of the crystal orientation distribution was performed on the basis of pole figures of the (200) reflection (see Figure S5 in Supplementary Information), since it is the most intense reflection in Figures 5c,e. The integration of the (200) reflection intensity followed the same procedure described above for P3HT, with a difference in the integration range that amounted  $q = 6.6 - 7.8 \text{ nm}^{-1}$ . The ratio  $I_{edge}/I_{face}$  of the

intensities corresponding to edge-on and face-on oriented crystals is given in **Figure 6** as a function of incident angle  $\alpha_i$ . As can be seen from the dependence in Figure 6, the fraction of edge-on oriented crystals in both P3BrHT films increases in the top layer of the film. Hence, it can be concluded that the edge-on crystals form at the interface of P3BrHT to vacuum, analogously to the behaviour observed for P3HT and the model in Figure 1. Consequently, we conclude that although Br-substitution of methyl end group on side chains suppresses the surface freezing in P3BrHT, it is not eliminated completely. Recalling that the orientation dependent interfacial energies control the surface freezing, the latter experimental outcomes in Figure 6 can imply that the interfacial energy difference  $\Delta\gamma_{s,fr}$  has been reduced in comparison with P3HT but still larger than zero and high enough to cause the surface freezing.

**Surface morphology of P3HT and P3BrHT films on graphene.** The surface morphology of P3BrHT films with thickness 21 and 35 nm on graphene was studied with peak force atomic force microscopy (AFM). The corresponding height and adhesion images shown in Figure 7 indicate that in both samples P3BrHT forms lamellar crystals. It is evident that the change of lamellae size with increasing film thickness is pronounced and drastic. According to our WAXS results, the thinner of two films possesses only face-on crystals, while 35 nm P3BrHT film has mixed crystal orientation with edge-on crystals at the top surface. Based on the chemical similarity between two semiconducting polymers, it could be fair to assume that the main

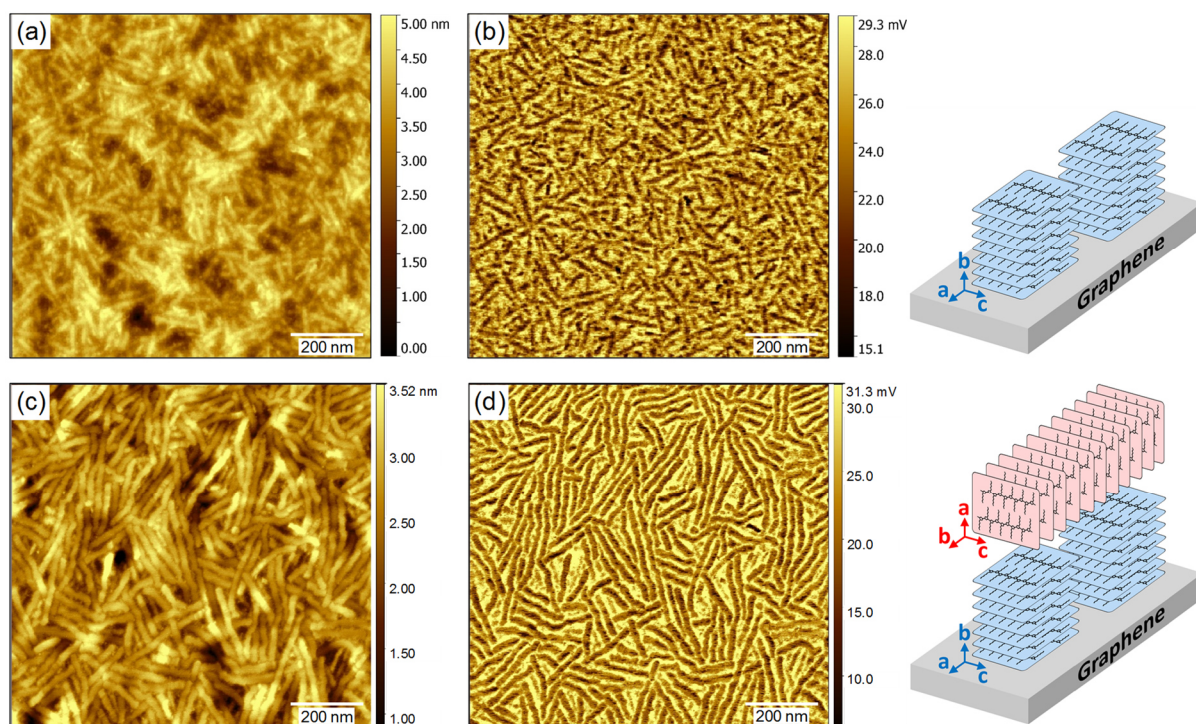


**Figure 7.** AFM height (a,c) and adhesion (b,d) images of P3BrHT films of thickness 21 nm (a,b) and 35 nm (c,d) on graphene. The size of images is same allowing a direct comparison of the lamellae size.

interaction responsible for crystallization in P3BrHT is intra- and interchain  $\pi$ - $\pi$  stacking formation, analogous to P3HT.<sup>5,33</sup> Since b crystal axis is the longest crystal axis in P3HT,<sup>5,33</sup> we can presume that the longest axis of P3BrHT lamellae also lies along the b axis of the crystals, which is the direction of  $\pi$ - $\pi$  stacking. It is then expected that the edge-on oriented lamellae have their b axis parallel to the film surface, whereas the b axis of the face-on lamellae is normal to the surface, as schematically illustrated in Figure 1 and in the corresponding sketches in **Figure 7**. Thus, the change of lamellae size at the top surface of the films with increasing film thickness is consistent with the change of the crystal orientation, as revealed by WAXS results in Figure 6, and supports our previous conclusions on the molecular alignment in polythiophenes summarized in Figure 1.

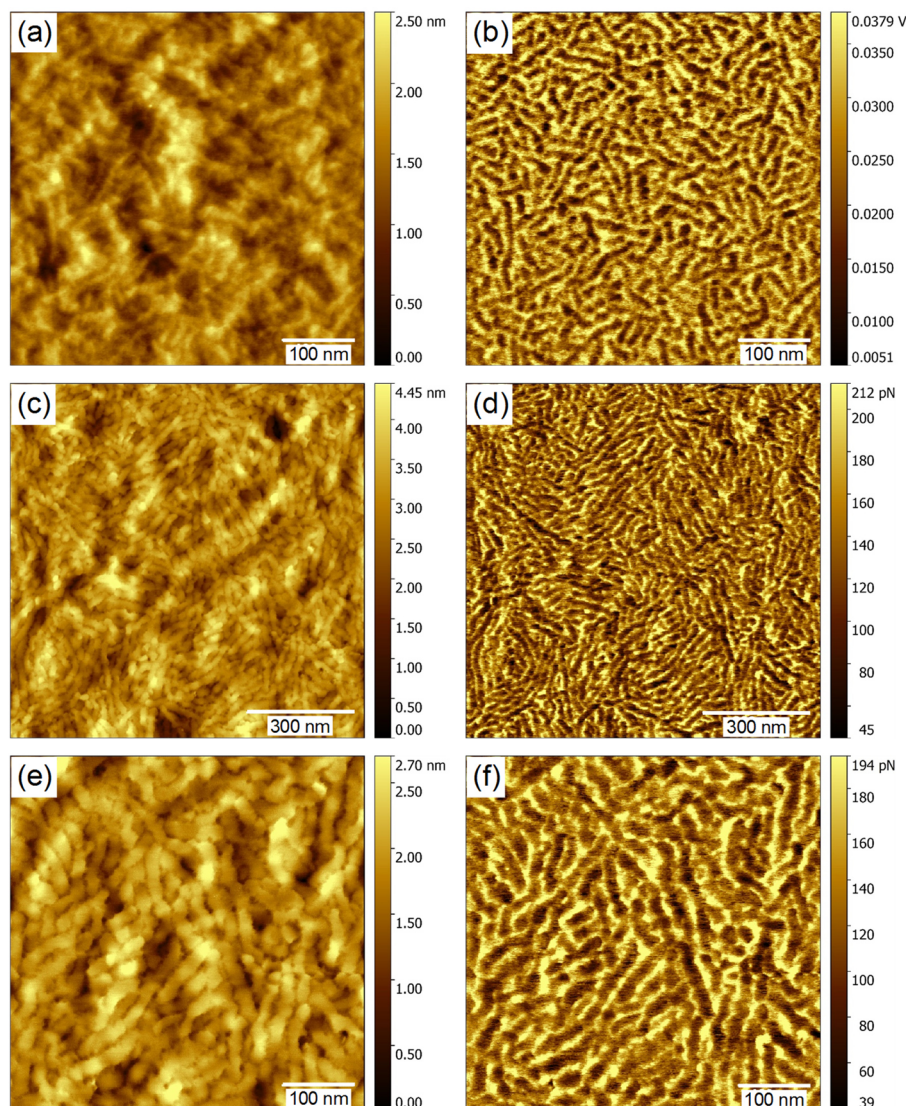


**Figure 8.** AFM height (a,c,e) and adhesion (b,d,f) images of P3HT films of thickness 31 nm (a,b) and 45 nm (c–f) on graphene. The size of images (a,b) and (e,f) is same allowing a direct comparison of the lamellae size.

The morphology of P3HT crystals at the top surface of films with thickness 31 and 45 nm can be seen in **Figure 8**. Comparison of the size of features visible in Figures 8a,b and 8e,f suggests that, unlike the results for P3BrHT above, no drastic change of lamellae length is observed for P3HT, which is in accordance with the WAXS results in Figures 2c,e and 3. A closer inspection, however, reveals that a bit thicker lamellae were formed in the thicker P3HT film. The observed increasing thickness of lamellae can presumably point at decreasing competition of different interfacial

orientations at the top surface with increasing film thickness. Indeed, although the fraction of edge-on crystals is highest at the top surface according to the results in Figure 4, a certain amount of face-on crystals was still observed even at the smallest incident angles probed the top surface of the corresponding P3HT films. Hence, we can assume that the competition of different crystal orientations occurred in the top layer of thin P3HT films as well and could hinder the growth of interfacial lamellar crystals. Consequently, the reduced or even vanished competition of orientations at the top surface of thicker films would imply a less hindered growth of edge-on lamellae and, as such, would result in an increased lamellar thickness. Moreover, the corresponding pole figures in Figure S2 in Supplementary Information showed the increasing amount of P3HT non-oriented crystals with increasing film thickness. According to our model of P3HT crystallization, such non-oriented crystals might have formed in-between the top edge-on and down face-on crystals as a result of the limited correlation length of two crystal orientations. Note that the thickness of crystalline layer formed during both prefreezing and surface freezing increases with decreasing temperature and diverges at the bulk melting point.<sup>10,27–32</sup> Cooling below the melting temperature with a rate faster than the crystal growth rate may result in multiple crystal nucleation events occurring in the residual melt and, consequently, in a loss of crystal orientation. We hypothesize that the latter can be a possible reason for the observed limited correlation length of face-on and edge-on crystals in thin P3HT films on graphene.

## DISCUSSION

In this work, a fundamental question of what determines the crystal orientation in thin films of polythiophenes was addressed. Based on the previous experimental results, we here assumed that while the vacuum interface induces surface freezing of P3HT with edge-on oriented crystals, the graphene surface causes prefreezing of P3HT chains and, thus, results in their face-on molecular alignment. To test this hypothesis, the crystal orientation in thin films of model semiconducting polymer P3HT and its derivative P3BrHT crystallized from the melt on a single layer graphene substrate was studied. The obtained results confirmed that P3HT on graphene has mixed edge-on and face-on crystal orientation. By using surface-sensitive grazing incidence WAXS, we were able to show that while face-on crystals appear at the interface to graphene, edge-on crystals are formed at the interface of P3HT to vacuum. It was observed that the mixed crystal orientation of P3HT is retained in films of various thickness, even as thin as 4-5 nm. The detected formation of P3HT edge-on crystals at the top film surface conform to the results of early studies of P3HT molecular orientation on SiO<sub>2</sub>/Si.<sup>26</sup> In view of the substrate and film thickness independence of the appearance of edge-on crystal orientation, we conclude that it is as a consequence of P3HT crystallization at the interface to vacuum. Hence, the mixed crystal orientation of P3HT on graphene results from competing interfacial orientations induced, on the one hand, by prefreezing of P3HT on graphene and, on the other hand, by surface freezing of P3HT chains to vacuum. According to the existing knowledge on surface freezing, the interfacial energy difference  $\Delta\gamma_{s,fr} = \gamma_{liq,vac} - (\gamma_{cry,vac} + \gamma_{cry,liq})$  is the driving force for the phenomenon and, as such, plays a key role in controlling it.

In order to suppress P3HT surface freezing and, consequently, the formation of edge-on crystals, we substituted the methyl end groups of P3HT side chains with more polar Br, expecting higher surface energies and lower  $\Delta\gamma_{s,fr}$ . The crystal orientation in the resultant polymer P3BrHT was studied in films of various thickness on graphene. It was evidenced that P3BrHT films with thickness up to about 26 nm have only face-on oriented crystals. Thus, we have tested the hypothesis of P3HT surface freezing and showed that indeed it can be inhibited by increasing polarity of end groups of polythiophene side chains. However, P3BrHT films with thickness higher than 26 nm on graphene exhibited the mixed crystal orientation with edge-on crystals formed at the top film surface, similarly to P3HT. The corresponding AFM study of the crystal morphology showed the pronounced change in size of lamellar crystals for thicker P3BrHT films, thus supporting the conclusions of the crystal orientation change obtained by grazing incidence WAXS. Hence, it can be concluded that although surface freezing of P3BrHT was hindered, it was not fully eliminated. It is worth mentioning that an alternative crystallization path, heterogeneous nucleation of liquids, fails to explain the observed behaviour of both P3HT and P3BrHT on graphene. According to classical nucleation theory, a foreign surface can reduce the energy barrier for crystal nucleation and result in an increased nucleation rate, which is proportional to the contact area.<sup>38</sup> For all our samples, the areas of both interfaces to graphene and vacuum were kept isometric. As such, if both interfaces induced crystallization of P3BrHT via heterogeneous nucleation, the appeared crystal nuclei would result in different crystal orientations for the samples of different thickness. As P3BrHT with thickness up to 26 nm shows a uniform face-on crystal alignment, which shifts to the mixed crystal orientation for just 10 nm thicker films, the described alternative scenario of heterogeneous nucleation becomes unlikely. We hypothesize

that the observed effects of surface freezing suppression can be enhanced by further modification of either P3HT side chains or its backbone. A direct experimental observation of P3HT surface freezing would be advantageous at this stage. Moreover, it should be emphasized that determination of surface energies, which are hardly accessible in experiments, of both investigated polymers could shed light on surface freezing and, therefore, pave the way to a complete face-on crystal orientation. It is expected that the latter will help to largely improve the efficiency of organic photovoltaics. Finally, we would like to stress that the presented results have a broad scientific relevance and are not limited to polythiophenes only. Indeed, here we were able to elucidate the important aspects of how side chain engineering can affect interfacial interactions and crystal orientation in thin films of polymers crystallized on solid surfaces. Since side chain engineering is a general widely used tool in improving material solubility and processing, the obtained results retain the relevance for many other functional macromolecules with side chain architecture subjected to various thin film applications in organic electronics and beyond.

## METHODS

**Materials.** P3HT was purchased from BASF SE ( $M_n = 15.6 \text{ kg}\cdot\text{mol}^{-1}$ ,  $D = 1.6$ , measured with size-exclusion chromatography with tetrahydrofuran (THF) as eluent and a polystyrene calibration). The monomer 3-(6-bromohexyl) thiophene was synthesized according to a published procedure.<sup>39</sup> All other chemicals were purchased by Sigma Aldrich or Fischer Scientific and used as received. The polymer P3BrHT was synthesized via Kumada catalyst transfer polymerization with *t*-butyl magnesium chloride (1.7 M in THF) and di-chloro[1,3-bis(diphenylphosphino)propane] Ni(dppp)Cl<sub>2</sub> as catalyst according to the published procedures ( $M_n = 13 \text{ kg}\cdot\text{mol}^{-1}$ ,  $D = 1.08$ ).<sup>40,41</sup> Both polymers, P3HT and P3BrHT, were purified via Soxhlet extraction using methanol, hexane, and chloroform, respectively. The chloroform fraction of the polymers was concentrated and precipitated in methanol to get the polymer powders.

A single-layer graphene on the ultra-flat SiO<sub>2</sub> substrates produced by Ted Pella, Inc. were purchased from PLANO GmbH (Wetzlar, Germany). The graphene sheets cover the 5x5 mm<sup>2</sup> diced substrate. According to Ted Pella, Inc., the ultra-flat SiO<sub>2</sub> substrates consist of a 200 nm thermally grown SiO<sub>2</sub> film on an ultra-flat silicon wafer with a thickness of 675  $\mu\text{m}$ .

**Thin film preparation.** Thin films of semiconducting polymers were prepared by spin coating a solution of P3HT and P3BrHT in chloroform on graphene substrates at 2000 rpm for 60 s at room temperature. The concentration of polymers in the solvent was varied from 0.06 wt% to 0.6 wt% to prepare the thin films with different thicknesses. The spin coated films were placed in a vacuum oven, heated to 285 °C for P3HT and 157 °C for P3BrHT, which are above their melting points, for 5 min and then slowly cooled down ( $\approx 1 \text{ }^\circ\text{C}\cdot\text{min}^{-1}$ ) to room temperature. The film thickness was

determined with the X-ray reflectivity for the films on 10x10 mm<sup>2</sup> SiO<sub>2</sub>/Si substrates prepared from the same solutions with various concentrations (see Table 1 in Supplementary Information).

**X-ray diffraction.** The WAXS experiments were performed using a SAXSLAB laboratory setup (Retro-F) (Copenhagen, Denmark) equipped with an AXO microfocus X-ray source (Dresden, Germany) and an AXO multilayer X-ray optics (ASTIX) as a monochromator for Cu-K $\alpha$  radiation ( $\lambda = 0.15418$  nm). A DECTRIS PILATUS3 R 300K detector (Daettwil, Switzerland) was used to record the 2D WAXS patterns. The measurements were performed in reflection geometry in vacuum at room temperature, and the sample to detector distance was around 89 mm. The incidence angle  $\alpha_i$  varied between 0.11° and 10°. The grazing incidence WAXS patterns at  $\alpha_i = 0.11 - 0.22^\circ$ , which is below the critical angle of SiO<sub>2</sub>  $\alpha_c^{SiO_2} \approx 0.24^\circ$  for Cu-K $\alpha$  radiation, were collected to observe all possible in-plane and out-plane reflections. The gradual variation of  $\alpha_i$  below the critical angles of the polymers  $\alpha_c^{P3HT} \approx 0.165^\circ$  and  $\alpha_c^{P3BrHT} \approx 0.174^\circ$ , which were determined from the X-ray reflectivity, resulted in gradually varied penetration depth of X-rays and, hence, allowed to study the crystal orientation in a film as a function of the penetration depth.<sup>26,36,37</sup> The higher incidence angles around 4 – 4.5° and 10° were used to visualize reflections at high  $q$  values perpendicular or nearly perpendicular to the graphene substrates. The detector images were converted into the reciprocal space map of scattering patterns with two components,  $q_z$  and  $q_r$ , being perpendicular and parallel to the sample surface, respectively.<sup>26</sup> On account of the special geometry of measurements, a certain area of the reciprocal space along the  $q_z$  axis was not accessible and appeared as a blank arc. Two additional blank vertical strips arose at

the positions where two of three adjacent parts of the detector meet, and were inactive regions of the detector.

**Atomic force microscopy (AFM).** AFM images were recorded in peak force tapping mode using a Bruker MultiMode 8 AFM with a Nanoscope V controller equipped with a ScanAsyst–Fluid+ cantilever ( $f_0 = 150$  kHz,  $k = 0.7$  Nm<sup>-1</sup>) purchased from Bruker. The cantilever was operated at the excitation frequency of 2 kHz. For the discussion of the surface morphology, the height and adhesion images were used. Adhesion images are a measure of the adhesive forces between the tip and the sample surface during tapping. An open-source software Gwyddion was used to edit and analyze the AFM images.<sup>42</sup>

## REFERENCES

- (1) Organic and Biological Optoelectronics; Rentzepis, P. M., Ed.; University of California, Irvine: Irvine, CA, 1993, pp 1–260.
- (2) Schopf, G.; Kossmehl, G. Polythiophenes – electrically conductive polymers. *Adv. Polym. Sci.* **1997**, 129, 1.
- (3) Handbook of Oligo- and Polythiophenes; Fishou, D., Ed.; Wiley VCh: New York, 1998.
- (4) Roncali, J. Conjugated poly(thiophenes): synthesis, functionalization, and applications. *J. Chem. Rev.* **1992**, 92, 711.
- (5) P3HT revisited – From molecular scale to solar cell; Ludwigs, S. Ed.; Springer: 2014, pp 1–232.
- (6) Liu, Y.; Zhao, J.; Li, Z.; Mu, C.; Ma, W.; Hu, H.; Jiang, K.; Lin, H.; Ade, H.; Yan, H. Aggregation and morphology control enables multiple cases of high-efficiency polymer solar cells. *Nature Communications* **2014**, 5, 5293.
- (7) Xu, T.; Yu, L. How to design low bandgap polymers for highly efficient organic solar cells. *Mater. Today* **2014**, 17 (1), 11–15.
- (8) Löhmann, A.-K.; Henze, T.; Thurn-Albrecht, T. Direct Observation of Prefreezing at the Interface Melt-Solid in Polymer Crystallization. *Proc. Natl. Acad. Sci. U. S. A.* **2014**, 111 (49), 17368–17372.
- (9) Flieger, A.-K.; Schulz, M.; Thurn-Albrecht, T. Interface-Induced Crystallization of Polycaprolactone on Graphite via First-Order Prewetting of the Crystalline Phase. *Macromolecules* **2018**, 51 (1), 189–194.
- (10) Dolynchuk, O.; Tariq, M.; Thurn-Albrecht, T. Phenomenological theory of first-order prefreezing. *J. Phys. Chem. Lett.* **2019**, 10 (8), 1942–1946.
- (11) Bäuerle, P.; Fischer, T.; Bidlingmaier, B.; Stabel, A.; Rabe, J. P. Oligothiophenes—Yet Longer? Synthesis, Characterization, and Scanning Tunneling Microscopy Images of Homologous, Isomerically Pure Oligo(alkylthiophene)s. *Angew. Chem., Int. Ed. Engl.* **1995**, 34, 303–307.
- (12) Stabel, A.; Rabe, J. P. Scanning tunnelling microscopy of alkylated oligothiophenes at interfaces with graphite. *Synth. Met.* **1994**, 67, 47–53.
- (13) Stecher, R.; Gompf, B.; Muentner, J. R. S.; Effenberger, F. Monolayers of Functionalized Oligothiophenes on Graphite—STM Investigation of the Influence of Intermolecular Interactions on the Epitaxy. *Adv. Mater.* **1999**, 11, 927–931.
- (14) Azumi, R.; Mena-Osteritz, E.; Boese, R.; Benet-Buchholzd, J.; Bäuerle, P. J. The longest oligothiophene ever examined by X-ray structure analysis. *Mater. Chem.* **2006**, 16, 728–735.
- (15) Azumi, R.; Götz, G.; Debaerdemaeker, T.; Bäuerle, P. Coincidence of the Molecular Organization of  $\beta$ -Substituted Oligothiophenes in Two-Dimensional Layers and Three-Dimensional Crystals. *Chem. – Eur. J.* **2000**, 6, 735–744.
- (16) Gesquière, A.; Abdel-Mottaleb, M. M. S.; De Feyter, S.; De Schryver, F. C.; Schoonbeek, F.; van Esch, J.; Kellogg, R. M.; Feringa, B. L.; Calderone, A.; Lazzaroni, R.; Bre`das, J. L. Molecular Organization of Bis-urea Substituted Thiophene Derivatives at the Liquid/Solid Interface Studied by Scanning Tunneling Microscopy. *Langmuir* **2000**, 16 (26), 10385–10391.
- (17) Mena-Osteritz, E.; Meyer, A.; Langeveld-Voss, B. M. W.; Janssen, R. A. J.; Meijer, E. W.; Bäuerle, P. Two-Dimensional Crystals of Poly(3-Alkyl- thiophene)s: Direct Visualization of Polymer Folds in Submolecular Resolution. *Angew. Chem., Int. Ed.* **2000**, 39 (15), 2679–2684.
- (18) Keg, P.; Lohani, A.; Fichou, D.; Lam, Y. M.; Wu, Y.; Ong, B. S.; Mhaisalkar, S. G. Direct Observation of Alkyl Chain Interdigitation in Conjugated Polyquarterthiophene Self-Organized on Graphite Surfaces. *Macromol. Rapid Comm.* **2008**, 29 (14), 1197–1202.

- (19)Gus'kova, O. A.; Mena-Osteritz, E.; Schillinger, E.; Khalatur, P. G.; Bäuerle, P.; Khokhlov, A. R. Self-Assembled Monolayers of  $\beta$ -Alkylated Oligothiophenes on Graphite Substrate: Molecular Dynamics Simulation. *J. Phys. Chem. C* **2007**, 111 (19), 7165–7174.
- (20)Kim, D. H.; Lee, H. S.; Shin, H.-J.; Bae, Y.-S.; Lee, K.-H.; Kim, S.-W.; Choi, D.; Choi, J.-Y. Graphene surface induced specific self-assembly of poly(3-hexylthiophene) for nanohybrid optoelectronics: from first-principles calculation to experimental characterizations. *Soft Matter* **2013**, 9 (22), 5355–5360.
- (21)Skrypnichuk, V.; Boulanger, N.; Yu, V.; Hilke, M.; Mannsfeld, S. C. B.; Toney, M. F.; Barbero, D. R. Enhanced Vertical Charge Transport in a Semiconducting P3HT Thin Film on Single Layer Graphene. *Adv. Funct. Mater.* **2015**, 25 (5), 664–670.
- (22)Skrypnichuk, V.; Wetzelaer, G.-J. A. H.; Gordiichuk, P. I.; Mannsfeld, S. C. B.; Herrmann, A.; Toney, M. F.; Barbero, D. R. Ultrahigh Mobility in an Organic Semiconductor by Vertical Chain Alignment. *Adv. Mater.* **2016**, 28 (12), 2359–2366.
- (23)Skrypnichuk, V.; Boulanger, N.; Yu, V.; Hilke, M.; Toney, M. F.; Barbero, D. R. Reduced crystallinity and enhanced charge transport by melt annealing of an organic semiconductor on single layer graphene. *J. Mater. Chem. C* **2016**, 4 (19), 4143–4149.
- (24)Boulanger, N.; Yu, V.; Hilke, M.; Toney, M. F.; Barbero, D. R. In situ probing of the crystallization kinetics of rr-P3HT on single layer graphene as a function of temperature. *Phys. Chem. Chem. Phys.* **2017**, 19 (12), 8496–8503.
- (25)Boulanger, N.; Yu, V.; Hilke, M.; Toney, M. F.; Barbero, D. R. Graphene induced electrical percolation enables more efficient charge transport at a hybrid organic semiconductor/graphene interface. *Phys. Chem. Chem. Phys.* **2018**, 20 (6), 4422–4428.
- (26)Balko, J.; Portale, G.; Lohwasser, R. H.; Thelakkat, M.; Thurn-Albrecht, T. Surface induced orientation and vertically layered morphology in thin films of poly(3-hexylthiophene) crystallized from the melt. *J. Mater. Res.* **2017**, 32 (10), 1957–1968.
- (27)Wu, X. Z.; Ocko, B. M.; Sirota, E. B.; Sinha, S. K.; Deutsch, M.; Cao, B. H.; Kim, M. W. Surface tension measurements of surface freezing in liquid normal alkanes. *Science* **1993**, 261, 1018–1021.
- (28)Ocko, B. M.; Wu, X. Z.; Sirota, E. B.; Sinha, S. K.; Gang, O.; Deutsch, M. Surface freezing in chain molecules: Normal alkanes. *Phys. Rev. E: Stat. Phys., Plasmas, Fluids, Relat. Interdiscip. Top.* **1997**, 55, 3164–3182.
- (29)Gautam, K. S.; Dhinojwala, A. Melting at alkyl side chain comb polymer interfaces. *Phys. Rev. Lett.* **2002**, 88, 145501.
- (30)Gautam, K. S.; Kumar, S.; Wermeille, D.; Robinson, D.; Dhinojwala, A. Observation of novel liquid-crystalline phase above the bulk-melting temperature. *Phys. Rev. Lett.* **2003**, 90, 215501.
- (31)Gang, O.; Wu, X. Z.; Ocko, B. M.; Sirota, E. B.; Deutsch, M. Surface freezing in chain molecules. II. Neat and hydrated alcohols. *Phys. Rev. E: Stat. Phys., Plasmas, Fluids, Relat. Interdiscip. Top.* **1998**, 58, 6086–6100.
- (32)Prasad, S.; Jiang, Z.; Sinha, S.K.; Dhinojwala, A. Partial crystallinity in alkyl side chain polymers dictates surface freezing. *Phys. Rev. Lett.* **2008**, 101, 065505.
- (33)Zen, A.; Saphiannikova, M.; Neher, D.; Grenzer, J.; Grigorian, S.; Pietsch, U.; Asawapirom, U.; Janietz, S.; Scherf, U.; Lieberwirth, I.; Wegner, G. Effect of Molecular Weight on the Structure and Crystallinity of Poly(3-hexylthiophene). *Macromolecules* **2006**, 39 (6), 2162–2171.
- (34)Balko, J.; Lohwasser, R.H.; Sommer, M.; Thelakkat, M.; Thurn-Albrecht, T. Determination of the crystallinity of semicrystalline poly(3-hexylthiophene) by means of wide-angle X-ray scattering. *Macromolecules* **2013**, 46, 9642–9651.
- (35)Schmode, P.; Schötz, K.; Dolynchuk, O.; Panzer, F.; Köhler, A.; Thurn-Albrecht, T.; Thelakkat, M. Influence of  $\omega$ -bromo substitution on structure and opto-electronic properties of homopolymers and gradient copolymers of 3-hexylthiophene. *Macromolecules* **2020**, *accepted*.

- (36)Factor, B. J.; Russell, T. P.; Toney, M. F. Grazing-incidence X-ray-scattering studies of thin-films of an aromatic polyimide. *Macromolecules* **1993**, *26*, 2847–2859.
- (37)Breiby, D.W.; Bunk, O.; Andreasen, J.W.; Lemke, H.T.; Nielsen, M.M. Simulating X-ray diffraction of textured films. *J. Appl. Crystallogr.* **2008**, *41*, 262–271.
- (38)Sear, R. Nucleation: theory and applications to protein solutions and colloidal suspensions. *J. Phys.: Condens. Matter* **2007**, *19*, No. 033101.
- (39)Zhai, L.; Pilston, R. L.; Zaiger, K. L.; Stokes, K. K.; McCullough, R. D. A Simple Method to Generate Side-Chain Derivatives of Regioregular Polythiophene via the GRIM Metathesis and Post-Polymerization Functionalization. *Macromolecules* **2003**, *36* (1), 61–64.
- (40)Lohwasser, R. H.; Thelakkat, M. Toward Perfect Control of End Groups and Polydispersity in Poly(3-Hexylthiophene) via Catalyst Transfer Polymerization. *Macromolecules* **2011**, *44* (9), 3388–3397.
- (41)Brendel, J. C.; Schmidt, M. M.; Hagen, G.; Moos, R.; Thelakkat, T. Controlled Synthesis of Water-Soluble Conjugated Polyelectrolytes Leading to Excellent Hole Transport Mobility. *Chem. Mater.* **2014**, *26*, 6, 1992–1998.
- (42)Nečas, D.; Klapetek, P. Gwyddion: an open-source software for SPM data analysis. *Cent. Eur. J. Phys.* **2012**, *10* (1), 181–188.

### Supplementary Information

**Table 1.** Dependence of film thickness on P3HT and P3BrHT concentration in chloroform. The films were produced by spin coating the respective solutions on SiO<sub>2</sub>/Si substrates at 2000 rpm for 60 s at room temperature. The film thickness was measured with the X-ray reflectivity.

Concentration (wt%)	Film thickness (nm)	
	P3HT	P3BrHT
0.06	4-5 <sup>1</sup>	–
0.25	31	21
0.35	45	26
0.48	–	35
0.6	≈100	46

<sup>1</sup> As the X-ray reflectivity curve of the thinnest P3HT film resulted in just a few interference fringes (Kissing fringes), the film thickness for this sample could not be determined as precise as for the rest of samples and amounted to about 4-5 nm.

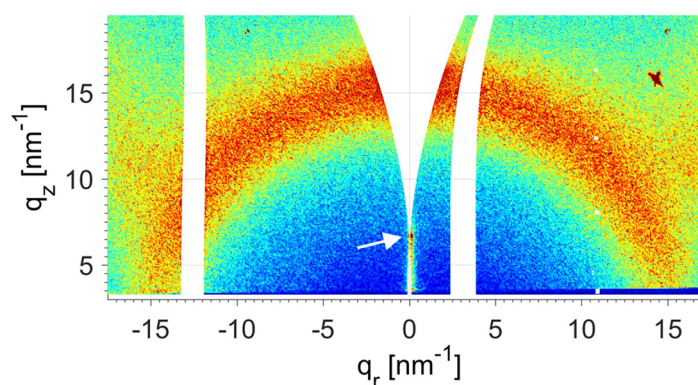


**Figure S1.** Reciprocal space map of the WAXS pattern of 21 nm thin PBr3HT on graphene measured at an incident angle of 4.5°. The white arrow points to the reflected beam position.

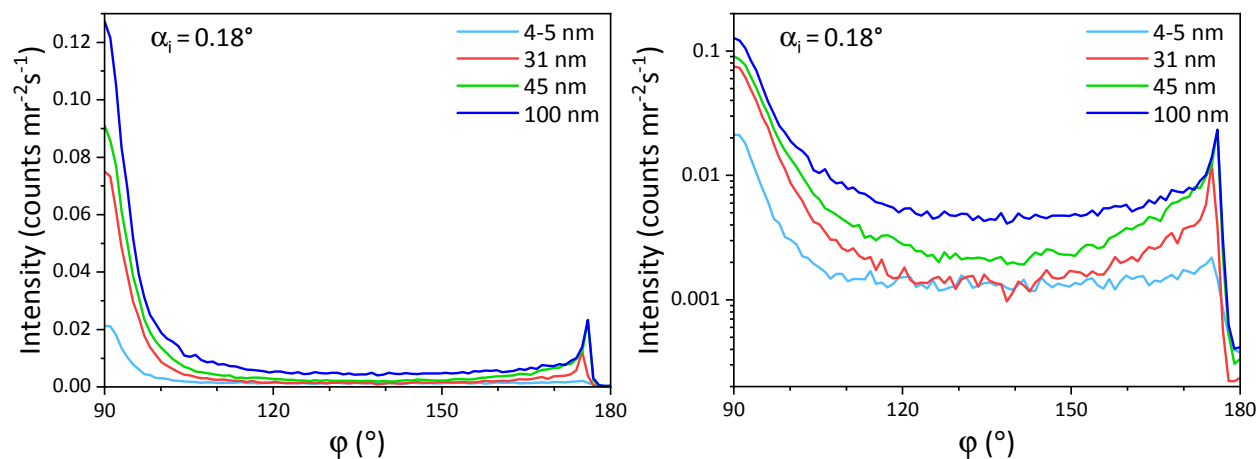


**Figure S2.** Pole figures of (100) reflection in linear (left) and logarithmic (right) scale of P3HT films of different thicknesses on graphene measured at angle of incidence  $\alpha_i = 0.18^\circ$ , which is above the critical angle of P3HT. The pole figures were extracted directly from the measured scattering patterns (Figures 2a and 3a,c,e in the main text) by integrating the intensity over the range  $q = 3.2 - 4.4 \text{ nm}^{-1}$  of the (100) reflection. The corresponding film thickness is given in each plot.

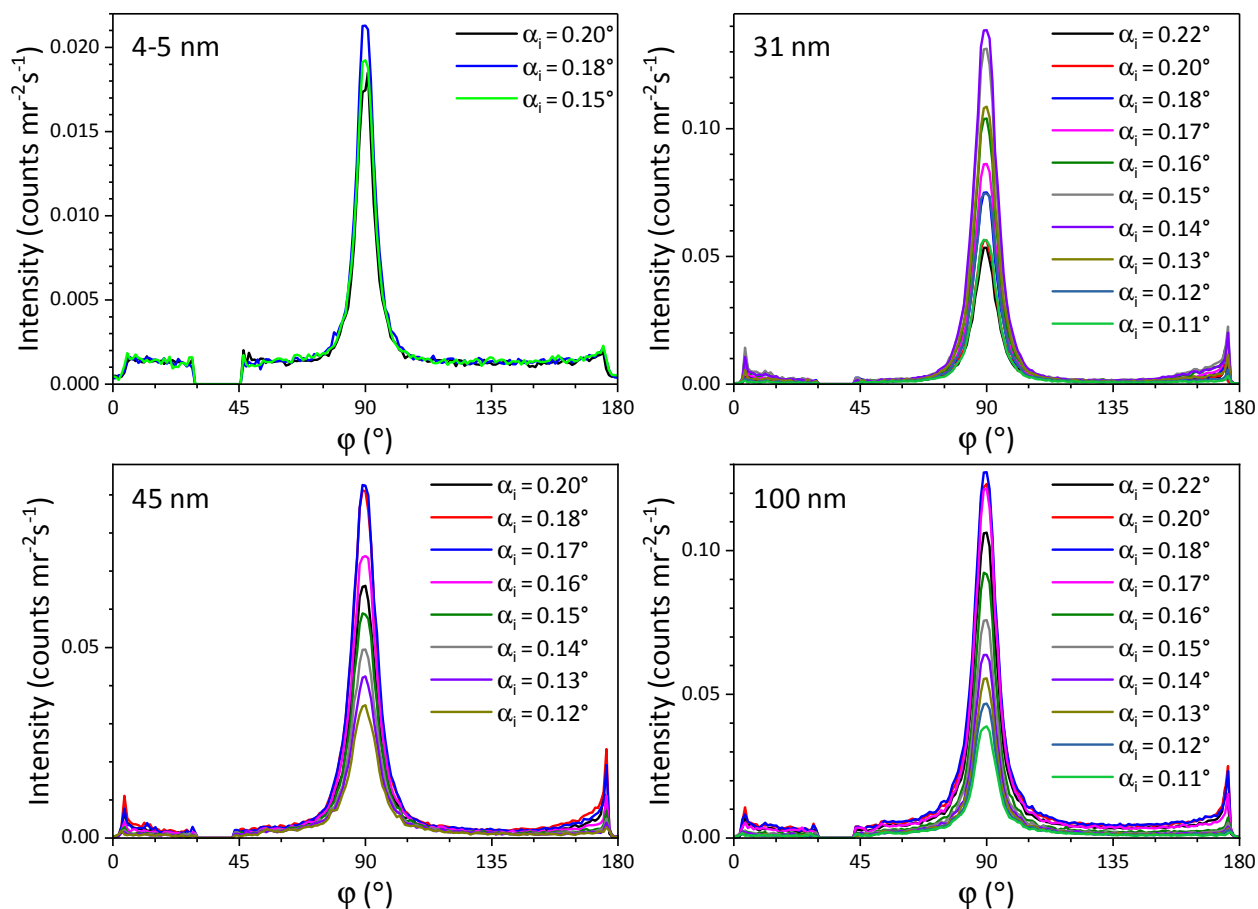


**Figure S3.** Pole figures of (100) reflection of P3HT films of different thicknesses on graphene for various angles of incidence  $\alpha_i$  above and below the critical angle of P3HT. The pole

figures were extracted directly from the measured scattering patterns by integrating the intensity over the range  $q = 3.2 - 4.4 \text{ nm}^{-1}$  of the (100) reflection. The corresponding film thickness is given in each plot.

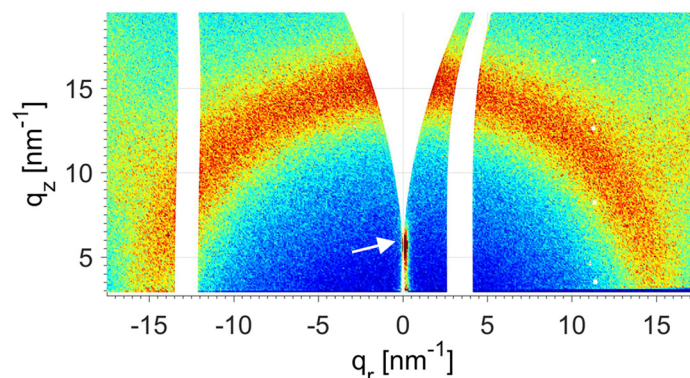


**Figure S4.** Reciprocal space map of the WAXS pattern of 26 nm thin PBr3HT on graphene measured at an incident angle of  $4^\circ$ . The white arrow points to the reflected beam position.

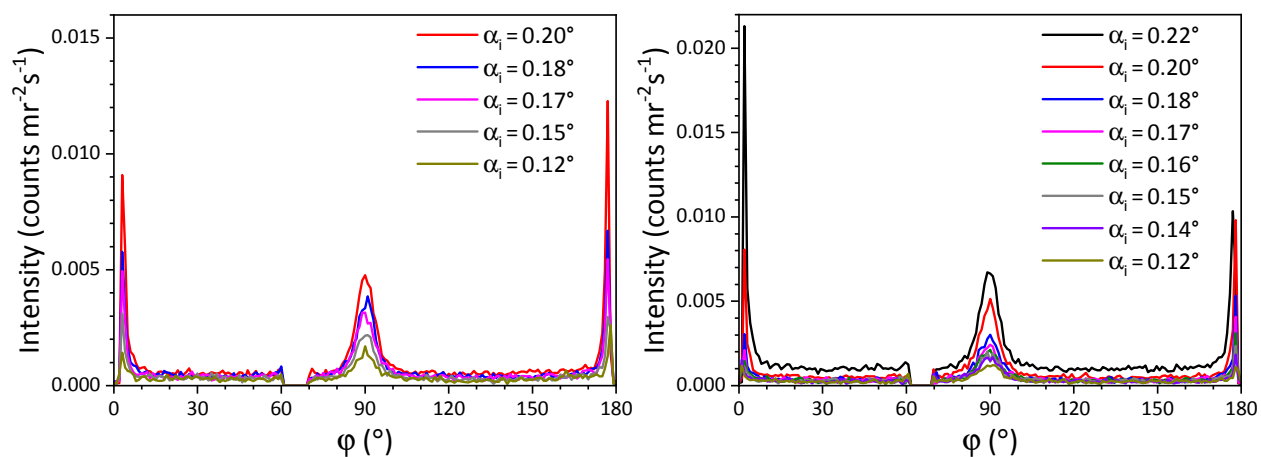


**Figure S5.** Pole figures of (200) reflection of 35 nm (left) and 46 nm (right) thin P3BrHT on graphene for various incident angles  $\alpha_i$  above and below the critical angle of P3BrHT. The pole figures were extracted directly from the measured scattering patterns by integrating the intensity over the range  $q = 6.6 - 7.8 \text{ nm}^{-1}$  of the (200) reflection.

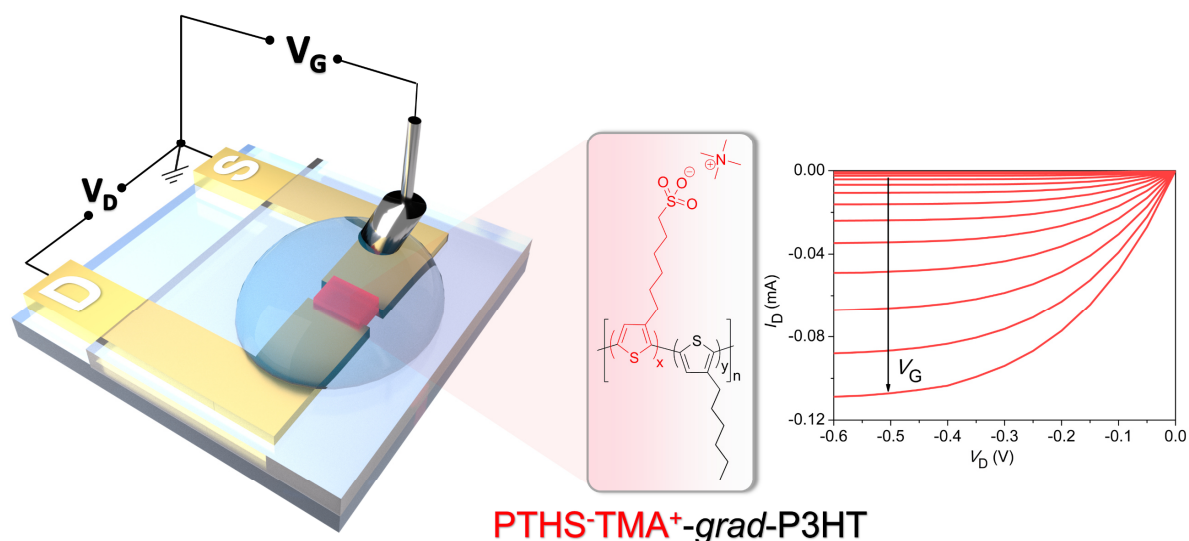
# Chapter 6:

## High Performance Organic Electrochemical Transistors Based on Conjugated Polyelectrolyte Copolymers

Philip Schmode <sup>†</sup>, David Ohayon <sup>‡</sup>, Paul M. Reichstein <sup>†</sup>, Achilleas Savva <sup>‡</sup>, Sahika Inal <sup>\* ‡</sup> and Mukundan Thelakkat <sup>\* †§</sup>

<sup>†</sup>Applied Functional Polymers, Department of Macromolecular Chemistry I and <sup>§</sup>Bavarian Polymer Institute, University of Bayreuth, Universitätsstr. 30, 95440 Bayreuth, Germany

<sup>‡</sup> Biological and Environmental Science and Engineering, King Abdullah University of Science and Technology (KAUST), Thuwal 23955-6900, Saudi Arabia



Reproduced with permission from *Chem. Mater.* **2019**, *31* (14), 5286–5295.

Copyright 2019 American Chemical Society

## ABSTRACT

A new generation of polythiophene-based polyelectrolytes are reported to address fundamental issues in an organic electrochemical transistor (OECT). In such devices, the semiconductor must be able to transport and store ions and to possess simultaneously a very high electronic mobility. For this, the ion-conducting 6-(thiophen-3-yl) hexane-1-sulfonate tetramethyl ammonium monomer (THS-TMA<sup>+</sup>) is copolymerized with the hole-conducting 3-hexylthiophene (3HT) to obtain copolymers, PTHS-TMA<sup>+</sup>-co-P3HT 1-3 with a gradient architecture. The copolymers having up to 50 mol% 3HT content are easily oxidizable and are crystalline. Consequently, for the copolymers, a higher stability in water is achieved, thus reducing the amount of cross-linker needed to stabilize the film. Furthermore, OECTs using copolymers with 75 and 50 mol% of PTHS-TMA<sup>+</sup> content exhibit 2-3 orders of magnitude higher ON/OFF ratio and an extremely lower threshold voltage (-0.15 V) compared to PTHS-TMA<sup>+</sup>. Additionally, high volumetric capacitance ( $C^* > 100 \text{ F/cm}^3$ ) is achieved, indicating that the ion transport is not hampered by the hydrophobic 3HT up to 50 mol%, for which a very high OECT hole mobility of  $0.017 \text{ cm}^2/\text{Vs}$  is also achieved. Thus, the concept of copolymerization to combine both ionic and electronic charge transport in an organic mixed conductor offers an elegant approach to obtain high performance OECT materials.

## 1. INTRODUCTION

Mixed conducting  $\pi$ -conjugated polymers are materials which can conduct both ions and electrons. Understanding the structure–property relationship of such organic mixed conductors is the key to developing new high-performance materials for modern applications.<sup>1</sup> This class of material is attractive for several applications that integrate solid or liquid electrolytes, such as thermoelectric devices,<sup>2</sup> electrochromic devices,<sup>3</sup> and organic electrochemical transistors (OECTs), which is a device configuration used for biosensing applications.<sup>4</sup> A class of polythiophenes that is widely studied for OECTs is PEDOT:PSS (poly(3,4-ethylenedioxythiophene):polystyrene sulfonate).<sup>5</sup> PEDOT:PSS consists of short PEDOT segments, which are p-doped by PSS of much higher molecular weight. It is synthesized in an uncontrolled manner and the short PEDOT oligomers already suffer from poor solubility, which makes it difficult to modify it synthetically. PEDOT:PSS is very suitable for depletion mode OECTs.<sup>5</sup> Another example is PEDOT-S, which consists of a PEDOT backbone, functionalized with an alkyl sulfonate side chain. This polymer or its blend with a conjugated polyelectrolyte was integrated into liposomes or lipid bilayers, enabling electronic conduction within the lipid membranes.<sup>6–8</sup> Current research is focused on developing new mixed conductors that show efficient electronic charge transport and can conduct and store ions simultaneously to improve the performance of such devices.<sup>5,9</sup> The focus has been on non-doped polymers, which are suitable for accumulation mode OECTs. P3HT constitutes the most widely studied p-type homopolymer for charge transport and structure formation both in solution and thin films. The crystallinity of P3HT strongly depends on the length of the polymer chain (optimum absolute molecular weight of around 12 kg/mol), therefore, also its ability to transport holes. Above this

molecular weight, chain folding takes place and the crystallinity and charge transport are affected negatively.<sup>10,11</sup> The synthesis of this polymer is of exceptional character due to its well-controlled chain growth mechanism utilizing Kumada catalyst-transfer polymerization (KCTP).<sup>12-15</sup> However, for application in biosensors, especially in OECTs that operate in aqueous media at gate voltages below 1 V, water compatibility, swelling, ion uptake, and high volumetric capacitance are additionally required. To achieve this, different polar derivatives of polythiophenes have been synthesized and tested in OECTs. The main strategy to obtain polar semiconducting polymers is to attach polar side chains to the  $\pi$ -conjugated polymer backbone, to facilitate ion uptake and transport within the polymer bulk, by maintaining the desired charge transport properties of conjugated polymers.<sup>16</sup> For example, polythiophene derivatives, equipped with ethylene glycol chains have shown promising performance in OECTs, due to their good ion transport and storage, combined with their high electronic charge transport properties. One example was reported by GIOVANNITTI ET AL. who synthesized the copolymer poly(2-(3,3'-bis(2-(2-(2-methoxyethoxy)ethoxy)ethoxy)-[2,2'-bithiophen]5-yl)thieno [3,2-b]thiophene), p(g2T-TT), via Stille polycondensation. So far, this material shows the best compromise between high electronic and ionic transport.<sup>16</sup> A compromise is needed since the ion conduction requires hydration and swelling of the polymer in aqueous media, whereas efficient electron transport is generally observed in highly crystalline hydrophobic conjugated polymers. Thus, designing a conjugated polymer with balanced ion and charge carrier transport is one of the biggest challenges in polymer science.<sup>1,9</sup>

Another class of non-doped polar semiconductors suitable for bioelectronics comprises conjugated polyelectrolytes. We reported different derivatives of poly[6-

(thiophen-3-yl) hexane-1-sulfonate tetraalkylammonium], PTHS-M<sup>+</sup> for the first time in 2014, where the thiophene is carrying extremely polar alkyl sulfonate groups as side chains and the counterion, M<sup>+</sup>, is the tetraalkylammonium.<sup>17</sup> PTHS-M<sup>+</sup> was obtained by a postpolymerization reaction of a precursor, which was polymerized in a well-controlled manner using KCTP. It showed good results toward a high ON current and high transconductance,  $g_m$ .<sup>18</sup> We could also show the importance of a controlled polymerization for this kind of conjugated polyelectrolytes.<sup>17</sup> Moreover, the influence of different M<sup>+</sup> cations on OECT properties was evaluated and we found the smallest tetramethylammonium (TMA<sup>+</sup>) to be the most suitable counterion.<sup>19</sup> However, the high solubility of the various PTHS-M<sup>+</sup> polyelectrolytes in polar or aqueous solvents entails difficulties during the OECT operation, because films delaminate upon exposure to water, necessitating the use of an external cross-linker.<sup>17,18</sup> However, this electrically insulating cross-linker dilutes the active material in the transistor channel and was shown, for the case of PEDOT:PSS, to enhance the water-stability of the film at the expense of its mixed (ionic and electronic) conductivity.<sup>20,21</sup> The drop in electrical conductivity upon inclusion of such crosslinkers stems from the changes in the film morphology.<sup>20,22</sup> Diligent choice of crosslinkers and optimization of their content have been proven to enhance both the electronic conductivity and mechanical stability of conjugated polymer films.<sup>23</sup> Furthermore, all of the PTHS-M<sup>+</sup> polyelectrolytes display a threshold voltage ( $V_{th}$ ) of around  $-0.5$  V in an OECT.<sup>18,19</sup> For biosensing applications where the recognition events lead to doping of the channel (that is, switching the transistor ON), materials with low  $V_{th}$  are desirable as at low external voltages applied, the devices consume less power, but also avoid possible Faradaic reactions that can take place in complex biological media rich with electroactive species and interfere with the device output. Here, we suggest a

solution to overcome the high-water solubility of PTHS-M<sup>+</sup> in general and to improve the relevant parameters in an OECT with the concept of copolymerization. In this work, we aimed at combining the best of both P3HT and PTHS-TMA<sup>+</sup> to take advantage of the above-mentioned features of each moiety that favor mixed conduction and to have polymers synthesized by well-controlled procedures such as KCTP. First, we synthesized three precursor copolymers, poly[3-(hexylthiophene)-co-3-(6-bromohexyl) thiophene], via KCTP with systematic variation in composition. Consequently, they were converted in a postpolymerization reaction to PTHS-TMA<sup>+</sup>-co-P3HT 1–3, containing the 3-hexylthiophene (3HT) moiety and the ion-conducting 6-(thiophen-3-yl) hexane-1-sulfonate tetramethylammonium (THS-TMA<sup>+</sup>) units. We investigated the structure in bulk via small angle X-ray scattering (SAXS) and aggregation properties in solution and thin films via UV–vis spectroscopy. Furthermore, we wanted to elucidate the structure–property relationship of these polymers considering their performance in OECTs. Besides characterizing the behavior of the polymers in microfabricated OECT channels, we determined their volumetric capacitance  $C^*$  via electrochemical impedance spectroscopy (EIS) as well as the OECT hole mobility from bandwidth measurements to probe mixed transport properties.<sup>24,25</sup> Also, the water uptake of the polymer films was investigated with a quartz crystal microbalance with dissipation monitoring (QCM-D). The overall analysis of the above parameters indicates the individual contributions of the P3HT and PTHS-TMA<sup>+</sup> moieties on mixed conduction properties and gives a blueprint to design novel polar conjugated polymers for OECTs by combining sufficient water compatibility and low threshold voltage with high capacitance and charge carrier transport.

## 2. EXPERIMENTAL SECTION

### 2.1. Materials

The monomers 3-(6-bromohexyl) thiophene 3BrHT and 3-(hexylthiophene) 3HT were synthesized according to the known procedures.<sup>26,27</sup> All other chemicals were purchased from Sigma-Aldrich or Fischer Scientific and used as received. The precursor copolymers poly[3-(6-bromohexyl)thiophene-co-3-(hexylthiophene)] P3BrHT-co-P3HT 1–3 were synthesized via Kumada catalyst-transfer polymerization with *t*-butyl magnesium chloride (1.7 M in tetrahydrofuran (THF)) and dichloro[1,3-bis-(diphenylphosphino)propane] Ni(dppp)Cl<sub>2</sub> as a catalyst according to the published procedures.<sup>26,28</sup>

*2.1.1. Synthesis of Bis(tetramethylammonium)sulfite.* 2.48 mL of dimethyl sulfite (27.2 mmol, 1 equiv) was slowly added to 21.8 mL of tetramethylammonium hydroxide solution (40 wt % in MeOH, 51.8 mmol, 1.9 equiv) while stirring. The salt solution was used without further purification. <sup>1</sup>H NMR: δ<sub>H</sub> (300 MHz; ppm, D<sub>2</sub>O): 3.30 (s, 12H).

*2.1.2. Synthesis of Poly[6-(thiophen-3-yl)hexane-1-sulfonate-co-3-(hexylthiophene)] Copolymers PTHS-TMA<sup>+</sup>-co-P3HT 1–3.* The precursor copolymers, P3BrHT-co-P3HT 1–3 (1 equiv), were dissolved in 30 mL of THF per 100 mg polymer at 40 °C and the mixture was degassed by a constant argon stream for 15 min. Bis-[tetramethylammonium] sulfite (1 M in MeOH, 10 equiv) was added and the mixture was kept at 40 °C for 4 h. Water was added, and the reaction mixture was dialyzed against Milli-Q water for purification. The solution was freeze-dried to yield a dark red solid. <sup>1</sup>H NMR: δ<sub>H</sub> (300 MHz; ppm, THF-d<sub>8</sub>/D<sub>2</sub>O): PTHS-TMA<sup>+</sup>-co-P3HT 2: 7.15 (s, 1H<sub>arom</sub>), 7.10 (s, 1H<sub>arom</sub>), 3.26 (s, 12H<sub>TMA</sub>), 2.86 (m, 6H), 1.98–0.78 (m, 18H).

## 2.2. Methods

2.2.1. *UV-Vis Spectroscopy.* UV-vis spectra were recorded on a Jasco V-670 spectrophotometer. All polymer solutions were measured at a concentration of 2 mg/mL. The spectra were recorded in quartz cuvettes with an internal diameter of 1 mm. The thin polymer films were spin-coated from methanol and from mixtures of methanol and THF on glass substrates.

2.2.2. *<sup>1</sup>H NMR.* Spectra were recorded in deuterated THF-d<sub>8</sub> and THF-d<sub>8</sub>/D<sub>2</sub>O on a Bruker Avance 250 spectrometer at 300 MHz at room temperature. Chemical shifts are noted in ppm and coupling constants in Hz. All spectra were calibrated according to the residual solvent peaks (THF-d<sub>8</sub>  $\delta$  = 3.58 ppm).

2.2.3. *Size Exclusion Chromatography (SEC).* SEC was performed on the precursor polymers P3HT-co-P3BrHT utilizing a Waters 515 HPLC pump and THF with 0.25 wt % tetrabutylammonium bromide as the eluent at a flow rate of 0.5 mL/min. A volume of 100  $\mu$ L of polymer solution (1–2 mg/mL) was injected with a 707 Waters autosampler into a column setup comprising a guard column (Agilent PLgel Guard MIXED-C, 5  $\times$  0.75 cm<sup>2</sup>, particle size 5  $\mu$ m) and two separation columns (Agilent PLgel MIXED-C, 30  $\times$  0.75 cm<sup>2</sup>, particle size 5  $\mu$ m). Polymer size distributions were monitored with a Waters 998 photodiode array detector at 254 nm and a Waters 414 refractive index detector. Narrowly distributed polystyrene standards were used for calibration and 1,2-dichlorobenzene as an internal reference.

2.2.4. *Matrix-Assisted Laser Desorption Ionization Spectroscopy with Time of Flight Detection Mass Spectroscopy Measurements (MALDI-ToF).* MALDI-ToF were performed with the precursor polymers P3HT-co-P3BrHT on a Bruker Reflex III mass spectrometer. For the copolymers, 1,8-dihydroxy-9,10-dihydroanthracen-9-one

(dithranol) was used as the matrix. The ratio of the mixture was 1000:1 (matrix/polymer).

*2.2.5. Photoelectron Spectroscopy in Air (PESA).* PESA measurements were recorded with a Riken Keiki AC-2 PESA spectrometer with a power setting of 20 nW and a power number of 0.3. Samples for PESA were prepared on glass substrates by spin-coating from a 10 mg/mL polymer solution.

*2.2.6. Small Angle X-ray Scattering (SAXS).* SAXS measurements were performed at a Double Ganehsa AIR purchased from SAXSLAB. A copper anode (MicoMax 007HF, Rigaku Corporation) was used as an X-ray source with an emission wavelength of  $\lambda = 0.154$  nm. Scattering intensity was recorded by a PILATUS 300 K detector in the scattering range from 0.0004 to 0.4 nm. The measurements were performed at room temperature and in 1 mm thick aluminum discs. The raw data were analyzed with the software SASfit and were corrected toward the background (air).

*2.2.7. Spectroelectrochemistry Measurements.* Thin films were prepared on indium tin oxide-coated glass substrates. For film preparation, PTHS-TMA<sup>+</sup>-co-P3HT 1 and 2 were mixed with the cross-linker (3-glycidylloxypropyl)trimethoxysilane (GOPS) (1 wt % PTHS-TMA<sup>+</sup>-co-P3HT 1, 2 + 0.5 wt % GOPS in methanol). The polymer films were cross-linked at 100 °C for 1.5 h. PTHS-TMA<sup>+</sup>-co-P3HT 3 films were spin-coated out of a MeOH/THF solution without the cross-linker because the copolymer is not water soluble. Measurements were carried out in 0.1 M aqueous NaCl solution using a UV-vis spectrometer (OceanOptics USB 2000+) integrated with an Ivium CompactStat potentiostat. A Pt mesh was used as the counter electrode and an

Ag/AgCl electrode as the reference electrode. The indicated voltages were applied versus VOC for 10 s until the current stabilized prior to the recording of the spectrum.

*2.2.8. Electrochemical Impedance Spectroscopy (EIS).* The electrochemical impedance spectra of polymer-coated electrodes ( $0.058 \text{ cm}^2$ ) were acquired using a Metrohm Autolab PGSTAT128N operated within a frequency range from 100 kHz to 0.1 Hz. The impedance spectra were measured in 0.1 M NaCl aqueous solution, using a standard Ag/AgCl as the reference electrode and a Pt mesh as the counter electrode. The measurements were performed either at open circuit conditions or at a direct current (DC) offset potential which enables the maximum achievable doping for the material and an alternating current (AC) amplitude of 10 mV. Once the spectra were recorded, they were fit to an equivalent circuit using native tool software Metrohm Autolab NOVA. For the fitting, the Randles circuit was used,  $R_{\text{electrolyte}}(R_{\text{polymer}}||C_{\text{polymer}})$ , and resulted in good quality fits. The extracted capacitance values were normalized by the measured film volume to determine the volumetric capacitance ( $C^*$ ) (see **Figure S8** for an example of the impedance spectra of films). The thickness of films was measured in the dry state with a Bruker Dektak profilometer. The same setup and measurement configuration were used to record cyclic voltammetry curves of the films.

*2.2.9. Quartz Crystal Microbalance with Dissipation Monitoring (QCM-D) Experiments.* QCM-D measurements were performed using a Q-sense analyzer (QE401, Biolin Scientific). First, the QCM-D response of the bare Au sensors in air was recorded, followed by the injection of the aqueous NaCl solutions into the chamber. This results in large shifts in frequency and dissipation due to the density differences between the two media. The measurements were then stopped, the sensors were removed, and polymer films were coated on the sensors. For the film

preparation, PTHS-TMA<sup>+</sup>-co-P3HT 1 and 2 were mixed with the cross-linker GOPS (1 wt % PTHS-TMA<sup>+</sup>-co-P3HT 1, 2 + 0.5 wt % GOPS in methanol). PTHS-TMA<sup>+</sup>-co-P3HT 3 layers were prepared without the cross-linker due to its hydrophobic nature. PTHS-TMA<sup>+</sup>-co-P3HT copolymer layers were spin-coated directly on the same sensor from a methanol and methanol/THF solution (10 mg/mL). The polymer films were cross-linked at 100 °C for 1.5 h. Then, the absolute differences in QCM-D signals for multiple overtones between the bare sensor and the PTHS-TMA<sup>+</sup>-co-P3HT-coated sensor, both in air and in 0.1 M NaCl, using the function “stitched data” of Q-soft software were compared. The change in dissipation is not exceeding 10 and the different overtones (3<sup>rd</sup>, 5<sup>th</sup>, and 7<sup>th</sup>) are overlapping (**Figure S7**). Therefore, the Sauerbrey equation is valid in this case because the change in dissipation of energy is small, which obviates the need for viscoelastic modeling. The detailed analysis of the swelling percentage calculation is as explained by SAVVA ET AL.<sup>29</sup>

*2.2.10. OECT Fabrication.* The devices were fabricated according to the parylene-C lift-off method reported previously.<sup>30</sup> Briefly, microscope glass slides were cleaned via sonication in 2% soap solution, acetone, and isopropyl alcohol and dried with N<sub>2</sub>. Connection pads and interconnects were deposited through a liftoff process using photolithographic patterning of two positive photoresists (LOR 5B and S1813). A subsequent metal deposition via sputtering of Cr (10 nm) and of Au (110 nm) and metal lift-off using NMP defines the Au lines. The first layer of parylene-C (1.6 μm), deposited together with a small amount of 3-(trimethoxysilyl)-propylmethacrylate (A-174 silane) to enhance adhesion, acts as an insulator to prevent disturbing capacitive effects at the metal-liquid interface. Subsequently, an antiadhesive layer was spin-coated using a dilution of industrial cleaner (2 wt %, Micro-90), and a second parylene-C sacrificial layer (2.1 μm) was deposited followed by a second

photolithographic patterning step and a subsequent plasma reactive ion etching step. All of the polymer solutions were prepared in methanol and methanol/THF at 10 mg/mL and spin-coated from a glass fiber filter with a 0.45  $\mu\text{m}$  pore diameter. PTHS-TMA<sup>+</sup>-co-P3HT 1, 2 polymer films were spin cast and cross-linked on the devices as described in QCM-D measurements. Peeling of the second parylene-C sacrificial layer defined the channel dimensions. The thickness of the polymer films was measured using a DEKTAK 150 stylus profilometer.

*2.2.11. OECT Characterization.* OECTs were characterized using a dual-channel source-meter unit (NI-PXI) with a custom-written control code in LabVIEW. All measurements were performed using an Ag/AgCl pellet (D = 2 mm  $\times$  H = 2 mm; Warner Instruments) as the gate electrode. NaCl solution (0.1 M) was contained in a poly(dimethylsiloxane) well on top of the OECTs, and the electrolyte volume was constant at 120  $\mu\text{L}$  for all measurements. The AC response time of the OECTs was calculated via bandwidth measurements, using the 3 dB cutoff frequency equivalent to 0.707 times the peak of transconductance, also known as the half-power point. The mobility ( $\mu_{\text{OECT}}$ ) was determined by applying a constant drain bias to the channel and a sinusoidal voltage pulse at the gate electrode ( $\Delta V_{\text{G}} = 10 \text{ mV}$ ) with a preset offset ( $V_{\text{G, offset}}$ ) and at varying frequencies. The frequency domain relation between the measured gate current ( $\Delta I_{\text{G}}$ ) and drain current ( $\Delta I_{\text{D}}$ ) involving hole/ electron transit time in the channel ( $\tau_{\text{e}}$ ) is:

$$\Delta I_{\text{G}}(f) = 2\pi f \tau_{\text{e}} \Delta I_{\text{D}}(f) \quad (1)$$

Matching the gate current and drain current derived impedance yields  $\tau_e$  as detailed by Rivnay et al.<sup>24</sup> Using the  $\tau_e$ , the channel length ( $L$ ), and the applied drain bias ( $V_D$ ), the hole mobility  $\mu_{OECT}$  can be estimated:

$$\mu_{OECT} = \frac{L^2}{\tau_e V_D} \quad (2)$$

### 3.RESULTS

The three conjugated copolyelectrolytes PTHS-TMA<sup>+</sup>-co-P3HT 1–3 were synthesized using a similar precursor route, as used for the PTHS-TBA<sup>+</sup> homopolymer by Brendel et al.<sup>18</sup> First, the precursor copolymers, poly[3-(6-bromohexyl)-thiophene-co-poly(3-hexyl) thiophene] P3BrHT-co-P3HT 1–3, were synthesized with three different feed-in ratios (75:25, 50:50, and 25:75). Both monomers, 3-hexylthiophene (3HT) and 3-(6-bromohexyl)-thiophene (3BrHT), were added together in a single batch. The polymerization resulted in a gradient copolymer because the monomer 3HT is built-in much faster compared to the monomer 3BrHT (see **Figure S1**). The method we used is KCTP that is well established for the synthesis of polythiophene derivatives with high molecular weight, low polydispersity, and high regioregularity.<sup>26,28</sup> We obtained three defined copolymers, namely P3BrHT-co-P3HT 1, 2, and 3, with low polydispersity ( $\mathcal{D} \leq 1.2$ ) and similar chain lengths (see **Figure 1a** for chemical structures). The built-in ratios of 3BrHT/3HT obtained from <sup>1</sup>H NMR are 70:30, 51:49, and 23:77, respectively, and these are comparable to the feed-in ratios of the monomers.

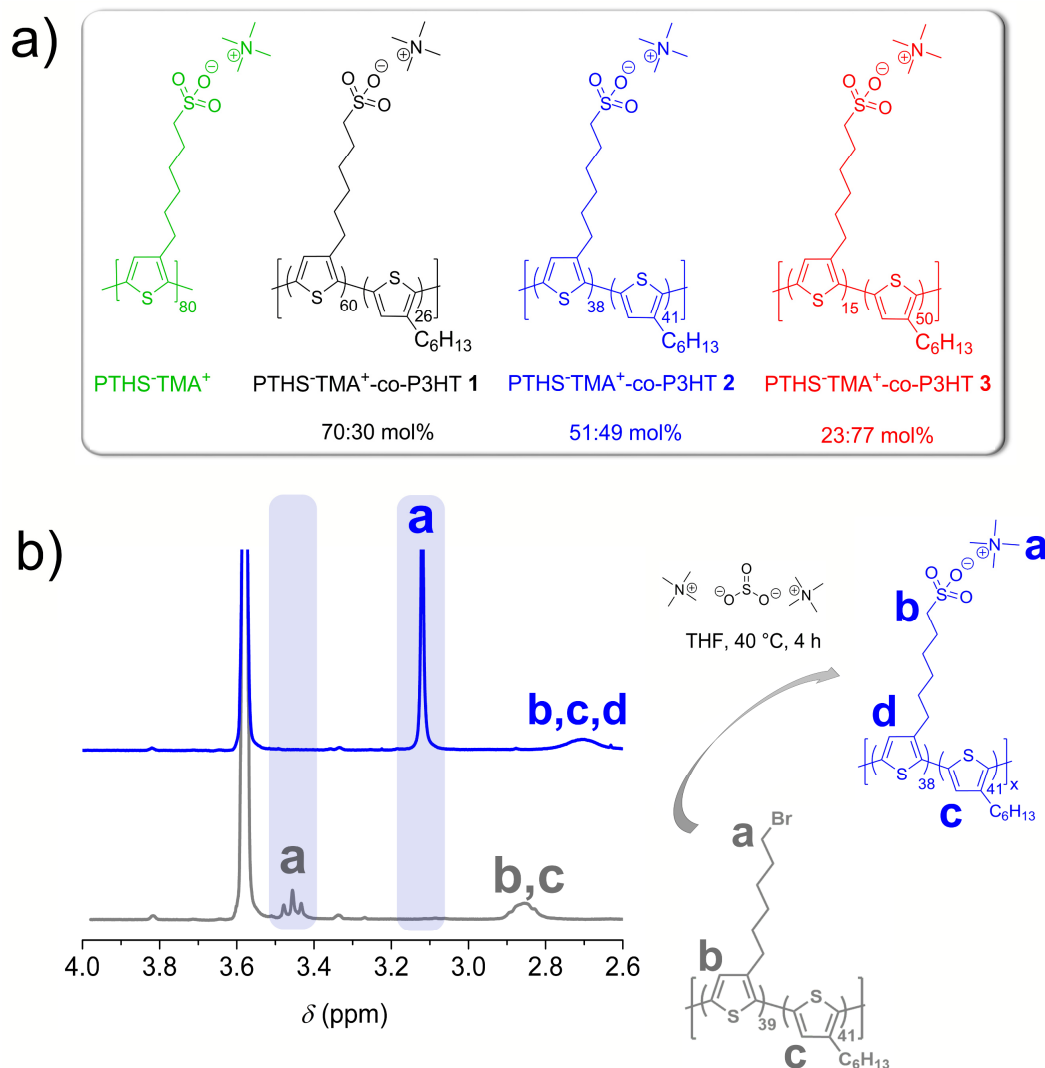


**Figure 1.** (a) Chemical structures of the PTHS-TMA<sup>+</sup>, PTHS-TMA<sup>+</sup>-co-P3HT 1 (70:30 mol %), PTHS-TMA<sup>+</sup>-co-P3HT 2 (49:51 mol %), and PTHS-TMA<sup>+</sup>-co-P3HT 3 (23:77 mol %). The number of repeating units were calculated out of the built-in ratios determined by <sup>1</sup>H NMR and from the molecular weight determined in MALDI-ToF experiments. (b) <sup>1</sup>H NMR spectra of the precursor polymer P3HT-co-P3BrHT 2 (blue) and the corresponding conjugated copolyelectrolyte PTHS-TMA<sup>+</sup>-co-P3HT 2 (red), measured in THF-d<sub>8</sub> and a mixture of D<sub>2</sub>O and THF-d<sub>8</sub>, respectively. The disappearance of signal a in the copolymer P3HT-co-P3BrHT 2 indicates a quantitative substitution of the bromine in the polymer side chain.

Absolute molecular weights of the precursor copolymers P3BrHT-co-P3HT 1 (19 kg/mol), P3BrHT-co-P3HT 2 (16 kg/mol), and P3BrHT-co-P3HT 3 (13 kg/mol), are measured with MALDI-ToF. In the following synthetic step, the conjugated copolyelectrolytes poly[6-(thiophen-3-yl) hexane-1-sulfonate-co-poly(3-

hexyl]thiophene] PTHS-TMA<sup>+</sup>-co-P3HT 1–3 with a tetramethylammonium counter cation were synthesized by a postpolymerization reaction. For this, the precursor polymers were dissolved in THF and a solution of bis-(tetramethylammonium)sulfite in methanol was added and stirred for 4 h at 40 °C. The substitution reaction was monitored with <sup>1</sup>H NMR spectroscopy. The complete disappearance of the triplet signal a of CH<sub>2</sub>Br protons in the precursor polymer, e.g., P3BrHT-coP3HT 2 indicates a quantitative substitution (see **Figure 1b**). Furthermore, the signal a of the methyl group of the counterion TMA<sup>+</sup> appears in the product. The shift of the protons b and c of the thiophene ring arises out of the difference in polarity of the solvent used for <sup>1</sup>H NMR spectroscopy. From the molecular weight of the repeating unit of 3-THS TMA<sup>+</sup> and the built-in ratio of both monomers, 3BrHT/3HT, the molecular weight of the final polyelectrolyte copolymers can be calculated for PTHS-TMA<sup>+</sup>-co-P3HT 1 (24 kg/mol), PTHS-TMA<sup>+</sup>-co-P3HT 2 (19 kg/mol), and PTHS-TMA<sup>+</sup>-co-P3HT 3 (13 kg/mol). PTHS-TMA<sup>+</sup>-co-P3HT 1–2 are soluble in common polar solvents like water, dimethyl sulfoxide (DMSO), methanol, ethylene glycol, and formamide. On the other hand, PTHS-TMA<sup>+</sup>-co-P3HT 3, the copolymer with the highest amount of nonpolar 3-hexylthiophene (77 mol %), is insoluble in water, but soluble in mixtures of an organic solvent such as tetrahydrofuran and water (see **Figure S2**). Thus, our polymerization technique led to three gradient copolyelectrolytes with differing water solubility behavior (maintaining water compatibility) prepared in a well-controlled manner. To investigate the structural properties in bulk of all of the copolyelectrolytes, we used small angle X-ray scattering (SAXS). The samples were annealed above the melting temperatures of the copolymers for 30 min under nitrogen to facilitate any possible crystallization from the melt.<sup>31,32</sup> As a comparison, the homopolymer PTHS-TMA<sup>+</sup> was measured at room temperature after annealing at 250 °C for 30 min under

nitrogen to ensure that the polymer is completely in the molten state before cooling. Out of thermogravimetric analysis, we validated that the polymer is not decomposing at this temperature (see **Figure S3**). **Figure 2** shows the scattering curves for the PTHS-TMA<sup>+</sup> homopolymer, as well as the scattering curves for the copolymers in the SAXS–wide-angle X-ray scattering (WAXS) regime at room temperature or the melt-crystallized samples. The [100] crystalline peak of the homopolymer PTHS-TMA<sup>+</sup> appears at a scattering vector  $q$  at around  $0.27 \text{ \AA}^{-1}$ .

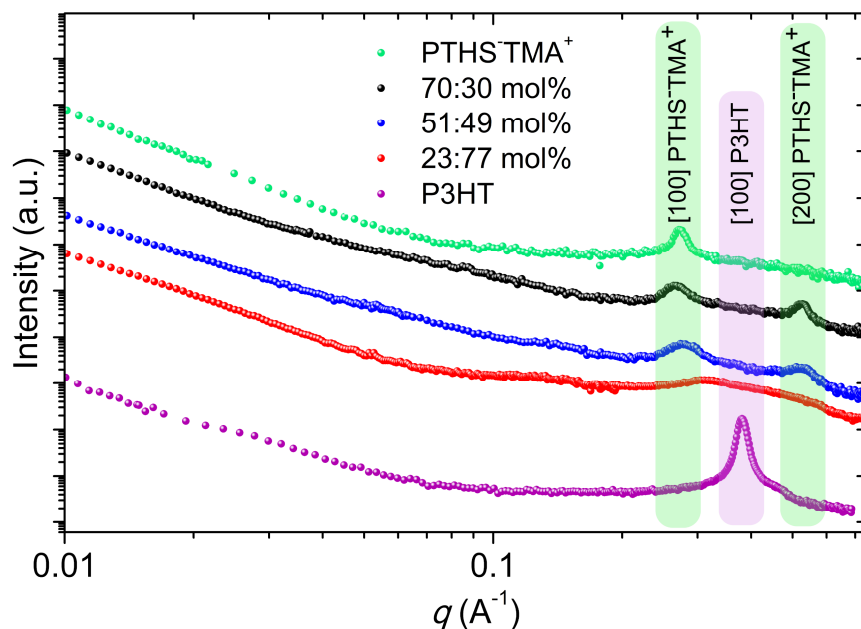


**Figure 2.** X-ray scattering in the SAXS/WAXS regime of the bulk materials PTHS-TMA<sup>+</sup>-co-P3HT (1 black, 2 blue and 3 red), the homopolymers P3HT (magenta), and PTHS-TMA<sup>+</sup> (green), which were annealed at the ambient temperature for 30 min under nitrogen.

This spectral feature is also present in the copolymers PTHS-TMA<sup>+</sup>-co-P3HT 1 and 2. In addition to this, in both of these copolymers, the [200] peak is also present at around  $q = 0.54\text{--}0.55 \text{ \AA}^{-1}$ . In PTHS-TMA<sup>+</sup>-co-P3HT 3 having the least amount of PTHS-TMA<sup>+</sup> content, no defined crystalline peaks due to the PTHS-TMA<sup>+</sup> moiety is observed, but only a broad amorphous halo is visible indicating that neither of the components crystallizes. Interestingly, the crystallization of P3HT is completely

suppressed in all copolymers including PTHS-TMA<sup>+</sup>-co-P3HT 3, the copolymer with the highest (77 mol %) 3HT content, because the typical [100] crystalline peak of P3HT at around  $q = 0.38 \text{ \AA}^{-1}$  is not visible. Thus, the PTHS-TMA<sup>+</sup> is hindering the crystallization of P3HT in these gradient types of copolymers. In addition, the [200] peak of PTHS-TMA<sup>+</sup> is visible in the copolymers at  $0.53 \text{ \AA}^{-1}$ , but not in the homopolymer. This suggests that the presence of the nonionic P3HT gradient segment improves the crystallization of the ionic component. Additional information about the aggregation behavior of the thiophene copolymers PTHS-TMA<sup>+</sup>-co-P3HT 1–3 in comparison with the homopolymer PTHS-TMA<sup>+</sup> can be extracted from the UV–Vis absorption spectra. SPANO ET AL. postulated that poly-3-hexylthiophene forms weak H-aggregates in films or bad solvents.<sup>33,34</sup> The solution spectra of the copolymers in a good solvent such as DMSO (PTHS-TMA<sup>+</sup>-co-P3HT 1 and 2) or THF/water 90:10 (PTHS-TMA<sup>+</sup>-co-P3HT 3) exhibit one broad and featureless absorption (**Figure S2**), with a peak maximum ranging from 432 to 450 nm.<sup>33,34</sup> This absorption peak can be attributed to the amorphous coil structure of polythiophenes. For polythiophenes, it is known that this peak shows a bathochromic shift with increasing molecular weight of the polymer, indicating the growth of the conjugated system, which saturates at around 450 nm.<sup>35</sup> When aggregates form, a bathochromic shift of about 100 nm and three distinct peaks are observed. These peaks can be attributed to transitions from the different vibrational states (0–2, 0–1, and 0–0 transitions).<sup>35</sup> In aqueous solutions (for PTHS-TMA<sup>+</sup>-co-P3HT 3, we used a water/THF mixture since it is not soluble in water alone and  $c = 2 \text{ mg/mL}$  for all polymers), PTHS-TMA<sup>+</sup> is highly aggregated, but the individual transition peaks cannot be distinguished (**Figure 3a**).

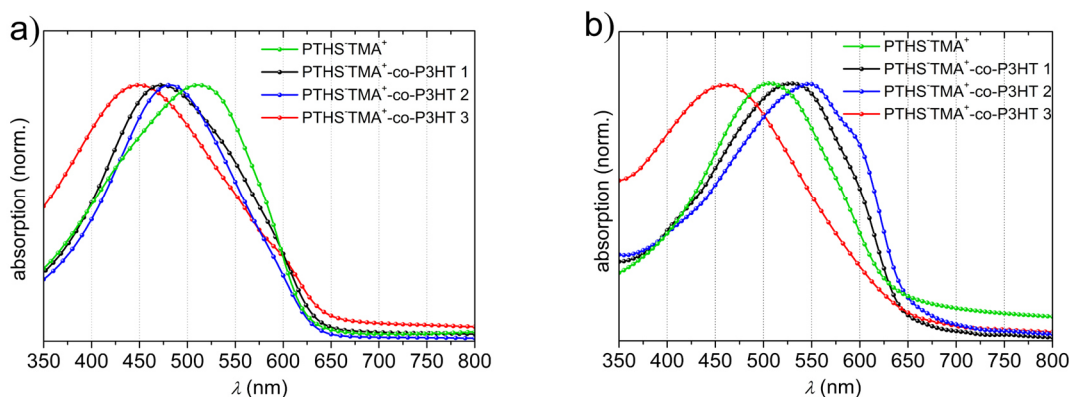


**Figure 3.** (a) Absorption spectra of PTHS-TMA<sup>+</sup>, PTHS-TMA<sup>+</sup>-co-P3HT 1, and PTHS-TMA<sup>+</sup>-co-P3HT 2 in H<sub>2</sub>O at a polymer concentration of 2 mg/mL. PTHS-TMA<sup>+</sup>-co-P3HT 3 was measured in a mixture of H<sub>2</sub>O/THF 90:10 vol %. (b) Thin-film spectra of PTHS-TMA<sup>+</sup> and PTHS-TMA<sup>+</sup>-co-P3HT 1–3. The thin polymer films were spin-coated from methanol and from mixtures of methanol and THF on glass slides.

Compared to the copolymers, a bathochromic shift is observed in the absorption spectrum of PTHS-TMA<sup>+</sup> ( $\lambda_{\max}$ : 502 nm), which indicates the aggregation of this species in water. With the increasing amount of nonpolar hexylthiophene in the copolymers, the aggregation gets more and more disrupted. Thus, PTHS-TMA<sup>+</sup>-co-P3HT 3 with about 75% 3HT content shows the smallest bathochromic shift among the three copolymers. For PTHS-TMA<sup>+</sup>-co-P3HT 1–3, in general, the relative amounts of disordered to H-aggregated chains can be assessed by comparing the absorption intensity of the respective species.<sup>33,34</sup> Even without quantitatively separating the spectra into the two contributions as would be required for a full analysis, it is evident that a higher P3HT content increases the fraction of disordered chains in water. This can be understood from the fact that we are observing the aggregates of the PTHS-TMA<sup>+</sup> fraction here rather than that of the P3HT part. This is in accordance with the fact that the crystallization of P3HT is fully suppressed in bulk as evidenced by X-ray diffraction analysis.

In contrast, aggregation behavior in thin films is different (**Figure 3b**). As deduced from the SAXS spectra in bulk as well as in absorption spectra in solution, PTHS-TMA<sup>+</sup>-co-P3HT 3 is not crystalline and does not aggregate in thin films, indicated by a featureless broad absorption with a maximum at around  $\lambda_{\max}$ : 460 nm. The homopolymer, PTHS-TMA<sup>+</sup>, shows a higher order in thin films compared to PTHS-TMA<sup>+</sup>-co-P3HT 3 ( $\lambda_{\max}$ : 506 nm) and has no pronounced shoulder at 610 nm. On the other hand, the copolymers with 25 and 50 mol % of hexylthiophene as the comonomer show higher ordered absorption in thin films, with a pronounced shoulder at 610 nm compared to PTHS-TMA<sup>+</sup>. According to SPANO ET AL. the quality of the polymeric aggregates can also be determined by the ratio of the absorbance of the 0–0 peak (at 610 nm) and the 0–1 peak (at ~510 nm).<sup>33,34</sup> A high  $A_{0-0}/A_{0-1}$  ratio indicates a high order in the polymer film. The  $A_{0-0}/A_{0-1}$  ratio of 0.74 and 0.67 for PTHS-TMA<sup>+</sup>-co-P3HT 2 and 1, respectively, can be extracted from the absorption spectra in a rough way without quantitatively analyzing the spectra for the individual contributions. Thus, for the copolymers PTHS-TMA<sup>+</sup>-co-P3HT 1 and 2, we achieved a higher chain order in the films through copolymerization with 3HT, compared to PTHS-TMA<sup>+</sup>. We next calculated the optical gap from the absorption edge in thin-film spectra resulting in similar values of about 2 eV for all polymers. The ionization potential ( $I_p$ ) values for PTHS-TMA<sup>+</sup> as well as for the copolymers PTHS-TMA<sup>+</sup>-co-P3HT 1–3 were calculated with photoelectron spectroscopy measurements in air (PESA, **Figure S4**). The ionization potentials of the copolymers PTHS-TMA<sup>+</sup>-co-P3HT 1 and 2 are slightly lower (–4.82 and –4.81 eV) than that of PTHS-TMA<sup>+</sup> (–4.94 eV). On the other hand, PTHS-TMA<sup>+</sup>-co-P3HT 3 exhibits a similar ionization potential ( $I_p$ ) (–4.97 eV) compared to PTHS-TMA<sup>+</sup>. Therefore, within possible error

limits of the PESA method, we could not clearly register any trend in ionization potentials.

To render the copolymers applicable in OECTs, it is desirable that the materials are able to undergo an oxidation (i.e., doping) process in an aqueous environment at low applied gate voltages to avoid co-oxidation of possible electroactive species in complex media (dopamine, uric acid, ascorbic acid, glutamate, etc.). Therefore, we monitored the changes in the absorption spectra of the polymer films in an aqueous electrolyte solution when they are subjected to an electrochemical doping potential, representing the operation conditions of an OECT. The measurements were performed in 0.1 M aqueous NaCl solution in the range between 0 and  $-0.9$  V vs Ag/AgCl, measured in steps of 0.1 V. Before starting the measurement, a de-doping potential was applied (0.2 V), to ensure that the polymer is in the pristine state before electrochemical doping. Upon application of a doping potential, the characteristic polaron absorption arises between 600 and 1100 nm, while the main  $\pi-\pi^*$  absorption ranging from 400 to 600 nm decreases for all of the copolymers (**Figure S5**).

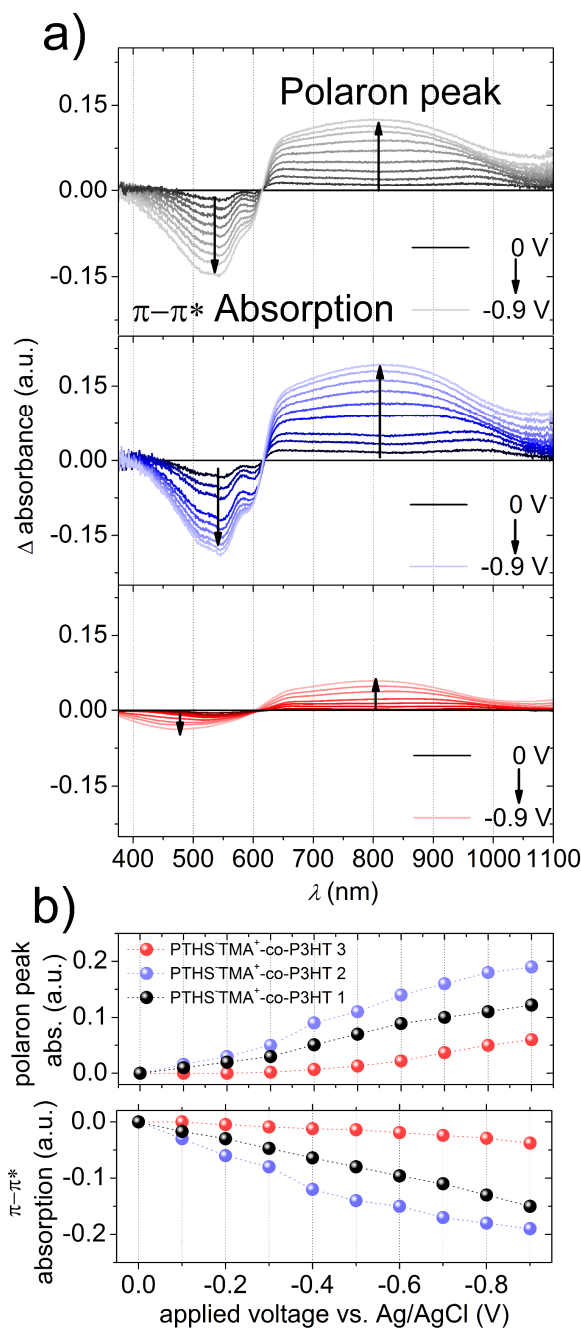


**Figure 4.** (a) Absolute changes in the absorption spectra of the copolymers obtained by subtracting the spectrum of each film in the neutral state (0 V) from that recorded under different applied potentials during the electrochemical oxidation of PTHS-TMA<sup>+</sup>-co-P3HT 1–3. The arrow indicates the direction of spectral changes and its length represents the degree of oxidation which is clearly much higher for PTHS-TMA<sup>+</sup>-co-P3HT 1 and 2 compared to 3. (b) Corresponding change in the intensities of the polaron peak at 820 nm (top) and  $\pi$ - $\pi^*$  absorption maximum (bottom).

Moreover, we observe a clear isosbestic point for all of the copolymers, indicating that the stoichiometry of the reaction remains unchanged during the electrochemical reaction and that no secondary reactions occur during the conversion of pristine polymer into the oxidized form (**Figure S5**). PTHS-TMA<sup>+</sup>-co-P3HT 3, the polymer with the highest amount of hydrophobic 3HT in the copolymer, exhibits a broad main absorption of nonaggregated coils, and an indication for oxidation can be observed only at applied voltages of around -0.4 V. For the copolymers with a higher amount of hydrophilic 3-HTS (PTHS-TMA<sup>+</sup>-co-P3HT 1 and 2), the onset of the oxidation in water can be already observed at very low applied potentials (-0.1 V). To quantify the oxidation of the films under applied voltages similar to the OECT measurement conditions, the absorption spectra of the copolymers in the neutral state (0 V) were subtracted from the absorption spectra of the copolymers under different applied potentials and the resulting spectra are plotted in **Figure 4**. These spectra clearly show the degree of decrease in the pristine  $\pi$ - $\pi^*$  absorption with a concomitant increase in polaron absorption. Figure 4b depicts the intensity of both the polaron peak and  $\pi$ - $\pi^*$  absorption under different applied potentials. At a potential of -0.6 V (relevant for OECT operation), PTHS-TMA<sup>+</sup>-co-P3HT 1 and 2 exhibit a considerably higher amount of oxidized species (5 to 6 times) compared to PTHS-TMA<sup>+</sup>-co-P3HT 3. The observed differences in the amount of oxidizable species can be understood as a combination of different parameters which make these copolymers different. For example, PTHS-TMA<sup>+</sup>-co-P3HT 1 and 2, which have higher amounts of the hydrophilic THS-TMA<sup>+</sup> comonomer, exhibit slightly lower  $I_p$  as well as better crystalline order compared to PTHS-TMA<sup>+</sup>-co-P3HT 3. Thus, it seems that the hydrophilic PTHS-TMA<sup>+</sup> segments undergo preferential oxidation compared to the hydrophobic hexylthiophene part at low applied voltages in water. This is also

consistent with cyclic voltammetry experiments that we performed for the copolymer films using 0.1 M NaCl as the electrolyte and an Ag/AgCl reference electrode and a Pt as the counter electrode (see **Figure S6**). Here, the polymers with a higher content of the ionic comonomer (PTHS-TMA<sup>+</sup>-co-P3HT 1 and 2) show a slightly earlier oxidation onset of around 0.15 V compared to PTHS-TMA<sup>+</sup>-co-P3HT 3, with an onset of 0.3 V.

An additional prerequisite for an OECT material is its capability of water uptake. The water-uptake/swelling process is monitored using QCM-D, a sensitive balance that can detect in-situ changes of the mass of a polymer film coated on a piezoelectric quartz crystal. When water is absorbed by the dry polymer film, the oscillation frequency ( $f$ ) of the QCM-D crystal decreases, which indicates an increased mass of the polymer film (see **Figure S7**). Furthermore, for a soft material, the dissipation ( $D$ ) increases because of the loss of energy during the water uptake.<sup>29</sup> We monitored the mass changes of thin polymer films (20–80 nm). For a higher amount of hydrophilic moiety 3THS-TMA<sup>+</sup>, the copolymer takes up more water. We measure 24% swelling for the polymer PTHS-TMA<sup>+</sup>-co-P3HT 1, 22% for PTHS-TMA<sup>+</sup>-co-P3HT 2, and 4% for PTHS-TMA<sup>+</sup>-co-P3HT 3, in agreement with the ionic monomer content in the polymer (70, 51, and 23 mol %, respectively). Therefore, the ability of the chains to swell strongly depends on the hydrophilic character of the copolymers and on the copolymer composition. Finally, we evaluated the performance of these copolymers in OECTs (**Figure 5a**). The microfabricated devices were prepared as described in the Experimental Section. In an OECT, the semiconducting film is in direct contact with the aqueous media and ions can be injected into the polymer film and modify the film conductivity.<sup>5,9,36</sup> The injection of the charges and infiltration of ions into the channel are initiated by the application of a gate voltage,  $V_G$ . The drain

voltage,  $V_D$ , is applied to read the current ( $I_D$ ) flowing in the channel, which is proportional to the number of holes (in p-type materials) therein.<sup>5,9,36</sup> OECTs convert small ionic signals in the electrolyte into large changes in the drain current.<sup>5,9,36</sup> The efficiency of this conversion is called transconductance,  $g_m$ , which defines the steady-state OECT performance expressed as follows:<sup>5,9,36,37</sup>

$$g_m = \frac{\partial I_D}{\partial V_G} = \frac{W \cdot d}{L} \cdot \mu_{\text{OECT}} \cdot C^* \cdot (V_{th} - V_G)$$

(3)

with  $W$  being the channel width,  $L$  the channel length,  $d$  the thickness of the film,  $\mu_{\text{OECT}}$  the OECT hole mobility,  $C^*$  the volumetric capacitance, and  $V_{th}$  the threshold voltage. Here, the product of the material-dependent parameters ( $\mu_{\text{OECT}} \cdot C^*$ ) was described by INAL ET AL.<sup>37</sup> as figure-of-merit to compare the performance of materials in OECTs. Polymers that exhibit a high  $C^*$  and  $\mu_{\text{OECT}}$  can store charges within the polymeric thin films efficiently and are able to transport holes or electrons well through their  $\pi$ -conjugated chains. **Figure 5b, c** summarizes the output and transfer characteristics of an exemplary OECT comprising PTHS-TMA<sup>+</sup>-co-P3HT 2 in the channel. For the copolymer PTHS-TMA<sup>+</sup>-co-P3HT 3, no transistor characteristics could be observed due to its highly hydrophobic nature resulting in very low swelling (4%) and inhibiting ion penetration/transport. In contrast, the copolymers with higher amounts of hydrophilic 3THS-TMA<sup>+</sup> in the copolymer show excellent OECT performance. The conductivity of the copolymers increases upon applying a doping potential because of interactions with Cl<sup>-</sup> anions, as we observe an increase in the drain current, consistent with the accumulation mode operation. Both  $g_m$  and  $I_D$  increase with an increase in  $V_G$ , while the threshold voltage is lower than -0.2 V for both copolymers.

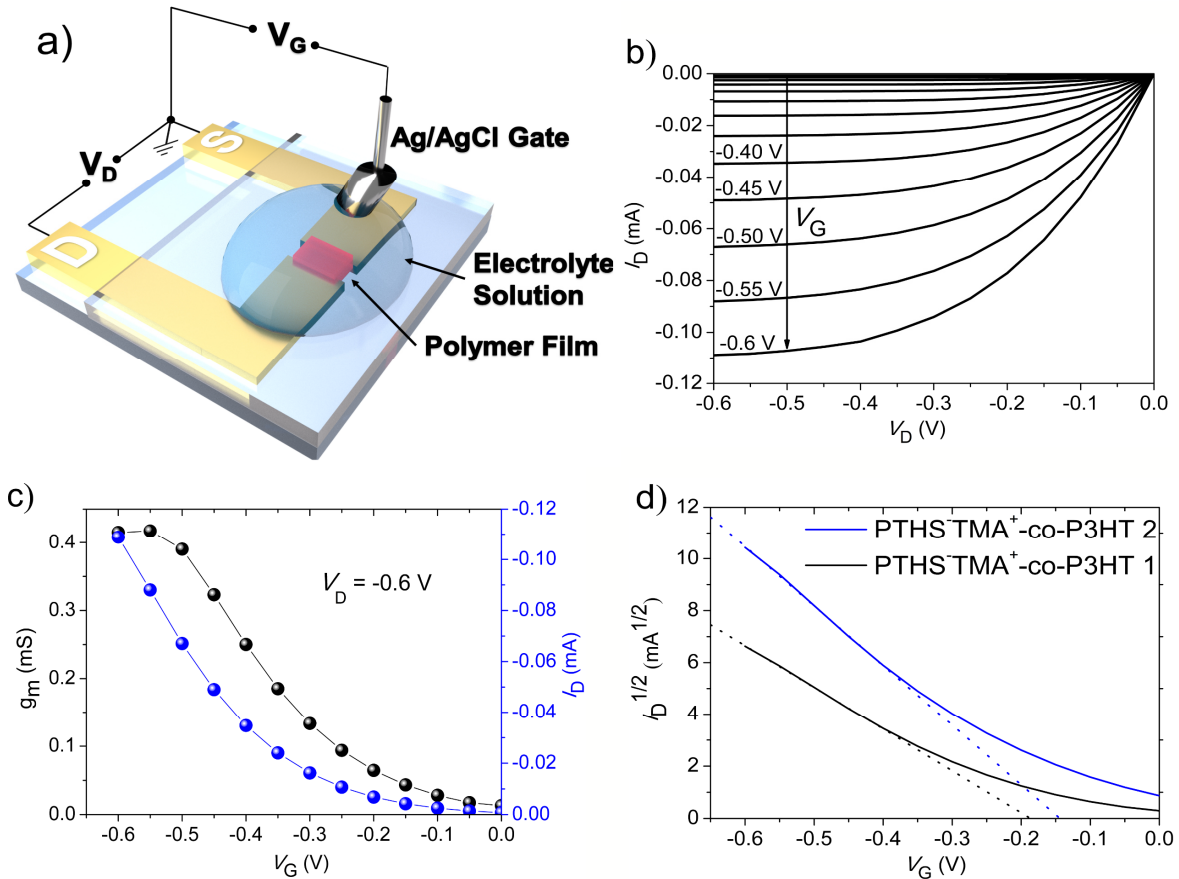


**Figure 5.** (a) Illustration of the setup of an OEET. The channel dimensions were  $W = 100 \mu\text{m}$  and  $L = 10 \mu\text{m}$  and the film thickness was about 60 nm. OEETs were operated in 0.1 M aqueous NaCl solution with an Ag/AgCl pellet as the gate electrode. (b) Output curves of PTHS-TMA<sup>+</sup>-co-P3HT 2 for gate voltages ( $V_G$ ) ranging from 0 to  $-0.6$  V, the data were recorded every  $-0.05$  V. The films were prepared with 0.5 wt % GOPS used as the cross-linker. (c) Transfer curve of PTHS-TMA<sup>+</sup>-co-P3HT 2 with the corresponding transconductance plotted vs  $V_G$  with  $V_D = -0.6$  V. (d)  $\sqrt{I_D}$  vs  $V_G$  plots of the OEETs comprising of PTHS-TMA<sup>+</sup>-co-P3HT 1 and 2. The threshold voltage,  $V_{th}$ , was determined by extrapolating the linear region of the curves. The intersection of the x-axis corresponds to the  $V_{th}$ .

$V_{th}$  is in fact drastically reduced when going from PTHS-M<sup>+</sup> ( $\sim -0.5$  V) to PTHS-TMA<sup>+</sup>-co-P3HT 1 and 2 ( $-0.20$ ,  $-0.15$  V). The reduction in  $V_{th}$  (correlating with the capability to electrochemically dope the films with Cl<sup>-</sup>) agrees with the observation of lower ionization potentials of PTHS-TMA<sup>+</sup>-co-P3HT 1 and 2 determined from PESA experiments (Figure S4). Given the same channel dimensions and device operation conditions, high transconductance values

(normalized by respective film thickness) were obtained for PTHS-TMA<sup>+</sup>-co-P3HT 2 ( $g_m = 70.49$  S/cm) and PTHS-TMA<sup>+</sup>-co-P3HT 1 ( $g_m = 23.40$  S/cm), compared to PTHS-TMA<sup>+</sup> ( $g_m = 20.45$  S/cm).<sup>19</sup> We achieved high ON/ OFF ratios of around  $10^4$ – $10^5$  (**Figure S12**), indicating an effective current amplification. Another OECT configuration, incorporating a planar, polymer-coated micron scale gold gate electrode ( $500 \times 500 \mu\text{m}^2$ ), was also tested (**Figures S10 and S11**). About half of the ON current was measured in this configuration, compared to the standard Ag/AgCl top-gate electrode. This configuration is much more relevant for utilizing OECT as an implantable device as the device integrates both the channel and the gate electrode in proximity. To determine the charge storage capability, we recorded the electrochemical impedance spectra of the polymers with no applied potential ( $V_{oc}$ ) and at a doping potential ( $V = -0.6$  V, **Figure S8**). From the impedance data, we extracted the capacitance of the polymer films, which were then normalized by their volume to get  $C^*$ . The copolymers with the relatively high amount of hydrophilic 3THS-TMA<sup>+</sup> comonomer (PTHS-TMA<sup>+</sup>-co-P3HT 1, 2) exhibit a  $C^*$  value of  $103 \pm 4$  F/cm<sup>3</sup>. For PTHS-TMA<sup>+</sup>-co-P3HT 3, the  $C^*$  drops to ca.  $31 \pm 6$  F/cm<sup>3</sup> because of the high amount of hydrophobic monomer (77 mol %) is not involved in ion storage or transport. The highest reported value for the PTHS-M<sup>+</sup> homopolymer is ca.  $124$  F/cm<sup>3</sup>.<sup>37</sup>

Thus, although we introduced a nonion-conducting, hydrophobic comonomer (3HT) to the polymer structure in copolymers 1 and 2, the ion transport and storage compared to the PTHS-M<sup>+</sup> homopolymer is not affected critically up to 50 mol % of 3HT incorporation. We next estimated the OECT hole mobility of the copolymers using bandwidth measurements (**Figure S13**). We obtained  $\mu_{OECT} = 0.009$  cm<sup>2</sup>/(V s) and  $\mu_{OECT} = 0.017$  cm<sup>2</sup>/(V s) for PTHS-TMA<sup>+</sup>-co-P3HT 1 and 2, respectively. Thus,

through incorporating the efficient hole conductor 3HT into the PTHS polymer structure, we achieved one order of magnitude higher hole mobilities compared to the highest reported value for the pure PTHS-M<sup>+</sup> homopolymer ( $\mu_{\text{OECT}} = 0.001 \text{ cm}^2/(\text{V s})$ ).<sup>37</sup> This, along with the high volumetric capacitance achieved, is remarkable and helpful for further design concepts of conjugated polyelectrolytes. To the best of our knowledge, the ionic copolyelectrolytes PTHS-TMA<sup>+</sup>-co-P3HT 1 and 2 are the best performing ionic polythiophene derivatives for accumulation mode OECTs reported to date. For example, if we compare the  $\mu_{\text{OECT}} \cdot C^*$  values of the copolymers with that of PTHS-TBA<sup>+</sup> ( $\mu_{\text{OECT}} \cdot C^* = 0.16 \text{ F}/(\text{cm V s})$ ), we observe almost one order of magnitude improvement.<sup>37</sup> However, we like to point out the differences in film preparation and the amount of cross-linker used in both cases. We summarize the OECT characteristics as well as the mixed conduction properties ( $\mu_{\text{OECT}}$ ,  $C^*$  and  $\mu_{\text{OECT}} \cdot C^*$ ) along with swelling values in **Table 1**.

**Table 1.** OEET characteristics and material dependent parameters for PTHS-TMA<sup>+</sup> and the copolymers PTHS-TMA<sup>+</sup>-co-P3HT 1, 2 and 3.  $g_m$  was measured at  $V_G = -0.6$  V and  $V_D = -0.6$  V and the average value out of 6 transistors was taken in account.  $V_{th}$  was determined from **Figure 5d** by extrapolating the linear region of the curve. The intersection of the x-axis corresponds to the  $V_{th}$ .  $C^*$  was extracted from electrochemical impedance spectra of the polymer films coated on Au electrodes recorded at a DC potential of -0.6 V or -0.7 V vs. Ag/AgCl.  $\mu_{OEET}$  was determined with bandwidth measurements (**Figure S13**). Swelling percentages were estimated from the QCM-D experiments (**Figure S7 and Table S1**).

Copolymer	$\mu_{OEET}$ (cm <sup>2</sup> /Vs)	$C^*$ (F/cm <sup>3</sup> )	$V_{th}$ (V)	Swelling (%)	Thickness (nm)	$g_m$ (S/cm)	$\mu_{OEET} \cdot C^*$ (F/cmVs)
PTHS-TMA <sup>+</sup> <sup>19</sup>	-	82	-0.45	-	20	20.45	-
PTHS-TMA <sup>+</sup> -co-P3HT 1	0.009 ± 0.0015	107 ± 6	-0.19	24	64±6	23.44	0.97
PTHS-TMA <sup>+</sup> -co-P3HT 2	0.017 ± 0.0036	100 ± 7	-0.15	22	61±5	70.49	1.7
PTHS-TMA <sup>+</sup> -co-P3HT 3	-	31 ± 6	-	4	88±9	-	-

#### 4. CONCLUSION

In this study, a new design strategy for high-performance mixed conductors was presented. We combined a holeconducting monomer (3HT) and an ion-conducting monomer (THS-TMA<sup>+</sup>) into one copolymer with a gradient architecture. By studying the structure–property relationship in thin films, we extracted design rules for new materials to be utilized in aqueous-based electrochemical devices such as the OECT. We achieved two highly ordered copolymers, PTHS-TMA<sup>+</sup>-coP3HT 1 and 2 and observed that the crystallization of the PTHS-TMA<sup>+</sup> segments in the copolymers is much more dominant and it is supported by the presence of the hydrophobic P3HT segments up to 50 mol %. As a consequence, the aggregation of the copolymers in thin films is higher compared to pure PTHS-TMA<sup>+</sup>, again indicative of a high chain order in PHTS-TMA<sup>+</sup>-co-P3HT 1 and 2 films. Moreover, through incorporating a hydrophobic comonomer like 3HT into the PTHS-TMA<sup>+</sup> structure, we could reduce the polymer solubility in water and therefore the amount of required cross-linker in the formulation by 50%. Furthermore, the threshold voltage  $V_{th}$  was reduced from ca.  $-0.5$  V (in PTHS-M<sup>+</sup>) to much lower values, i.e.,  $-0.15$  to  $-0.20$  V, attributed to the slightly lower oxidation potential and improved oxidizability of the copolymers as observed in spectroelectrochemistry. We also monitored the water uptake using QCM-D studies, which shows that the copolymer with the highest amount of THS-TMA<sup>+</sup> (around 70 mol %) swells the most (up to 24% swelling). The important material parameters for high-performance OECTs, i.e.,  $C^*$  and  $\mu_{OECT}$ , were determined using electrochemical impedance spectroscopy and bandwidth measurements, respectively. The copolymers showed very high values of  $C^*$ , which indicates that the ion transport through the polymer morphology is not disrupted by the hydrophobic comonomer in a gradient architecture. The hole mobility in OECTs

increased for the copolymers PHTS-TMA<sup>+</sup>-co-P3HT 1 and 2 compared to PTHS-TMA<sup>+</sup> by 1 order of magnitude. This can be attributed to the higher order in the copolymer films. Finally, the copolymers delivered a high ON current, high transconductance, and high ON/OFF ratios in OECTs. The best performing material in this study was PTHS-TMA<sup>+</sup>-co-P3HT 2 because it shows the best compromise between swelling, i.e., ion uptake as well as ion transport, high hole mobility, easy oxidizability, and low oxidation potential. Thus, this study enables a better understanding of how to tune the properties of conjugated polyelectrolytes, in this case PTHS-TMA<sup>+</sup>, to achieve a better performance in aqueous electrolyte-gated electrochemical transistors. To what extent the gradient architecture plays a role in the observed improvement of the OECT parameters can be quantified only after studying a similar series of block copolymers, in which the P3HT and PTHS-TMA<sup>+</sup> segments are clearly separated from one another.

## 5. References

- (1) Rivnay, J.; Inal, S.; Collins, B. A.; Sessolo, M.; Stavrinidou, E.; Strakosas, X.; Tassone, C.; Delongchamp, D. M.; Malliaras, G. G. Structural Control of Mixed Ionic and Electronic Transport in Conducting Polymers. *Nature Communications* **2016**, *7* (1).
- (2) Russ, B.; Gludell, A.; Urban, J. J.; Chabynyc, M. L.; Segalman, R. A. Organic Thermoelectric Materials for Energy Harvesting and Temperature Control. *Nature Reviews Materials* **2016**, *1*, 16050.
- (3) Mallikarjuna, K.; Kim, H. Highly Transparent Conductive Reduced Graphene Oxide/Silver Nanowires/Silver Grid Electrodes for Low-Voltage Electrochromic Smart Windows. *ACS Applied Materials & Interfaces* **2019**, *11* (2), 1969–1978.
- (4) Rivnay, J.; Owens, R. M.; Malliaras, G. G. The Rise of Organic Bioelectronics. *Chemistry of Materials* **2014**, *26* (1), 679–685.
- (5) Inal, S.; Rivnay, J.; Suiu, A.-O.; Malliaras, G. G.; McCulloch, I. Conjugated Polymers in Bioelectronics. *Accounts of Chemical Research* **2018**, *51* (6), 1368–1376.
- (6) Johansson, P. K.; Julleson, D.; Elfving, A.; Liin, S. I.; Musumeci, C.; Zeglio, E.; Elinder, F.; Solin, N.; Inganäs, O. Electronic Polymers in Lipid Membranes. *Scientific Reports* **2015**, *5*, 11242.
- (7) Zeglio, E.; Schmidt, M. M.; Thelakkat, M.; Gabrielsson, R.; Solin, N.; Inganäs, O. Conjugated Polyelectrolyte Blend as Photonic Probe of Biomembrane Organization. *ChemistrySelect* **2016**, *1* (14), 4340–4344.
- (8) Zeglio, E.; Schmidt, M. M.; Thelakkat, M.; Gabrielsson, R.; Solin, N.; Inganäs, O. Conjugated Polyelectrolyte Blends for Highly Stable Accumulation-Mode Electrochemical Transistors. *Chemistry of Materials* **2017**, *29* (10), 4293–4300.
- (9) Moser, M.; Ponder, J. F.; Wadsworth, A.; Giovannitti, A.; McCulloch, I. Materials in Organic Electrochemical Transistors for Bioelectronic Applications: Past, Present, and Future. *Advanced Functional Materials* **2018**, 1807033.
- (10) Balko, J.; Lohwasser, R. H.; Sommer, M.; Thelakkat, M.; Thurn-Albrecht, T. Determination of the Crystallinity of Semicrystalline Poly(3-Hexylthiophene) by Means of Wide-Angle X-Ray Scattering. *Macromolecules* **2013**, *46* (24), 9642–9651.
- (11) Singh, C. R.; Gupta, G.; Lohwasser, R.; Engmann, S.; Balko, J.; Thelakkat, M.; Thurn-Albrecht, T.; Hoppe, H. Correlation of Charge Transport with Structural Order in Highly Ordered Melt-Crystallized Poly(3-Hexylthiophene) Thin Films. *Journal of Polymer Science Part B: Polymer Physics* **2013**, *51* (12), 943–951.
- (12) Yokoyama, A.; Miyakoshi, R.; Yokozawa, T. Chain-Growth Polymerization for Poly(3-Hexylthiophene) with a Defined Molecular Weight and a Low Polydispersity. *Macromolecules* **2004**, *37* (4), 1169–1171.
- (13) Sheina, E. E.; Liu, J.; Iovu, M. C.; Laird, D. W.; McCullough, R. D. Chain Growth Mechanism for Regioregular Nickel-Initiated Cross-Coupling Polymerizations. *Macromolecules* **2004**, *37* (10), 3526–3528.
- (14) Miyakoshi, R.; Yokoyama, A.; Yokozawa, T. Catalyst-Transfer Polycondensation. Mechanism of Ni-Catalyzed Chain-Growth Polymerization Leading to Well-Defined Poly(3-Hexylthiophene). *Journal of the American Chemical Society* **2005**, *127* (49), 17542–17547.

- (15) Iovu, M. C.; Sheina, E. E.; Gil, R. R.; McCullough, R. D. Experimental Evidence for the Quasi-“Living” Nature of the Grignard Metathesis Method for the Synthesis of Regioregular Poly(3-Alkylthiophenes). *Macromolecules* **2005**, *38* (21), 8649–8656.
- (16) Giovannitti, A.; Sbircea, D.-T.; Inal, S.; Nielsen, C. B.; Bandiello, E.; Hanifi, D. A.; Sessolo, M.; Malliaras, G. G.; McCulloch, I.; Rivnay, J. Controlling the Mode of Operation of Organic Transistors through Side-Chain Engineering. *Proceedings of the National Academy of Sciences* **2016**, *113* (43), 12017–12022.
- (17) Brendel, J. C.; Schmidt, M. M.; Hagen, G.; Moos, R.; Thelakkat, M. Controlled Synthesis of Water-Soluble Conjugated Polyelectrolytes Leading to Excellent Hole Transport Mobility. *Chemistry of Materials* **2014**, *26* (6), 1992–1998.
- (18) Inal, S.; Rivnay, J.; Leleux, P.; Ferro, M.; Ramuz, M.; Brendel, J. C.; Schmidt, M. M.; Thelakkat, M.; Malliaras, G. G. A High Transconductance Accumulation Mode Electrochemical Transistor. *Advanced Materials* **2014**, *26* (44), 7450–7455.
- (19) Schmidt, M. M.; ElMahmoudy, M.; Malliaras, G. G.; Inal, S.; Thelakkat, M. Smaller Counter Cation for Higher Transconductance in Anionic Conjugated Polyelectrolytes. *Macromolecular Chemistry and Physics* **2018**, *219* (2), 1700374.
- (20) ElMahmoudy, M.; Inal, S.; Charrier, A.; Uguz, I.; Malliaras, G. G.; Sanaur, S. Tailoring the Electrochemical and Mechanical Properties of PEDOT:PSS Films for Bioelectronics. *Macromolecular Materials and Engineering* **2017**, *302* (5), 1600497.
- (21) Zhang, S.; Kumar, P.; Nouas, A. S.; Fontaine, L.; Tang, H.; Cicoira, F. Solvent-Induced Changes in PEDOT:PSS Films for Organic Electrochemical Transistors. *APL Materials* **2015**, *3* (1), 014911.
- (22) Håkansson, A.; Han, S.; Wang, S.; Lu, J.; Braun, S.; Fahlman, M.; Berggren, M.; Crispin, X.; Fabiano, S. Effect of (3-Glycidyloxypropyl)Trimethoxysilane (GOPS) on the Electrical Properties of PEDOT:PSS Films. *J. Polym. Sci. Part B: Polym. Phys.* **2017**, *55* (10), 814–820.
- (23) Mantione, D.; del Agua, I.; Schaafsma, W.; ElMahmoudy, M.; Uguz, I.; Sanchez-Sanchez, A.; Sardon, H.; Castro, B.; Malliaras, G. G.; Mecerreyes, D. Low-Temperature Cross-Linking of PEDOT:PSS Films Using Divinylsulfone. *ACS Appl. Mater. Interfaces* **2017**, *9* (21), 18254–18262.
- (24) Rivnay, J.; Ramuz, M.; Leleux, P.; Hama, A.; Huerta, M.; Owens, R. M. Organic Electrochemical Transistors for Cell-Based Impedance Sensing. *Applied Physics Letters* **2015**, *106* (4), 043301.
- (25) Bernards, D. A.; Malliaras, G. G. Steady-State and Transient Behavior of Organic Electrochemical Transistors. *Advanced Functional Materials* **2007**, *17* (17), 3538–3544.
- (26) Lohwasser, R. H.; Thelakkat, M. Toward Perfect Control of End Groups and Polydispersity in Poly(3-Hexylthiophene) via Catalyst Transfer Polymerization. *Macromolecules* **2011**, *44* (9), 3388–3397.
- (27) Zhai, L.; Pilston, R. L.; Zaiger, K. L.; Stokes, K. K.; McCullough, R. D. A Simple Method to Generate Side-Chain Derivatives of Regioregular Polythiophene via the GRIM Metathesis and Post-Polymerization Functionalization. *Macromolecules* **2003**, *36* (1), 61–64.
- (28) Lohwasser, R. H.; Gupta, G.; Kohn, P.; Sommer, M.; Lang, A. S.; Thurn-Albrecht, T.; Thelakkat, M. Phase Separation in the Melt and Confined Crystallization as the Key to Well-Ordered Microphase Separated Donor–Acceptor Block Copolymers. *Macromolecules* **2013**, *46* (11), 4403–4410.

- (29) Savva, A.; Cendra, C.; Giugni, A.; Torre, B.; Surgailis, J.; Ohayon, D.; Giovannitti, A.; McCulloch, I.; Di Fabrizio, E.; Salleo, A.; et al. Influence of Water on the Performance of Organic Electrochemical Transistors. *Chemistry of Materials* **2019**, *31* (3), 927–937.
- (30) Wustoni, S.; Savva, A.; Sun, R.; Bihar, E.; Inal, S. Enzyme-Free Detection of Glucose with a Hybrid Conductive Gel Electrode. *Adv. Mater. Interfaces* **2019**, *6* (1), 1800928.
- (31) Wu, Z.; Petzold, A.; Henze, T.; Thurn-Albrecht, T.; Lohwasser, R. H.; Sommer, M.; Thelakkat, M. Temperature and Molecular Weight Dependent Hierarchical Equilibrium Structures in Semiconducting Poly(3-Hexylthiophene). *Macromolecules* **2010**, *43* (10), 4646–4653.
- (32) Balko, J.; Rinscheid, A.; Wurm, A.; Schick, C.; Lohwasser, R. H.; Thelakkat, M.; Thurn-Albrecht, T. Crystallinity of Poly(3-Hexylthiophene) in Thin Films Determined by Fast Scanning Calorimetry. *Journal of Polymer Science Part B: Polymer Physics* **2016**, *54* (18), 1791–1801.
- (33) Spano, F. C.; Clark, J.; Silva, C.; Friend, R. H. Determining Exciton Coherence from the Photoluminescence Spectral Line Shape in Poly(3-Hexylthiophene) Thin Films. *The Journal of Chemical Physics* **2009**, *130* (7), 074904.
- (34) Spano, F. C.; Yamagata, H. Vibronic Coupling in J-Aggregates and Beyond: A Direct Means of Determining the Exciton Coherence Length from the Photoluminescence Spectrum. *The Journal of Physical Chemistry B* **2011**, *115* (18), 5133–5143.
- (35) Brown, P. J.; Thomas, D. S.; Köhler, A.; Wilson, J. S.; Kim, J.-S.; Ramsdale, C. M.; Sirringhaus, H.; Friend, R. H. Effect of Interchain Interactions on the Absorption and Emission of Poly(3-Hexylthiophene). *Physical Review B* **2003**, *67* (6).
- (36) Rivnay, J.; Inal, S.; Salleo, A.; Owens, R. M.; Berggren, M.; Malliaras, G. G. Organic Electrochemical Transistors. *Nature Reviews Materials* **2018**, *3*, 17086.
- (37) Inal, S.; Malliaras, G. G.; Rivnay, J. Benchmarking Organic Mixed Conductors for Transistors. *Nature Communications* **2017**, *8* (1).

## 6.Supporting Information

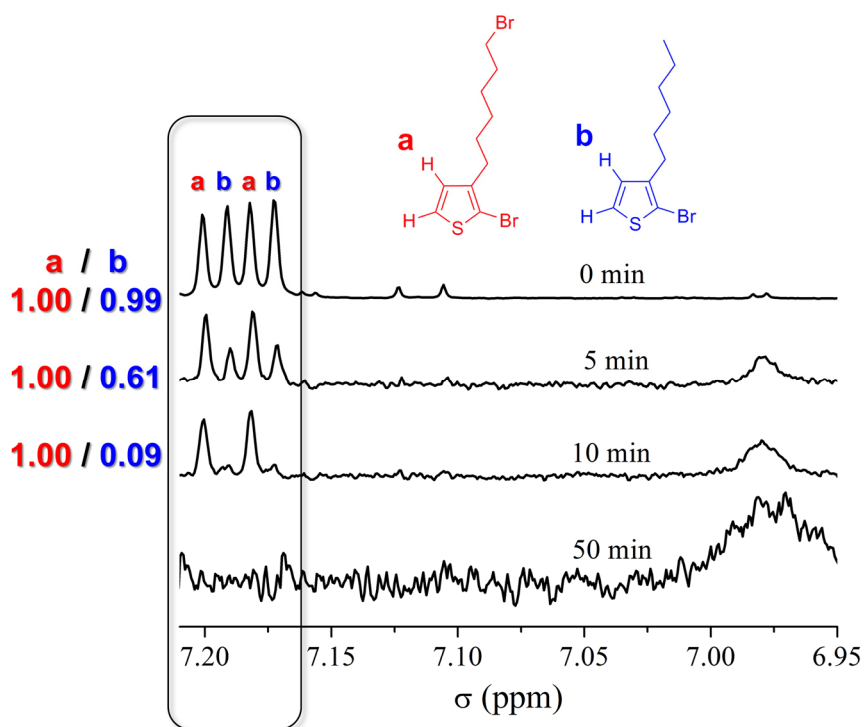


**Figure S1:**  $^1\text{H-NMR}$  kinetic study of the copolymerization of P3BrHT-co-P3HT 2 in a 50:50 mol% in THF solution. During the copolymerization, samples were withdrawn to study the kinetics of the copolymerization. The samples were quenched with aqueous hydrochloric acid, to enable determination of the remaining active monomer ratios. 3-hexylthiophene (blue) compared to 3-(6-bromohexyl) thiophene (red) is consumed much faster into the copolymer, resulting in a gradient type of copolymer.

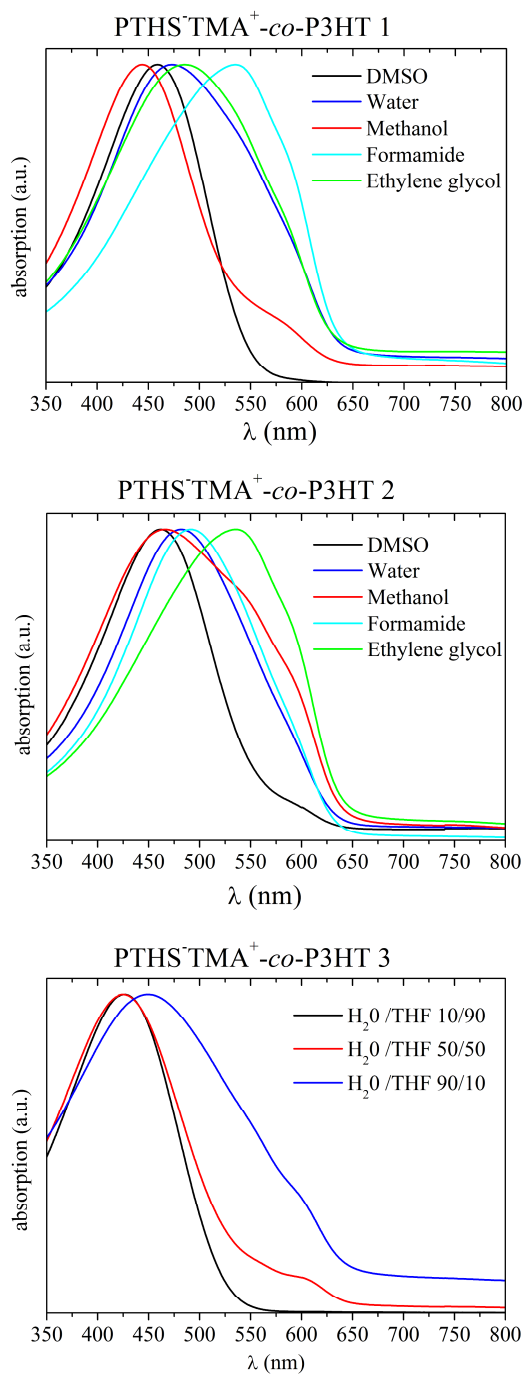


**Figure S2:** Absorption spectra of PTHS<sup>-</sup>TMA<sup>+</sup>-co-P3HT 1-3, measured in different solvents at a polymer concentration of 0.02 mg/mL.

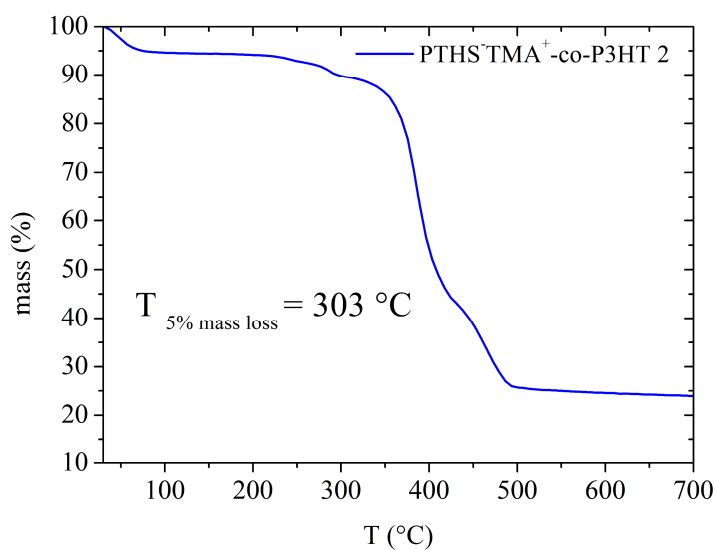


**Figure S3:** TGA measurement of PTHS-TMA<sup>+</sup>-co-P3HT 2 under nitrogen atmosphere with a heating rate of 10 K/min in a temperature range from 30 °C to 700 °C.

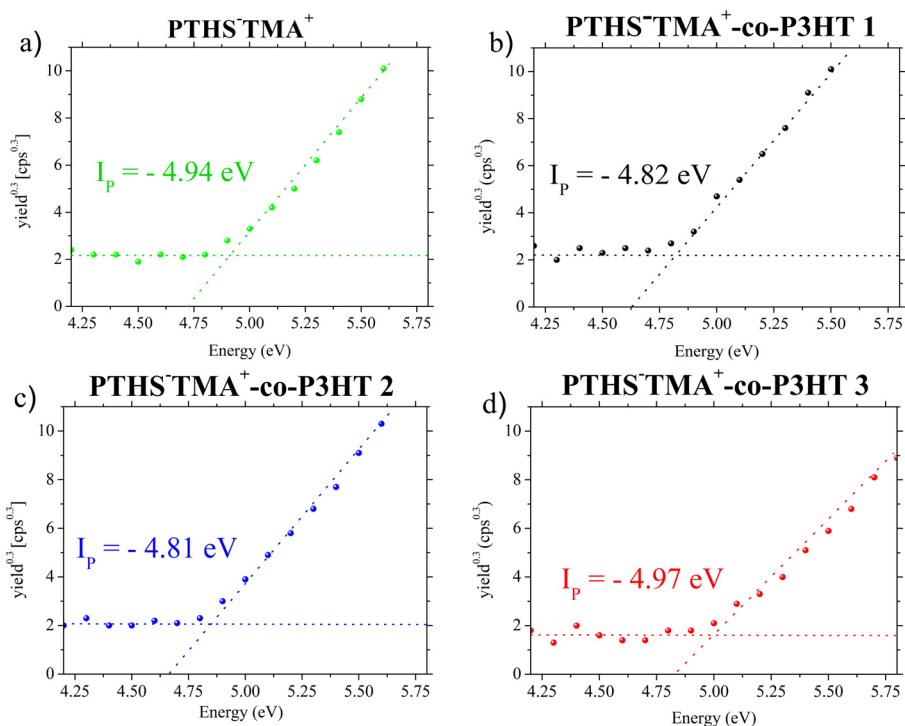


**Figure S4:** a) - d) Photoelectron spectroscopy in air (PESA) measurements of PTHS-TMA<sup>+</sup> and PTHS-TMA<sup>+</sup>-co-P3HT 1-3 on thin polymer films on glass substrates.  $I_p$  values were determined by interception of the both linear fitting curves.

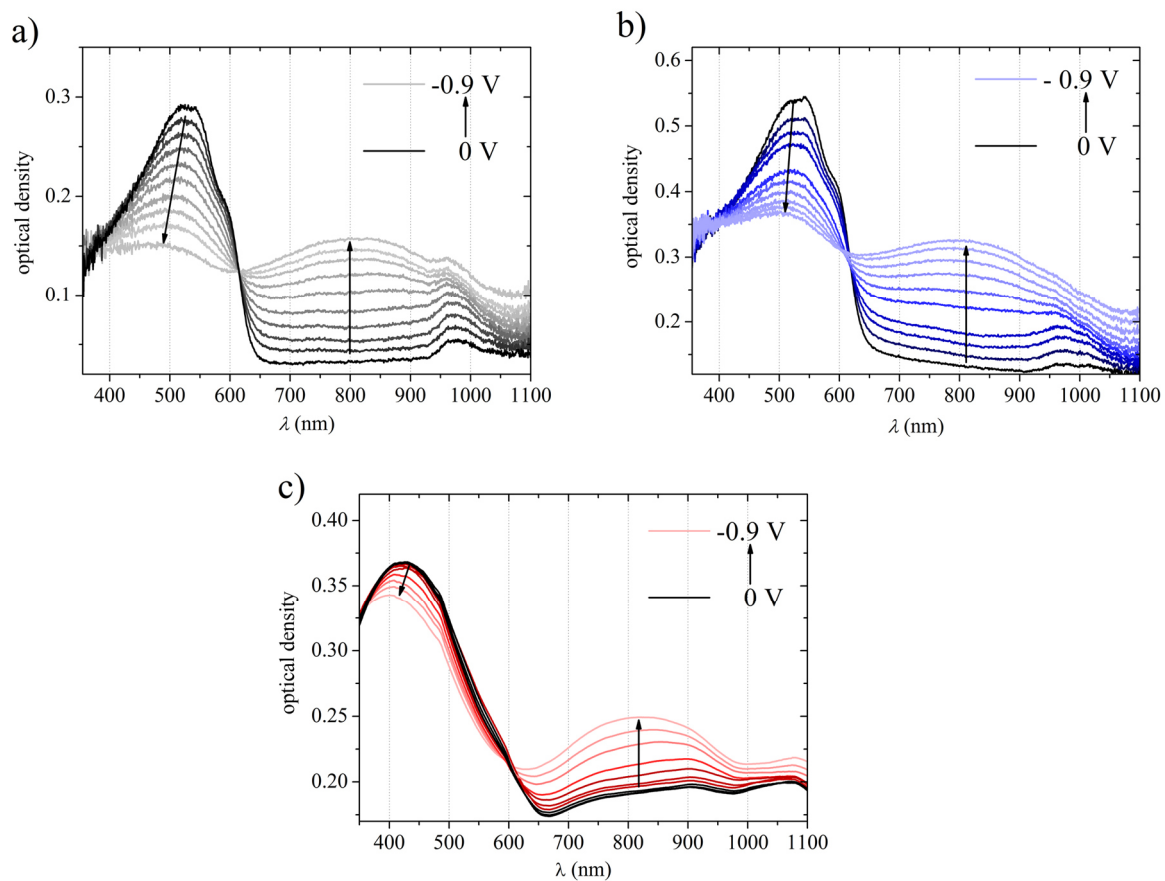


**Figure S5:** a-c) Spectroelectrochemistry measurements of thin polymer films on ITO of PTHS-TMA<sup>+</sup>-co-P3HT 1-3 respectively. The spectra were measured in 0.1 M NaCl when the films were biased from 0 V to -0.9 V in a three-electrode setup with an Ag/AgCl reference electrode and a Pt counter electrode.

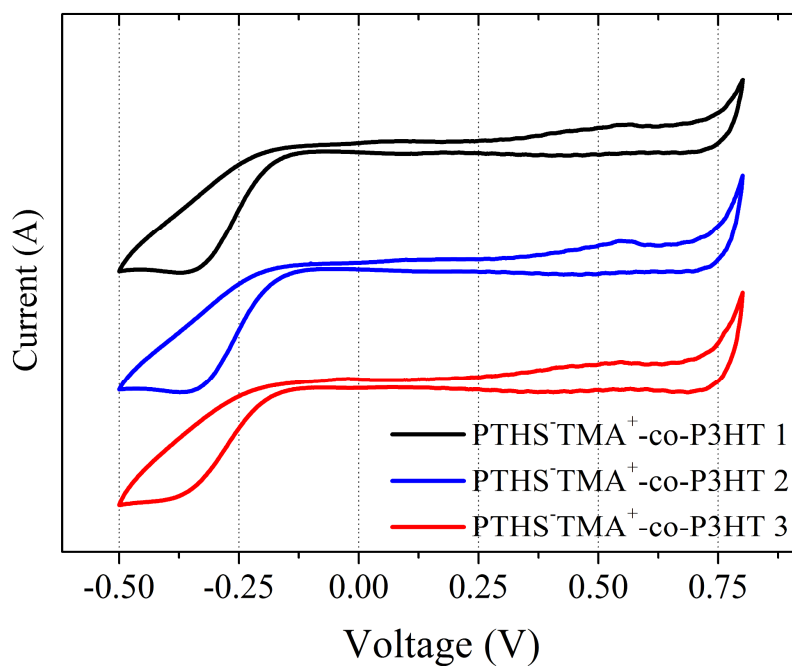


**Figure S6:** Cyclic voltammetry (CV) measurements of the copolymer films were recorded using a potentiostat (Autolab PGstat128N, MetroOhm) with a Ag/AgCl reference electrode and a Pt counter electrode. CV curves were acquired at a scan rate of 50 mV s<sup>-1</sup> in NaCl solution (0.1 M, aqueous).

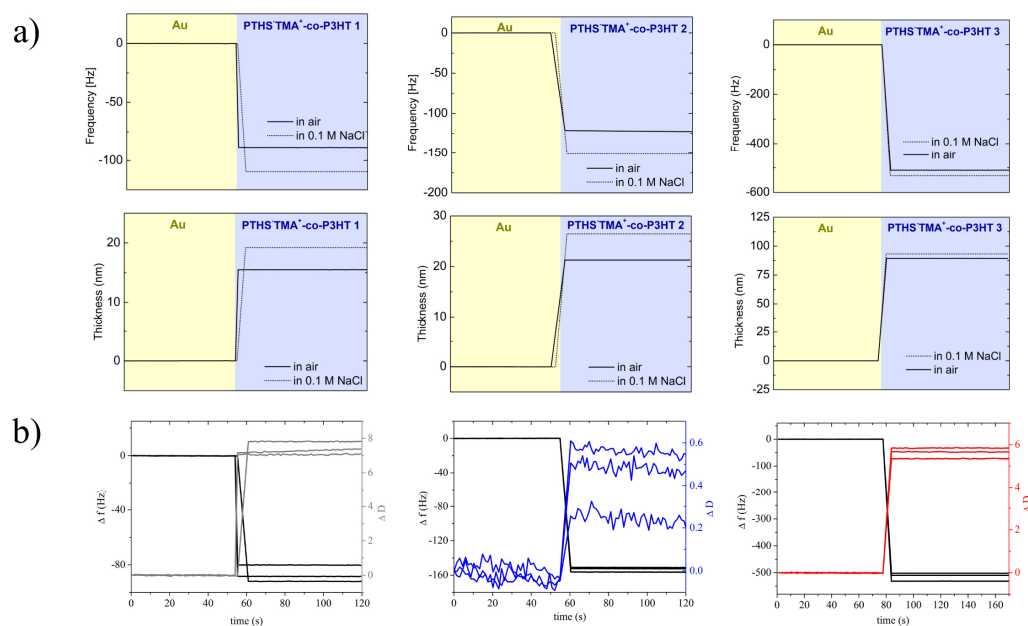


**Figure S7:** a) Shifts of the QCM-D frequency ( $\Delta f$ ) and the calculated thicknesses of the copolymer films. Spectra were recorded in air and in aqueous 0.1 M NaCl solution. For all three copolymers, the 5<sup>th</sup> overtone was used for calculations based on Sauerbrey model. b) Changes in  $\Delta f$  as well as dissipation of energy ( $\Delta D$ ) for these copolymers before and during the injection of 0.1 M NaCl solution into the chambers. The 3<sup>rd</sup>, 5<sup>th</sup> and 7<sup>th</sup> overtone are shown.

**Table S1:** Dry and wet thicknesses of the copolymer films after swelling in 0.1 aqueous NaCl solution. The thickness was calculated using Sauerbrey equation. The 5<sup>th</sup> overtone was used for calculation.

Copolymer	Dry thickness (nm)	Thickness after swelling (nm)	Swelling (%)
PTHS-TMA <sup>+</sup> -co-P3HT 1	21.9	26.6	24
PTHS-TMA <sup>+</sup> -co-P3HT 2	15.4	19.3	22
PTHS-TMA <sup>+</sup> -co-P3HT 3	89.14	92.8	4

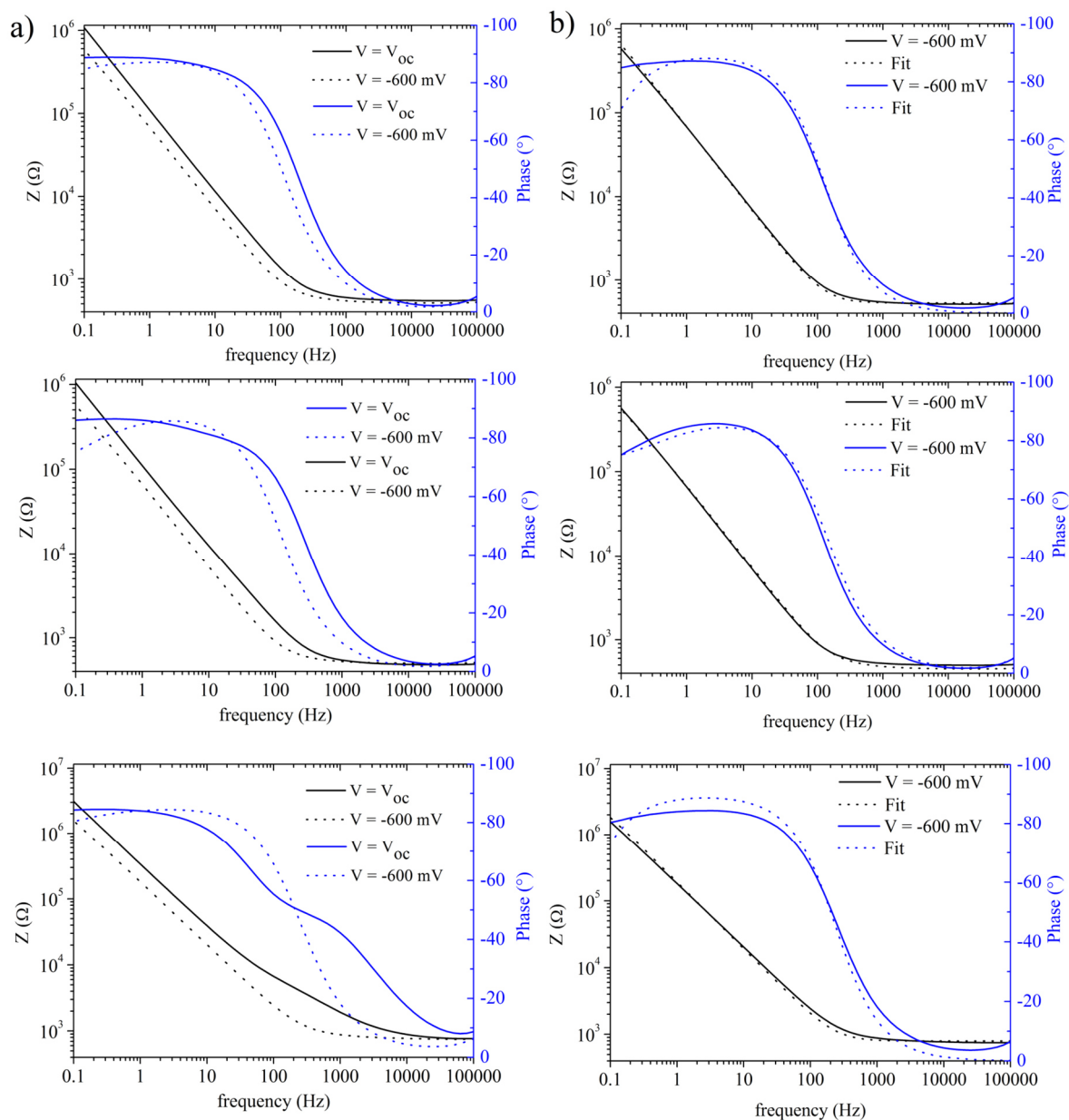


**Figure S8:** a) Electrochemical impedance spectra of the copolymers PTHS-TMA<sup>+</sup>-co-P3HT 1-3 (from top to bottom, 1 to 3) recorded at  $V_{oc}$  and at the doping potential that attains the maximum transconductance ( $V = -0.6$  V) in NaCl solution (0.1 M). b) Fitted electrochemical impedance spectra. Randles circuit was used for fitting the impedance and the phase spectrum,  $R_{electrolyte}(R_{polymer}||C_{polymer})$  at a doping potential ( $V = -0.6$  V). Following chi-fitting values were noted: 0.146 (PTHS-TMA<sup>+</sup>-co-P3HT 1), 0.146 (PTHS-TMA<sup>+</sup>-co-P3HT 2) and 0.765 (PTHS-TMA<sup>+</sup>-co-P3HT 3).

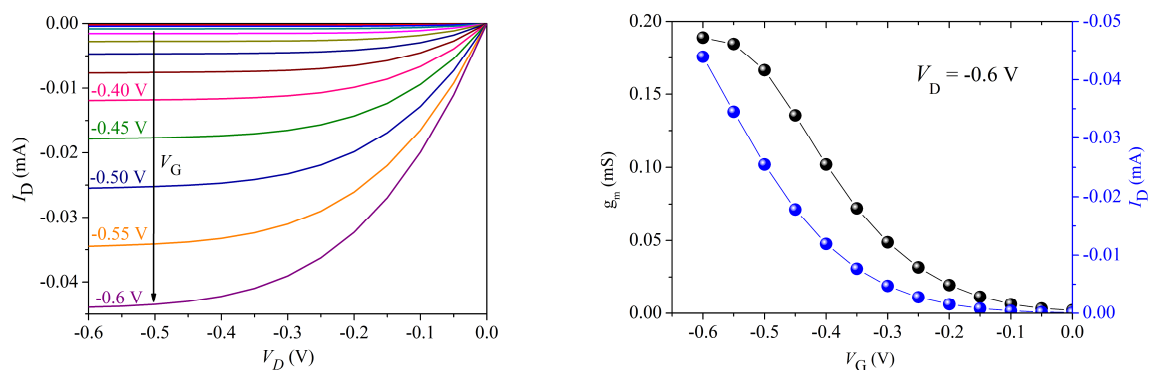


**Figure S9:** Output curve of PTHS-TMA<sup>+</sup>-co-P3HT 1 for gate voltages ranging from 0 V to -0.60 V ( $\Delta V = -0.05$  V) (left). The transfer curve of PTHS-TMA<sup>+</sup>-co-P3HT 1 with the corresponding transconductance values (right).

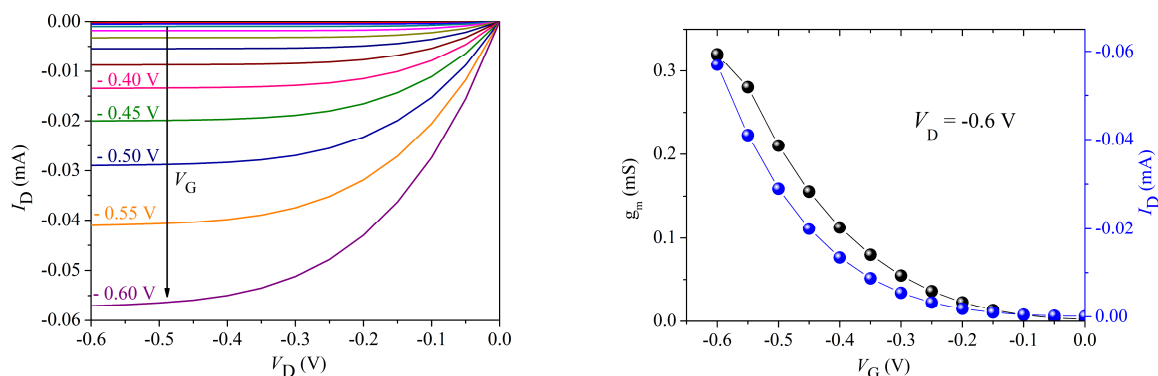


**Figure S10:** Output curves of PTHS-TMA<sup>+</sup>-co-P3HT 2 for gate voltages ranging from 0 V to -0.60 V ( $\Delta V = -0.05$  V) (left). The transfer curve of PTHS-TMA<sup>+</sup>-co-P3HT 2 with the corresponding transconductance values (right). Here, we use a PTHS-TMA<sup>+</sup>-co-P3HT 2 coated, micron scale, planar gold electrode instead of an Ag/AgCl top-gate electrode.

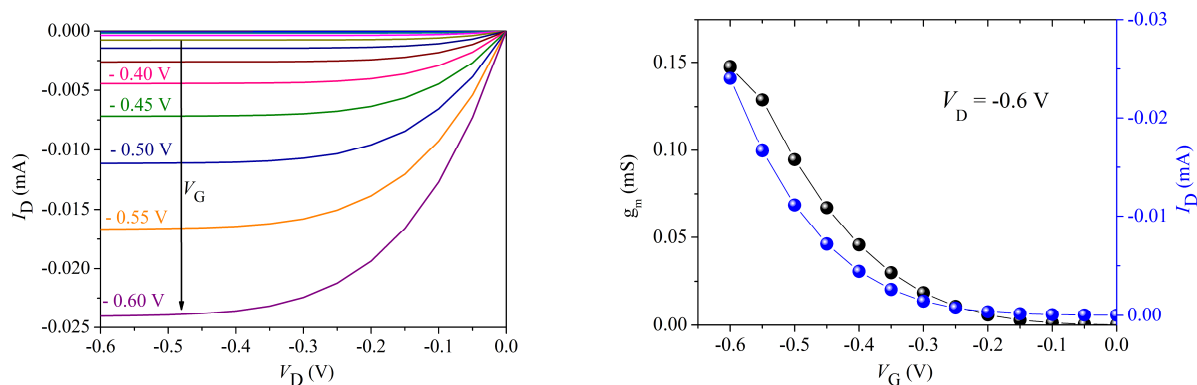


**Figure S11:** Output curves of PTHS-TMA<sup>+</sup>-co-P3HT 1 for gate voltages ranging from 0 V to -0.60 V ( $\Delta V = -0.05$  V) (left). Transfer curve of PTHS-TMA<sup>+</sup>-co-P3HT 1 with corresponding transconductance values (right). Here, we use a PTHS-TMA<sup>+</sup>-co-P3HT 1 coated, micron scale, planar gold electrode instead of an Ag/AgCl top-gate electrode.

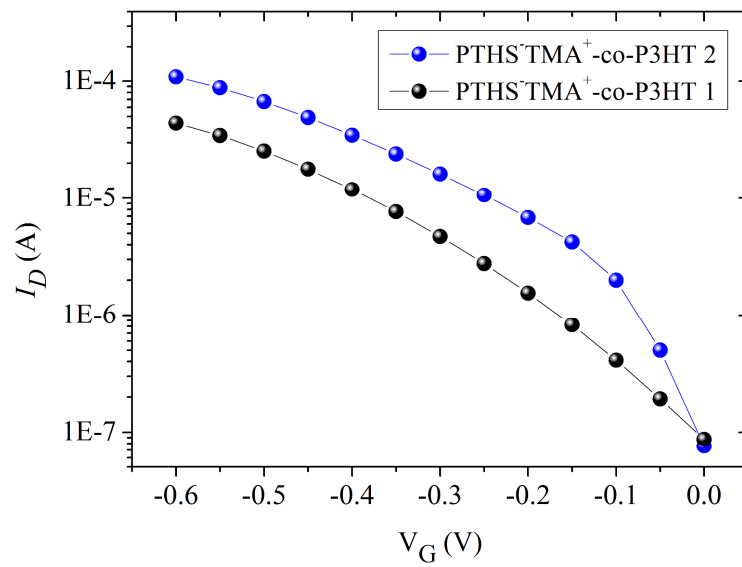


**Figure S12:** Plot of drain current vs. gate voltage of PTHS-TMA<sup>+</sup>-co-P3HT 1 and 2 OECTs at a  $V_D$  of -0.6 V and  $V_G$  ranging from 0 V to -0.60 V with a step of  $\Delta V_G = -0.05$  V.

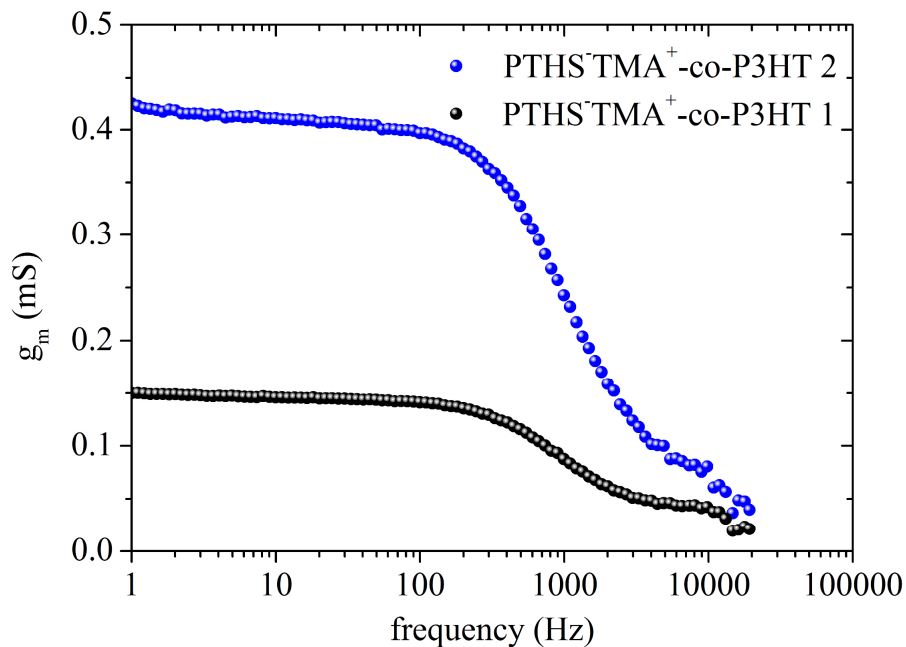


**Figure S13:** Transconductance vs. frequency curve of the copolymer PTHS-TMA<sup>+</sup>-co-P3HT 1 and 2. The devices were biased at a constant  $V_D$  and  $V_G$  of -0.6 V.

# Chapter 7:

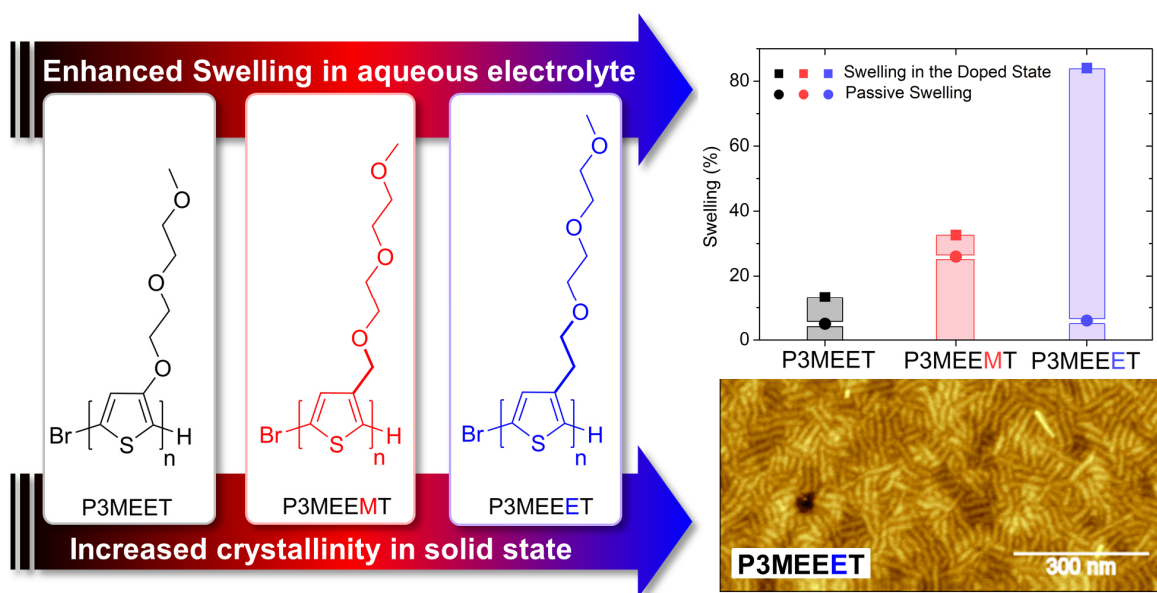
## The Key Role of Side Chain Linkage in Structure Formation and Mixed Conduction of Ethylene Glycol Substituted Polythiophenes

Philip Schmode <sup>†</sup>, Achilleas Savva <sup>‡</sup>, Robert Kahl <sup>||</sup>, David Ohayon <sup>‡</sup>, Florian Meichsner <sup>†</sup>, Oleksandr Dolynchuk <sup>||</sup>, Thomas Thurn-Albrecht <sup>||</sup>, Sahika Inal\* <sup>‡</sup> and Mukundan Thelakkat\* <sup>†§</sup>

<sup>†</sup>Applied Functional Polymers and <sup>§</sup>Bavarian Polymer Institute, University of Bayreuth, Universitätsstr. 30, 95440 Bayreuth, Germany

<sup>‡</sup> Biological and Environmental Science and Engineering, King Abdullah University of Science and Technology (KAUST), Thuwal 23955-6900, Saudi Arabia

<sup>||</sup>Experimental Polymer Physics Group, Martin Luther University Halle-Wittenberg, Von-Danckelmann-Platz 3, 06120 Halle, Germany



Reproduced with permission from *ACS Appl. Mater. Interfaces* **2020**, 12 (11), 13029-13039.

Copyright 2020 American Chemical Society

## ABSTRACT

Functionalizing conjugated polymers with polar ethylene glycol side chains enables enhanced swelling and facilitates ion transport in addition to electronic transport in such systems. Here we investigate three polythiophene homopolymers (P3MEET, P3MEEMT and P3MEEET), having differently linked (without, methyl and ethyl spacer, respectively) diethylene glycol side chains. All the polymers were tested in organic electrochemical transistors (OECTs). They show drastic differences in the device performance. The highest  $\mu_{\text{OECT}} C^*$  product of 11.5 F/cmVs was obtained for ethyl spaced P3MEEET. How the injection and transport of ions is influenced by the side-chain linkage was studied with electrochemical impedance spectroscopy (EIS), which shows a dramatic increase in volumetric capacitance from  $80 \pm 9$  up to  $242 \pm 17$  F/cm<sup>3</sup> on going from P3MEET to P3MEEET. Thus, ethyl-spaced P3MEEET exhibits one of the highest reported volumetric capacitance values among p-type polymers. Moreover, P3MEEET exhibits in dry thin films an OFET hole mobility of 0.005 cm<sup>2</sup>/Vs, highest among the three, which is one order of magnitude higher than for P3MEEMT. The extracted hole mobility from OECT (oxidized swollen state) and the hole mobility in solid state thin films (OFET) show contradictory trends for P3MEEMT and P3MEEET. In order to understand exactly the properties in the hydrated and dry states, the crystal structure of the polymers was investigated with WAXS and GIWAXS and the water uptake under applied potential was monitored using E-QCMD. These measurements reveal an amorphous state for P3MEET and a semicrystalline state for P3MEEMT and P3MEEET. On the other hand, E-QCMD confirms that P3MEEET swells ten times more than P3MEEMT in the oxidized state. Thus, the importance of the ethyl spacer towards crystallinity and mixed-conduction properties was clearly demonstrated, emphasizing the impact of side chain-linkage of

diethylene glycol. This detailed study offers a better understanding how to design high performance organic mixed conductors.

## 1. INTRODUCTION

Side-chain engineering of conjugated polymers (semiconductors) is one of the most powerful strategies to modify the properties such as crystallinity, charge transport and solubility of conjugated polymers.<sup>1</sup> Especially polar side chains are of great interest in conjugated polymers, because they create a permanent dipole, decrease the dielectric constant, reduce the  $\pi$ - $\pi$  stacking distance, enable enhanced swelling, facilitating simultaneous ionic and electronic transport (mixed conduction)<sup>2-4</sup>. In specific examples, it was also demonstrated that this modification improves the doping efficiency due to the higher miscibility of dopant molecules within the hydrophilic side chains.<sup>5</sup> In 2014, we demonstrated that conjugated polyelectrolytes (with ionic side chains) based on polythiophenes obtained using controlled polymerization are suitable candidates for mixed conduction.<sup>6,7</sup> However, due to their high solubility in water, device operation could only be realized after cross-linking the material. A strategy to reduce the amount of cross-linkers (which dilute the active semiconductor) is provided by copolymers of conjugated polyelectrolytes and hydrophobic conjugated polymers.<sup>8</sup> Mixed conductors based on ethylene glycol (EG) substituted conjugated polymers are viable alternatives to conjugated polyelectrolytes. Their non-ionic hydrophilic EG side chains have been reported to facilitate ion transport and storage during biasing in aqueous electrolytes.<sup>2,9</sup> Thus, these polar conjugated polymers carrying EG side chains are potential candidates for biomedical and bioengineering applications and do not require any additional cross-linkers in aqueous media.<sup>10</sup> In general, the mixed conductors are attractive materials for several applications, such as thermoelectric devices, electrochromic displays and

bioelectronics.<sup>8,9,11,12</sup> The widely studied class of p-type semiconductors for bioelectronics still comprises of polythiophene derivatives, due to their high crystallinity, excellent charge carrier properties, high solubility and the feasibility of a controlled synthesis. The synthesis of substituted polythiophenes is of exceptional character, due to the quasi living polymerization character of the Kumada catalyst transfer polymerization, which was initially developed for poly-3-hexylthiophene (P3HT).<sup>13–15</sup> For bioelectronic applications, materials must show an excellent balance between a high ion transport and a high electronic charge transport, both of which are strongly correlated to the morphology of the polymers.<sup>16,17</sup> Both these properties are often contradictory, because ion conduction requires hydration, swelling and free volume of the polymer in aqueous medium, whereas high hole transport is generally observed in highly crystalline non-polar conjugated polymers.<sup>18</sup> For bioelectronic applications, organic electrochemical transistors (OECTs) provide a promising device configuration. In OECTs, small changes in ion fluxes in an electrolyte result in large changes in electrical output current, that is the channel current.<sup>19</sup> Here, the semiconductor material is in the channel which is in direct contact with the (typically aqueous) medium. During the operation of a p-type accumulation mode OECT, a small voltage applied at the gate electrode,  $V_G (< 1 \text{ V})$ , injects anions into the channel compensating for the holes injected from the contacts, resulting in increased conductivity of the semiconductor.<sup>19</sup> Because of the change in the channel conductivity, the current between source and drain  $I_G$  increases.<sup>18</sup> The steady-state performance of OECTs can be expressed by their transconductance,  $g_m$ . The product  $\mu_{\text{OECT}} C^*$  of OECT mobility ( $\mu_{\text{OECT}}$ ) and volumetric capacitance ( $C^*$ ) was reported as figure of merit value, to benchmark the mixed conduction properties of materials and predict their performance in OECTs.<sup>16</sup> This product can be extracted from eq 1, using

the measured transconductance  $g_m$ ,  $V_{th}$  the threshold voltage,  $V_G$  the applied gate bias, and the geometry dependent OECT parameters such as the channel width ( $W$ ) and channel length ( $L$ ), as well as the channel thickness  $d$ .

$$g_m = \frac{\partial I_D}{\partial V_G} = \frac{W \cdot d}{L} \cdot \mu_{OECT} \cdot C^* \cdot (V_{th} - V_G) \quad (1)$$

The most studied polymer in OECTs is still poly(3,4-ethylenedioxythiophene) polystyrenesulfonate (PEDOT:PSS) due to its commercial availability, good mixed conductivity in doped state and high  $\mu_{OECT}$  ( $1.9 \text{ cm}^2\text{V}^{-1} \text{ s}^{-1}$ ) and moderate  $C^*$  values ( $39 \text{ Fcm}^{-3}$ ).<sup>16</sup> PEDOT:PSS is available only in doped state and therefore the OECTs are operated in depletion mode. On the other hand, un-doped p-type conjugated copolymers equipped with EG sidechains and thienothiophene moieties working under accumulation mode have already reached  $\mu C^*$  product values of around  $300 \text{ Fcm}^{-1}\text{V}^{-1} \text{ s}^{-1}$ . The best performing polymer of this class is poly(2-(3,3'-bis(2-(2-(2-methoxyethoxy)ethoxy)ethoxy)-[2,2'-bithiophen]5 yl)thieno [3,2-b]thiophene), p(g2T-TT).<sup>20-22</sup> In these materials, the ability of water molecules to form hydrogen bonds with EG allows swelling and facile ion penetration, necessary for electrochemical (i.e., bulk) doping. Also the fact that EG substituted polythiophenes are less soluble in water necessitates the use of external cross-linkers (also used in PEDOT:PSS) superfluous, which is advantageous for bioelectronics.<sup>23</sup> Another example of polythiophenes functionalized with EG sidechains was reported by Flagg et. al.<sup>24</sup> They studied the influence of the size of the doping anion in OECTs using poly(3-{[2-(2-methoxyethoxy)ethoxy]methyl} thiophene-2,5-diyl) (P3MEEMT). They found that compared to P3HT, P3MEEMT has faster anion injection rates, which was attributed to the hydration of the P3MEEMT crystal lattice. However, the impact of the nature of the linkage of the ethylene glycol side chain on mixed conduction and OECT

performance was not systematically studied up to now. The first report regarding the importance of the EG linkage came from another field, viz. Li<sup>+</sup>-conduction for battery applications.<sup>25</sup> They investigated polythiophene derivatives with diethylene glycol side chains, where the first oxygen of the glycol side chain is directly connected to the thiophene core (P3MEET), or via a methyl spacer (P3MEEMT). They showed that the Li<sup>+</sup>-ion conductivity (using added LiTFSI salt) increases in P3MEET.<sup>25</sup> But these polymers are neither studied for their mixed conduction properties nor compared in OECTs or OFETs.

Motivated by this observation of the large difference in Li<sup>+</sup>-ion conduction, we wanted to investigate the influence of the nature of diethylene glycol linkage on mixed conduction, crystallinity and performance in OFET and OECT devices by systematical comparative studies. For this purpose, three ethylene glycol functionalized polythiophene derivatives were synthesized by controlled polymerization using KCTP. The diethylene glycol side chains were linked either with no spacer (P3MEET), with a methyl spacer (P3MEEMT) or an ethyl spacer (P3MEEET). For a detailed comparative study of polymers prepared under same conditions, we synthesized the known polymers (P3MEET and P3MEEMT) and extended the series to a new polymer having ethyl spacer, P3MEEET. We elucidate the impact of EG side-chain linkage on the interplay of structure formation, swelling, volumetric capacitance and charge carrier mobility resulting in efficient mixed conduction properties. The three polymers differ in all the above properties drastically. For understanding these drastic differences in properties among the three polymers, we carried out first solid-state studies in thin films and bulk samples using OFET, XRD and AFM. These studies reveal that the crystallinity of P3MEEET reaches the highest value of 58 % in this series. Also, only P3MEEET showed a

lamellar morphology in thin film. In line with these properties, P3MEEET with ethyl spacer linked EG side chain shows the best performance in OECT. From OECT measurements, the highest figure of merit value ( $\mu C^*$  product) of  $11.5 \text{ Fcm}^{-1}\text{V}^{-1} \text{ s}^{-1}$  and highest volumetric capacitance of  $242 \pm 17 \text{ F/cm}^3$  was determined for this ethyl-spacer polymer P3MEEET. To enable an explanation of the extraordinary OECT performance of P3MEEET, the ionic charge storage capability was quantified using electrochemical impedance spectroscopy. This study reveals a linear increase of the volumetric capacitance  $C^*$  upon increasing the spacer length. E-QCMD measurements were carried out to evaluate the differences in water/ion uptake of the polymer films upon applying a doping potential in aqueous electrolyte. Out of these comprehensive and systematic studies, both in thin dry films and hydrated doped state of this series of three diethylene glycol functionalized polythiophenes, we could elucidate the unique properties associated with an ethyl spacer linkage of diethylene glycol in substituted polythiophenes.

## 2. EXPERIMENTAL SECTION

**2.1. Materials.** All chemicals were purchased from Sigma Aldrich or Fischer Scientific and used as received. P3HT was purchased from BASF SE ( $M_n = 15.6 \text{ kg/mol}$ ,  $\bar{D} = 1.6$ , measured with SEC with THF as eluent and a polystyrene calibration). The detailed monomer and polymer synthesis are described in the Supporting Information.

**2.2. Methods.** *2.2.1.  $^1\text{H-NMR}$ .*  $^1\text{H-NMR}$ . Spectra were recorded in deuterated chloroform on a Bruker Avance 250 spectrometer at 300 MHz at room temperature. Chemical shifts are noted in ppm and coupling constants in Hz. All spectra were calibrated according to the residual solvent peaks ( $\text{CHCl}_3 \delta = 7.26 \text{ ppm}$ ).

*2.2.2. Size exclusion chromatography (SEC).* SEC was performed utilizing a Waters 515 HPLC pump and THF with 0.25 wt% tetrabutylammonium bromide (TBAB) as eluent at a flow rate of 0.5 mL/min. A volume of 100  $\mu$ L of polymer solution (1-2 mg/mL) was injected with a 2707 Waters auto-sampler into a column setup comprising a guard column (Agilent PLgel Guard MIXED-C, 5  $\times$  0.75 cm, particle size 5  $\mu$ m) and two separation columns (Agilent PLgel MIXED-C, 30  $\times$  0.75 cm, particle size 5  $\mu$ m). Polymer size distributions were monitored with a Waters 998 photodiode array detector at 254 nm and a Waters 414 refractive index detector. Narrow distributed polystyrene standards were used for calibration and 1,2-dichlorobenzene as an internal reference.

*2.2.3. Differential Scanning Calorimetry (DSC):* A Perkin Elmer DSC 7 was used with a heating/cooling rate of 10 K/min. All samples 1st cooling and 2nd heating shown except for P3MEEMT: multiple measurements were conducted: max temperature increased gradually increased in steps of 10  $^{\circ}$ C from 80 to 130 $^{\circ}$ C, two measurement runs each, measurement shown is 2nd measurement to 110 $^{\circ}$ C.

*2.2.3. Wide angle x-ray scattering (WAXS).* Microfocus: A SAXSLAB laboratory Setup (Retro-F) (Copenhagen, Denmark) was used. As x-ray source, an AXO microfocus was used, with an AXO multilayer monochromator (Cu-K $_{\alpha}$  radiation  $\lambda=0.15418$  nm, ASTIX) purchased from X-ray optics. For 2D Scattering patterns, a Dectris PILATUS R 300K detector (Daettwil, Switzerland) was used. SAXSGUI v2.19.02 was used for data reduction of the WAXS and SAXS patterns. All measurements were conducted under vacuo and WAXS in transmission, GIWAXS in reflection. Sample to Detector distance is around 89 mm. All samples measured in ordered temperature region and in melt, P3HT, P3MEEET during cooling run, P3MEEMT and P3MEET during heating run.

*2.2.4. Spectroelectrochemistry Measurements.* Thin films were prepared on ITO coated glass substrates. Measurements were carried out using a UV-Vis spectrometer (OceanOptics USB 2000+) integrated with an Ivium CompactStat potentiostat. A Pt mesh was used as the counter electrode and an Ag/AgCl electrode as the reference electrode. The indicated voltages were applied versus  $V_{oc}$  for 10 s until the current stabilized prior to recording of the spectrum.

*2.2.5. Electrochemical Impedance Measurements (EIS).* Electrochemical impedance spectroscopy (EIS) for determination of capacitance was measured on polymer coated electrodes with a Metrohm Autolab PGSTAT128N at a frequency range between 100 kHz to 0.1 Hz. The impedance spectra of the gate of the OECT (0.003364 cm<sup>2</sup> area) were measured in 0.1 M NaCl aqueous solution, using a standard Ag/AgCl as the reference electrode and a Pt mesh as the counter electrode. The measurements were performed at a DC offset potential which enables the maximum achievable doping for the material and an AC amplitude of 10 mV. Once the spectra were recorded, they were fit to equivalent circuit using native tool software Metrohm Autolab NOVA. For fitting, Randle's circuit was used,  $R_{electrolyte}(R_{polymer}||C_{polymer})$ , and resulted in good fit quality. The capacitance values that are extracted were normalized by the measured film volume to determine volumetric capacitance ( $C^*$ ). Thickness of films was measured in the dry state with a Bruker Dektac profilometer. See SI **Figure 10** for an example of experimental determination of volumetric capacitance.

*2.2.6. Organic Field Effect Transistors (OFETs):* Bottom gate/bottom contact organic field effect transistors (OFET Gen4) were purchased from Fraunhofer IPMS. N-doped silicon (doping at the surface  $n \sim 3 \times 10^{17} \text{ cm}^{-3}$ ) was used as the surface and gate electrode. The dielectric consists of a 230 nm layer of silicon oxide. Each substrate

consisted of 16 devices with a constant channel width of 10 nm and varying channel length of 2.5–20  $\mu\text{m}$ . The source and drain electrodes were a 30 nm thick gold layer on a 10 nm ITO adhesion layer. The devices were prepared by cleaning in acetone and subsequently in iso-propanol in an ultrasonic bath for 10 min, followed by 15 min treatment in an ozone oven at 50  $^{\circ}\text{C}$  and subsequent silanization by 45 min treatment in a bath of 1 wt% octadecyltrichlorosilane (ODTS) in toluene at 60  $^{\circ}\text{C}$ . The devices were rinsed with toluene and *i*-propanol and dried. Thin polymer films were spin cast from 5 mg/mL chloroform solutions at a spinning speed of 3000 rpm under ambient conditions. All devices were stored and measured under nitrogen atmosphere. The I-V-characteristics were measured using an Agilent B1500 semiconductor parameter analyzer. Using eq. (2) the charge carrier mobilities were calculated from the slope of the  $(I^d)^{0.5}$ – $V_g$  plots.

$$I_d = \frac{W}{2L} C_i \mu (V_g - V_t)^2 \quad (2)$$

**2.2.7. Atomic Force Microscopy (AFM).** Measurements were performed on a Bruker MultiMode 8 AFM with a Nanoscope V controller equipped with a ScanAsystFluid+ cantilever ( $f_0 = 150$  kHz,  $k = 0.7$   $\text{Nm}^{-1}$ ) from Bruker. An excitation frequency of 2 kHz was used. Height and adhesion images (reflect strength of adhesive forces btw. Tip and surface) were recorded. Editing was done with open source software Gwyddion.

**2.2.8. OECT Fabrication.** The devices were fabricated according to the parylene-C lift-off method reported previously.<sup>26</sup> Standard glass microscope slides were cleaned via sonication in 2 % soap solution, acetone and isopropyl alcohol and dried with  $\text{N}_2$ . Connection pads and interconnects were deposited through a lift-off process using

photolithographic patterning of two positive photoresists (LOR 5B and S1813). A subsequent metal deposition via sputtering of Cr (10 nm) and of Au (110 nm) and metal lift-off using NMP defines the Au lines. A first layer of parylene C (1.6  $\mu\text{m}$ ), deposited together with a small amount of 3-(trimethoxysilyl) propyl methacrylate (A-174 Silane) to enhance adhesion, acts as an insulator to prevent disturbing capacitive effects at the metal liquid interface. Subsequently, an antiadhesive layer was spin-coated using a dilution of industrial cleaner (2 wt %, Micro-90), and a second parylene-C sacrificial layer (2.1  $\mu\text{m}$ ) is deposited. To define the contact pads and the channel of the OEECT, a second photolithographic patterning step using a thick positive photoresist (AZ9260) and AZ developer is used to protect the parylene-C layers from a subsequent plasma reactive ion etching step. All the polymer solutions were prepared in chloroform at 10 mg/mL and spin-coated from a glass fiber filter with 0.45  $\mu\text{m}$  pore diameter. Peeling of the second parylene-C sacrificial layer defines the channel dimensions. The thickness of the channels was measured using a DEKTAK 150 stylus profilometer.

*2.2.9. OEECT Characterization.* OEECTs were characterized using a dual-channel source-meter unit (NI-PXI) with custom-written control code in LabVIEW. All measurements were performed using an Ag/AgCl pellet (D = 2 mm  $\times$  H = 2 mm; Warner Instruments) as the gate electrode. The aqueous electrolytes were contained in a PDMS well on top of the OEECTs, and the electrolyte volume was constant at 120  $\mu\text{L}$  for all measurements.

*2.2.10. E-QCM-D Swelling Experiments.* Electrochemical Quartz crystal microbalance with dissipation monitoring: We performed EQCM-D measurements using a Q-sense analyzer (QE401, Biolin Scientific). Swelling measurements were performed as follows. First, we recorded the QCM-D response of the bare Au

sensors in the air, followed by the injection of the  $\text{NaCl}_{(\text{aq.})}$  0.1 M solutions into the chamber. This resulted in large shifts in frequency ( $f$ ) and dissipation of energy ( $D$ ), due to the density differences between the two media. The measurements were then stopped, the sensors were removed, and polymer films were spun cast directly on the same sensor from a 10 mg/mL chloroform solution at 1000 rpm. The absolute  $f$  value for each polymer coated sensor was obtained both in air and in  $\text{NaCl}_{(\text{aq.})}$  0.1 M, after the  $f$  signal was perfectly flat (i.e.,  $f < 0.5$  Hz) assuring that the system is in equilibrium. We then compared the absolute difference in  $f$  for multiple overtones between the bare sensor and the polymer coated sensors, both in air and in  $\text{NaCl}_{(\text{aq.})}$  0.1 M by using the function “stitched data” of Q-soft software. This function compares the selected datasets based on the raw frequencies measured and excludes the effect of the different densities between the two media (**Figure S11**). Thus, the difference of the  $f$  values of the stitched data is directly analogous to the thickness of the polymer in both media, which is calculated by using the Sauerbrey equation below (**eq. 3**). EQCM-D measurements were performed using Autolab PGstat128N potentiostat coupled with Q-sense electrochemistry module. The three-electrode setup was comprised of Ag/AgCl reference, Pt counter and Au/polymer EQCM-D sensor as the working electrode. The physical modelling of the two measured parameters, the  $f$  and  $D$ , is related to the viscoelastic properties of the film. On the one hand, a rigid film shows zero  $D$  as there are theoretically no energy losses (no viscoelasticity) and Sauerbrey equation can be used to quantify the mass ( $m$ ), using only one overtone as described in equation 3:

$$\Delta m = (-17.7)/n \Delta f_n \quad (3)$$

On the other hand, a thicker and/or softer film, does not follow the motion of the crystal and leads to energy losses during the oscillation. We approximate thicker

and/or soft films to behave like a Kelvin-Voigt element, which means that they exhibit both viscous and elastic characteristics acting in parallel (viscoelastic). A Kelvin-Voigt element has a complex shear modulus as described in equation 4:

$$G^* = \mu + 2\pi i f \eta \quad (4)$$

where  $G^*$  is the complex shear modulus,  $\mu$  is elasticity ( $\text{kgm}^{-1}\text{s}^{-2}$ ),  $\eta$  is viscosity ( $\text{kgm}^{-1}\text{s}^{-1}$ ) and  $f$  is the frequency. To calculate the mass changes of a thick, viscoelastic film, complex shear modulus was analysed and fitted using at least three frequency and dissipation of energy overtones. Q-Tools and D-find software were used for the modelling and data analysis. Since the polymer films are becoming soft and uptake a significant amount of water under doping potentials, we used the Kelvin-Voigt viscoelastic (VSE) model to fit the data. To quantify the mass correctly, we used the  $f$  and  $D$  data of three different overtones (3rd, 5th and 7th). The good quality of the fits guaranteed the accurate mass calculation accumulated within the films upon applied potentials.

### 3. RESULTS AND DISCUSSION

Three diethylene glycol functionalized thiophene monomers were synthesized, differing in the linkage of diethylene glycol side chain respective to the thiophene core in order to obtain the three polymers, P3MEET, P3MEEMT and P3MEEET (**Figure 1b**). The detailed monomers and polymer synthesis can be found in the supporting information (**Scheme S1**). For the polymer synthesis, we used the well-established Kumada Catalyst Transfer polymerization, with [1,3-bis(diphenylphosphino)propane] dichloronickel (II) ( $\text{Ni}(\text{dppp})\text{Cl}_2$ ) as catalyst and tert-butyl magnesium chloride as Grignard metathesis reagent. All the polymerization reactions proceeded for four hours, which is noticeably longer than for 3-

hexylthiophene monomer.<sup>13</sup> We assume that the catalyst Ni(dppp)Cl<sub>2</sub> probably coordinates to the ethylene glycol side chain (not only to the thiophene backbone), and so prolongs the polymerization.

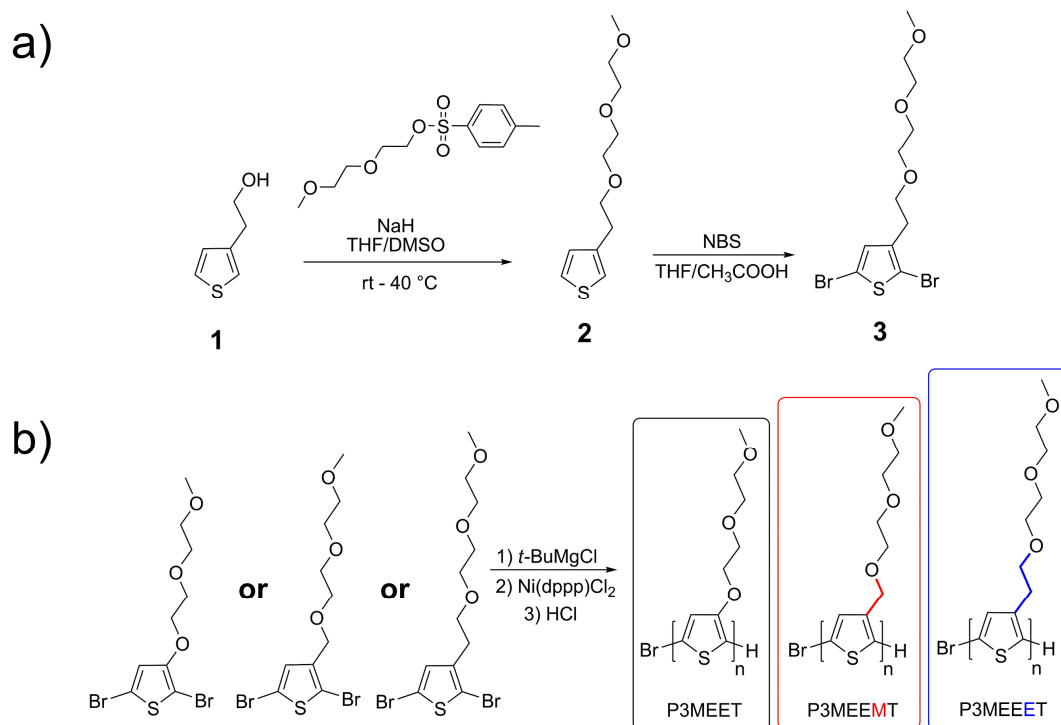


**Figure 1:** a) Newly developed synthetic route for the thiophene monomer 3MEEET (3) with an ethyl spacer. b) Kumada catalyst transfer polymerization procedure to obtain the polymers P3MEET (black), P3MEEMT (red) and P3MEEET (blue).

The polymers have narrow dispersity ( $\bar{D}$  1.08 to 1.4) and appreciably high molecular weight ( $\sim$  12 kg/mol) required for charge carrier transport, as determined with SEC measurements in THF. In the case of P3MEET, under our polymerization conditions in THF, we reached a maximum molecular weight of 10 kg/mol due to its limited solubility in THF and the relatively high reactivity of the monomer. The final polymers were purified using precipitation and Soxhlet extraction methods. P3MEEMT and P3MEEET are highly soluble in common solvents for polythiophenes, such as tetrahydrofuran and chloroform.

TGA studies reveal that the thermal stability of the polymers increases in the series from without spacer to ethyl spacer linkage of the EG unit. The lower thermal stability of P3MEET can be attributed mainly to the electron withdrawing effect of a directly connected EG unit (**Figure S1**). In differential scanning calorimetry experiments (DSC, **Figure S2**), a melting point for P3MEEET at 122 °C and a weak melting point for P3MEEMT at 99 °C can be observed, whereas P3MEET is an amorphous material. Both melting points as well as the melting enthalpies are noticeably lower compared to that of the benchmark polythiophene P3HT. These results indicate that EG side chains lead to reduced molecular order. The hole mobility in the dry state was extracted out of organic field effect transistors (OFETs). The hole mobility of the polymers was investigated in bottom-gate (Si) and bottom-contact (Au) devices with a silicon oxide layer as dielectric containing two different channels ranging from 10 to 20  $\mu\text{m}$ . The polymer films were directly spin-coated from chloroform onto the substrates. By plotting the square root of the drain current  $I_D$  versus the gate voltage  $V_G$  the hole mobility can be estimated. The average value for the hole mobility was taken out of 4 transistor measurements. The output and transfer curves of the OFET measurements are depicted in **Figure S3**. Here, we observe a clear difference in the charge carrier mobility.

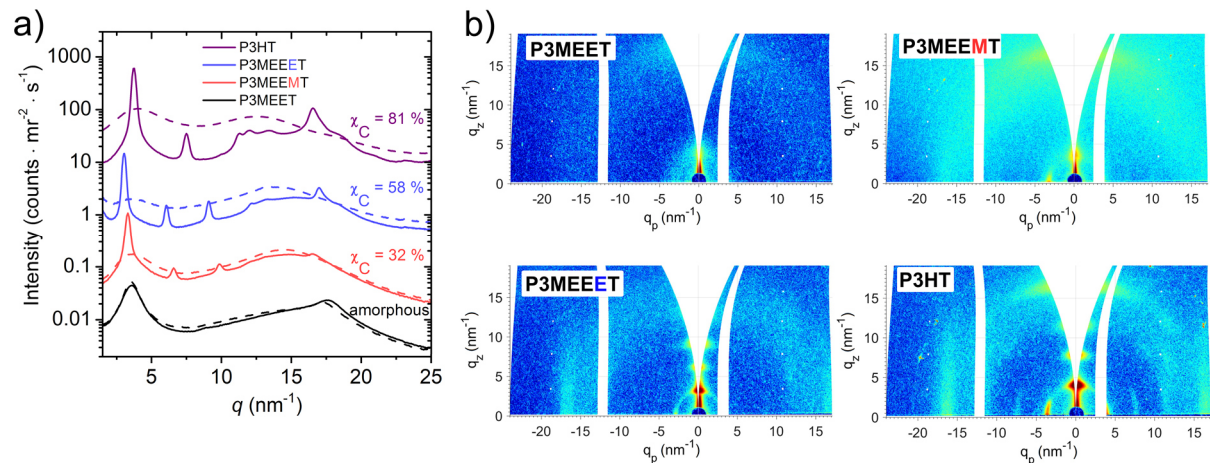


**Figure 2:** a) WAXS patterns of P3HT, P3MEEET, P3MEEMT and P3MEET. All samples were measured in ordered state (solid lines) and in the melt (dashed lines). b) Reciprocal space maps from GIWAXS of thin films of P3MEET, P3MEEMT, P3MEEET, and P3HT measured at an incident angle  $\alpha_i = 0.20^\circ$ . After spin coating, the polymer films except P3MEET were melt-crystallized in vacuo (P3HT, P3MEEET), respectively annealed (P3MEEMT at  $70^\circ\text{C}$ ).

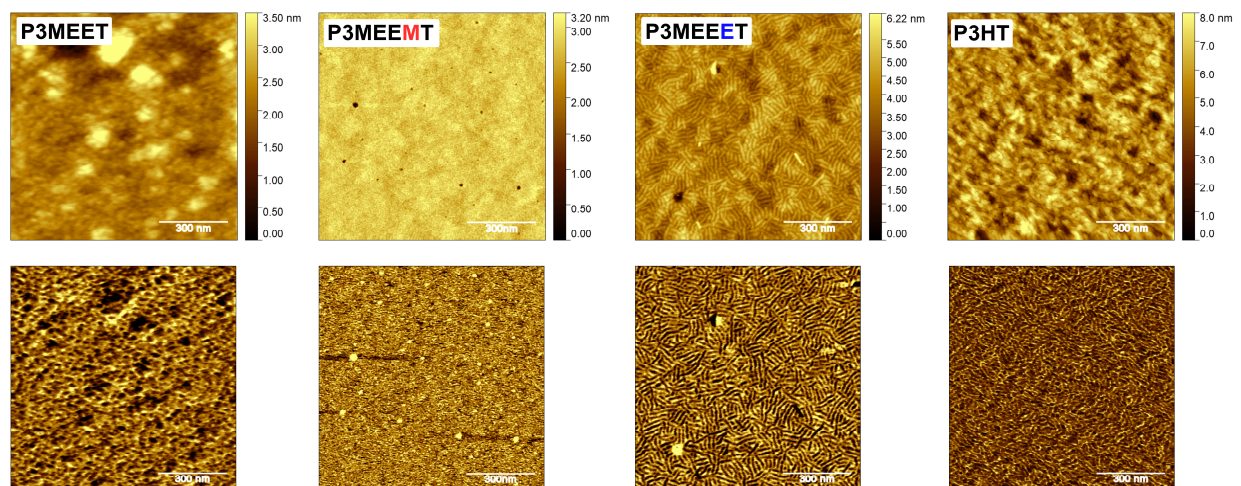


**Figure 3:** AFM pictures of P3MEET, P3MEEMT, P3MEEET, and P3HT recorded using peak force tapping mode. The height images are displayed in the upper row and the adhesion images are displayed in the lower row.

P3MEEET exhibits one order of magnitude higher hole mobility ( $0.005\text{ cm}^2/\text{Vs}$ ) compared to P3MEEMT ( $0.0003\text{ cm}^2/\text{Vs}$ ). With P3MEET, no transistor behavior could be observed. Compared to benchmark polythiophene P3HT, P3MEEET shows only one order of magnitude lower hole mobility and at the same time the highest reported value for a polar polythiophene homopolymer in transistors.<sup>27</sup>

To relate and possibly understand the differences in the hole mobility in the solid-state state of the different polymers in terms of microscopic structure, we performed X-ray scattering experiments in the bulk and in thin films. **Figure 2a** shows WAXS scattering pattern measured in transmission. All polymers except P3MEET were measured in the ordered state (solid line) and in the melt (dashed lines), whereby the exact temperature program for the different samples was adjusted according to their phase behavior observed in DSC (**Figure S2**). Generally, with decreasing length of the alkyl spacer between the first oxygen in the side chain and the polythiophene backbone, we observe a clear trend of decreasing order. This trend can be quantified in terms of the crystallinity, as estimated from the different intensities of the amorphous scattering contribution in between the first two Bragg-reflections according to Balko et. al.<sup>28</sup> For P3HT, the scattering pattern measured at 275 °C and at 20 °C after cooling from the melt is shown. The crystallinity amounts to 81 % comparable to values obtained in our previous studies.<sup>28</sup> For P3MEEET the measurement in the melt state was taken at 140 °C. While the crystal structure of P3MEEET is obviously similar to P3HT, the crystallinity shows a reduced value of 58%. For P3MEEMT the scattering pattern measured at 70 °C during a heating run is shown, as the sample does not recrystallize during cooling from the melt (150 °C), probably due to sample degradation. At this temperature the polymer is most well-ordered. In addition to a further reduced crystallinity of only 32 %, the (020) Bragg reflection is less pronounced. P3MEET finally shows only one much broader peak at the expected position of the (100) peak, which presumably corresponds to an amorphous structure. The measurement shown was taken at 20 °C as prepared and at 100°C. According to the earlier studies of P3HT crystal structure the lattice parameters of a monoclinic unit cell of P3HT were calculated from the WAXS peaks

in Figure 2a (see Table 1).<sup>28,29</sup> Note that to determine the crystalline structure of the polymers precisely, a well oriented sample would be needed. As the GIWAXS patterns (Figure 2b) of both P3MEEMT and P3MEEET show only a few diffraction peaks, the crystal structure could not be determined from these measurements alone. However, the qualitative similarity between the WAXS of P3HT and P3MEEMT and P3MEEET suggests a similarity in their crystal structure. As such, we estimated the lattice parameters  $a$  and  $b$  for P3MEEMT and P3MEEET under the assumption of a monoclinic crystal lattice with the same angle  $\gamma$  as for P3HT (**Table 1**). While the  $b$  parameter does not show any significant change, the monotonic increase of the parameter  $a$  when going from P3HT to P3MEEET is expected, as the side chains become more voluminous.

Apart from molecular order or crystallinity, also molecular orientation can have a strong influence on transport properties. We therefore performed grazing incidence X-ray diffraction (GIWAXS, incident angle of  $\alpha_i = 0.20^\circ$ ) experiments; the results are shown in **Figure 2b**). Complementary measurements taken at an incident angle  $\alpha_i = 10^\circ$  in order to access regions of higher  $q$  on the meridian gave consistent results and are shown in the Supporting Information (**Figure S4**). The polymer films were spin coated onto Si-substrates and afterwards melt-crystallized in vacuo during slow cooling to room temperature. The film thicknesses used were approx. 20-30 nm. In all polymers, besides the amorphous P3MEET, the (100) peak is clearly visible with orientation perpendicular and parallel to the substrate, indicating a mixed crystal orientation, but to different degrees. P3MEEET shows the strongest edge-on component. Overall, unlike the effects on crystallinity, we did not observe any strongly pronounced influence of the diethylene glycol linkage on the molecular orientation of ethylene glycol substituted polythiophenes on a Si substrate. Similar

trends as in the scattering experiments could be observed in AFM images taken from the thin film samples used for GIWAXS.

**Table 1:** Crystal lattice parameters of P3HT, P3MEEMT and P3MEEET calculated from the corresponding WAXS patterns.

Polymer	<i>a</i>	<i>b</i>	<i>c</i>	$\gamma$
	(nm)	(nm)	(nm)	(°)
P3HT	1.677	0.757	0.788	92.7
P3MEEMT <sup>a</sup>	1.820	0.755	-	92.7 <sup>b</sup>
P3MEEET	2.071	0.744	-	92.7 <sup>b</sup>

a) Values calculated from WAXS measurement taken at 20°C to allow for comparison between materials. b) Values assumed based on similarity of scattering patterns to P3HT.

The AFM was operated in peak force tapping mode and **Figure 3** shows height and adhesion images. Consistent with the strong edge-on orientation of P3MEEET a very clear lamellar structure was observed for this sample. The morphology of P3HT appears somewhat weaker, as it is often found for commercial samples, but still well visible. For the other two samples P3MEEMT and P3MEET no clear structures can be discerned, consistent with the lower degree of order observed for these samples in the WAXS and GIWAXS data. Summarizing the results obtained from the structure analysis, the differences in the measured hole mobility in the investigated polymers can be explained neither by a change in the  $\pi$ - $\pi$ -stacking distance nor by a change in the crystal orientation, which are known to have a strong influence on the charge carrier mobility.<sup>30</sup> Although further factors of influence cannot be ruled out, we suggest that the differences in the observed hole mobility are mainly caused by the differences in crystallinity.

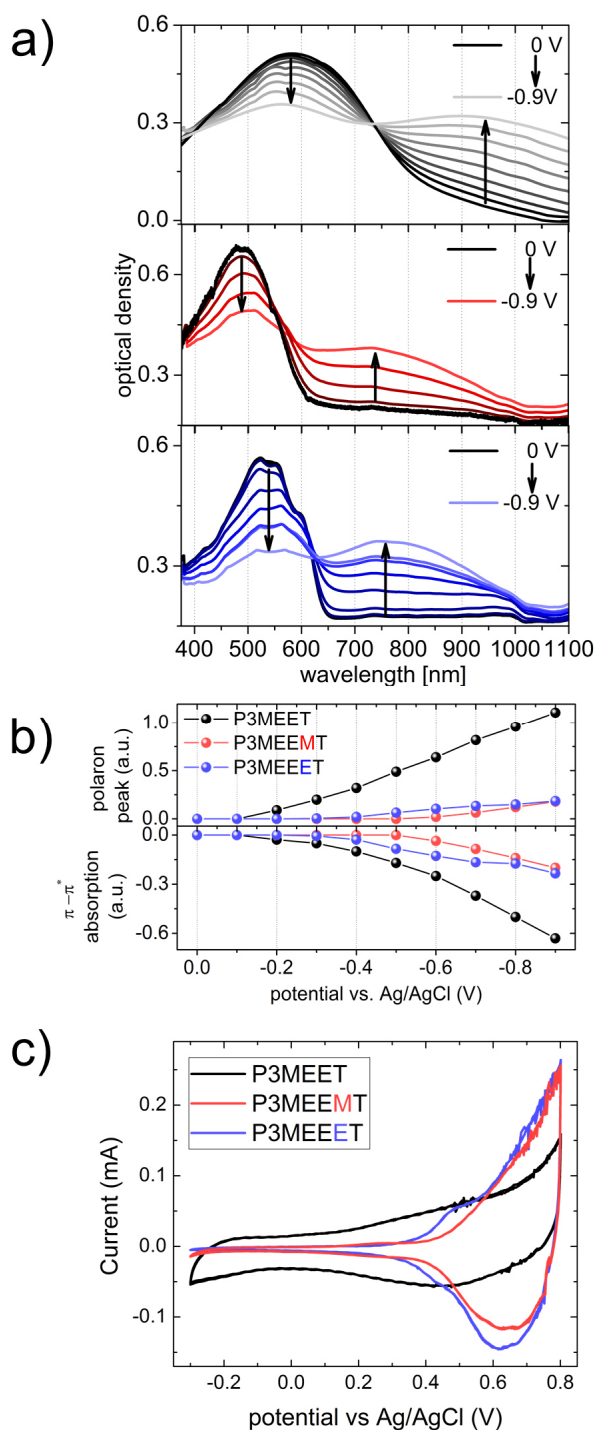


**Figure 4:** a) Spectroelectrochemistry measurements of polymer films on ITO of P3MEEET (blue), P3MEEMT (red) and P3MEET (black) respectively. The UV-Vis spectra were measured in 0.1 M NaCl when the films were biased from 0 V to -0.9 V in a three-electrode setup with an Ag/AgCl reference electrode and a Pt counter electrode. b) Changes in the intensities of polaron peak (top) and  $\pi-\pi^*$  absorption maximum (bottom), obtained from the difference spectra (Figure S6). c) Cyclic voltammetry (CV) measurements of the copolymer films were recorded with an Ag/AgCl reference electrode and a Pt counter electrode. CV curves were acquired at a scan rate of  $50 \text{ mV s}^{-1}$  in NaCl solution (0.1 M, aqueous).

oxidation at doping potentials applied in an aqueous medium and how the nature of the diethylene glycol side chain linkage affects the oxidation behavior of these polymers. This was investigated with spectroelectrochemistry (SEC) and cyclic voltammetry experiments in 0.1 M NaCl aqueous electrolyte. **Figure 4a** shows the UV-VIS spectra of the films subject to doping potentials (0 V to -0.9 V, in steps of -0.1 V, the neutral state is at 0 V, close to the open circuit potential,  $V_{oc}$ ). In **Figure S5**, the relative changes in SEC spectra obtained by subtracting the pristine spectrum at 0 V (i.e., before application of voltage) from the spectrum of each oxidized state reached by varying doping potentials are shown. For all the three polymers, the main  $\pi$ - $\pi^*$  associated absorption intensity decreases and concomitantly a red-shifted polaron peak starts growing upon application of a doping potential. The evolution of the decreasing  $\pi$ - $\pi^*$  absorption maximum and the growing polaron peak is depicted in **Figure 4b**. The onset, as well as the oxidation of P3MEEMT and P3MEEET in aqueous solution is comparable, regarding the extent of oxidation. The intensity of the polaron peak of P3MEET is substantially higher than that of the polymers with spacers when biased at the same doping voltages. Moreover, the onset of the oxidation for P3MEET is very low at around -0.2 V, whereas the polymers containing methyl and ethyl spacers exhibit higher onsets of about -0.5 to -0.6 V. Both observations can be explained as due to the ease of oxidation of P3MEET, which in turn can be attributed to its low ionization potential. This agrees very well with the photon electron spectroscopy in air (PESA) results discussed later. Furthermore, we recorded cyclic voltammetry (CV) curves of the polymer films in 0.1 M NaCl solution (**Figure 4c**). As expected from PESA and SEC studies, a drastic difference on the oxidation onset is observed; P3MEET showing an early onset at 0.1V. P3MEEMT and P3MEEET on the other hand show pronounced oxidation in contact with the

electrolyte, with oxidation onset for P3MEEMT at around 0.5 V and for P3MEEET at around 0.4 V, which also corresponds to the threshold voltage  $V_{th}$  observed in OECT operation as discussed below.

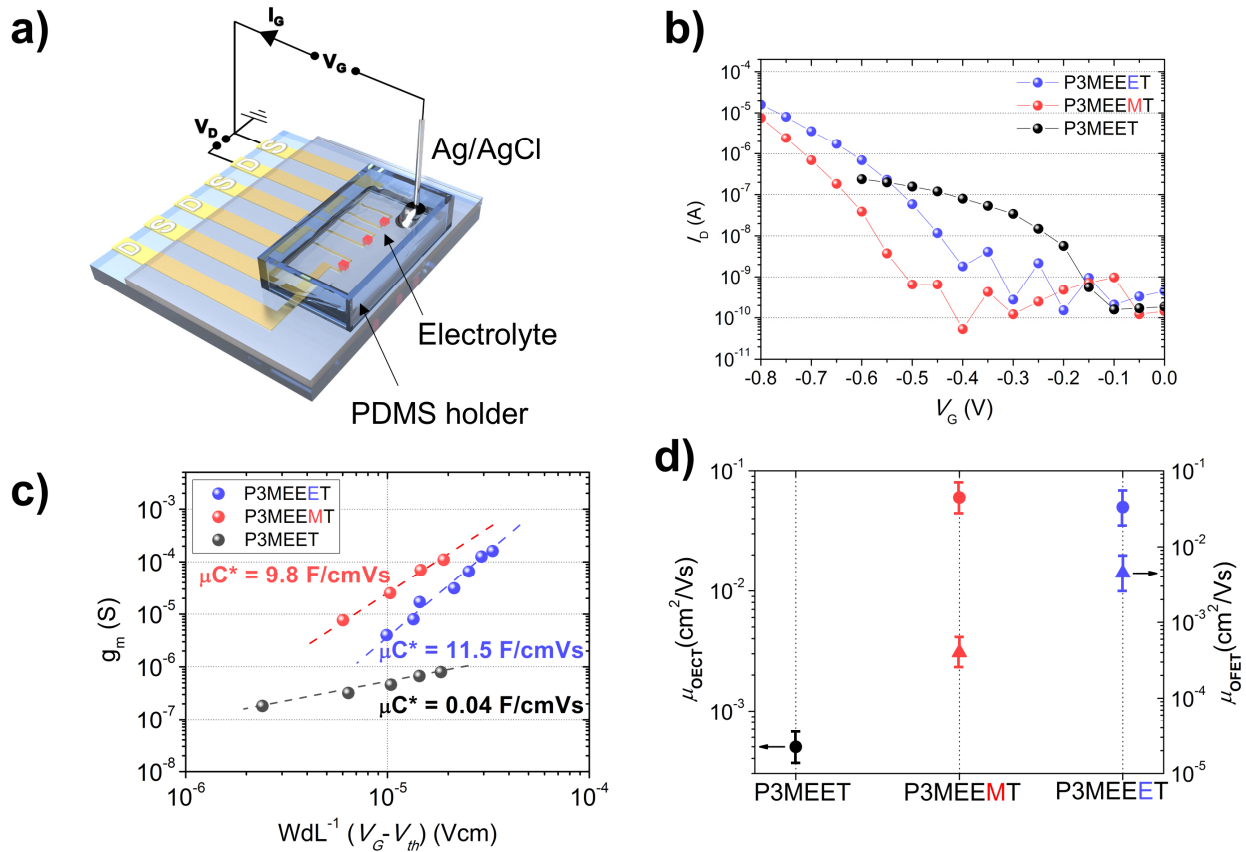


**Figure 5:** a) Illustration of an organic electrochemical transistor. The channel dimensions were  $W=100\ \mu\text{m}$  and  $L=10\ \mu\text{m}$ . OECTs were operated in 0.1 M aqueous NaCl solution with an Ag/AgCl pellet used as gate electrode. b) Transfer curve of P3MEET, P3MEEMT and P3MEEET.  $V_D = -0.6\ \text{V}$  for P3MEET and  $V_D = -0.8\ \text{V}$  for the other two polymers. c) Extracting the  $\mu C^*$  product from the plot of transconductance  $g_m$  vs. the channel geometry and operation parameters. Dashed lines indicate the fits. d) OECT hole mobility extracted in the hydrated state plotted against the bulk hole mobility estimated from organic field effect transistors (OFETs, bottom-gate, bottom-contact geometry).

Since all polymers exhibit oxidation behavior in aqueous environment at low applied voltages ( $<0.7\ \text{V}$  vs Ag/AgCl), the next step is to test them in OECT devices in order to quantify the mixed conduction properties. **Figure 5a** illustrates the OECT geometry which was used to examine the mixed conduction properties of the three functionalized polythiophenes. The fabrication of the devices is described in the

supporting information.<sup>31</sup> **Figure 5b** depicts the transfer curves of OECTs comprising these three polymers operated in 0.1 M NaCl solution (see the output curves and additional transfer curves in **Figure S7, S8 and S9**). We measured comparable thicknesses for the polymer films, between 90 and 100 nm, patterned on microscale Au patterns adjacent to the channels. Amongst all OECTs, the maximum drain current  $I_D$  was observed for the ethyl spacer derivative, P3MEEET, whereas the maximum transconductance (at a gate voltage  $V_G = -0.8$  V) was measured for P3MEEMT and P3MEEET. The OECT characteristics are summarized in **Table 2**. Notably, P3MEET in which the diethylene glycol side chain is directly connected to the thiophene backbone exhibits a very low threshold voltage  $V_{th}$  of -0.18 V, compared to the polymers with a methyl and an ethyl spacer. This can be mainly attributed to the increased electron withdrawing effect of the directly connected oxygen in P3MEET making this polymer easily oxidizable. To understand the differences in the threshold voltages, the ionization energies ( $I_P$ ) were measured using photon electron spectroscopy measurements in air (PESA, **Figure S9**). These measurements reveal that the  $I_P$  value is the lowest for P3MEET ( $I_P = -4.5$  eV) compared to the other two polymers with methyl or ethyl spacers, which explains the observed low threshold voltage in OECT operation for the former. This is also in agreement with the SEC and CV results discussed above. In comparison with the  $I_P$  value of P3HT (-4.67 eV)<sup>32</sup>, P3MEEMT and P3MEEET show similar values. This can be possibly explained by the lower electron withdrawing effect of the side chain in P3MEEMT and P3MEEET, which originates from the direct oxygen connection in P3MEET.

**Table 2:** Summary of the polymer properties: molecular weight, polydispersity, thermal properties and the mixed conduction properties volumetric capacitance  $C^*$ , the normalized transconductance  $g_m$  and the material dependent  $\mu_{\text{OECT}} C^*$  product.

Polymer	$M_n(\bar{D})^a$ (kg/mol)	$T_m^b$ (°C)	$\Delta H_m^b$ (J/g)	Volumetric Capacitance $C^*^c$ (F/cm <sup>3</sup> )	Threshold Voltage $V_{th}^d$ (V)	$I_p^e$ (eV)	Transcond uctance $g_m^f$ (S/cm)	Figure of Merit $\mu_{\text{OECT}} C^*^g$ (F/cmVs)
P3MEET	10 (1.43)	-	-	80±9	-0.18	-4.50	0.02	0.04±0.01
P3MEEMT	12 (1.21)	99	2.0	160±12	-0.66	-4.70	12.3	9.8±1.1
P3MEEET	13 (1.08)	122	8.6	242±17	-0.57	-4.66	20.4	11.5±1.4

a) SEC, with THF as eluent and against polystyrene standards. b) DSC in nitrogen atmosphere and a heating rate of 10 K/min. c) Electrical impedance spectroscopy (EIS) on Au electrodes with a DC voltage of 0.6 V (for P3MEET) or 0.8 V vs Ag/AgCl (for P3MEEMT and P3MEEET). d)  $V_{th}$  was determined from Figure S7 by extrapolating the linear region of the curve. e) Ionization potentials were estimated with PESA experiments (Figure S9) f)  $g_m$  at  $V_G = -0.6$  V and  $V_D = -0.8$  V and normalized by the film thickness. g) The  $\mu_{\text{OECT}} C^*$  product was extracted from Figure 5c.

In order to determine the  $\mu_{\text{OECT}} C^*$  product, **eq 1** was used. By plotting the transconductance  $g_m$  against the channel geometry and operation parameters of the OECT,  $\mu_{\text{OECT}} C^*$  can be estimated from the slope of the curve fit to the linear regime (**Figure 5c**). In aqueous 0.1 M NaCl solution, the  $\mu_{\text{OECT}} C^*$  product for P3MEEMT (9.8 F/cmVs) and P3MEEET (11.5 F/cmVs) are similar and considerably higher than that for P3MEET (0.04 F/cmVs). Thus, P3MEEET with ethyl-spacer is the most promising candidate for bioelectronic applications. It is also to be noted that all these polymers were tested in OECTs without the need of any cross-linker. It is known that OECT characteristics depend also on the nature of the electrolyte.<sup>20</sup> An electrolyte containing divalent anions or anions with different polarity may result in an increased capacitance and/or increased charge carrier mobility of the semiconductor, which can be applied in the case of P3MEEET to further improve the performance of the OECTs made thereof.

To investigate the charge storage capability, measurements of electrochemical impedance spectroscopy (**Figure S10**) of the polymers were recorded for the film before doping ( $V = V_{oc}$ ) and at a doping potential that gives the maximum transconductance ( $V = -0.8$  V for P3MEEMT and P3MEEET and  $-0.6$  V for P3MEET vs Ag/AgCl). The impedance data were fit to Randle's circuit  $R_{electrolyte}(R_{polymer}||C_{polymer})$  to extract the capacitance of the polymers, which was then normalized by the volume of the films to estimate the volumetric capacitance  $C^*$ . The volumetric capacitance increases from  $80 \pm 9$  to  $160 \pm 12$  and  $242 \pm 17$  F/cm<sup>3</sup> when going from P3MEET without a spacer to P3MEEMT and P3MEEET having a methyl or an ethyl spacer. The volumetric capacitance of P3MEEET is in the range of the highest reported value for the benchmark-type mixed conductor polymer p(g2T-TT).<sup>16</sup> The electrochemical charging in undoped (p-type) conjugated polymers involves simultaneous anion injection from the electrolyte and hole injection from the metal electrodes. Thus, a capacitor is formed between these two carriers, which is the origin of the capacitance of the polymer film. Proctor et. al. described that the volumetric capacitance  $C^*$  can be directly associated with the density of these anion/hole pairs in the polymer.<sup>33</sup> We attribute the increase in  $C^*$  to better accessibility of the mobile holes to the penetrating anions. Sivaraman et. al. linked the increased capacitance of P3HT with a higher crystallinity and order.<sup>34</sup> They attributed an increase in capacitance in higher crystalline P3HT derivatives to a decreased resistance for ion motion in the film. Furthermore, they observed that the highly disordered amorphous phase poses more restriction to the drift of ions. Thus, an increased volumetric capacitance  $C^*$  in P3MEEET, compared to P3MEEMT and P3MEET can be explained by the higher crystalline order and their regioregularity. Additionally, the high capacitance of P3MEEET can be well-understood if the swelling

and water/ion uptake of this polymer is considered as discussed later. Based on the capacitance values and the  $\mu_{\text{OECT}} C^*$  product extracted from OECT measurements, the hole mobility  $\mu_{\text{OECT}}$  of the three polythiophenes can be estimated.  $\mu_{\text{OECT}}$  describes the mobility in the swollen oxidized state under OECT operation and therefore strongly depends on the structural order of the polymer in the swollen and oxidized state, as well as the used electrolyte. High hole mobility in polythiophenes is generally observed in well-ordered systems, thus a large swelling in OECT operation can lower the effective hole mobility of the system, if the morphology or crystallinity in electrolyte medium is unfavorable for charge hopping.<sup>21</sup>.

From OECT measurements, similar hole mobilities were obtained for P3MEEMT and P3MEEET (0.06 cm<sup>2</sup>/Vs and 0.05 cm<sup>2</sup>/Vs), whereas P3MEET exhibits a lower mobility in the swollen state (5.2 ·10<sup>-4</sup> cm<sup>2</sup>/Vs). Comparing the  $\mu_{\text{OECT}}$  values (measured in hydrated state) to the  $\mu_{\text{OFET}}$  values obtained in thin dry films allows us to draw conclusions regarding the change in structure or morphology due to swelling (**Figure 5d**). It is very interesting to note that P3MEET is clearly an OECT material although it did not show any transistor characteristics in OFET configuration, indicating that swelling might have a positive influence on the charge transport for this polymer. On the other hand, P3MEEET (with the highest crystallinity in solid state), which showed one order of magnitude higher OFET mobility compared to P3MEEMT, forfeit this advantage in swollen state in OECT devices.

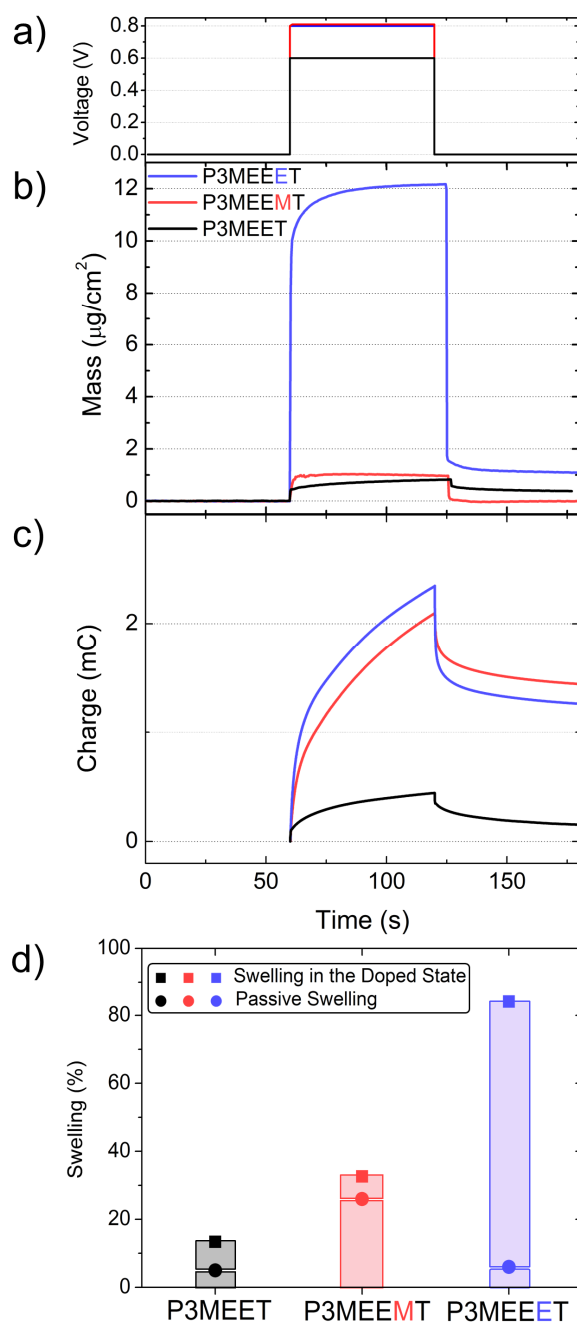


**Figure 6:** a) Doping potential profile applied to the polymer films, 0.8 V for P3MEEMT and P3MEEET and 0.6 V for P3MEET vs Ag/AgCl. b) mass change and c) the corresponding charge recorded as the polymers were doped. All measurements were performed in NaCl 0.1 M with an Ag/AgCl reference and Pt counter electrode, and the polymer film was deposited on QCM-D crystal with an area of  $0.7854 \text{ cm}^2$ . d) The swelling percentage of polymer films as they were exposed to the electrolyte and upon the application of the doping potential.

These results can be understood only if the swelling behavior of the three polymers are studied under applied voltages. In order to understand the influence of EG linkage on swelling and water/ion uptake properties of these conjugated polymers, we used electrochemical quartz crystal microbalance with dissipation monitoring (EQCM-D).<sup>35–37</sup> EQCM-D allows monitoring of mass exchange between an electrically active film and an electrolyte as the film undergoes electrochemical doping/de-doping. Here we study, simultaneously, the mass (ions and water) taken-up by the polymer films and the amount of charge generated during the electrochemical doping. First, we measure the passive swelling of the three polymers cast on QCM-D sensors as they are exposed to 0.1 M NaCl solution. The passive swelling percentage was calculated using Sauerbrey model (**Eq. 3**).<sup>23,35</sup> The pristine films swell 5 % ± 2 % (P3MEET), 26 % ± 8 % (P3MEEMT) and 6 % ± 3 % (P3MEEET) of their initial mass when exposed to the electrolyte (**Figure S11**). Here we observe that degree of passive swelling follows the order; P3MEEMT (methyl spacer) > P3MEEET (ethyl spacer) > P3MEET.

This order completely changes when measuring the amount of mass uptake triggered by a doping potential. The voltage pulses used for each polymer film are also the voltages that enabled the maximum transconductance. Upon application of a doping potential to the films (with a magnitude that corresponds to the maximum transconductance in OECTs), we monitor tremendous differences in the water and ion uptake (**Figure 6b** and **d**). Due to the large changes in the dissipation, we used a Kelvin-Voigt viscoelastic model to interpret the swelling behavior and to calculate the mass uptake.<sup>38</sup> P3MEEET takes up noticeably more mass compared to P3MEEMT and P3MEET. The total mass (water and Cl<sup>-</sup> ions) accumulating inside P3MEEET during oxidation is about 12 μg/cm<sup>2</sup>, whereas P3MEET and P3MEEMT take up

around  $1.0 \mu\text{g}/\text{cm}^2$  (see **Figure S12** for the recorded raw frequency and dissipation changes). This 12 times higher mass uptake of P3MEEET during the penetration of electrolyte anions is by far the highest value reported up to date, compared to other mixed conductors, as well as the benchmark accumulation mode material p(g2T-TT) when it is doped to approximately to the same oxidized state.<sup>20,21</sup> Furthermore, the charge recorded from these films in-situ upon electrochemical doping with  $\text{Cl}^-$  ions is calculated to be  $2.33 \cdot 10^{-3} \text{ C}$  for the P3MEEET film and  $2.1 \cdot 10^{-3} \text{ C}$  for the P3MEEMT film, while it is  $4.4 \cdot 10^{-4} \text{ C}$  for P3MEET, which were then normalized by the film thickness, resulting in  $45.4 \text{ C}/\text{cm}$  for P3MEET,  $135.5 \text{ C}/\text{cm}$  for P3MEEMT and  $153.3 \text{ C}/\text{cm}$  for P3MEEET. These values are well in line with the volumetric capacitance calculated from the electrochemical impedance spectra of films recorded in OECT channels (**Figure S10**) and demonstrate the improvement in the ionic charging of the ethylene glycol functionalized polythiophenes as a result of side-chain engineering. Why exactly an ethyl-spacer linked diethylene glycol (in P3MEEET) causes this strong ability of water and ion uptake in the oxidized state compared to no spacer or methyl spacer is not yet fully understood. Additionally, it seems that the  $\mu_{\text{OECT}}$  values also correlate with the charging in the hydrated system. The observed swelling in E-QCMD measurements for P3MEET (with no measurable  $\mu_{\text{OFET}}$  mobility) resulting in measurable  $\mu_{\text{OECT}}$  also supports this assumption. However, we like to point out that mixed conduction in differently swollen and differently oxidized systems is very complex and difficult to be correlated with the individual material properties in solid state, for example the charge carrier mobilities in thin dry films.

#### 4. CONCLUSION

A detailed study of the impact and importance of the nature of linkage of diethylene glycol side chain functionalized polythiophene derivatives towards the mixed conduction and solid-state properties was presented. Three defined polythiophenes equipped with diethylene glycol side chains (P3MEET, P3MEEMT and P3MEEET), varying the side-chain linkage respective to the thiophene backbone (without, methyl and ethyl spacer), were synthesized in a controlled manner with similar molecular weights and low polydispersity. The suitability of these polymers for OECT applications was tested using SEC, UV-Vis and CV measurements performed in an aqueous medium. We found that the low oxidation onset observed for P3MEET correlates with the low ionization energy measured with PESA. The solid-state hole mobility of the polymers was determined using OFET configuration. Here, P3MEEET exhibits the highest reported value ( $0.005 \text{ cm}^2/\text{Vs}$ ) for a polar polythiophene homopolymer and this is one order of magnitude higher compared to the polymer with methyl spacer (P3MEEMT). This increase in the solid-state hole mobility can be attributed to the higher crystallinity of P3MEEET compared to P3MEEMT as revealed by the WAXS. The differences in molecular order were also confirmed by AFM, where only P3MEEET shows a lamellar morphology. A possible application in bioelectronic devices was tested with organic electrochemical transistors in 0.1 M NaCl. Drastic differences in the performance of the three conjugated polymers could be observed, where P3MEEET (ethyl spacer) shows the best mixed conduction properties with a  $\mu_{\text{OECT}} C^*$  product of 11.5 (F/cmVs). To understand the influence of linkage of diethylene glycol side chain and the extraordinary performance of P3MEEET, the ionic charge storage capability was tested using electrochemical impedance spectroscopy. This study reveals a linear increase of the volumetric

capacitance  $C^*$  upon increasing the spacer length. This can be presumably attributed to a better accessibility of the diethylene glycol side chain and thus an enhanced ion transport, as well as a higher order of P3MEEET. P3MEEET exhibits a volumetric capacitance of around  $242 \pm 17 \text{ F/cm}^3$ , which is in the range of the highest reported values for p-type organic mixed conductors.<sup>16</sup> From OECT device characteristics, the hole mobility ( $\mu_{\text{OECT}}$ ) of the polymers in the hydrated state was extracted. The  $\mu_{\text{OECT}}$  of the P3MEEMT and P3MEEET are almost identical in the swollen state. The differences in water uptake and swelling were monitored with E-QCM-D experiments, without (passive swelling) and under applied doping potential. P3MEEET takes up 12 times more water and ions than P3MEET and P3MEEMT in the oxidized state. The charge uptake derived from the same measurements correlate well with the volumetric capacitance. Thus, the nature of linkage, which may seem to be trivial plays an enormously important role in deciding the complex interplay of swelling, ion uptake and charge transport in OECTs. We conclude that this systematic and comparative study combining various interdisciplinary characterization techniques gives insights into determining factors influencing mixed conduction. Overall, this contribution emphasizes the crucial role of side-chain engineering in diethylene glycol substituted polythiophenes towards high performance polymeric mixed conductors.

## 5. REFERENCES

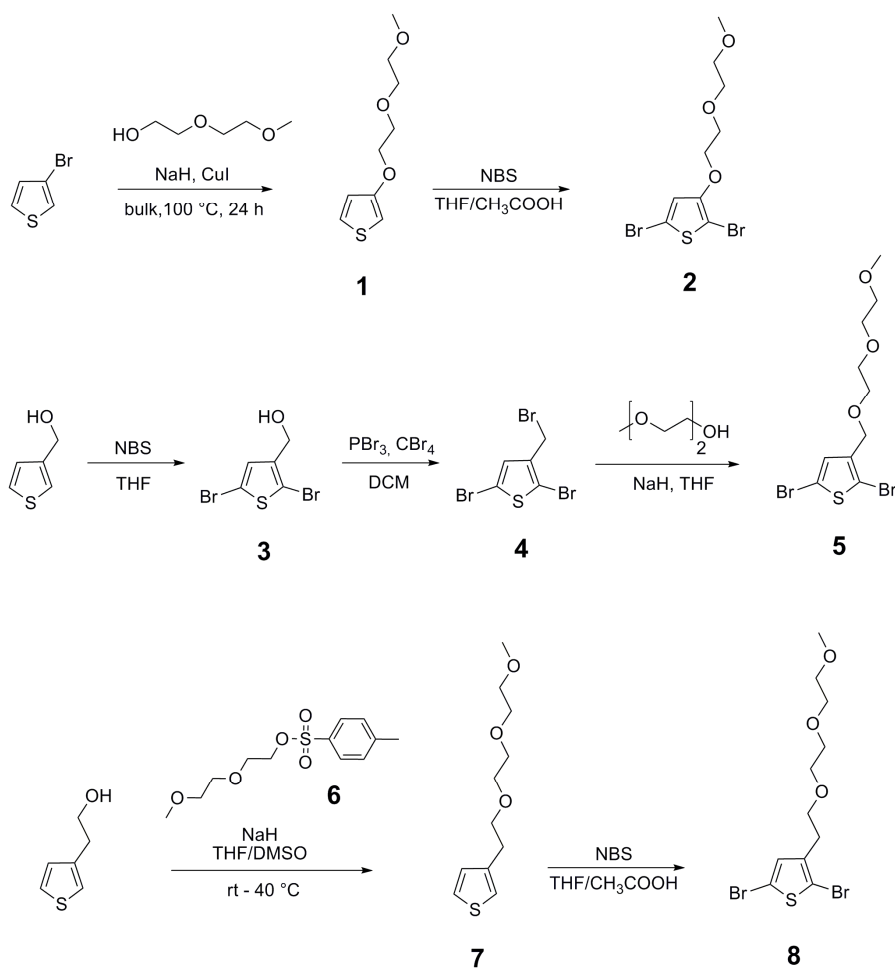
- (1) Mei, J.; Bao, Z. Side Chain Engineering in Solution-Processable Conjugated Polymers. *Chemistry of Materials* **2014**, *26* (1), 604–615.
- (2) Giovannitti, A.; Maria, I. P.; Hanifi, D.; Donahue, M. J.; Bryant, D.; Barth, K. J.; Makdah, B. E.; Savva, A.; Moia, D.; Zetek, M.; Barnes, P. R. F.; Reid, O. G.; Inal, S.; Rumbles, G.; Malliaras, G. G.; Nelson, J.; Rivnay, J.; McCulloch, I. The Role of the Side Chain on the Performance of N-Type Conjugated Polymers in Aqueous Electrolytes. *Chemistry of Materials* **2018**, *30* (9), 2945–2953.
- (3) Liu, J.; Qiu, L.; Alessandri, R.; Qiu, X.; Portale, G.; Dong, J.; Talsma, W.; Ye, G.; Sengrian, A. A.; Souza, P. C. T.; Loi, M. A.; Chiechi, R. C.; Marrink, S. J.; Hummelen, J. C.; Koster, L. J. A. Enhancing Molecular N-Type Doping of Donor-Acceptor Copolymers by Tailoring Side Chains. *Adv. Mater.* **2018**, *30* (7), 1704630.
- (4) Meng, B.; Song, H.; Chen, X.; Xie, Z.; Liu, J.; Wang, L. Replacing Alkyl with Oligo(Ethylene Glycol) as Side Chains of Conjugated Polymers for Close  $\pi$ - $\pi$  Stacking. *Macromolecules* **2015**, *48* (13), 4357–4363.
- (5) Kiefer, D.; Giovannitti, A.; Sun, H.; Biskup, T.; Hofmann, A.; Koopmans, M.; Cendra, C.; Weber, S.; Anton Koster, L. J.; Olsson, E.; Rivnay, J.; Fabiano, S.; McCulloch, I.; Müller, C. Enhanced N-Doping Efficiency of a Naphthalenediimide-Based Copolymer through Polar Side Chains for Organic Thermoelectrics. *ACS Energy Lett.* **2018**, *3* (2), 278–285.
- (6) Brendel, J. C.; Schmidt, M. M.; Hagen, G.; Moos, R.; Thelakkat, M. Controlled Synthesis of Water-Soluble Conjugated Polyelectrolytes Leading to Excellent Hole Transport Mobility. *Chemistry of Materials* **2014**, *26* (6), 1992–1998.
- (7) Schmidt, M. M.; ElMahmoudy, M.; Malliaras, G. G.; Inal, S.; Thelakkat, M. Smaller Counter Cation for Higher Transconductance in Anionic Conjugated Polyelectrolytes. *Macromolecular Chemistry and Physics* **2018**, *219* (2), 1700374.
- (8) Schmode, P.; Ohayon, D.; Reichstein, P. M.; Savva, A.; Inal, S.; Thelakkat, M. High Performance Organic Electrochemical Transistors Based on Conjugated Polyelectrolyte Copolymers. *Chem. Mater.* **2019**, *31* (14), 5286–5295.
- (9) Inal, S.; Rivnay, J.; Suiu, A.-O.; Malliaras, G. G.; McCulloch, I. Conjugated Polymers in Bioelectronics. *Accounts of Chemical Research* **2018**, *51* (6), 1368–1376.
- (10) Zhao, H.; Zhu, B.; Sekine, J.; Luo, S.-C.; Yu, H. Oligoethylene-Glycol-Functionalized Polyoxothiophenes for Cell Engineering: Syntheses, Characterizations, and Cell Compatibilities. *ACS Applied Materials & Interfaces* **2012**, *4* (2), 680–686.
- (11) Collier, G. S.; Pelse, I.; Reynolds, J. R. Aqueous Electrolyte Compatible Electrochromic Polymers Processed from an Environmentally Sustainable Solvent. *ACS Macro Lett.* **2018**, *7* (10), 1208–1214.
- (12) Goel, M.; Heinrich, C. D.; Krauss, G.; Thelakkat, M. Principles of Structural Design of Conjugated Polymers Showing Excellent Charge Transport toward Thermoelectrics and Bioelectronics Applications. *Macromol. Rapid Commun.* **2019**, 1800915.
- (13) Lohwasser, R. H.; Thelakkat, M. Toward Perfect Control of End Groups and Polydispersity in Poly(3-Hexylthiophene) via Catalyst Transfer Polymerization. *Macromolecules* **2011**, *44* (9), 3388–3397.
- (14) Iovu, M. C.; Sheina, E. E.; Gil, R. R.; McCullough, R. D. Experimental Evidence for the Quasi-“Living” Nature of the Grignard Metathesis Method for the Synthesis of Regioregular Poly(3-Alkylthiophenes). *Macromolecules* **2005**, *38* (21), 8649–8656.

- (15) Yokoyama, A.; Miyakoshi, R.; Yokozawa, T. Chain-Growth Polymerization for Poly(3-Hexylthiophene) with a Defined Molecular Weight and a Low Polydispersity. *Macromolecules* **2004**, *37* (4), 1169–1171.
- (16) Inal, S.; Malliaras, G. G.; Rivnay, J. Benchmarking Organic Mixed Conductors for Transistors. *Nature Communications* **2017**, *8* (1).
- (17) Paulsen, B. D.; Tybrandt, K.; Stavrinidou, E.; Rivnay, J. Organic Mixed Ionic–Electronic Conductors. *Nat. Mater.* **2019**.
- (18) Simon, D. T.; Gabrielsson, E. O.; Tybrandt, K.; Berggren, M. Organic Bioelectronics: Bridging the Signaling Gap between Biology and Technology. *Chemical Reviews* **2016**, *116* (21), 13009–13041.
- (19) Rivnay, J.; Inal, S.; Salleo, A.; Owens, R. M.; Berggren, M.; Malliaras, G. G. Organic Electrochemical Transistors. *Nature Reviews Materials* **2018**, *3* (2), 17086.
- (20) Cendra, C.; Giovannitti, A.; Savva, A.; Venkatraman, V.; McCulloch, I.; Salleo, A.; Inal, S.; Rivnay, J. Role of the Anion on the Transport and Structure of Organic Mixed Conductors. *Adv. Funct. Mater.* **2019**, *29* (5), 1807034.
- (21) Savva, A.; Cendra, C.; Giugni, A.; Torre, B.; Surgailis, J.; Ohayon, D.; Giovannitti, A.; McCulloch, I.; Di Fabrizio, E.; Salleo, A.; Rivnay, J.; Inal, S. Influence of Water on the Performance of Organic Electrochemical Transistors. *Chemistry of Materials* **2019**, *31* (3), 927–937.
- (22) Giovannitti, A.; Sbircea, D.-T.; Inal, S.; Nielsen, C. B.; Bandiello, E.; Hanifi, D. A.; Sessolo, M.; Malliaras, G. G.; McCulloch, I.; Rivnay, J. Controlling the Mode of Operation of Organic Transistors through Side-Chain Engineering. *Proceedings of the National Academy of Sciences* **2016**, *113* (43), 12017–12022.
- (23) ElMahmoudy, M.; Inal, S.; Charrier, A.; Uguz, I.; Malliaras, G. G.; Sanaur, S. Tailoring the Electrochemical and Mechanical Properties of PEDOT:PSS Films for Bioelectronics. *Macromolecular Materials and Engineering* **2017**, *302* (5), 1600497.
- (24) Flagg, L. Q.; Bischak, C. G.; Onorato, J. W.; Rashid, R. B.; Luscombe, C. K.; Ginger, D. S. Polymer Crystallinity Controls Water Uptake in Glycol Side-Chain Polymer Organic Electrochemical Transistors. *Journal of the American Chemical Society* **2019**, *141* (10), 4345–4354.
- (25) Dong, B. X.; Nowak, C.; Onorato, J. W.; Strzalka, J.; Escobedo, F. A.; Luscombe, C. K.; Nealey, P. F.; Patel, S. N. Influence of Side-Chain Chemistry on Structure and Ionic Conduction Characteristics of Polythiophene Derivatives: A Computational and Experimental Study. *Chemistry of Materials* **2019**, *31* (4), 1418–1429.
- (26) Wustoni, S.; Savva, A.; Sun, R.; Bihar, E.; Inal, S. Enzyme-Free Detection of Glucose with a Hybrid Conductive Gel Electrode. *Adv. Mater. Interfaces* **2019**, *6* (1), 1800928.
- (27) Heinrich, C. D.; Thelakkat, M. Poly-(3-Hexylthiophene) Bottlebrush Copolymers with Tailored Side-Chain Lengths and High Charge Carrier Mobilities. *Journal of Materials Chemistry C* **2016**, *4* (23), 5370–5378.
- (28) Balko, J.; Lohwasser, R. H.; Sommer, M.; Thelakkat, M.; Thurn-Albrecht, T. Determination of the Crystallinity of Semicrystalline Poly(3-Hexylthiophene) by Means of Wide-Angle X-Ray Scattering. *Macromolecules* **2013**, *46* (24), 9642–9651.
- (29) Balko, J.; Portale, G.; Lohwasser, R. H.; Thelakkat, M.; Thurn-Albrecht, T. Surface Induced Orientation and Vertically Layered Morphology in Thin Films of Poly(3-Hexylthiophene) Crystallized from the Melt. *J. Mater. Res.* **2017**, *32* (10), 1957–1968.

- (30) Mei, J.; Kim, D. H.; Ayzner, A. L.; Toney, M. F.; Bao, Z. Siloxane-Terminated Solubilizing Side Chains: Bringing Conjugated Polymer Backbones Closer and Boosting Hole Mobilities in Thin-Film Transistors. *J. Am. Chem. Soc.* **2011**, *133* (50), 20130–20133.
- (31) Wustoni, S.; Combe, C.; Ohayon, D.; Akhtar, M. H.; McCulloch, I.; Inal, S. Membrane-Free Detection of Metal Cations with an Organic Electrochemical Transistor. *Adv. Funct. Mater.* **2019**, *29* (44), 1904403.
- (32) Liu, F.; Chen, D.; Wang, C.; Luo, K.; Gu, W.; Briseno, A. L.; Hsu, J. W. P.; Russell, T. P. Molecular Weight Dependence of the Morphology in P3HT:PCBM Solar Cells. *ACS Appl. Mater. Interfaces* **2014**, *6* (22), 19876–19887.
- (33) Proctor, C. M.; Rivnay, J.; Malliaras, G. G. Understanding Volumetric Capacitance in Conducting Polymers. *J. Polym. Sci. Part B: Polym. Phys.* **2016**, *54* (15), 1433–1436.
- (34) Sivaraman, P.; Mishra, S. P.; Bhattacharyya, A. R.; Thakur, A.; Shashidhara, K.; Samui, A. B. Effect of Regioregularity on Specific Capacitance of Poly(3-Hexylthiophene). *Electrochimica Acta* **2012**, *69*, 134–138.
- (35) Savva, A.; Wustoni, S.; Inal, S. Ionic-to-Electronic Coupling Efficiency in PEDOT:PSS Films Operated in Aqueous Electrolytes. *J. Mater. Chem. C* **2018**, *6* (44), 12023–12030.
- (36) Rodahl, M.; Kasemo, B. A Simple Setup to Simultaneously Measure the Resonant Frequency and the Absolute Dissipation Factor of a Quartz Crystal Microbalance. *Review of Scientific Instruments* **1996**, *67* (9), 3238–3241.
- (37) Rodahl, M.; Höök, F.; Krozer, A.; Brzezinski, P.; Kasemo, B. Quartz Crystal Microbalance Setup for Frequency and Q-factor Measurements in Gaseous and Liquid Environments. *Review of Scientific Instruments* **1995**, *66* (7), 3924–3930.
- (38) Höök, F.; Rodahl, M.; Brzezinski, P.; Kasemo, B. Energy Dissipation Kinetics for Protein and Antibody–Antigen Adsorption under Shear Oscillation on a Quartz Crystal Microbalance. *Langmuir* **1998**, *14* (4), 729–734.

## 6. SUPPORTING INFORMATION

### Synthesis



**Scheme S1:** Complete synthetic route of the used ethylene glycol thiophene monomers.

*Synthesis of 3-[2-(2-methoxyethoxy) ethoxy] thiophene (1)*

A dry 250-mL Schlenk tube, was flushed with N<sub>2</sub> and charged with sodium hydride (6.0 g (60% in mineral oil), 0.15 mol) and anhydrous DMF (25 mL). The reaction flask was cooled down to 0 °C, whereupon anhydrous 1-DEGMME (60 mL, 0.48 mol) was added dropwise from the addition funnel over a 30-minute time period. The solution was allowed to stir for additional 1 hour to assure complete consumption of NaH, while the temperature was maintained at 0 °C. To this reaction mixture, 3-bromothiophene (16.3 g, 0.10 mol) and CuBr (1.44 g, 0.01 mol) were added. The ice bath was replaced with an oil bath and the solution was heated up to ~ 110 °C. After 30 minutes at the elevated temperature, an aliquot was taken out, quenched with a 1 M aqueous solution of NH<sub>4</sub>Cl, extracted with diethyl ether (Et<sub>2</sub>O), and subjected to NMR analysis. Note, if a relative abundance of the starting material was detected, an equimolar amount of CuBr was added and the reaction was allowed to proceed for an additional 30 minutes at the elevated temperature. The material was then poured into a 1 M aqueous solution of NH<sub>4</sub>Cl (100 mL) and stirred for 10 minutes. The organic phase was extracted with hexane and dried over anhydrous magnesium sulfate (MgSO<sub>4</sub>). After the product was filtered, the solvent was removed by rotary evaporation. The crude product was purified via column chromatography with hexane: ethylacetate 7:3 as eluent to yield 17.1 g (93%) of 3-hexyloxythiophene as a colorless oil.

<sup>1</sup>H-NMR: δ<sub>H</sub> (300 MHz; ppm, CDCl<sub>3</sub>): 0.93 (t, 3H), 1.42 (m, 6H), 1.79(m, 2H), 3.97 (t, 2H), 6.25 (dd, 1H), 6.78 (dd, 1H), 7.19 (dd, 1H)

*Synthesis of 2,5-dibromo-3-[2-(2-methoxyethoxy)ethoxy]thiophene (2)*

14.7 g 3-[2-(2-methoxyethoxy) ethoxy] thiophene (72.6 mmol) and 29.7 g N-bromosuccinimide (166.7 mmol) were dissolved under argon and under the exclusion of light at RT in a mixture of dry THF and acetic acid (74 mL/74 mL). The reaction mixture was stirred for 3 h. Afterwards, the solvent was removed by rotary evaporation. The resulting residue was washed with hexanes, filtered, and purified using column chromatography on silica gel with hexanes/ ethyl acetate 9:1 as the eluent (R<sub>f</sub> = 0.16). The product was dried over anhydrous MgSO<sub>4</sub>. After filtration, the solvent was removed by rotary evaporation. The compound was dried under vacuum (yield 78 %).

$^1\text{H-NMR}$ :  $\delta_{\text{H}}$  (300 MHz; ppm,  $\text{CDCl}_3$ ): 0.93 (t, 3H), 1.42 (m, 6H), 1.79 (m, 2H), 3.97 (t, 2H), 6.78 (dd, 1H).

#### *Synthesis of 2,5-dibromo-3-thiophenemethanol (3)*

3-Thiophenemethanol (5.0 g, 44 mmol) was dissolved in THF (40 mL) in a dried 100 mL round bottom flask. The flask was degassed with nitrogen for 15 min before being sealed under a nitrogen atmosphere. NBS (16.445 g, 92.4 mmol) was added gradually to the reaction mixture (over 10 minutes) and the reaction was run at room temperature overnight. The solution was passed through a plug of Celite to remove residual NBS, then THF was removed by rotary evaporation. The product was dissolved in diethyl ether, then rinsed with 1M sodium hydroxide solution and water. The organic layer was concentrated and the product was eluted over silica gel using hexane:ethyl acetate (80:20). The solvent was removed by rotary evaporation to yield the desired product (10.0 g, 85% yield) as a white solid.

$^1\text{H-NMR}$ :  $\delta_{\text{H}}$  (300 MHz; ppm,  $\text{CDCl}_3$ ): 4.60 (s, 2H) and 6.70 (s, 1H).

#### *Synthesis of 2,5-dibromo-3-bromomethylthiophene (4)*

8 g 2,5-Dibromo-3-thiophenemethanol (29.9 mol) in dry methylene chloride (100 mL) was added to a 250 mL flask and sealed under a nitrogen atmosphere. The flask was placed in an ice water bath, and the mixture stirred for 20 min. Phosphorus tribromide (2.9 mL, 30.5 mmol) was added dropwise to the solution over a 15 min period. The reaction was run at room temperature for 5 hours, then quenched with a 10% sodium bicarbonate solution. The organic solution was passed through a plug of Celite, rinsed with water, and dried over magnesium sulfate. The solution was filtered and dried using rotary evaporation to yield the product (5.8 g, 94% yield) as a light yellow solid.

$^1\text{H-NMR}$ :  $\delta_{\text{H}}$  (300 MHz; ppm,  $\text{CDCl}_3$ ): 4.80 (s, 2H) and 6.7 (s, 2H).

*Synthesis of 2,5-dibromo-3-{2-[2-(2-methoxyethoxy)ethoxy]ethoxymethyl} thiophene (5)*

Diethylene glycol monomethyl ether (4.4 g, 36.5 mmol) was dissolved in THF (125 mL) in a 2-neck 250 mL flask and equipped with an addition funnel and septum with nitrogen inlet. Sodium hydride (0.92 g, 23.1 mol) was added, and after hydrogen gas evolution had ceased, the flask was sealed under a nitrogen atmosphere. 2,5-dibromo-3-bromomethylthiophene (6.8 g, 20.3 mol) was dissolved in THF (25 mL) and added dropwise to the reaction mixture at room temperature over the course of 10 minutes. Stirring was continued for 4 hours. The mixture was then run through a plug of Celite and the solvent was removed by rotary evaporation. The crude product was eluted over silica gel with a 7:3 hexane:ethyl acetate mixture. The second of two UV active spots, seen by TLC, was collected and dried to provide the product (9.1 g, 75% yield) as a yellow liquid.

$^1\text{H-NMR}$ :  $\delta_{\text{H}}$  (300 MHz; ppm,  $\text{CDCl}_3$ ): 3.30 (s, 3H), 3.5-3.7 (m, 12H), 4.60 (s, 2H), 6.70 (s, 1H).

*Synthesis of 2-(2-methoxyethoxy)ethyl tosylate (6)*

A solution of 25.0 g diethylene glycol monomethyl ether (208 mmol) in 70 mL pyridine was cooled down to 0 °C and 37.6 g *p*-toluene sulfonyl chloride (197 mmol) was added and stirred at room temperature for 4 h. Water was added, and the product was extracted with dichloromethane. The organic phase was washed with hydrochloric acid (1 M) and water. The solution was dried over  $\text{Na}_2\text{SO}_4$  and the organic solvents was removed by evaporation. The colourless product was obtained after purification by a silica plug with hexane/EtoAc (1:1) as eluent (41.2 g, 73 % Yield).

$^1\text{H-NMR}$ :  $\delta_{\text{H}}$  (300 MHz; ppm,  $\text{CDCl}_3$ ): 7.28 (m, 2 H), 6.94 (m, 1 H), 3.43 (t, 2 H), 2.65 (t, 2 H), 1.86 (t, 2 H), 1.7 – 1.2 (m, 6 H).

*Synthesis of 3-(2-(2-(2-Methoxyethoxy)ethoxy)ethyl)thiophene (7)*

4.92 g 3-thiophene ethanol (38.40 mmol) were dissolved in 75 mL THF and 25 mL DMSO and 1.77 g NaH (46.08 mol) were added portion wise under stirring. After 30

min of stirring a solution of 11.03 g 2-(2-methoxyethoxy) ethyl tosylate (40.32 mmol) in 50 mL THF was added under stirring. The beige solution changed to red/orange and was stirred for 2 h at room temperature and afterwards for 17 h at 40 °C. To quench the solution 50 mL of a saturated NH<sub>4</sub>Cl solution was added. The colour shifted from beige to red/brown and the grey precipitate was dissolved. The organic phase was separated, and the water phase was washed three times with EtOAc, afterwards the organic phase was washed two times with a saturated NH<sub>4</sub>Cl solution and two times with a saturated NaCl solution. The product was obtained by drying over Na<sub>2</sub>SO<sub>4</sub> and evaporation of the organic solvents. After purification with a silica plug and hexane/EtOAc (7:3) as eluent, the first and only UV-active fraction was collected (7 g, 79 % Yield).

<sup>1</sup>H-NMR: δ<sub>H</sub> (300 MHz; ppm, CDCl<sub>3</sub>): 7.24 (d, 1 H), 7.03 (m, 1 H), 6.98 (d, 1 H), 3.69 (t, 2 H), 3.65 – 3.61 (m, 6 H), 3.56 (m, 2 H), 3.39 (s, 3 H), 2.93 (t, 2 H).

#### *Synthesis of 2,5-Dibromo-3-(2-(2-(2-methoxyethoxy)ethoxy)ethyl)thiophene (8)*

Under the exclusion of light 7.0 g of 3-(2-(2-(2-methoxyethoxy)ethoxy)ethyl)thiophene (30.4 mmol) was dissolved in 125 mL THF and 11.4 g of *N*-bromo succinimide (63.8 mmol) was added stepwise at room temperature. After stirring for one hour the product was extracted with EtOAc and washed with water and saturated NaCl solution. The organic phase was dried over Na<sub>2</sub>SO<sub>4</sub> and the solvent was evaporated. The product was obtained after purification by a silica plug with hexane/EtOAc (7:3) as eluent (7.95 g, 68 % Yield).

<sup>1</sup>H-NMR: δ<sub>H</sub> (300 MHz; ppm, CDCl<sub>3</sub>): 6.89 (s, 1 H), 3.67-3.61 (m, 8 H), 3.58-3.54 (m, 2 H), 3.39 (s, 3 H), 2.81 (t, 2 H).

#### *General procedure for Kumada catalyst transfer polymerization of the ethylene glycol monomers*

The ethylene glycol thiophene monomer (1 equ.) was added to a dry flask under argon and the vessel was evacuated once again and flushed with nitrogen. Then the concentration was set with dry THF to 0.5 mol/l and *t*-butylmagnesiumchloride (1.22 M in THF, 0.96 eq.) was added dropwise. The reaction mixture was stirred for 20 h under the exclusion of light. Then the reaction mixture was diluted with dry THF to 0.1 mol/l. The respective amount of Ni(dppp)Cl<sub>2</sub> (suspension in 2-3 ml dry THF) was

added in one portion to start the polymerization. After 4 h the polymerization was quenched with water. The mixture was concentrated, and the polymer was precipitated in methanol. Furthermore, the polymer was purified by Soxhlet extraction with methanol, hexane and chloroform and dried under vacuum.

SEC: P3MEET:  $M_n = 10$  kg/mol,  $\bar{D} = 1.43$ , P3MEEMT:  $M_n = 12$  kg/mol,  $\bar{D} = 1.21$ , P3MEEET:  $M_n = 13$  kg/mol,  $\bar{D} = 1.08$ .

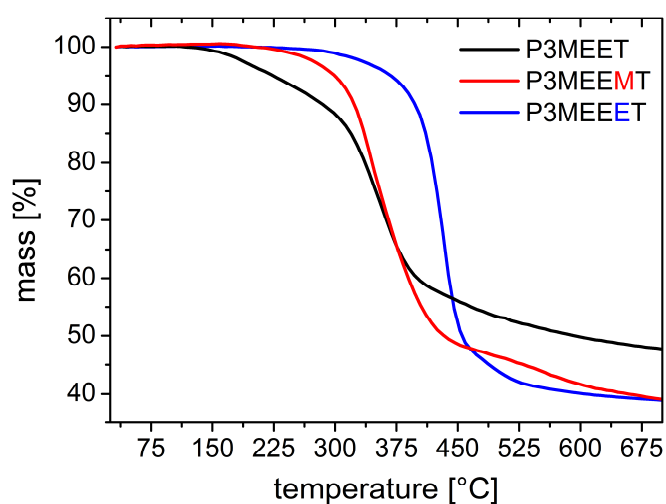


**Figure S1:** Thermogravimetric analysis (TGA) measurement P3MEET, P3MEEMT and P3MEEET under nitrogen atmosphere with a heating rate of 10 K/min in a temperature range from 30 °C to 700 °C.

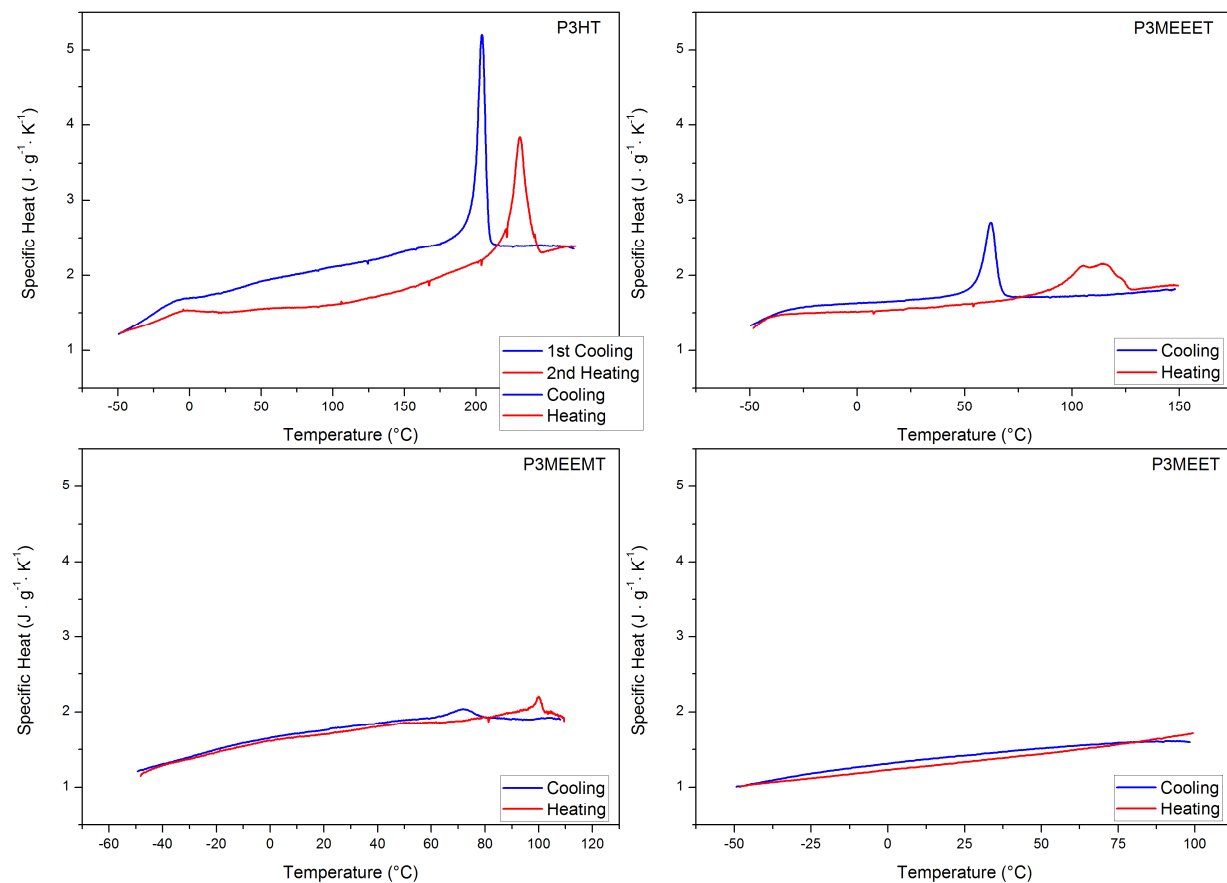


**Figure S2:** Differential scanning calorimetry (DSC) scans of P3MEET, P3MEEMT and P3MEEET under nitrogen, with a heating and cooling rate of 10 K/min. In all samples the 1<sup>st</sup> cooling and the 2<sup>nd</sup> heating run are shown.

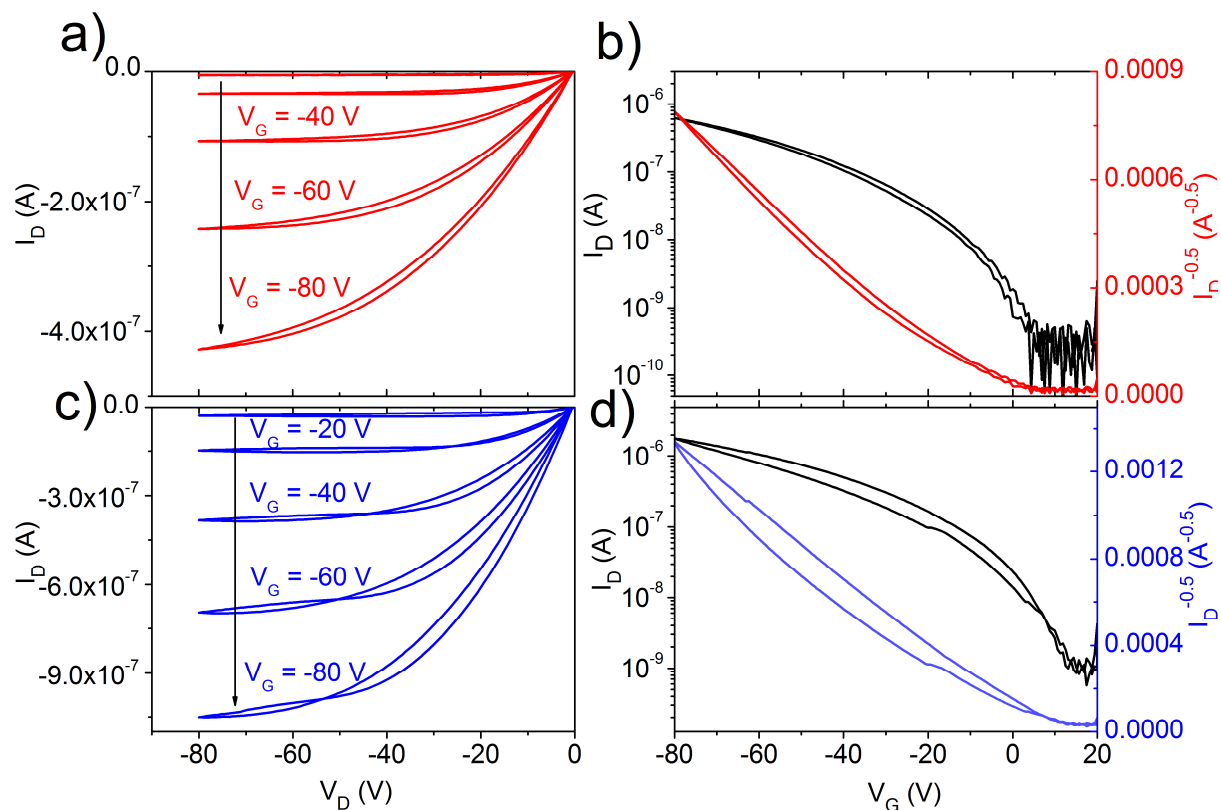


**Figure S3:** a) and c): Output curve of P3MEEMT (red) and P3MEEET (blue). b) and d): p-transfer curves of P3MEEMT (red) and P3MEEET (blue). With P3MEET no transistor characteristics were observed.

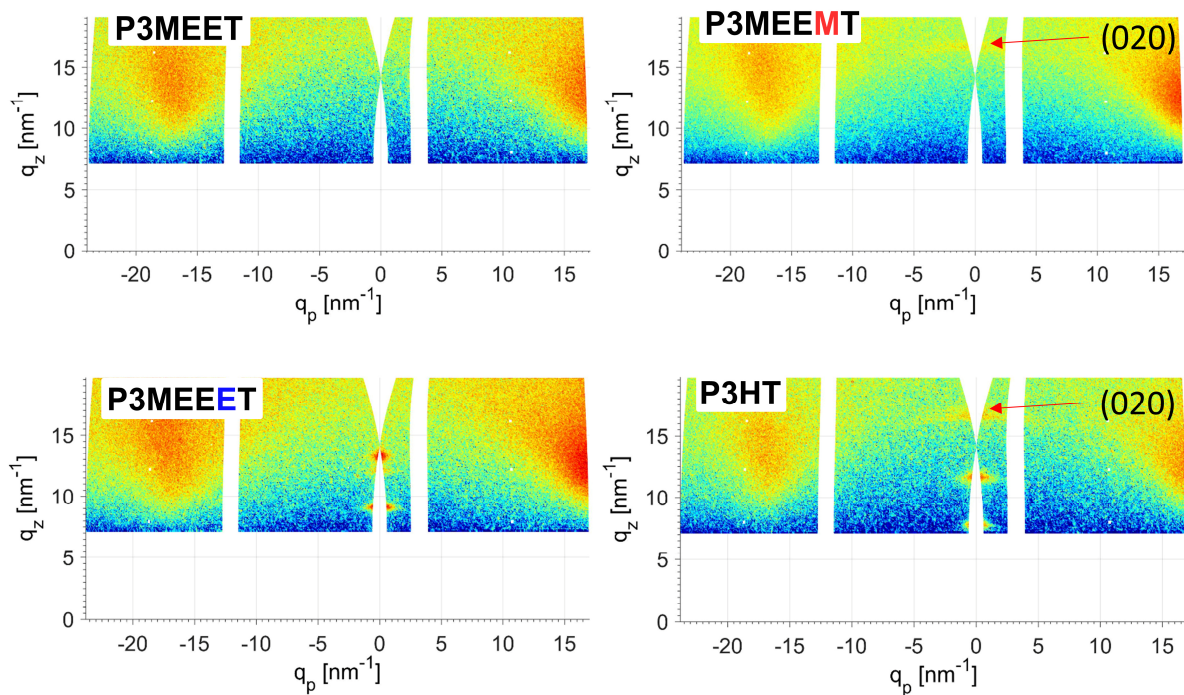


**Figure S4:** Reciprocal space maps from GIWAXS of thin films of P3MEET, P3MEEMT, P3MEEET and P3HT measured at an incident angle  $\alpha_i = 10^\circ$ . After spin coating, the polymer

films except P3MEET were melt-crystallized in vacuo (P3HT, P3MEEET), respectively annealed (P3MEEMT at 70 °C).

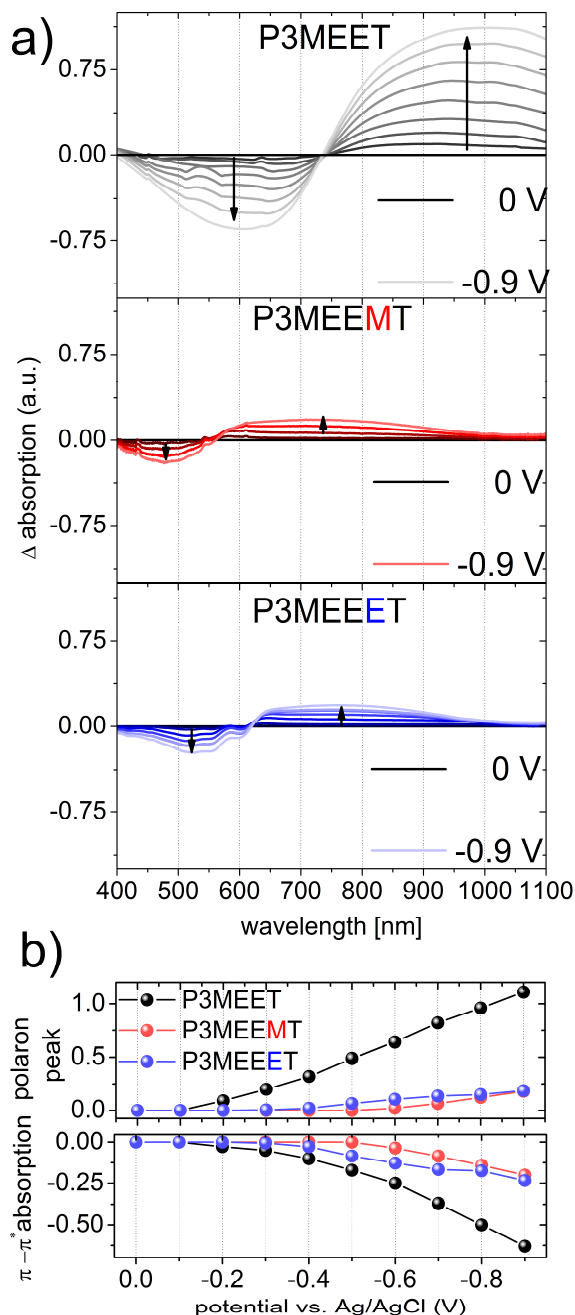


**Figure S5:** Difference spectra obtained by subtracting the absorption spectra of the copolymers in the neutral state (0 V) from the absorption spectra under different applied potentials during the in situ electrochemical oxidation of P3MEET, P3MEEMT and P3MEEET by applying a potential from 0 to -900 mV.

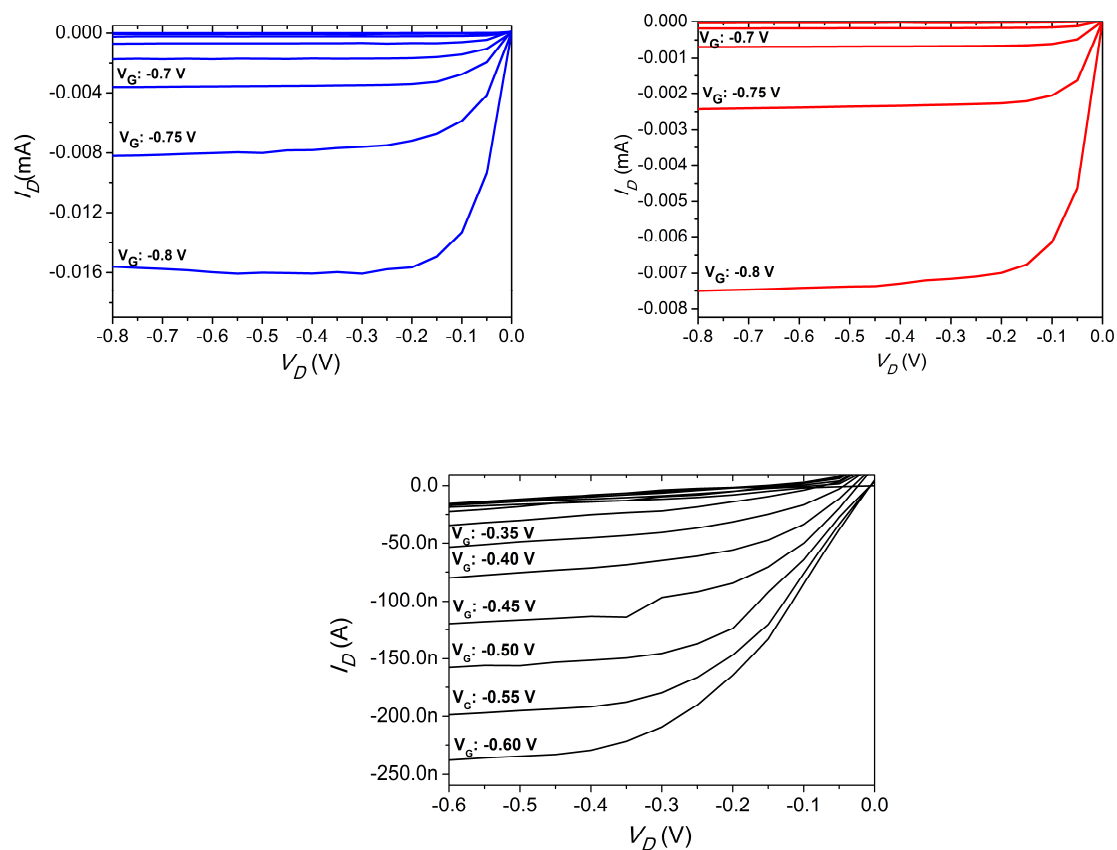


**Figure S6:** Output curves of P3MEEET (blue), P3MEEMT (red) and P3MEET (black) for gate voltages ranging from 0 V to -0.80 V ( $\Delta V = -0.05$  V) and 0 V to -0.60 V respectively.

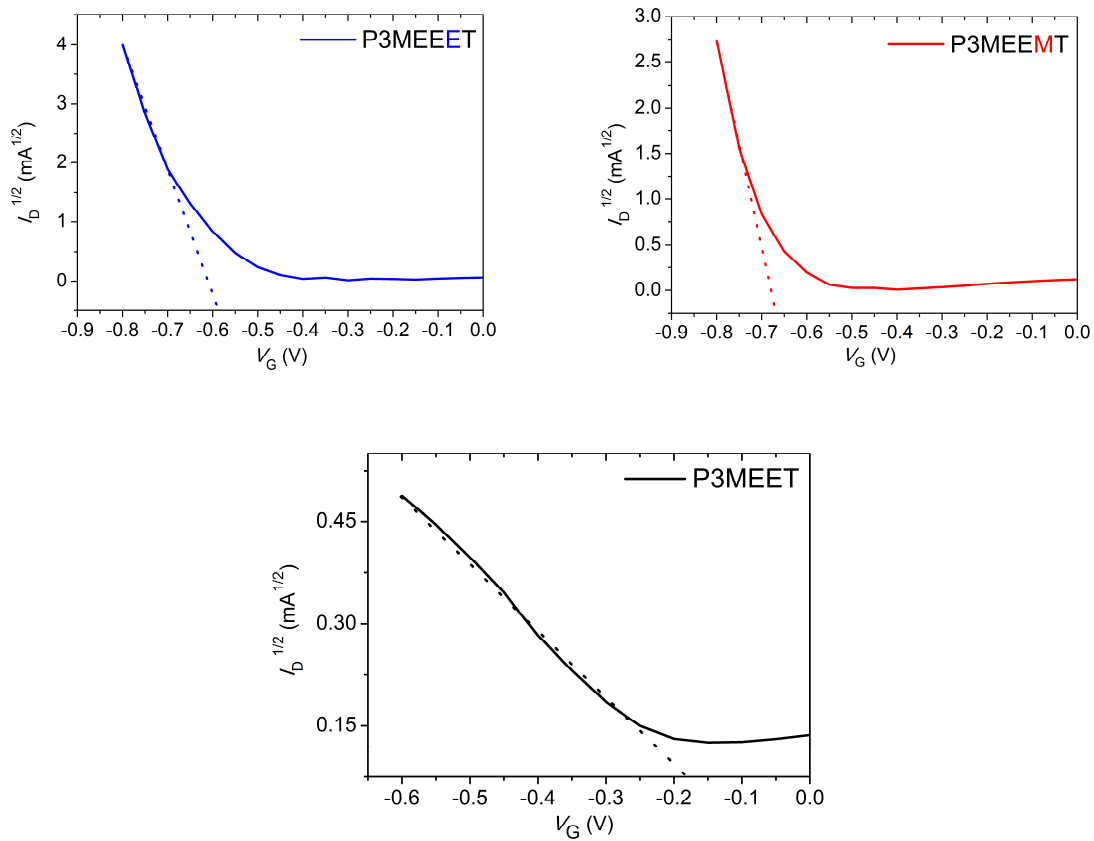


**Figure S7:**  $\sqrt{I_D}$  vs.  $V_G$  plots of the OECTs comprising of P3MEET, P3MEEMT and P3MEEET. The threshold voltage,  $V_{th}$ , was determined by extrapolating the linear region of the curves. The intersection of the x-axis corresponds to the  $V_{th}$ .

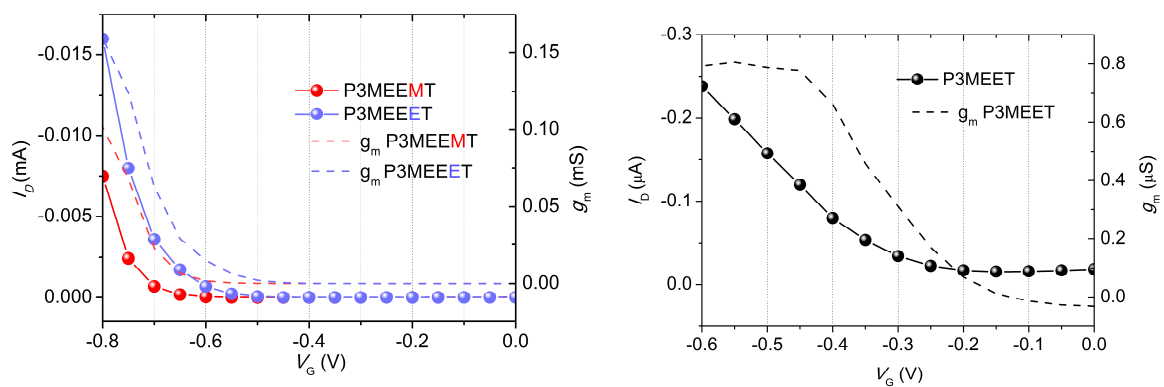


**Figure S8:** Transfer curve of P3MEEMT, P3MEEET (left) and P3MEET (right) with corresponding transconductance values (right).

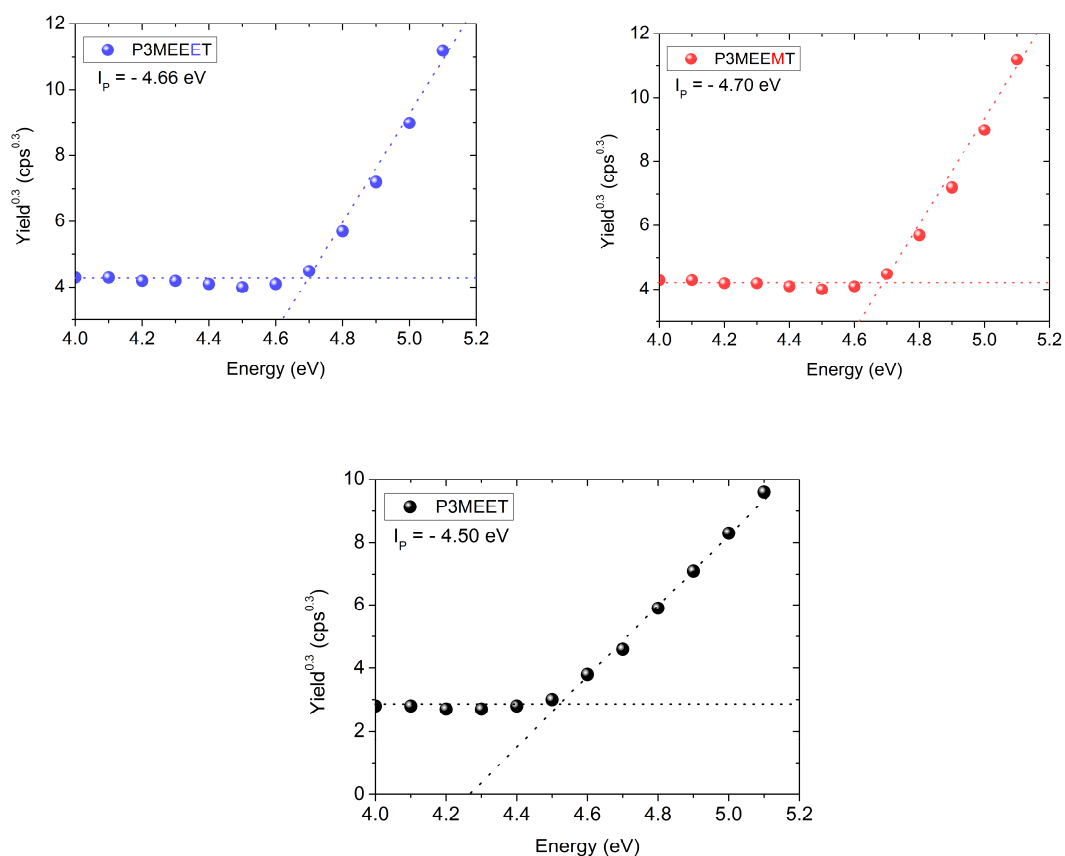


**Figure S9:** Photoelectron spectroscopy in air (PESA) measurements of P3MEEET (blue), P3MEEMT (red) and P3MEET (black) on thin polymer films on glass substrates. I<sub>p</sub> values were determined by interception of the both linear fitting curves.

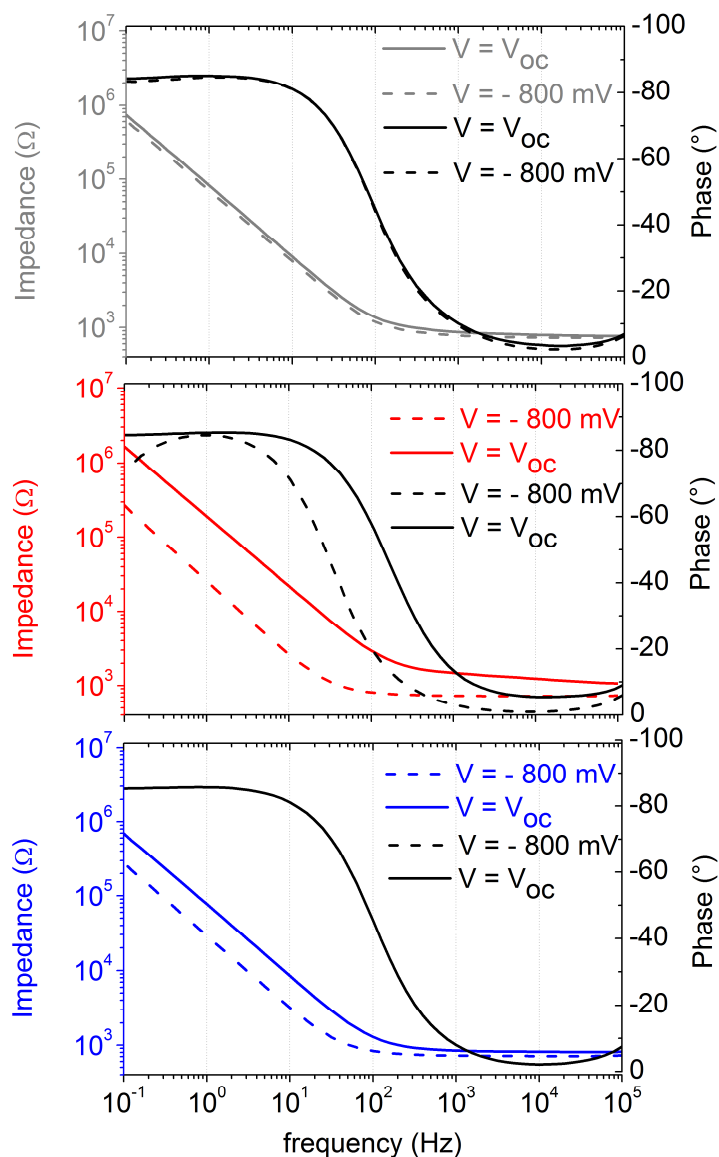


**Figure S10:** Electrochemical impedance spectra of P3MEEET (blue), P3MEEMT (red) and P3MEET (black) recorded at  $V_{oc}$  and at the doping potential that attains the maximum transconductance ( $V = -0.8$  V P3MEEMT and P3MEEET and  $-0.6$  V for P3MEET) in NaCl solution (0.1 M). Randles circuit was used for fitting the impedance and the phase spectrum,  $R_{Electrolyte}(R_{Polymer}||C_{Polymer})$  at a doping potential ( $V = -0.8$  V and  $-0.6$  V respectively). Following chi-fitting values were noted: 0.180 (P3MEEET), 0.223 (P3MEEMT) and 0.813 (P3MEET).

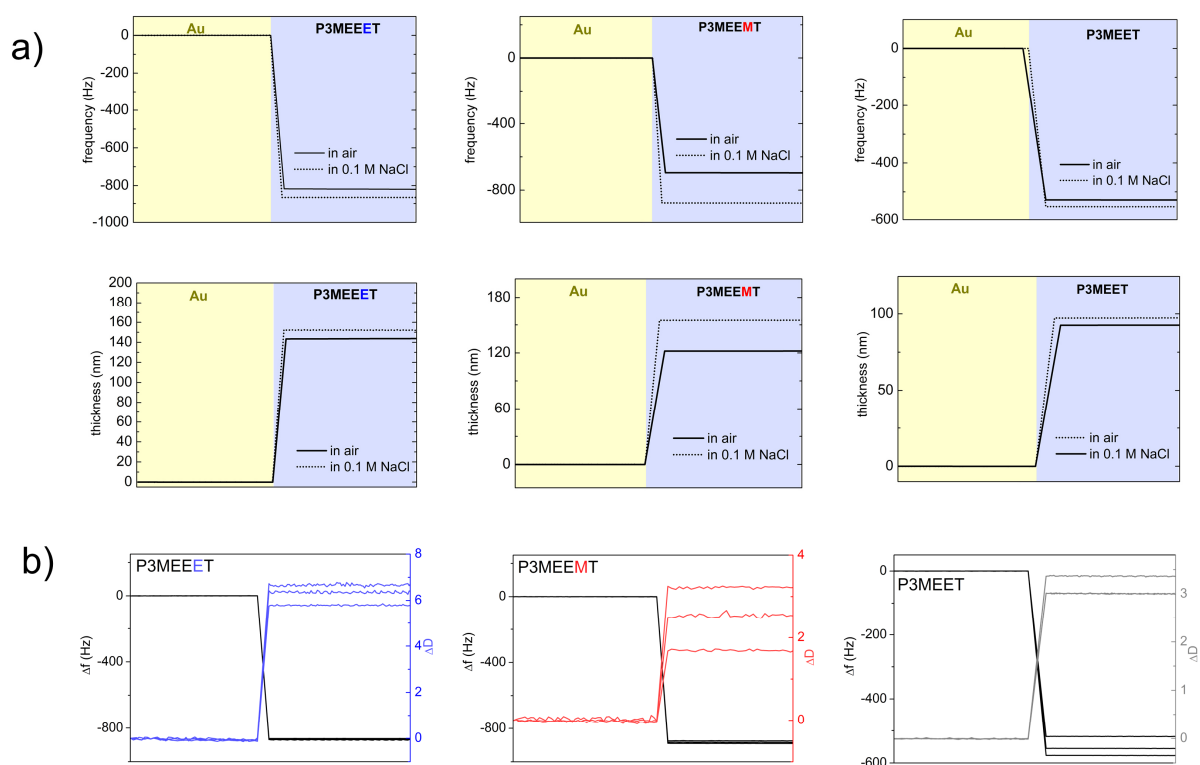


**Figure S11:** a) Shifts of the QCM-D frequency ( $\Delta f$ ) and the calculated thicknesses of P3MEEET (blue), P3MEEMT (red) and P3MEET (black) films. Spectra were recorded in air and in aqueous 0.1 M NaCl solution. For all three copolymers, the 7th overtone was used for calculations based on Sauerbrey model. b) Changes in  $\Delta f$  as well as dissipation of energy ( $\Delta D$ ) for these copolymers before and during the injection of 0.1 M NaCl solution into the chambers. The 3rd, 5th and 7th overtone are shown.

**Table S1:** Dry and wet thicknesses of the copolymer films after swelling in 0.1 aqueous NaCl solution. The thickness was calculated using Sauerbrey equation. The 7<sup>th</sup> overtone was used for calculation.

Copolymer	Dry thickness (nm)	Thickness after swelling (nm)	Swelling (%)
P3MEET	92	97	5
P3MEEMT	122	155	26
P3MEEET	143	152	6

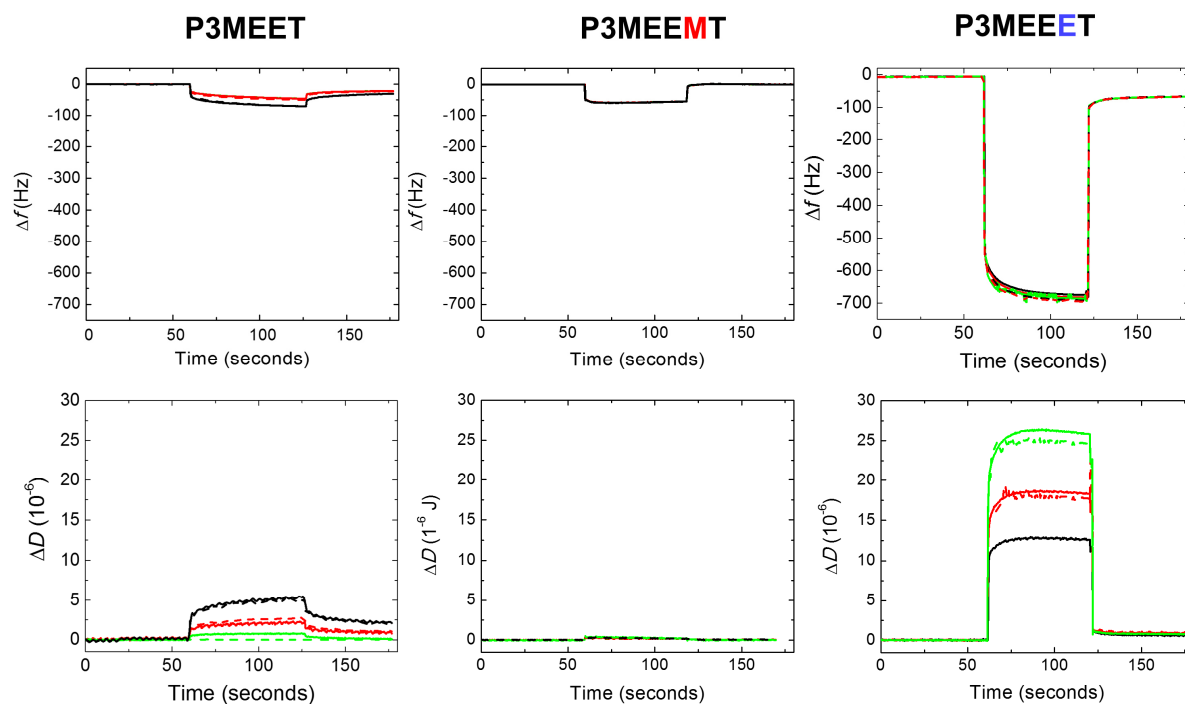


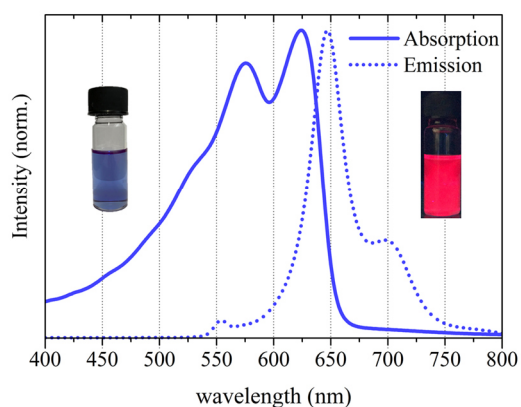
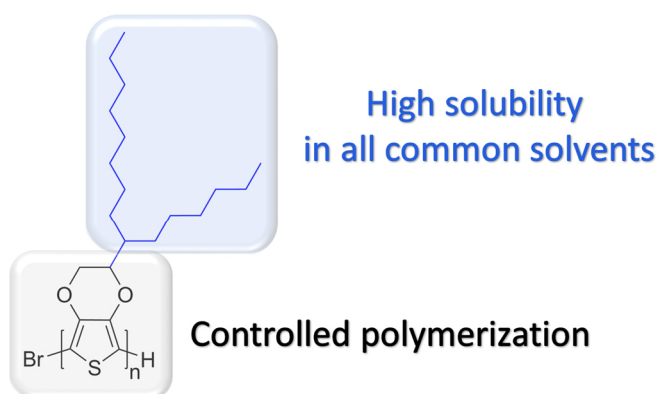
**Figure S12:** Raw frequency shifts and changes in dissipation (3<sup>rd</sup>, 5<sup>th</sup> and 7<sup>th</sup> overtone is shown) of the E-QCM study upon applying a doping potential of -0.6 V for P3MEET and -0.8 V for P3MEEMT and P3MEEET. The mass uptake, as well as the charge of the systems after ion injection were calculated using viscoelastic modelling.

# Chapter 8:

## A highly Soluble alkyl substituted PEDOT via Kumada Catalyst Transfer Polymerization

Philip Schmode,<sup>†</sup> Mahima Goel,<sup>†</sup> Florian Meichsner,<sup>†</sup> and Mukundan Thelakkat\*,<sup>†§</sup>

<sup>†</sup> Applied Functional Polymers, Department of Macromolecular Chemistry I and <sup>§</sup>Bavarian Polymer Institute, University of Bayreuth, Universitätsstr. 30, 95440 Bayreuth, Germany



*Intended for Submission*

## **ABSTRACT**

PEDOT:PSS [poly(3,4-ethylenedioxythiophene) polystyrene sulfonate] is one of the widely used p-doped hole conductor in the field of conducting polymers. In general, PEDOT is insoluble in any solvent and therefore for practical applications, a dispersion of PEDOT/PSS in polar solvents is used. In this work, highly soluble PEDOT homopolymers were obtained using Kumada Catalyst Transfer Polymerization (KCTP) of a newly synthesized EDOT monomer carrying a branched alkyl substituent on the 1,4-dioxane ring. The resulting polymers, PEDOT-C<sub>6</sub>C<sub>8</sub> 1 and 2, were prepared with a high control in molecular weight and low dispersity. Through the introduction of a branched alkyl side chain, the polymers exhibit excellent solubility in all common solvents such as hexane, tetrahydrofuran or chloroform. These polymers exhibit strong aggregation as evidenced by the UV-Vis spectroscopy. Moreover, these polymers are easily p-doped in thin films leading to conductivity values of 10<sup>-3</sup> S/cm<sup>-1</sup>, even when doped with low amounts (10 mol%) of a dopant, spiro-OMeTAD(TFSI)<sub>2</sub>. The field effect charge carrier mobility could be determined in pristine (undoped) material in bottom gate bottom contact OFETs ( $\mu_{\text{hole}} = 5 \cdot 10^4 \text{ cm}^2\text{V}^{-1}\text{s}^{-1}$ ). This new design concept of soluble PEDOT homopolymers with well-controlled molecular weights provides with solution-processable derivative in the established field of PEDOT/PSS.

$\pi$ -conjugated semiconducting polymers as well as their doped counterparts called conducting polymers, which show a good charge transport, low oxidation potential and a high stability of the oxidized state, are of great interest in the field of organic thermoelectrics, solar cells and in organic bioelectronics.<sup>1-3</sup> The most widely used p-type conducting polymer in devices is PEDOT:PSS [poly(3,4-ethylenedioxythiophene) polystyrene sulfonate], because it is commercially available, mainly transparent within low thicknesses and exhibits high conductivity.<sup>4</sup> PEDOT: PSS is mixture of two ionomers, where PSS has the function of doping the short PEDOT segments and stabilizing its oxidized state. In this mixture, the short PEDOT segments (5-15 units) are surrounded by the PSS chains with a much higher molecular weight.<sup>5</sup> However, PSS is in itself an insulator, and therefore dilutes the active PEDOT material. This inherent limitation has instigated recent interest in developing new PEDOT homopolymers, which are themselves highly soluble, processable as films and then oxidizable for different applications such as bioelectronics, and thermoelectrics. The key challenge in synthesizing such PEDOT homopolymers is to keep up sufficient solubility, while still reaching high molecular weights, because, PEDOT gets insoluble after only a few repeating units. In addition, the useful electrical properties of PEDOT: PSS, e.g. high conductivity caused by the high tendency of oxidation should also be maintained in the new PEDOT homopolymers. Most of the research on soluble poly-3,4-dialkoxy thiophenes is done on 3,4-propylenedioxythiophene derivatives, because they are synthetically much more easily accessible.<sup>6,7</sup> Incorporating suitable side chains is a viable strategy, also in other conjugated polymers like P3HT, to improve the solubility and processability of the resulting polymer. Bhardwaj et al. functionalized an EDOT monomer with a hexyl side chain and used the controlled polymerization technique of KCTP to achieve a PEDOT-C<sub>6</sub> homopolymer.<sup>8</sup> Nevertheless, they

achieved a polymer with low molecular weight of 4 kg/mol, so the hexyl side chains did not enhance the solubility of the final polymer sufficiently. In low band gap polymers, the common way to increase the solubility is to introduce branched side chains.<sup>9</sup> We adopted this concept, to synthesize a new generation of dibrominated EDOT monomer, in order to obtain a high molecular weight PEDOT homopolymer soluble in common organic solvents. In this study we present the first reported high molecular weight, low polydispersity and highly soluble PEDOT homopolymer, which was synthesized in a living fashion, utilizing KCTP. A new monomer synthesis route was developed to obtain an EDOT monomer with a branched 2-hexyldecyl (C<sub>6</sub>C<sub>8</sub>) side chain. The two resulting highly defined polymers, differing in the polymer chain lengths, were investigated with spectro electrochemistry measurements, to evaluate their oxidizability. Furthermore, a comparative study of the charge carrier mobility in organic field effect transistors, as well as the electrical conductivity when doped with spiro-OMeTAD(TFSI)<sub>2</sub> is shown.<sup>10–12</sup>

Side chain-functionalized EDOT monomers can be prepared using two methods: I) Commercially available EDOT precursor molecules e.g. hydroxymethyl EDOT or bromomethyl EDOT are functionalized with a solubilizing side chain or II) by attaching a side chain via a trans-etherification reaction with a diol and 3,4 dimethoxy thiophene. In this study, we adopted the latter method for preparing the new monomer 5,7-dibromo-2-(pentadecan-7-yl)-2,3-dihydrothieno[3,4-b] [1,4] dioxine (Br<sub>2</sub>-EDOT-C<sub>6</sub>C<sub>8</sub>). For obtaining the diol, the branched alcohol, 2-hexyldecan-1-ol was in a first step oxidized to the aldehyde followed by a Wittig reaction with methyltriphenylphosphonium bromide resulting in the corresponding alkene, which was dihydroxylated with ruthenium (III) chloride.<sup>13</sup> The trans-etherification between the diol and 3,4-dimethoxythiophene results in EDOT-C<sub>6</sub>C<sub>8</sub> monomer carrying a branched

C<sub>6</sub>C<sub>8</sub> side chain. For the use in the Kumada catalyst transfer polymerization, a further dibromination step is necessary, which was accomplished using NBS in a mixture of CH<sub>3</sub>COOH and THF (**Figure 1**). The KCTP is a powerful synthetic method to generate well-defined polythiophenes with high regioregularity, low dispersity and high molecular weight.<sup>14–17</sup> In this type of catalyst transfer polymerization an active Grignard monomer can be formed in situ from the dihalide monomers via a Grignard metathesis reaction with *t*-butyl magnesium bromide. The polymerization is started by the addition of the nickel catalyst dichloro[1,3-bis(diphenylphosphino)propane] nickel Ni(dppp)Cl<sub>2</sub> and the [M]<sub>0</sub>/[Cat] ratio determines the molecular weight. After 4 h, the polymerization was quenched with water and the polymer was precipitated in methanol, resulting in a dark black solid. Two well defined PEDOT-C<sub>6</sub>C<sub>8</sub> **1** and **2** polymers with different molecular weight were synthesized. We chose two different monomer to nickel catalyst ratios [M]<sub>0</sub>/[Ni(dppp)Cl<sub>2</sub>] (30/1 and 10/1) to synthesize two different polymers PEDOT-C<sub>6</sub>C<sub>8</sub> **1** and **2**, resulting in theoretical molecular weights of 3500 g/mol and 10500 g/mol, the detailed synthetic procedure and characterization has been given in the supporting Information. To determine the molecular weight distribution and Dispersity of PEDOT-C<sub>6</sub>C<sub>8</sub> **1** and **2**, we used size exclusion chromatography (SEC) and MALDI –Tof analysis (Table 1). SEC measurements revealed well defined polymers with low polydispersity, but two identical molecular weights for the two polymers However, difference in molecular weights could be clearly resolved in MALDI- Tof analysis, resulting in peak molecular weights of 3 kg/mol (~ 9 repeating units) and 10 kg/mol (~ 27 repeating units), respectively (**Figure S2**).The second peak of the spectra of PEDOT-C<sub>6</sub>C<sub>8</sub> **1** can be attributed to the double charged species of the ionized polymer (+2). The similarity of the molecular weights as determined with SEC technique can be explained by the fact that, at around nine repeating units the hydrodynamic radius does not change

any more, after which the spectra remains unchanged for both the PEDOT-C<sub>6</sub>C<sub>8</sub> polymers, mainly Br/H end groups were obtained. In Both MALDI-Tof spectra the molecular weight of the repeating unit (352 g/mol) could be found (Figure S2).

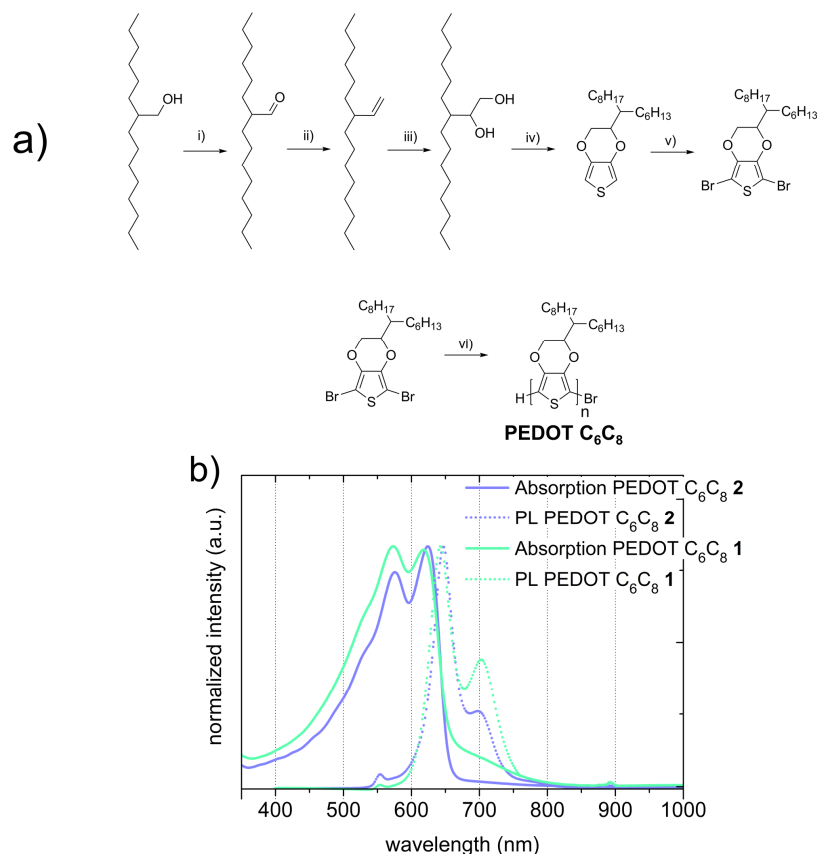


**Figure 1:** a) Monomer Synthesis of Br<sub>2</sub>-EDOT-C<sub>6</sub>C<sub>8</sub>; **i)** 2-hexyldecan-1-ol, oxalyl chloride, TEA, - 72 °C **ii)** KO<sup>t</sup>-Bu, Methyltriphenylphosphonium bromide, -78 °C, **iii)** NaIO<sub>3</sub>, RuCl<sub>3</sub>, RT, acetone, water, ethyl acetate, RT **iv)** 3,4-dimethoxythiophene, *p*-TsOH, toluene, reflux **v)** NBS, CH<sub>3</sub>COOH/THF, RT. Polymer Synthesis of PEDOT-C<sub>6</sub>C<sub>8</sub> 1 and 2:**vi)** *t*-BuMgCl, THF, RT, Ni(dppp)Cl<sub>2</sub>, H<sub>2</sub>O. b) UV-Vis absorption and photoluminescence measurements of PEDOT-C<sub>6</sub>C<sub>8</sub> in THF solution, with a polymer concentration of 0.02 mg/ml.

**Table 1:** Characteristics of the two synthesized copolymers PEDOT-C<sub>6</sub>C<sub>8</sub> 1 & 2, determined via SEC and MALDI-ToF experiments.

	[M]/[Ni]	Theoretical Molecular weight	M <sub>n</sub> , SEC <sup>a</sup>	M <sub>p</sub> , MALDI-ToF <sup>b</sup>	D <sub>SEC</sub> <sup>a</sup>	Repeating units <sup>c</sup>
	(mol)	(kg/mol)	(kg/mol)	(kg/mol)		
PEDOT-C <sub>6</sub> C <sub>8</sub> 1	10	3.5	10	3	1.38	9
PEDOT-C <sub>6</sub> C <sub>8</sub> 2	30	10.5	9.5	9.8	1.19	27

a: SEC with polystyrene calibration and THF as eluent.

b: Dithranol was used as matrix material, dilution 1:1000.

c: Calculated from peak molecular weight determined in MALDI-ToF.

UV-Vis studies in THF solution reveal, that both polymers exhibit vibronically resolved absorption spectra, from which qualitative information regarding aggregation in solution can be deduced. Both polymers exhibit highly ordered absorption spectra, where the 0-0 transition for both polymers peak can be distinguished at 638 nm and the 0-1 transition peak at 584 nm, respectively. Without further quantifying the absorption spectra by separating the spectra into the different contributions (amorphous and crystalline part), it can be stated that both PEDOT polymers are highly aggregated in every solvent we tested (chloroform, hexane, THF etc.), we couldn't observe a random coil absorption for both polymers. We investigated the thermal stability of the polymers with TGA and observed, that even the lower molecular weight polymer PEDOT-C<sub>6</sub>C<sub>8</sub> 1 is stable until 321 °C (T<sub>5%weight loss</sub>) under nitrogen.

The tendency of oxidation was monitored with spectro electrochemistry measurements. Here we monitored the changes in the absorption spectra of the polymer films in an aqueous electrolyte solution when they are subjected to an

electrochemical doping potential. As a typical SEC measurement and the difference absorption spectrum, plots are shown for PEDOT-C<sub>6</sub>C<sub>8</sub> 2 in Figure 1a (measurement of PEDOT-C<sub>6</sub>C<sub>8</sub> 1 can be found in Figure S3). The measurements were performed in 0.1 M aqueous NaCl solution in a potential range between 0 V and -0.9 V vs Ag/AgCl, measured in steps of 0.1 V. Before starting the measurement, a de-doping potential was applied (0.2 V), to ensure that the polymer is in the neutral state before electrochemical doping. Upon applying a doping potential, the characteristic polar absorption between 680 nm and 1100 nm arises, while in the meantime the main  $\pi$ - $\pi^*$  absorption completely vanishes, which make these polymers attractive for transparent electrode applications (**Figure 2a**, S3). To quantify the oxidation in thin film under applied voltages the absorption spectra of the copolymers in the neutral state (0 V) were subtracted from the absorption spectra of the copolymers under different applied potentials and the difference spectra are plotted in (**Figure 2b**). Here, a small difference is observed in the onset potentials, where PEDOT-C<sub>6</sub>C<sub>8</sub> 1 shows a little lower onset. However, the amount of oxidized species saturates at about 0.8 V for both polymers, indicating that probably the oxidation mechanism and the tendency of oxidation in both polymers are similar.

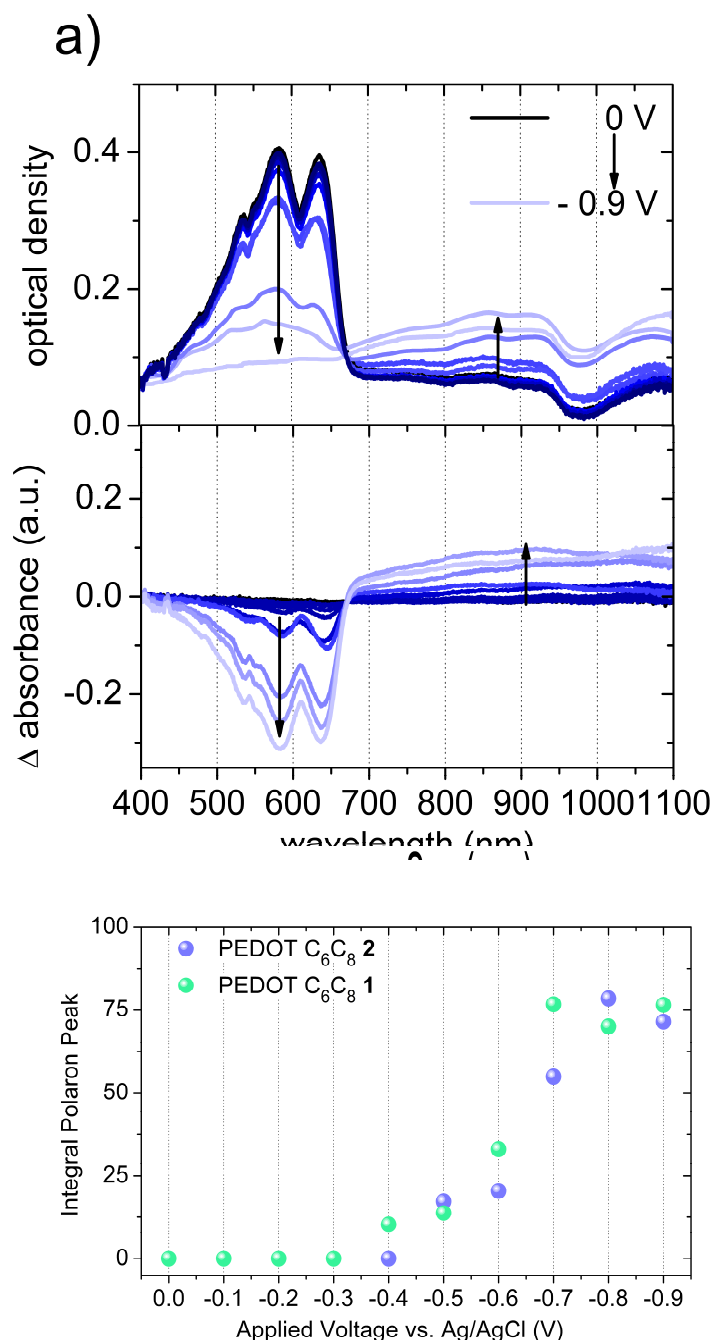


**Figure 2:** a) Spectro electrochemistry measurements of thin polymer films on ITO of PEDOT-C<sub>6</sub>C<sub>8</sub> 2 respectively. The spectra were measured in 0.1 M NaCl when the films were biased from 0 V to -0.9 V in a three-electrode setup with an Ag/AgCl reference electrode and a Pt counter electrode. Difference spectra obtained by subtracting the absorption spectra of the copolymers in the neutral state (0 V) from the absorption spectra under different applied potentials during the in situ electrochemical oxidation of PEDOT-C<sub>6</sub>C<sub>8</sub> 2 by applying a potential from 0 to -900 mV. The pristine absorption in the 400-680 nm range decreases with a concomitant increase in polaron absorption in the range of 680 to 1100 nm. The arrow indicates the direction of spectral changes. b) Correlation of the concentration of polarons indicated by the integrals (obtained by integrating the area under the curve between 680 – 1100 nm corresponding to the rising polaron peak vs. applied potential.

The hole mobility of the pristine PEDOT polymers were investigated in commercially available bottom-gate (Si) and bottom-contact (Au) substrates with a silicon oxide layer as dielectric containing different channels ranging from 10 to 20  $\mu\text{m}$  using OFET devices. The polymer films were directly spin-coated from THF onto the substrates. By plotting the square root of the drain current  $I_D$  versus the gate voltage  $V_G$  the hole mobility can be estimated (see eq. 1). Promising hole mobilities of  $1.6 \cdot 10^{-4} \text{ cm}^2\text{V}^{-1}\text{s}^{-1}$  (PEDOT-C<sub>6</sub>C<sub>8</sub> 1) and  $5 \cdot 10^{-4}$  (PEDOT-C<sub>6</sub>C<sub>8</sub> 2) were obtained, with an ON/OFF ratio in the range from  $2 \cdot 10^3$  -  $9 \cdot 10^3$ . The dependency of the molecular weight on the hole transport is also not that pronounced, unlike as known for many other polythiophenes, as P3HT.<sup>18</sup> In P3HT, the optimum hole transport is achieved with about 70 repeating units.<sup>18</sup> On the contrary, in the case of the the PEDOT polymers, almost the same mobility is observed, when the high and low molecular weight PEDOT polymers were compared.

PEDOT is an interesting polymer, if its electrical conductivity can be improved by doping. Therefore, to further investigate the chemical doping of these polymers, partially oxidized spiro-OMeTAD (TFSI)<sub>2</sub> was added as a dopant. This dopant has partially filled HOMO orbitals and therefore can accept electrons from the polymer valence band via HOMO-HOMO electron transfer. In this process, the polymer gets doped (partially oxidized to radical cations) and the dopant gets reduced to less oxidized species. If the polymer can delocalize and transport the charges, the conductivity can be improved. The electrical conductivities of pristine and doped polymers in thin films were measured on as cast and annealed films after 12 hours of exposure to air using interdigitated electrodes as described in experimental part. The corresponding data have been shown in the **Figure 3**. PEDOT-C<sub>6</sub>C<sub>8</sub> 2 in its pristine state, exhibited an electrical conductivity of  $1.04 \cdot 10^{-7} \text{ S cm}^{-1}$ , which increases more

than three orders of magnitude to a conductivity of  $3.58 \cdot 10^{-4} \text{ S cm}^{-1}$ , when doped with 10 mol% of spiro- (TFSI)<sub>2</sub>. This indicates that spiro-OMeTAD (TFSI)<sub>2</sub> can be used as a promising p-type dopant for PEDOT type polymers. So far, spiro-OMeTAD (TFSI)<sub>2</sub> has been mainly used as an additive to pristine spiro-OMeTAD (TFSI)<sub>2</sub> to improve the electrical conductivity of charge transport layers in perovskite solar cells.<sup>11</sup>

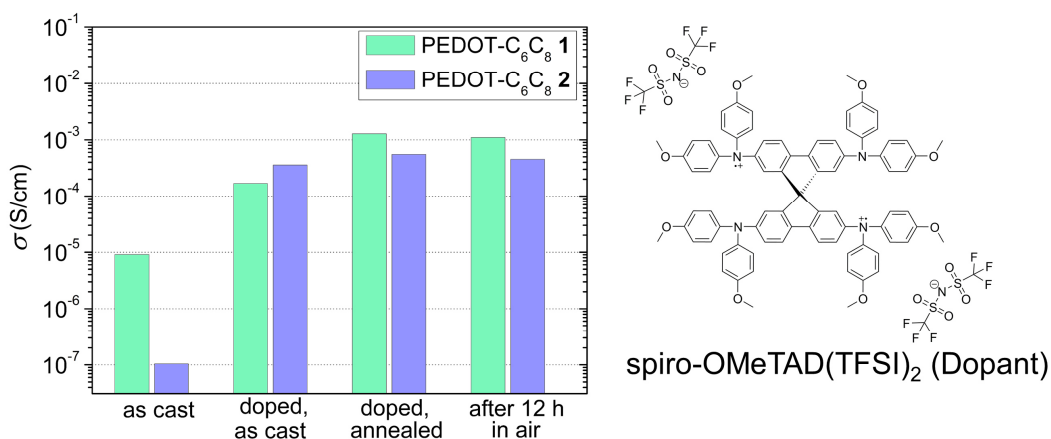


**Figure 3:** Electrical Conductivities (as cast, doped as cast, doped annealed and after 12 h in air) of PEDOT-C<sub>6</sub>C<sub>8</sub> 1 and 2, which were doped with 10 mol% of as well as the chemical structure of the dopant.

Further, to investigate the effect of annealing on the conductivity of pristine and doped films, we annealed the films at 100 °C for 30 min under nitrogen atmosphere. Our measurements indicated that although there is a slight increase in the conductivity of pristine polymer films, annealing does not significantly enhance the conductivity of doped films. To probe the stability of doped films in air, we exposed these films to air for 12 h at 100 °C and found that the conductivity of doped films remains almost unchanged confirming high stability of doped polymer films in air. To test the influence of molecular weight on the polymer doping efficiency, we compared PEDOT-C<sub>6</sub>C<sub>8</sub> 1 (M<sub>n</sub> = 3500 g/mol), having same repeating unit mass, but about one-third the molecular weight as compared to PEDOT-C<sub>6</sub>C<sub>8</sub> 2. We found that the conductivity of pristine films

was one order of magnitude higher ( $\sigma = 9.12 \cdot 10^{-6}$ ) in lower molecular weight polymer. It seems, that the lower molecular weight PEDOT polymer exhibits a higher tendency of oxidation. However, the conductivity of doped films showed no difference with respect to the molecular weight of the polymers. Additionally, as in the case of PEDOT-C<sub>6</sub>C<sub>8</sub> 2, the electrical conductivity of doped PEDOT-C<sub>6</sub>C<sub>8</sub> 1 films were two to three orders higher than pristine polymer PEDOT-C<sub>6</sub>C<sub>8</sub> 1, stable under argon, and does not show any decay once the doped films were exposed to air. Thus, the exceptional stability of the doped state of PEDOT polymers can be shown in this study. Table 2 summarizes the parameters determined with OFET and conductivity measurements.

**Table 2:** OFET characteristics of PEDOT-C<sub>6</sub>C<sub>8</sub> 1 and 2 determined in bottom-gate (Si), bottom-contact (Au) transistors. The hole mobility  $\mu_{\text{hole}}$ , was estimated out of the transfer curves (Figure S4, S5). Conductivity measurement of the polymers as cast, doped as cast with spiro-OMeTAD (TFSI)<sub>2</sub> and the conductivity after storing the film in air for 12 h. The thickness of the polymers was determined with a Dektak Stylus profilometer.

	OFET		Conductivity $\sigma$			Thickness (nm)
	$\mu_{\text{hole, average}}$ (cm <sup>2</sup> V <sup>-1</sup> s <sup>-1</sup> )	ON/OFF ratio	$\sigma_{\text{pristine, as cast}}$ (Scm <sup>-1</sup> )	$\sigma_{\text{doped, as cast}}$ (Scm <sup>-1</sup> )	$\sigma_{\text{in air}}$ (Scm <sup>-1</sup> )	
PEDOT-C <sub>6</sub> C <sub>8</sub> 1	$1.6 \cdot 10^{-4}$	$2 \cdot 10^3$	$9.12 \cdot 10^{-6}$	$1.28 \cdot 10^{-3}$	$1.10 \cdot 10^{-3}$	95±9
PEDOT-C <sub>6</sub> C <sub>8</sub> 2	$5 \cdot 10^{-4}$	$9 \cdot 10^3$	$1.04 \cdot 10^{-7}$	$5.53 \cdot 10^{-4}$	$4.53 \cdot 10^{-4}$	105±10

In this work, we present for the first time, controlled polymerization of a highly soluble PEDOT homopolymer with much higher molecular weight than those reported upto now. A new monomer synthesis route was developed, to obtain the EDOT monomer Br<sub>2</sub>-EDOT C<sub>6</sub>C<sub>8</sub>, carrying branched alkyl chains. With this monomer, defined polymers with molecular weights up to 10 kg/mol and low polydispersity's were achieved. This polymer PEDOT-C<sub>6</sub>C<sub>8</sub> 2 with higher molecular weight is highly soluble and easily processable. Also, the strong tendency of oxidation is maintained in both polymers. When applying a doping potential, the main  $\pi$ - $\pi^*$  absorption is completely vanished, which makes these polymers highly attractive for transparent electrodes. Furthermore, the hole mobility estimated with organic field effect transistors is very promising. Upon doping with spiro-OMeTAD (TFSI)<sub>2</sub> the electrical conductivity increases drastically (3-4 orders of magnitude), even at low dopant concentrations (10 mol%). Also, the stability

of the oxidized state is remarkable after 12 h under ambient conditions. Highly oxidizable, stable and easily processable p-type materials, like PEDOT-C<sub>6</sub>C<sub>8</sub>, are potential candidates for applications like thermoelectrics and bioelectronics.

## REFERENCES

- (1) Wu, X.; Surendran, A.; Ko, J.; Filonik, O.; Herzig, E. M.; Müller-Buschbaum, P.; Leong, W. L. Ionic-Liquid Doping Enables High Transconductance, Fast Response Time, and High Ion Sensitivity in Organic Electrochemical Transistors. *Adv. Mater.* **2019**, *31* (2), 1805544.
- (2) Kee, S.; Kim, H.; Paleti, S. H. K.; El Labban, A.; Neophytou, M.; Emwas, A.-H.; Alshareef, H. N.; Baran, D. Highly Stretchable and Air-Stable PEDOT:PSS/Ionic Liquid Composites for Efficient Organic Thermoelectrics. *Chem. Mater.* **2019**, *31*, 9, 3519-3526.
- (3) Vaagensmith, B.; Reza, K. M.; Hasan, M. N.; Elbohy, H.; Adhikari, N.; Dubey, A.; Kantack, N.; Gaml, E.; Qiao, Q. Environmentally Friendly Plasma-Treated PEDOT:PSS as Electrodes for ITO-Free Perovskite Solar Cells. *ACS Appl. Mater. Interfaces* **2017**, *9* (41), 35861–35870.
- (4) Fan, Z.; Ouyang, J. Thermoelectric Properties of PEDOT:PSS. *Adv. Electron. Mater.* **2019**, 1800769.
- (5) Ouyang, J. Solution-Processed PEDOT:PSS Films with Conductivities as Indium Tin Oxide through a Treatment with Mild and Weak Organic Acids. *ACS Appl. Mater. Interfaces* **2013**, *5* (24), 13082–13088.
- (6) Österholm, A. M.; Ponder, J. F.; De Keersmaecker, M.; Shen, D. E.; Reynolds, J. R. Disentangling Redox Properties and Capacitance in Solution-Processed Conjugated Polymers. *Chem. Mater.* **2019**, *31* (8), 2971–2982.
- (7) Ponder, J. F.; Pittelli, S. L.; Reynolds, J. R. Heteroatom Role in Polymeric Dioxyselenophene/Dioxythiophene Systems for Color and Redox Control. *ACS Macro Lett.* **2016**, *5* (6), 714–717.
- (8) Bhardwaj, D.; Shahjad; Gupta, S.; Yadav, P.; Bhargav, R.; Patra, A. All Conjugated Poly(3-Hexylthiophene)-Block-Poly(Hexyl-3,4-Ethylenedioxythiophene) Copolymers. *ChemistrySelect* **2017**, *2* (29), 9557–9562.
- (9) Weller, T.; Breunig, M.; Mueller, C. J.; Gann, E.; McNeill, C. R.; Thelakkat, M. Fluorination in Thieno[3,4-c]Pyrrole-4,6-Dione Copolymers Leading to Electron Transport, High Crystallinity and End-on Alignment. *J. Mater. Chem. C* **2017**, *5* (30), 7527–7534.
- (10) Cappel, U. B.; Daeneke, T.; Bach, U. Oxygen-Induced Doping of Spiro-MeOTAD in Solid-State Dye-Sensitized Solar Cells and Its Impact on Device Performance. *Nano Lett.* **2012**, *12* (9), 4925–4931.
- (11) Nguyen, W. H.; Bailie, C. D.; Unger, E. L.; McGehee, M. D. Enhancing the Hole-Conductivity of Spiro-OMeTAD without Oxygen or Lithium Salts by Using Spiro(TFSI)<sub>2</sub> in Perovskite and Dye-Sensitized Solar Cells. *J. Am. Chem. Soc.* **2014**, *136* (31), 10996–11001.
- (12) Goel, M.; Siegert, M.; Krauss, G.; Mohanraj, J.; Hochgesang, Adrian, J.; Heinrich, C. D.; Fried, M.; Pflaum, J.; Thelakkat, M. HOMO – HOMO Electron Transfer: An Elegant Strategy for p-Type Doping of Polymer Semiconductors towards Thermoelectric Applications. *Unpubl. Results*.
- (13) Plietker, B.; Niggemann, M. An Improved Protocol for the RuO<sub>4</sub>-Catalyzed Dihydroxylation of Olefins. *Org. Lett.* **2003**, *5* (18), 3353–3356. <https://doi.org/10.1021/ol035335a>.
- (14) Lohwasser, R. H.; Thelakkat, M. Toward Perfect Control of End Groups and Polydispersity in Poly(3-Hexylthiophene) via Catalyst Transfer Polymerization. *Macromolecules* **2011**, *44* (9), 3388–3397.
- (15) Lohwasser, R. H.; Gupta, G.; Kohn, P.; Sommer, M.; Lang, A. S.; Thurn-Albrecht, T.; Thelakkat, M. Phase Separation in the Melt and Confined Crystallization as the Key to Well-Ordered Microphase Separated Donor–Acceptor Block Copolymers. *Macromolecules* **2013**, *46* (11), 4403–4410.
- (16) Yokoyama, A.; Miyakoshi, R.; Yokozawa, T. Chain-Growth Polymerization for Poly(3-Hexylthiophene) with a Defined Molecular Weight and a Low Polydispersity. *Macromolecules* **2004**, *37* (4), 1169–1171.
- (17) Sheina, E. E.; Liu, J.; Iovu, M. C.; Laird, D. W.; McCullough, R. D. Chain Growth Mechanism for Regioregular Nickel-Initiated Cross-Coupling Polymerizations. *Macromolecules* **2004**, *37* (10), 3526–3528.

- (18) Singh, C. R.; Gupta, G.; Lohwasser, R.; Engmann, S.; Balko, J.; Thelakkat, M.; Thurn-Albrecht, T.; Hoppe, H. Correlation of Charge Transport with Structural Order in Highly Ordered Melt-Crystallized Poly(3-Hexylthiophene) Thin Films. *J. Polym. Sci. Part B Polym. Phys.* **2013**, *51* (12), 943–951.

## Supplementary Information

### Methods

*<sup>1</sup>H-NMR.* Spectra were recorded in deuterated CDCl<sub>3</sub> on a Bruker Avance 250 spectrometer at 300 MHz at room temperature. Chemical shifts are noted in ppm and coupling constants in Hz. All spectra were calibrated according to the residual solvent peaks (CDCl<sub>3</sub> δ=7.26 ppm).

*Size exclusion chromatography (SEC).* SEC was performed utilizing a Waters 515 HPLC pump and THF with 0.25 wt% tetrabutylammonium bromide (TBAB) as eluent at a flow rate of 0.5 mL/min. A volume of 100 µL of polymer solution (1-2 mg/mL) was injected with a 707 Waters auto-sampler into a column setup comprising a guard column (Agilent PLgel Guard MIXED-C, 5 × 0.75 cm, particle size 5 µm) and two separation columns (Agilent PLgel MIXED-C, 30 × 0.75 cm, particle size 5 µm). Polymer size distributions were monitored with a Waters 998 photodiode array detector at 254 nm and a Waters 414 refractive index detector. Narrow distributed polystyrene standards were used for calibration and 1,2-dichlorobenzene as an internal reference.

*UV-Vis Spectroscopy.* UV-Vis spectra were recorded on a Jasco V-670 spectrophotometer. All polymer solutions were measured at a concentration of 0.02 mg/ml. The spectra were recorded in quartz cuvettes with an internal diameter of 10 mm. The thin polymer films were spin-coated from methanol and from mixtures of methanol and THF on glass substrates.

*Spectroelectrochemistry Measurements.* Thin films were prepared on ITO coated glass substrates. Measurements were carried out using a UV-Vis spectrometer (OceanOptics USB 2000+) integrated with an Ivium CompactStat potentiostat. A Pt mesh was used as the counter electrode and an Ag/AgCl electrode as the reference

electrode. The indicated voltages were applied versus  $V_{OC}$  for 10 s until the current stabilized prior to recording of the spectrum.

*Organic Field Effect Transistors (OFETs):* Bottom gate/bottom contact organic field effect transistors (OFET Gen4) were purchased from Fraunhofer IPMS. N-doped silicon (doping at the surface  $n \sim 3 \times 10^{17} \text{ cm}^{-3}$ ) was used as the surface and gate electrode. The dielectric consists of a  $230 \pm 10 \text{ nm}$  layer of silicon oxide. Each substrate consisted of 16 devices with a constant channel width of 10 mm and varying channel length of 2.5–20  $\mu\text{m}$ . The source and drain electrodes were a 30 nm thick gold layer on a 10 nm ITO adhesion layer. The devices were prepared by cleaning in acetone and subsequently in iso-propanol in an ultrasonic bath for 10 min, followed by 15 min treatment in an ozone oven at 50 °C and subsequent silanization by 45 min treatment in a bath of 1 wt% octadecyltrichlorosilane (ODTS) in toluene at 60 °C. The devices were rinsed with toluene and *i*-propanol and dried. Thin polymer films were spin cast from 6 mg/mL chloroform solutions at a spinning speed of 3000 rpm under ambient conditions. All devices were stored and measured under nitrogen atmosphere. The I-V-characteristics were measured using an Agilent B1500 semiconductor parameter analyzer. Using eq. (1) the charge carrier mobilities were calculated from the slope of the  $(I_d)^{0.5} - V_g$  plots.

$$I_d = \frac{W}{2L} C_i \mu (V_g - V_t)^2 \quad (1)$$

*Conductivity  $\sigma$  Measurements:* Prepared substrates (OFET Gen 4) were purchased from Fraunhofer IPMS. In these substrates, an n-doped silicon (doping at the surface  $n \approx 3 \times 10^{17} \text{ cm}^{-3}$ ) bulk layer has a  $230 \pm 10 \text{ nm}$  layer of silicon oxide as the dielectric layer. The source and drain electrodes were a 30 nm thick gold layer on a 10 nm ITO adhesion layer. The substrates were cleaned with acetone and subsequently with iso-

propanol in an ultrasonic bath for 5 minutes. The polymers (10 mg mL<sup>-1</sup>) and appropriate amounts of dopant (MDR = 0.1, where, MDR is defined as; moles of oxidized Spiro-OMeTAD(TFSI)<sub>2</sub>: moles of repeating unit) were dissolved at room temperature in THF and thin films were spin coated (1000 rpm for 90 s) on precleaned substrates for conductivity measurements. All steps of sample preparation were performed in argon filled glovebox. Each substrate (chip) consists of four groups with four identical transistors, with a channel length of 2.5, 5, 10 and 20 μm respectively and a constant channel width of 1cm. For calculating conductivity, the source-drain current  $I_{DS}$  was measured as a function of the source-drain voltage  $V_{DS}$  ( $\pm 2$  V), without applying a gate potential  $V_G$ . An increase in the drain potential  $V_{DS}$  led to a linear increase in the current  $I_{DS}$ . From the linear fit of the I-V plots, the slope of was used to calculate the conductivity using the following equation:

$$\sigma = \frac{\text{slope} \cdot L}{W \cdot d} \quad (2)$$

Where, L is channel length, W is channel width (1cm constant) and d is the layer thickness, which was measured with Dektak Profilometer.

## Experimental

### (1) Synthesis 2-hexyldecanal

25 mL DMSO in 620 mL DCM was added to a dry Schlenk flask under nitrogen atmosphere. Thereafter, 12.4 mL (144 mmol, 1.40 eq.) oxalyl chloride was added at -72 ° C and stirred for 30 min. Then, at -72 ° C, 25 g (103 mmol) 1,2-hexyldecan-1-ol were added and stirred again for 30 minutes. Subsequently, 73.8 mL (532 mmol, 5.16 eq.) NEt<sub>3</sub> was added dropwise and reacted at r.T. for 24 hours. 30 ml deionized water were added to the reaction mixture which then was extracted 3 times with 30 ml of diethyl ether. The organic phase was washed with a 10% HCl solution. Subsequently, the reaction product was washed with a saturated NaHCO<sub>3</sub> solution and with a saturated NaCl. The crude product was purified via column chromatography over silica with ethyl acetate: hexane 1:5. (Yield: 23.1 g, 93 %)

<sup>1</sup>H-NMR: δ<sub>H</sub> (300 MHz; ppm, CDCl<sub>3</sub>): 0.88 (t, 6H), 1.14-1.7 (m, 24H), 2.22 (m, 1H), 9.57 (d, 1H)

### (2) Synthesis 2-hexyldecene

41 g (115 mmol, 1.2 eq.) methyltriphenylphosphonium bromide was dissolved in 580 mL THF at -78 °C in a dry Schlenk tube under nitrogen. Meanwhile, 12.9 g (114.8 mmol, 1.2 eq.) potassium *tert*-butoxide was dissolved in dry THF and added to the reaction mixture. The mixture was stirred for 1 h at -78 °C. 23 g 2-hexyldecanal (96 mmol, 1 eq.) were dissolved in 96 mL THF and slowly added to the mixture at -78 °C and stirred for 1 h. Then, the reaction mixture was allowed to warm up to room temperature and stirred overnight. The mixture was diluted with 250 mL hexane and filtered over Celite. The raw product was purified via column chromatography over silica with n-hexane as eluent. (Yield: 14.7 g, 65 %)

$^1\text{H-NMR}$ :  $\delta_{\text{H}}$  (300 MHz; ppm,  $\text{CDCl}_3$ ): 0.88 (t, 6H), 1.14-1.42 (m, 24H), 1.94 (s, 1H), 4.88-5.01 (m, 1H), 5.43-5.6 (m, 2H)

*(3) Synthesis of 3-hexylundecane-1,2-diol*

The synthesis was done according to Plietker et al., with minor modifications.<sup>13</sup> 18 mL  $\text{H}_2\text{SO}_4$  (18.3 mmol, 0.2 eq.) and 29.4 g  $\text{NaIO}_4$  (137 mmol, 1.5 eq.) were dissolved in 60 mL water in a flask and cooled down to 0 °C. An aqueous suspension of 95 mg  $\text{RuCl}_3$  (0.46 mmol, 0.005 eq.) in 5 mL water was added slowly to the solution. 274 mL ethyl acetate were added, and the suspension was stirred for 5 min. 274 mL acetonitrile were added, and the suspension was again stirred for 5 min. 22 g 2-hexyldecene (91 mmol, 1 eq.) was slowly added and the mixture was stirred for 5 min. The reaction mixture was poured into saturated solutions of 690 mL  $\text{NaHCO}_3$  and 910 mL  $\text{Na}_2\text{S}_2\text{O}_3$ . The organic phase was dried over  $\text{Na}_2\text{SO}_4$ . The product was purified via column chromatography over silica with n-hexane: EA 5:1.

(Yield: 9.73 g, 39 %)

$^1\text{H-NMR}$ :  $\delta_{\text{H}}$  (300 MHz; ppm,  $\text{CDCl}_3$ ): 0.88 (t, 6H), 1.14-1.42 (m, 24H), 2.01 (s, 1H), 3.50-3.59 (m, 1H), 3.61-3.77 (m, 2H)

*(4) Synthesis of 2-(pentadecan-7-yl)-2,3-dihydrothieno[3,4-b][1,4] dioxine*

To a three-necked flask equipped with an argon purge 3,4-dimethoxythiophene 1 (1 g, 6.935 mmol) were added, 3-hexylundecane-1,2-diol (3.779 g, 13.87 mmol), *p*-toluenesulfonic acid monohydrate (0.120 g, 3.467 mmol), and 25 mL dry toluene. The solution was heated at 90 °C for 24 h. After this time, another two equivalents of the

diol were added, and the reaction was conducted for another 3 h before it was allowed to cool to room temperature. The reaction mixture was mixed with ethyl acetate and washed twice with a saturated sodium bicarbonate solution. After removal of the solvent, the remaining crude product was isolated by column chromatography (silica gel, hexane/dichloromethane 8/2).

(Yield: 1.54 g, 63 %)

$^1\text{H-NMR}$ :  $\delta_{\text{H}}$  (300 MHz; ppm,  $\text{CDCl}_3$ ): 0.90 (t, 6H), 1.14-1.42 (m, 24H), 1.68 (s, 1H), 3.95-4.03 (m, 2H), 4.06-4.13 (q, 1H), 4.14-4.20 (dd, 1H), 6.31 (s, 2H)

*(5) Synthesis of 5,7-dibromo-2-hexyl-2,3-dihydrothieno[3,4-b] [1,4] dioxine*

NBS (1.633g, 9.173 mmol) was dissolved in a mixture of THF (30 ml) and acetic acid (30 ml) and cooled to 0 °C using an ice bath. 2-(pentadecan-7-yl)-2,3-dihydrothieno[3,4-b] [1,4] dioxine (1.54 g, 4.368 mmol) was added against an argon stream dropwise at 0 °C and the solution was stirred at RT for 4 h under the exclusion of light. The solution was then extracted with diethylether and washed with water, saturated solution of sodium bicarbonate and 1 molar solution of sodium hydroxide. The organic phase was dried over anhydrous  $\text{MgSO}_4$ , filtered and concentrated. The raw product was purified by column chromatography over silica with hexane/DCM 8/2 as eluent.

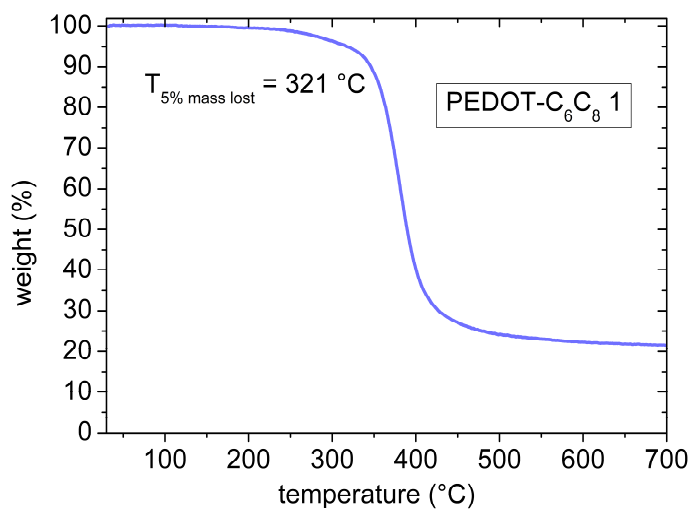
(Yield: 1.87 g, 84 %)

$^1\text{H-NMR}$ :  $\delta_{\text{H}}$  (300 MHz; ppm,  $\text{CDCl}_3$ ): 0.90 (t, 6H), 1.14-1.42 (m, 24H), 1.68 (s, 1H), 3.95-4.03 (m, 2H), 4.06-4.13 (q, 1H), 4.14-4.20 (dd, 1H)

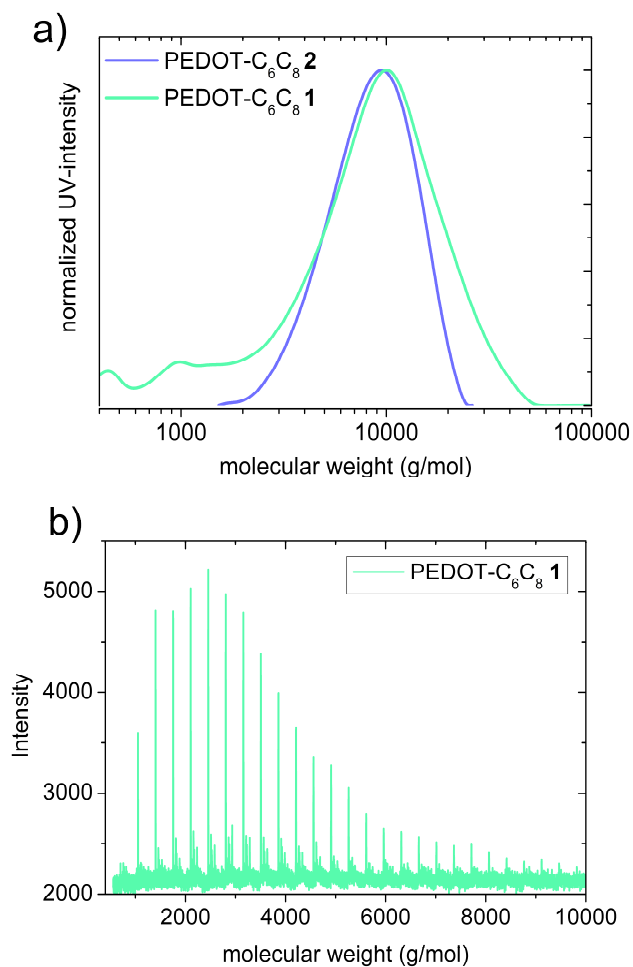
(6) Synthesis of Poly(2-(pentadecan-7-yl)-2,3-dihydrothieno[3,4-b] [1,4] dioxine)  
PEDOT-C<sub>6</sub>C<sub>8</sub>

5,7-dibromo-2-hexyl-2,3-dihydrothieno[3,4-b] [1,4] dioxine (1 eq.) was added to a dry flask under argon and the vessel was evacuated once again and flushed with nitrogen. Then the concentration was set with dry THF to 0.5 mol/l and *t*-butylmagnesiumchloride (1.22 M in THF, 0.96 eq.) was added dropwise. The reaction mixture was stirred for 20 h under the exclusion of light. Then the reaction mixture was diluted with dry THF to 0.1 mol/l. The respective amount of Ni(dppp)Cl<sub>2</sub> (suspension in 2-3 ml dry THF) was added in one portion to start the polymerization. After 4 h the polymerization was quenched with water. The mixture was concentrated, and the polymer was precipitated in methanol. Furthermore, the polymer was purified by Soxhlet extraction with hexane, methanol and chloroform and dried under vacuum.

<sup>1</sup>H-NMR: δ<sub>H</sub> (300 MHz; ppm, CDCl<sub>3</sub>): 0.88 (t, 6H), 1.14-1.42 (m, 24H), 1.94 (s, 1H), 4.01-4.57 (m, 4H).



**Figure S1:** TGA measurement of PEDOT-C<sub>6</sub>C<sub>8</sub> 1 under nitrogen with a heating rate of 10 K/min.



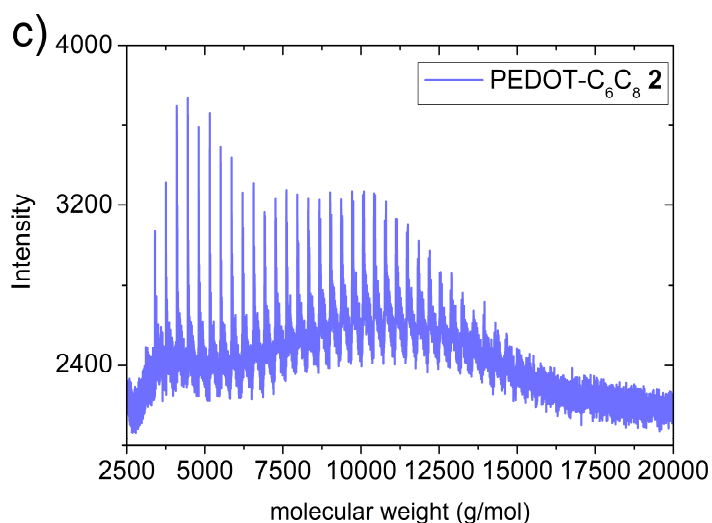


**Figure S2:** a) SEC chromatograms, measured with THF as eluent and narrowly distributed polystyrene as standard materials. (b) MALDI-ToF spectra were recorded with dithranol as matrix.

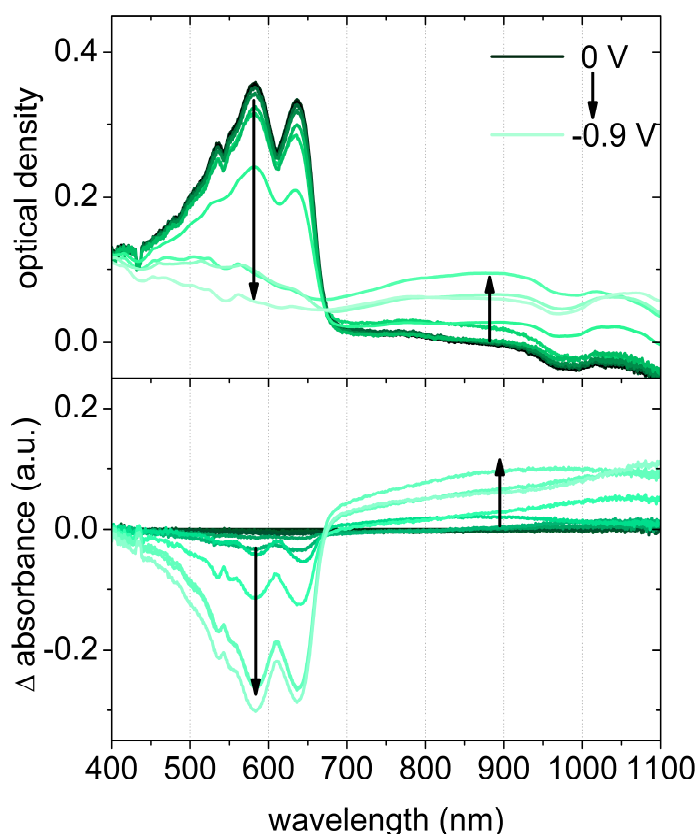


**Figure S3:** a) Spectro electrochemistry measurements of thin polymer films on ITO of PEDOT-C<sub>6</sub>C<sub>8</sub> 1 respectively. The spectra were measured in 0.1 M NaCl when the films were biased from 0 V to -0.9 V in a three-electrode setup with an Ag/AgCl reference electrode and a Pt counter electrode. Difference spectra obtained by subtracting the absorption spectra of the copolymers in the neutral state (0 V) from the absorption spectra under different applied potentials during the in situ electrochemical oxidation of PEDOT-C<sub>6</sub>C<sub>8</sub> 2 by applying a potential from 0 to -900 mV. The pristine absorption in the 400-680 nm range decreases with

a concomitant increase in polaron absorption in the range of 680 to 1100 nm. The arrow indicates the direction of spectral changes.

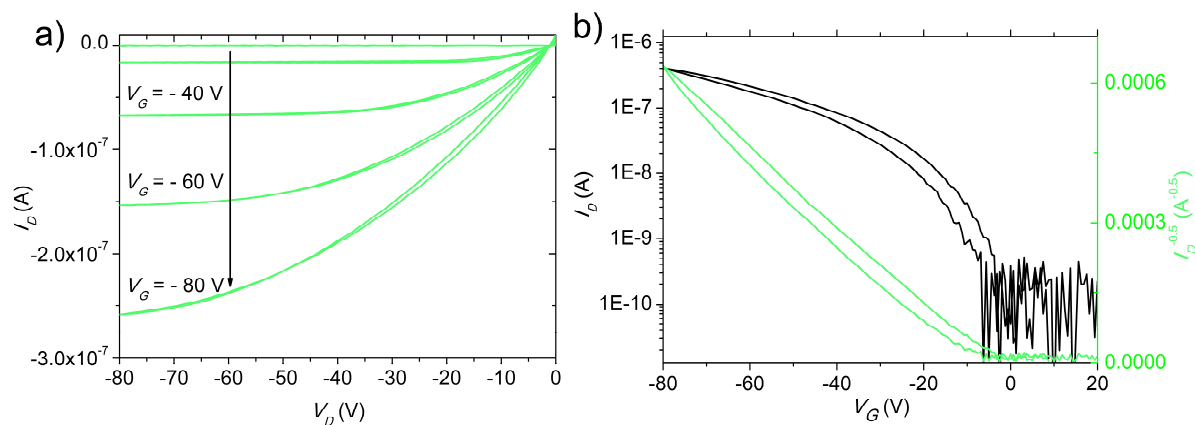


**Figure S4:** OEFT Output (a) and transfer curve (b) of PEDOT-C<sub>6</sub>C<sub>8</sub> 1, measured in a bottom-gate (Si), bottom-contact (Au) geometry in range from 0 V to -80 V.

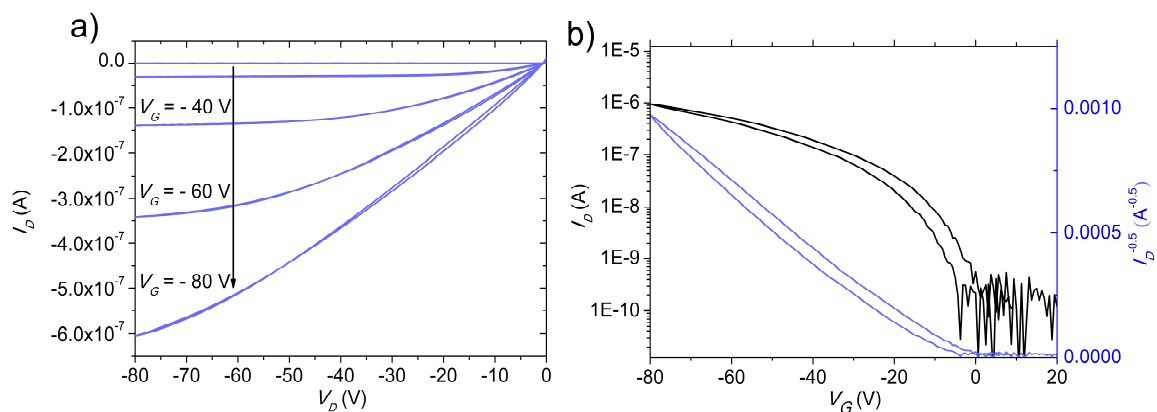


**Figure S5:** OEFT Output (a) and transfer curve (b) of PEDOT-C<sub>6</sub>C<sub>8</sub> 2, measured in a bottom-gate (Si), bottom-contact (Au) geometry in range from 0 V to -80 V.

**Table S1:** Summary of the measured conductivities (as cast, annealed at 100 °C for 5 min, annealed at 100 °C for 30 min, in air: 30 min, in air: 120 min, in air: 12 h) with the corresponding channel length of the transistor (2.5, 5, 10 and 20  $\mu\text{m}$ ) of PEDOT-C<sub>6</sub>C<sub>8</sub> 1, doped with 10 mol% of spiro-OMeTAD (TFSI)<sub>2</sub>.

PEDOT-C <sub>6</sub> C <sub>8</sub> 1 doped Thickness: 94.55nm	Conductivity (S cm <sup>-1</sup> ) Channel length (2.5 $\mu\text{m}$ )	Conductivity (S cm <sup>-1</sup> ) Channel length (5 $\mu\text{m}$ )	Conductivity (S cm <sup>-1</sup> ) Channel length (10 $\mu\text{m}$ )	Conductivity (S cm <sup>-1</sup> ) Channel length (20 $\mu\text{m}$ )	Conductivity (S cm <sup>-1</sup> ) Average of four channels
<b>As cast</b>	$1.58 \cdot 10^{-4}$	$1.58 \cdot 10^{-4}$	$2.11 \cdot 10^{-4}$	$1.48 \cdot 10^{-4}$	$1.69 \cdot 10^{-4}$
<b>Annealed at 100 °C for 5 min</b>	$5.29 \cdot 10^{-4}$	$5.28 \cdot 10^{-4}$	$7.40 \cdot 10^{-4}$	$8.46 \cdot 10^{-4}$	$6.60 \cdot 10^{-4}$
<b>Annealed at 100 °C for 30 min</b>	$1.32 \cdot 10^{-3}$	$1.05 \cdot 10^{-3}$	$1.05 \cdot 10^{-3}$	$1.69 \cdot 10^{-3}$	$1.28 \cdot 10^{-3}$
<b>In Air: 30 min</b>	$1.05 \cdot 10^{-3}$	$1.05 \cdot 10^{-3}$	$1.05 \cdot 10^{-3}$	$1.27 \cdot 10^{-3}$	$1.10 \cdot 10^{-3}$
<b>In Air: 120 min</b>	$1.05 \cdot 10^{-3}$	$1.05 \cdot 10^{-3}$	$1.05 \cdot 10^{-3}$	$1.27 \cdot 10^{-3}$	$1.10 \cdot 10^{-3}$
<b>In Air: 12 h</b>	$1.05 \cdot 10^{-3}$	$1.05 \cdot 10^{-3}$	$1.05 \cdot 10^{-3}$	$1.27 \cdot 10^{-3}$	$1.10 \cdot 10^{-3}$

**Table S2:** Summary of the measured conductivities (as cast, annealed at 100 °C for 5 min, annealed at 100 °C for 30 min, in air: 30 min, in air: 120 min, in air: 12 h) with the corresponding channel length of the transistor (2.5, 5, 10 and 20  $\mu\text{m}$ ) of pristine PEDOT- $\text{C}_6\text{C}_8$  1.

: PEDOT- $\text{C}_6\text{C}_8$ 1  pristine  Thickness: 54.71 nm	Conductivity ( $\text{S cm}^{-1}$ )  Channel length (2.5 $\mu\text{m}$ )	Conductivity ( $\text{S cm}^{-1}$ )  Channel length (5 $\mu\text{m}$ )	Conductivity ( $\text{S cm}^{-1}$ )  Channel length (10 $\mu\text{m}$ )	Conductivity ( $\text{S cm}^{-1}$ )  Channel length (20 $\mu\text{m}$ )	Conductivity ( $\text{S cm}^{-1}$ )  Average of four channels
<b>As cast</b>	-	$9.12 \cdot 10^{-6}$	$9.13 \cdot 10^{-6}$	-	$9.12 \cdot 10^{-6}$
<b>Annealed at 100 °C for 5 min</b>	$9.14 \cdot 10^{-6}$	$9.13 \cdot 10^{-6}$	$1.82 \cdot 10^{-6}$	$0.73 \cdot 10^{-6}$	$5.20 \cdot 10^{-6}$
<b>Annealed at 100 °C for 30 min</b>	-	$9.13 \cdot 10^{-6}$	$1.82 \cdot 10^{-6}$	$1.10 \cdot 10^{-6}$	$4.02 \cdot 10^{-6}$
<b>In Air: 30 min</b>	$18.2 \cdot 10^{-6}$	$9.13 \cdot 10^{-6}$	$3.65 \cdot 10^{-6}$	$3.65 \cdot 10^{-6}$	$8.66 \cdot 10^{-6}$
<b>In Air: 120 min</b>	$22.8 \cdot 10^{-6}$	$18.2 \cdot 10^{-6}$	$7.31 \cdot 10^{-6}$	$3.65 \cdot 10^{-6}$	$12.99 \cdot 10^{-6}$
<b>In Air: 12 h</b>	$31.9 \cdot 10^{-6}$	$54.8 \cdot 10^{-6}$	$1.10 \cdot 10^{-6}$	$7.3 \cdot 10^{-6}$	$23.78 \cdot 10^{-6}$

**Table S3:** Summary of the measured conductivities (as cast, annealed at 100 °C for 5 min, annealed at 100 °C for 30 min, in air: 30 min, in air: 120 min, in air: 12 h) with the corresponding channel length of the transistor (2.5, 5, 10 and 20 μm) of PEDOT-C<sub>6</sub>C<sub>8</sub>2, doped with 10 mol% of spiro-OMeTAD (TFSI)<sub>2</sub>.

PEDOT-C <sub>6</sub> C <sub>8</sub> 2 doped Thickness: 104.71nm	Conductivity (S cm <sup>-1</sup> ) Channel length (2.5 μm)	Conductivity (S cm <sup>-1</sup> ) Channel length (5 μm)	Conductivity (S cm <sup>-1</sup> ) Channel length (10 μm) <sup>1,10</sup>	Conductivity (S cm <sup>-1</sup> ) Channel length (20μm)	Conductivity (S cm <sup>-1</sup> ) Average of four channels
<b>As cast</b>	4.77 · 10 <sup>-4</sup>	2.86 · 10 <sup>-4</sup>	2.86 · 10 <sup>-4</sup>	3.82 · 10 <sup>-4</sup>	3.58 · 10 <sup>-4</sup>
<b>Annealed at 100 °C for 5 min</b>	4.77 · 10 <sup>-4</sup>	4.77 · 10 <sup>-4</sup>	4.77 · 10 <sup>-4</sup>	3.82 · 10 <sup>-4</sup>	4.53 · 10 <sup>-4</sup>
<b>Annealed at 100 °C for 30 min</b>	4.77 · 10 <sup>-4</sup>	4.77 · 10 <sup>-4</sup>	4.77 · 10 <sup>-4</sup>	5.73 · 10 <sup>-4</sup>	5.53 · 10 <sup>-4</sup>
<b>In Air: 30 min</b>	4.77 · 10 <sup>-4</sup>	4.77 · 10 <sup>-4</sup>	4.77 · 10 <sup>-4</sup>	3.82 · 10 <sup>-4</sup>	4.53 · 10 <sup>-4</sup>
<b>In Air: 120 min</b>	4.77 · 10 <sup>-4</sup>	4.77 · 10 <sup>-4</sup>	4.77 · 10 <sup>-4</sup>	3.82 · 10 <sup>-4</sup>	4.53 · 10 <sup>-4</sup>
<b>In Air: 12 h</b>	4.77 · 10 <sup>-4</sup>	4.77 · 10 <sup>-4</sup>	4.77 · 10 <sup>-4</sup>	3.82 · 10 <sup>-4</sup>	4.53 · 10 <sup>-4</sup>

**Table S4:** Summary of the measured conductivities (as cast, annealed at 100 °C for 5 min, annealed at 100 °C for 30 min, in air: 30 min, in air: 120 min, in air: 12 h) with the corresponding channel length of the transistor (2.5, 5, 10 and 20 μm) of pristine PEDOT-C<sub>6</sub>C<sub>8</sub>2.

PEDOT-C <sub>6</sub> C <sub>8</sub> 2	Conductivity (S cm <sup>-1</sup> )				
pristine Thickness: 44.32 nm	Channel length (2.5 μm)	Channel length (5 μm)	Channel length (10 μm)	Channel length (20μm)	Average of four channels
<b>As cast</b>	0.56 · 10 <sup>-7</sup>	1.12 · 10 <sup>-7</sup>	1.12 · 10 <sup>-7</sup>	1.35 · 10 <sup>-7</sup>	1.04 · 10 <sup>-7</sup>
<b>Annealed at 100 °C for 5 min</b>	5.64 · 10 <sup>-7</sup>	1.12 · 10 <sup>-7</sup>	1.12 · 10 <sup>-7</sup>	0.32 · 10 <sup>-7</sup>	2.05 · 10 <sup>-7</sup>
<b>Annealed at 100 °C for 30 min</b>	45.1 · 10 <sup>-7</sup>	6.76 · 10 <sup>-7</sup>	4.51 · 10 <sup>-7</sup>	3.16 · 10 <sup>-7</sup>	1.49 · 10 <sup>-6</sup>
<b>In Air: 30 min</b>	3.38 · 10 <sup>-6</sup>	0.90 · 10 <sup>-6</sup>	1.24 · 10 <sup>-6</sup>	1.80 · 10 <sup>-6</sup>	1.83 · 10 <sup>-6</sup>
<b>In Air: 120 min</b>	8.46 · 10 <sup>-6</sup>	2.25 · 10 <sup>-6</sup>	2.25 · 10 <sup>-6</sup>	3.16 · 10 <sup>-6</sup>	4.03 · 10 <sup>-6</sup>
<b>In Air: 12 h</b>	16.9 · 10 <sup>-6</sup>	6.20 · 10 <sup>-6</sup>	6.76 · 10 <sup>-6</sup>	3.61 · 10 <sup>-6</sup>	8.37 · 10 <sup>-6</sup>

## 9. Appendix: Unpublished data: Materials Synthesis, Characterization and OECT Device Fabrication

### 9.1. Amphiphilic Polythiophene-based Blockcopolymers – Synthesis and characterization

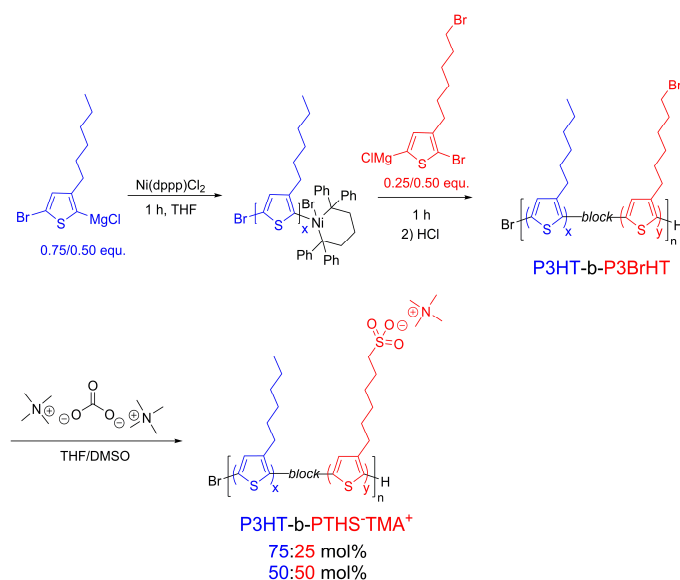


**Figure 1:** Schematic Illustration of the sequential blockcopolymerization and the polymer analogous conversion of the P3HT-b-P3BrHT Blockcopolymer to the conjugated polyelectrolyte P3HT-b-PTHS-TMA<sup>+</sup>.

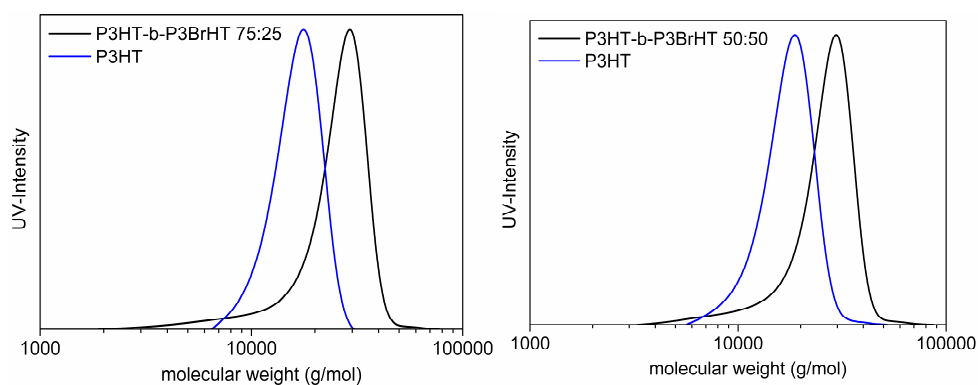


**Figure 2:** SEC profiles of the blockcopolymerization of P3HT-b-P3BrHT 75:25 (left) and 50:50 (right). The first block of 3HT is shown in blue, the final Blockcopolymer is illustrated in black.

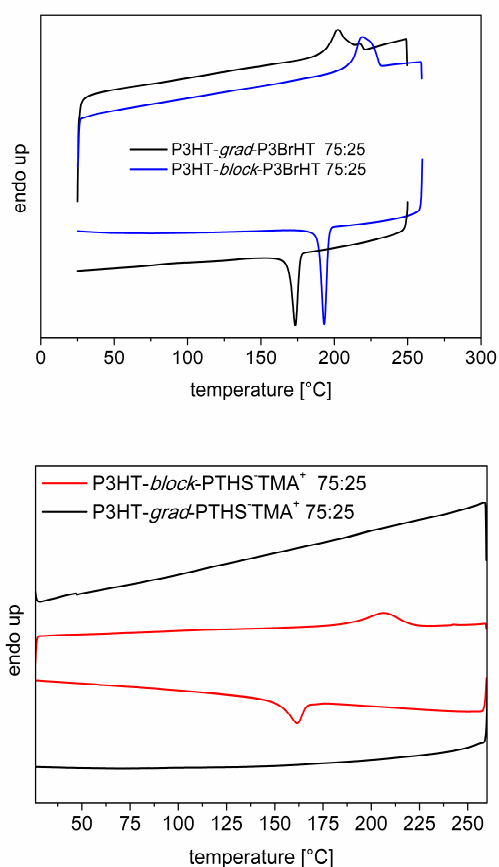


**Figure 3:** DSC measurements of the precursor polymers P3HT-grad-P3BrHT 75:25, P3HT-block-P3BrHT 75:25, P3HT-grad-PTHS-TMA<sup>+</sup> 75:25 and P3HT-block-PTHS-TMA<sup>+</sup> 75:25, measured with a heating rate of 10 K/min under nitrogen atmosphere. The first cooling and the second heating curve are shown.

**Table 1:** Thermal Properties of P3HT-grad-P3BrHT 75:25, P3HT-block-P3BrHT 75:25, P3HT-grad-PTHS-TMA<sup>+</sup> 75:25 and P3HT-block-PTHS-TMA<sup>+</sup> 75:25, measured with DSC.

	$T_{m, peak}$ (°C)	$\Delta H_m$ (J/g)	$T_{c, peak}$ (°C)
P3HT-grad-P3BrHT 75:25	203	17.5	175
P3HT-block-P3BrHT 75:25	225	18.6	194
P3HT-grad-PTHS-TMA <sup>+</sup> 75:25	-	-	-
P3HT-block-PTHS-TMA <sup>+</sup> 75:25	208	8.9	174

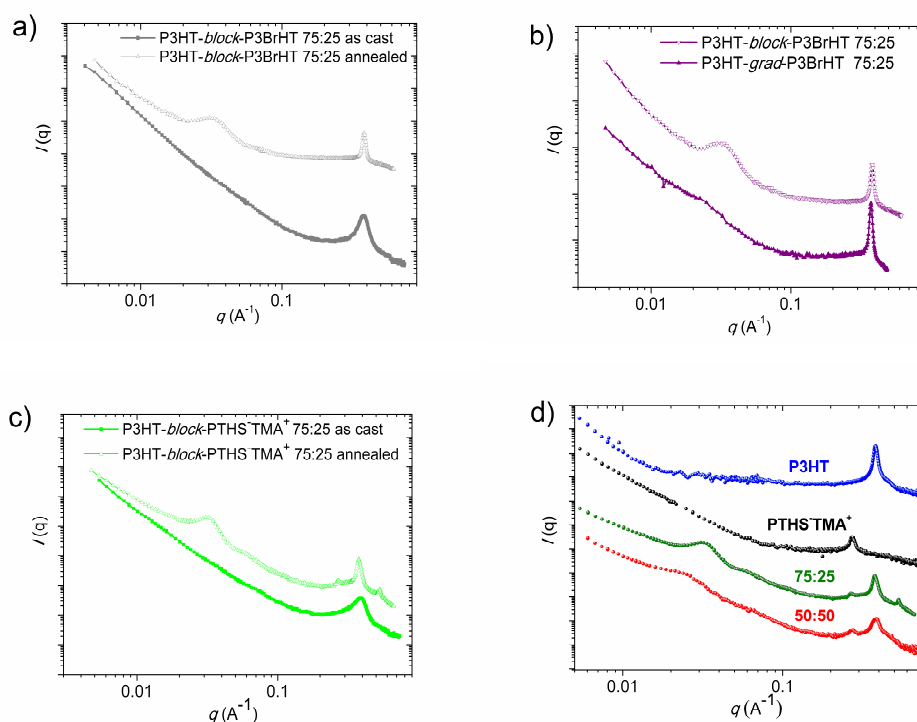


**Figure 4:** SAXS/WAXS measurements of (a) P3HT-block-P3BrHT 75:25 as cast and annealed, (b) P3HT-block-P3BrHT 75:25 vs. P3HT-grad-P3BrHT 75:25, (c) P3HT-block-PTHS-TMA<sup>+</sup> 75:25 as cast and annealed and (d) P3HT, PTHS-TMA<sup>+</sup>, P3HT-block-PTHS-TMA<sup>+</sup> 75:25 and P3HT-block-PTHS-TMA<sup>+</sup> 50:50.

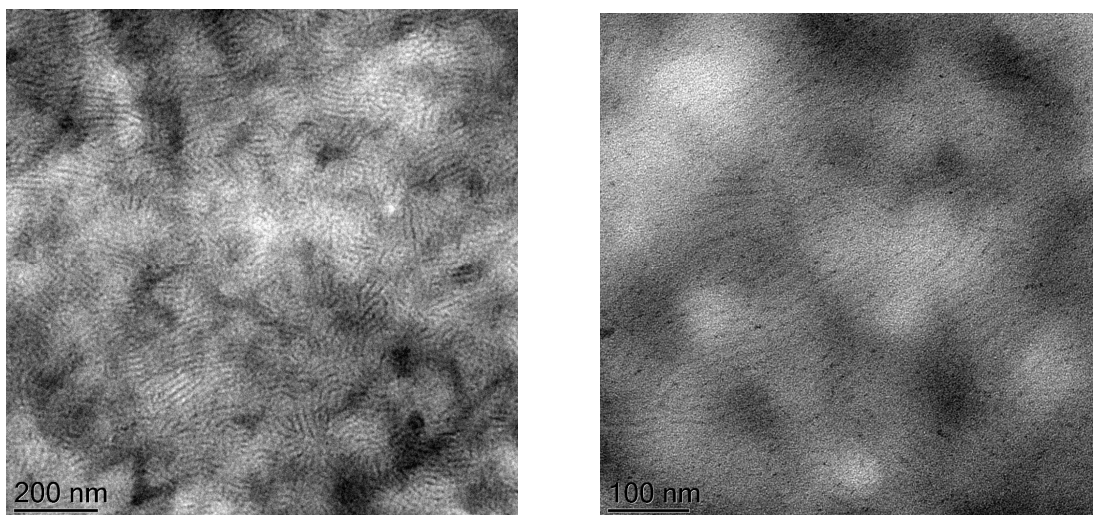


**Figure 5:** TEM images of P3HT-block-PTHS-TMA<sup>+</sup> 75:25. The sample was heated up to 250 °C and then slowly cooled down to room temperature with a cooling rate of 1 K/min. The polymer sample was then stained with OsO<sub>4</sub>.

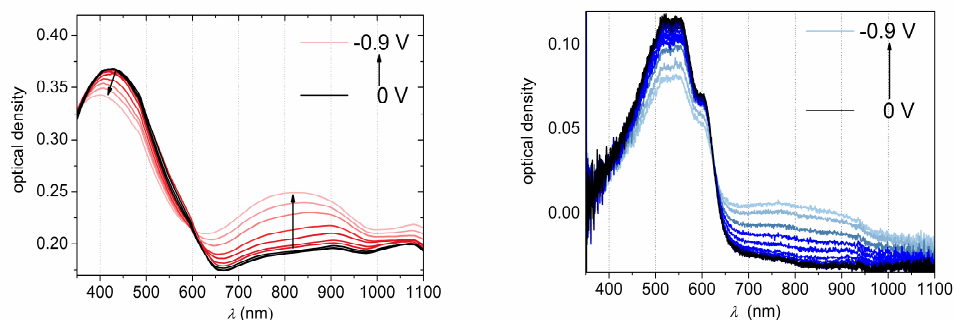


**Figure 6:** (a) Spectro electrochemistry measurements of polymer films on ITO of P3HT-grad-PTHS-TMA<sup>+</sup> 75:25 (left) and P3HT-block-PTHS-TMA<sup>+</sup> 75:25 (right). The UV-Vis spectra were measured in 0.1 M NaCl when the films were biased from 0 to -0.9 V in a three-electrode setup with an Ag/AgCl reference electrode and a Pt counter electrode.

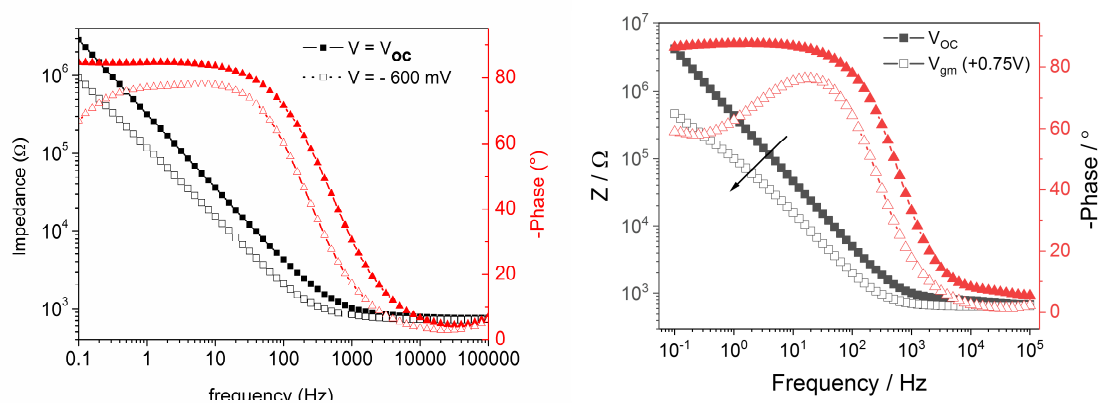


**Figure 7:** Electrochemical impedance spectra of P3HT-block-PTHS-TMA<sup>+</sup> 75:25 (left) and P3HT-block-PTHS-TMA<sup>+</sup> 50:50 (right) recorded at  $V_{oc}$  and at the doping potential that attains the maximum transconductance  $g_m$  ( $V = -0.75$  V) in NaCl solution (0.1 M). Randles circuit was used for fitting the impedance and the phase spectrum ( $R_{Electrolyte}(R_{Polymer}||C_{Polymer})$ ) at a doping potential of  $V = 0.75$  V. Following chi-fitting values were noted: 0.150 (P3HT-block-PTHS-TMA<sup>+</sup> 50:50) and 0.198 (P3HT-block-PTHS-TMA<sup>+</sup> 75:25).

9. Appendix: *Unpublished data: Materials Synthesis, Characterization and OECT Device Fabrication*

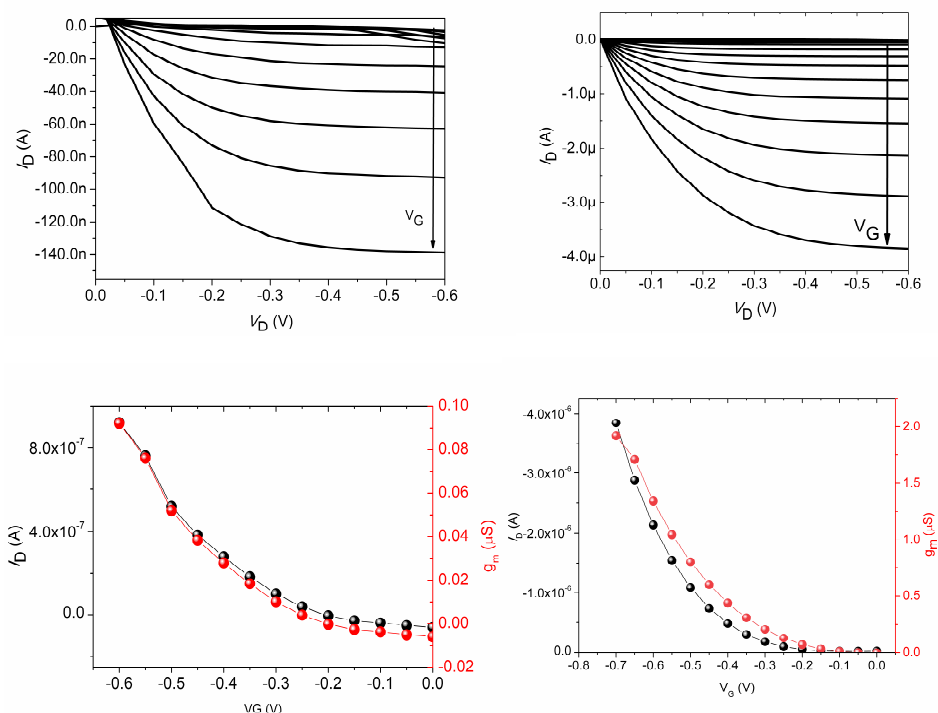


**Figure 8:** OECT output and transfer curves of P3HT-block-PTHS-TMA<sup>+</sup> 75:25 (left) and P3HT-block-PTHS-TMA<sup>+</sup> 50:50 (right) for gate voltages ranging from 0 V to -0.6 V ( $\Delta V = -0.05$  V) and 0 V to -0.7 V respectively ( $\Delta V = -0.05$  V). The transfer curve at a drain voltage of  $V_D = -0.6$  V is shown.

**Table 2.** OECT Characteristics and Material-Dependent Parameters for the Copolymers P3HT-grad-PTHS-TMA<sup>+</sup> 75:25, P3HT-block-PTHS-TMA<sup>+</sup> 75:25, P3HT-grad-PTHS-TMA<sup>+</sup> 50:50 and P3HT-block-PTHS-TMA<sup>+</sup> 50:50.

	$M_n$ (Đ)	$C^*$	$g_{m, \max.}$	$V_{th}$	$\mu_{OECT}$	Passive Swelling
	(kg/mol)	(F/cm <sup>3</sup> )	( $\mu$ S)	(V)	(cm <sup>2</sup> /Vs)	(%)
P3HT-grad-PTHS-TMA <sup>+</sup> 75:25	15 (1.20)	31	-	-	-	4
P3HT-block-PTHS-TMA <sup>+</sup> 75:25	21 (1.08)	63	0.09	-0.33	$7.23 \cdot 10^{-4}$	14
P3HT-grad-PTHS-TMA <sup>+</sup> 51:49	17 (1.18)	100	400	-0.15	0.017	22
P3HT-block-PTHS-TMA <sup>+</sup> 50:50	23 (1.10)	66	2	-0.21	$7.23 \cdot 10^{-3}$	n.d.

SEC was performed on the precursor copolymers P3HT-co-P3BrHT with polystyrene calibration and THF as eluent.  $g_m$  was measured at  $V_G = -0.6$  V and  $V_D = -0.6$  V and the average value out of six transistors was taken into account.  $C^*$  was extracted from electrochemical impedance spectra of the polymer films coated on Au electrodes recorded at a DC potential of -0.6 or -0.7 V vs Ag/AgCl.  $\mu_{OECT}$  was determined with bandwidth measurements. Swelling percentages were estimated from the QCM-D experiments and calculated with Sauerbrey equation.

## 9.2. High-Performance Organic Electrochemical Transistors Based on Conjugated Polyelectrolyte Copolymers – Part 2

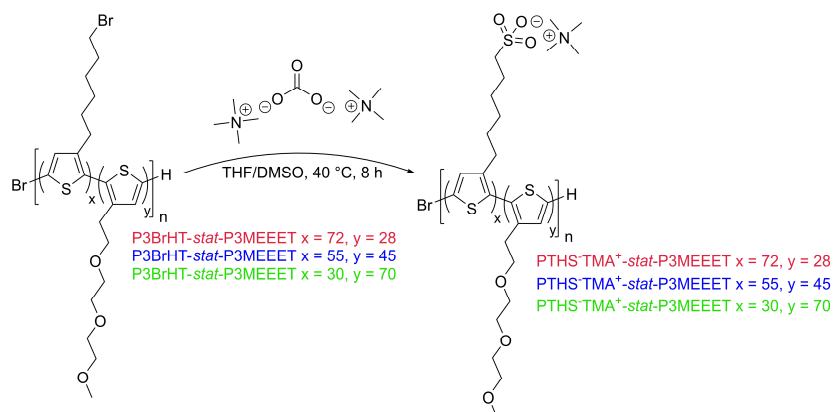


**Figure 1:** Chemical Structures of the precursor polymer P3BrHT-stat-P3MEEET and the conjugated polyelectrolyte PTHS-TMA<sup>+</sup>-stat-P3MEEET with three different copolymer compositions.

**Table 1.** Properties of the three synthesized precursor polymers P3BrHT-stat-P3MEEET. Both monomers form a statistical type of copolymer in all three compositions in one batch.

Copolymer	$M_n$ (kg/mol)	$M_p$ (kg/mol)	$\bar{D}$	Built-in ratio
P3BrHT-stat-P3MEEET 75:25	14	19	1.30	72:28
P3BrHT-stat-P3MEEET 50:50	20	26	1.16	55:45
P3BrHT-stat-P3MEEET 25:75	16	21	1.35	30:70

## 9. Appendix: Unpublished data: Materials Synthesis, Characterization and OECT Device Fabrication

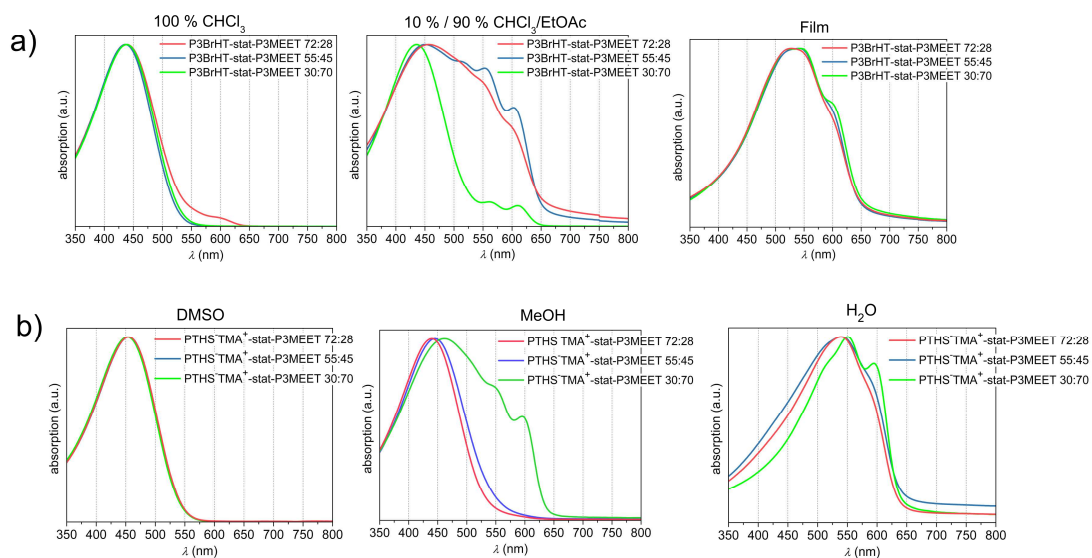


**Figure 2:** Absorption spectra of the (a) P3BrHT stat P3MEEET copolymers in solution and thin film, as well as solution absorption spectra of (b) PTHS-TMA<sup>+</sup>-stat-P3MEEET in DMSO, methanol and water at a polymer concentration of 0.02 mg/mL.

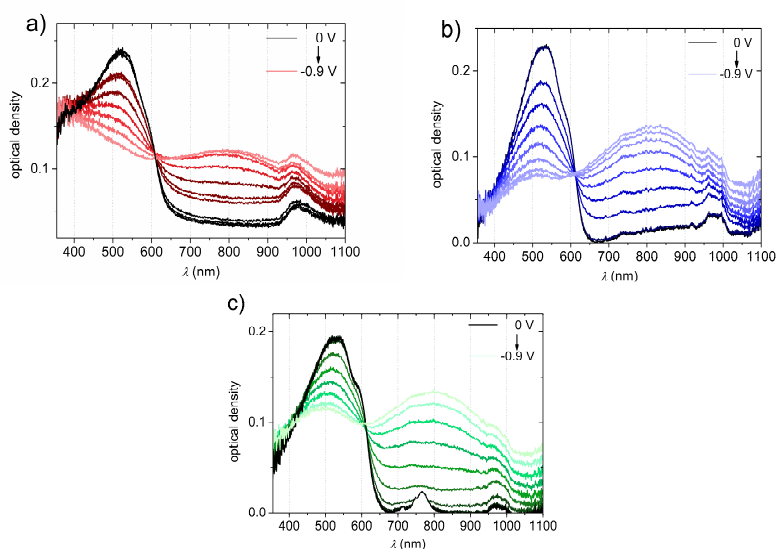


**Figure 3:** Spectroelectrochemistry measurements of polymer films on ITO of PTHS-TMA<sup>+</sup>-stat-P3MEEET 72:28 (a), PTHS-TMA<sup>+</sup>-stat-P3MEEET 55:45 (b), and PTHS-TMA<sup>+</sup>-stat-P3MEEET 30:70 (c). The UV-Vis spectra were measured in 0.1 M NaCl when the films were biased from 0 to -0.9 V in a three-electrode setup with an Ag/AgCl reference electrode and a Pt counter electrode.

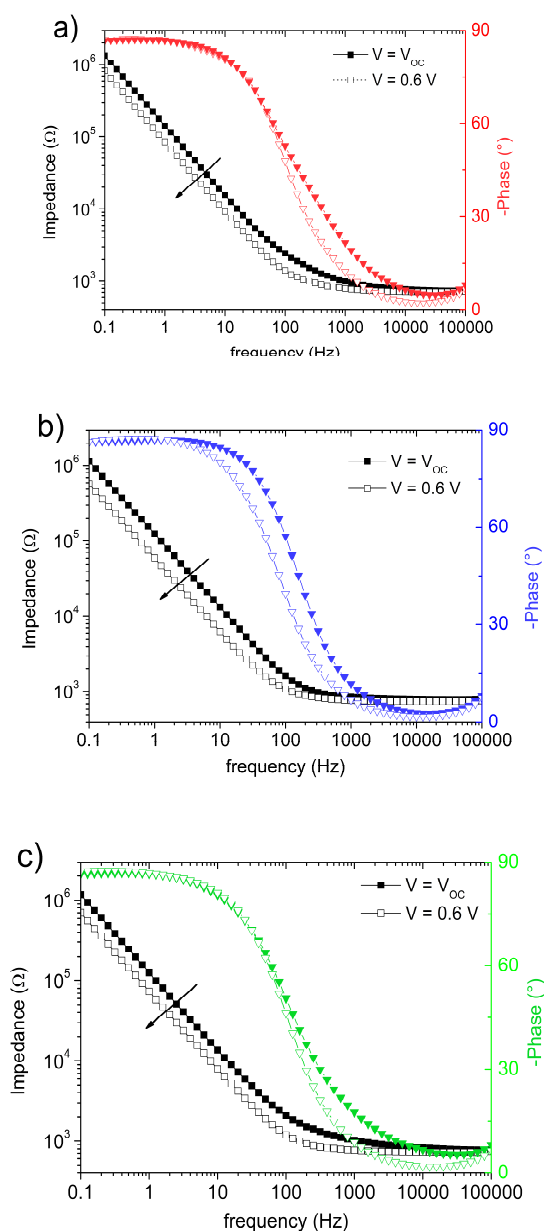


**Figure 4:** a) Electrochemical impedance spectra of the copolymers (a) PTHS-TMA<sup>+</sup>-stat-P3MEEET 72:28, (b) PTHS-TMA<sup>+</sup>-stat-P3MEEET 55:45 and (c) PTHS-TMA<sup>+</sup>-stat-P3MEEET 30:70 recorded at  $V_{oc}$  and at the doping potential that attains the maximum transconductance ( $V = -0.6$  V) in NaCl solution (0.1 M). Randles circuit was used for fitting the impedance and the phase spectrum,  $R_{electrolyte}(R_{polymer}||C_{polymer})$  at a doping potential ( $V = -0.6$  V). Following chi-fitting values were noted: 0.144 (PTHS-TMA<sup>+</sup>-stat-P3MEEET 72:28), 0.155 (PTHS-TMA<sup>+</sup>-stat-P3MEEET 55:45) and 0.122 (PTHS-TMA<sup>+</sup>-stat-P3MEEET 30:70).

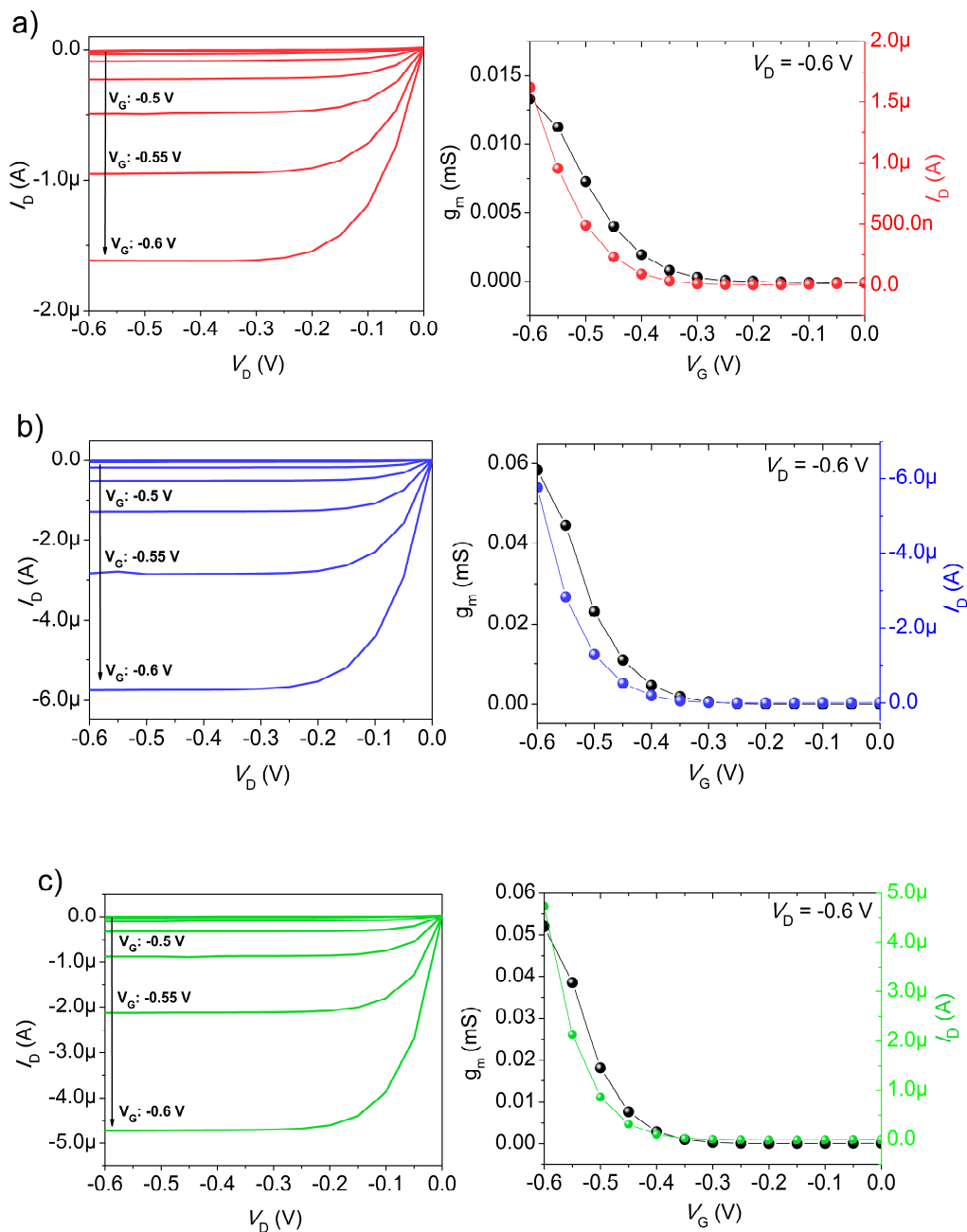


**Figure 5:** Output curve of copolymers (a) PTHS-TMA<sup>+</sup>-stat-P3MEEET 72:28, (b) PTHS-TMA<sup>+</sup>-stat-P3MEEET 55:45 and (c) PTHS-TMA<sup>+</sup>-stat-P3MEEET 30:70 for gate voltages ranging from 0 V to -0.60 V ( $\Delta V = -0.05$  V) (left), together with the transfer curve with the corresponding transconductance values (right).

**Table 2:** OECT Characteristics and Material-Dependent Parameters for PTHS-TMA<sup>+</sup> and the Copolymers PTHS-TMA<sup>+</sup>-co-P3MEEET copolymers.

	$\mu_{\text{OECT}}$ (cm <sup>2</sup> /Vs)	$C^*$ (F/cm <sup>3</sup> )	$V_{\text{th}}$ (V)	passive swelling (%)	thickness (nm)	$g_m$ (S/cm)	$\mu \cdot C^*$ (F/cmVs)
PTHS-TMA <sup>+</sup>		82	-0.45		20	20.45	
PTHS-TMA <sup>+</sup> - stat- P3MEEET 72:28	$2.83 \cdot 10^{-5}$	63	-0.32	35	118	11	0.0018
PTHS-TMA <sup>+</sup> - stat- P3MEEET 55:45	0.002	143	-0.37	21	105	57.1	0.29
PTHS-TMA <sup>+</sup> - stat- P3MEEET 30:70	0.002	153	-0.38	6	110	47.2	0.1

$g_m$  was measured at  $V_G = -0.6$  V and  $V_D = -0.6$  V and the average value out of six transistors was taken into account.  $C^*$  was extracted from electrochemical impedance spectra of the polymer films coated on Au electrodes recorded at a DC potential of  $-0.6$  or  $-0.7$  V vs Ag/AgCl (**Figure 4**).  $\mu_{\text{OECT}}$  was determined with bandwidth measurements. The thickness of the polymer films was measured with a Dektak profilometer. Swelling percentages were estimated from the QCM-D experiments using Sauerbrey equation.

### 9.3. Appendix: Organic Electrochemical Transistors - Microelectrode Design, Device Preparation and Characterization

Organic electrochemical transistors (OECTs) are the widely used device configuration in the field of organic bioelectronics. Their special features and their working principle are described in chapter 1. The fabrication of these transistors is quite challenging, and the use of a high-quality clean room is indispensable. The fabrication follows a so called “polymer lift-off” method. Here, the active channel material (organic semiconductor) is only located in a small cavity in the channel, which is defined by the polymer profile (See **Figure 1**). This is important, because the contact between the gold contacts and the aqueous electrolyte should be prevented, to avoid Faradaic reactions and capacitive effects during the measurement.

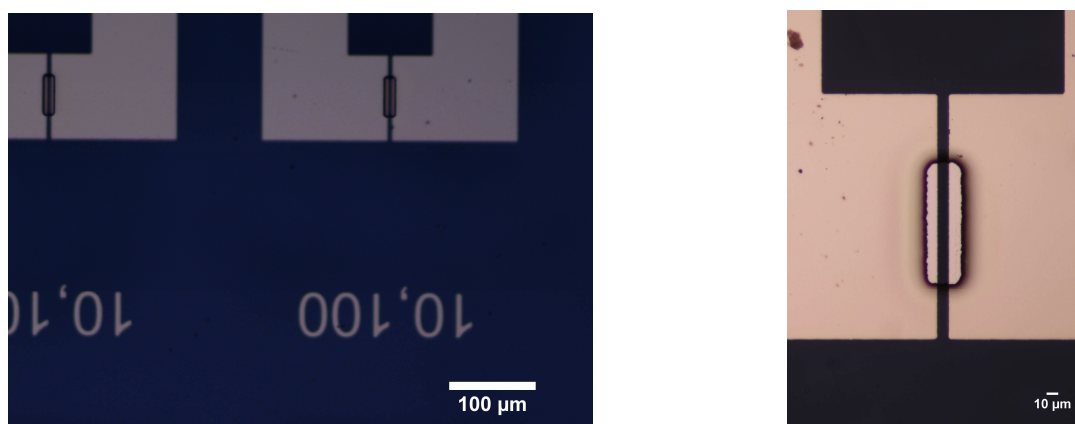


**Figure 1:** Microscope images of the channel geometry used in OECT with planar electrode set-ups.

To establish this type of measurements in the AFUPO group, we designed new OECT substrates in cooperation with the Fraunhofer ENAS in Chemnitz. Here we decided to take the advantage of an increased output current observed with interdigitated electrodes, compared to the standard used planar electrodes. The device configuration, as well as the polymer etching profile are shown in **Figure 2**.

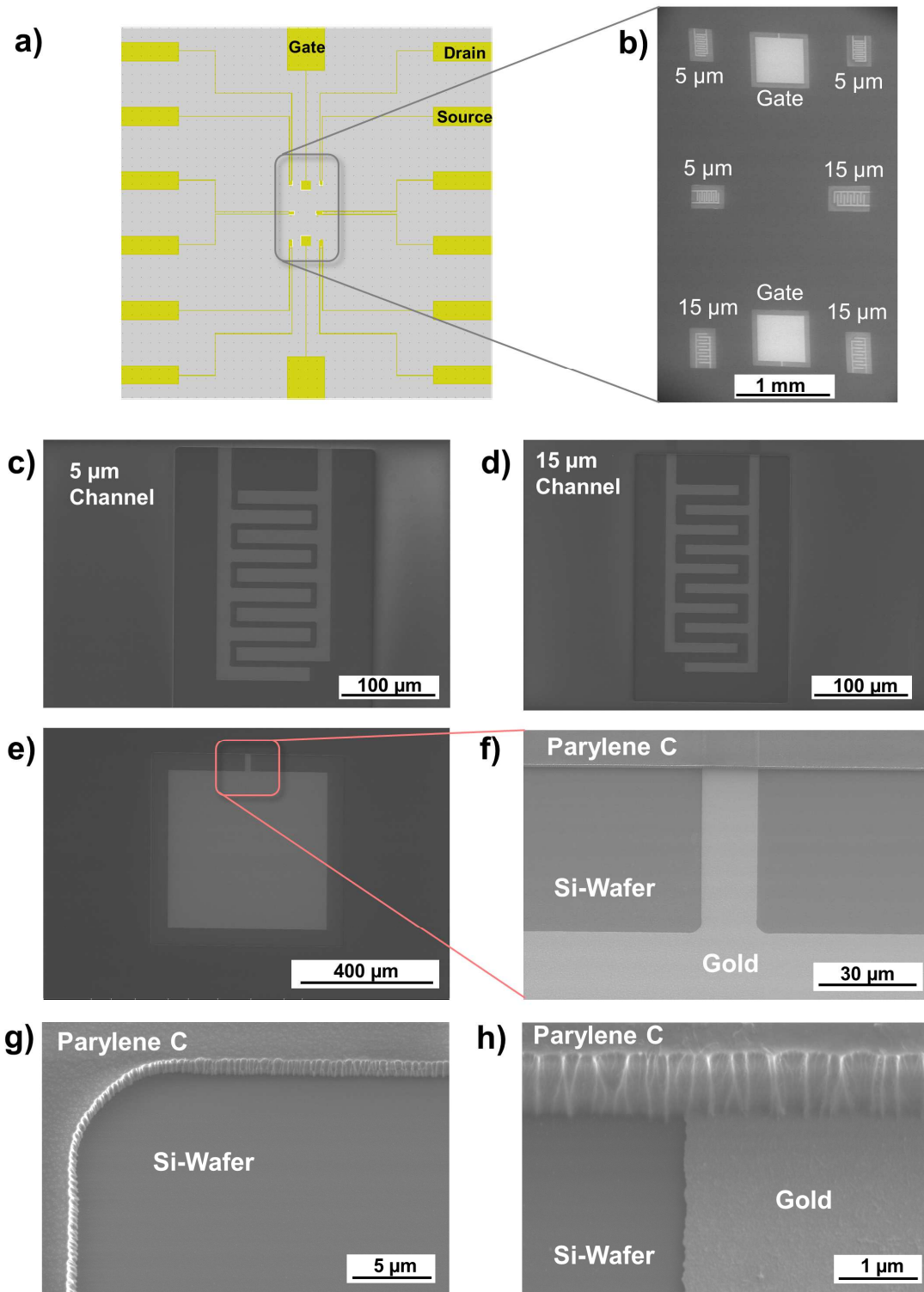


**Figure 2:** a) Illustration of the designed OEET substrate. b) ESEM image of the etched active area consisting of three transistors with a channel length of 5 μm, three transistors with a channel length of 15 μm and two square gold electrodes with an area of 500 x 500 μm<sup>2</sup>. c) and d) ESEM images of the two different etched interdigitated electrodes. e) ESEM image of the square gold gate electrode. f) Magnification of the square gold electrode and their etching profile. g) and h) ESEM images of the parylene C etching of the active areas of the transistors.

In the following, the detailed fabrication route will be described.

*1) Cleaning of the glass slides:*

The microscope glasses are first cleaned in a 2% Hellmanex solution in an ultrasonic bath for 20 min, then for 20 min in an acetone/isopropanol mixture (80/20). After that, the substrates were rinsed with isopropanol and dried with argon.

*2) Defining gold contacts*

- Cover substrate with LOR 5B (photo resist, ~ 1 ml) (no dynamic dispense)
- Then spin-coat with (a) 500 rpm/250 acc./10s and then (b) 3500 rpm/1750 acc./35s.
- Bake for 7 min at 180 °C
- Start spin coater (500 rpm/250 acc./10 sec) and dispense S1813 during spinning, then spin with 3500 rpm/1750 acc./35s (dynamic dispense).
- Bake for 1 min at 110 °C.
- First mask aligning step with a mask, followed by 30 s development step in Microposit MF-319 (Constantly pipette developer towards sample surface during development; After development submerge in DI water, rinse lightly at sink and dry with N<sub>2</sub> gun).
- Check at least one substrate under microscope that everything is well developed, and sharp edges can be seen.

*3) Plasma cleaning and surface activation*

- Reactive sputtering of 10 nm Cr and then 100 nm of Au.

- After sputtering, soak substrates in NMP at 70 °C for 2 h and then an RT overnight.
- Soaking in acetone/IPA overnight and then ultra-sonification for 15-20 min.
- If not all gold is removed, rub with Q-tip lightly to assist lift-off metal. Then rinse with IPA, dry with air gun and check under microscope.

#### 4) *Parylene C deposition*

- Before deposition, the surface is activated with oxygen plasma for 1 min.
- For adhesion promotion, small amounts of 3-(trimethoxysilyl) propyl methacrylate (Silane A-174) was placed at the inner wall of the evaporation chamber.
- Weigh 2.7 g of PaC dimer (~ 1.6  $\mu\text{m}$  of parylene C) and start evaporation procedure.
- Spin-coat a soap interfacial layer on top of the parylene C layer (3 wt% soap solution, 1000rpm/30 sec) and let it dry for 15 min.
- Weigh 3.5 g PaC dimer (~ 2.1  $\mu\text{m}$  of parylene C) and evaporate the second parylene C layer.

#### 5) *Deposition of the Channel mask*

- Start spin coater (500 rpm/250 acc./10 sec) and dispense AZ9260 during spinning, then spin with 3500 rpm/1750 acc./35s (dynamic resist dispense).
- Bake for 2 min at 110 °C.
- Mask aligning step, followed by 7 min development step in Microposit MF-319 (Constantly pipette developer towards sample surface during development; After development submerge in DI water, rinse lightly at sink and dry with N<sub>2</sub> gun).

- Check at least one substrate under microscope that everything is well developed, and sharp edges can be seen.

#### 6) Parylene C etching

- Perform a chamber cleaning step before etching
- Etch substrates ( $O_2/SF_6$  plasma) for 10 minutes and inspect them under the microscope for complete etching.
- If etching is not complete (particles on the gold electrode are visible) continue with 1 min etching and inspect again.
- After complete etching, clean substrates with acetone and IPA respectively.

In the following, the detailed OECT measurement procedure is described.

- 1) Spin-coat polymer solution in the middle of the OECT substrate (usually 20-40  $\mu$ l of the polymer solution). Inspect afterwards under the microscope, if the channel and the gate electrodes are covered with the polymer.
- 2) If the gate and channel is sufficient covered with the material, peel-off the first parylene C layer with a tape **before** any additional annealing step.
- 3) Anneal at 120 °C for 90 min under Argon if GOPS is used.
- 4) The Ag/AgCl gate electrode must be activated every time before measurement (Once a day is sufficient). Therefore, put the gate electrode in a diluted bleach solution (e.g. Domestos) for 15 min, and rinse the electrode afterwards with DI water and dry it with nitrogen.
- 5) Wash the PDMS holder with DI water and ethanol and then dry it with nitrogen.

- 6) Put the PDMS holder on a tape and then on the substrate. The active area of the substrate must be placed in the middle of the hole of the holder.
- 7) Fill the cavity of the PDMS holder with the measurement media (~80  $\mu\text{l}$ ), usually 0.1 M<sub>aqueous</sub> NaCl solution.
- 8) Connect the source and drain electrodes with the parameter analyzer, a contact the Ag/AgCl with electrolyte solution.
- 9) Measure the transistor characteristics till a saturation of the drain current  $I_D$  can be observed.
- 10) After the measurement rinse the channels with DI water and dry it with nitrogen. Also clean the PDMS holder with DI water and ethanol respectively and dry with nitrogen. Furthermore, the Ag/AgCl gate electrode is also rinsed with DI water and dried.

## PUBLIKATIONSLISTE

Schmode, P.; Ohayon, D.; Reichstein, P. M.; Savva, A.; Inal, S.; Thelakkat, M. High-Performance Organic Electrochemical Transistors Based on Conjugated Polyelectrolyte Copolymers. *Chem. Mater.* **2019**, *31* (14), 5286–5295.

<https://doi.org/10.1021/acs.chemmater.9b01722>

Schmode, P.; Savva, A.; Kahl, R.; Ohayon, D.; Meichsner, F.; Dolynchuk, O.; Thurn-Albrecht, T.; Inal, S.; Thelakkat, M. The Key Role of Side Chain Linkage in Structure Formation and Mixed Conduction of Ethylene Glycol Substituted Polythiophenes. *ACS Appl. Mater. Interfaces* **2020**, *12* (11), 13029–13039.

<https://doi.org/10.1021/acsami.9b21604>.

Schmode, P.; Schötz, K.; Dolynchuk, O.; Panzer, F.; Köhler, A.; Thurn-Albrecht, T.; Thelakkat, M. Influence of  $\omega$ -Bromo Substitution on Structure and Optoelectronic Properties of Homopolymers and Gradient Copolymers of 3-Hexylthiophene. *Macromolecules* **2020**, *53* (7), 2474–2484.

<https://doi.org/10.1021/acs.macromol.0c00352>

Dolynchuk, O.; Schmode, P.; Fischer, M.; Thurn-Albrecht, T.; Thelakkat, M. Elucidating the effect of interfacial interactions on crystal orientations in thin films of polythiophenes Intended for Submission to *Nature Communications* in 2020.

Schmode, P.; Goel, M.; Meichsner, F.; Thelakkat, M. A highly Soluble and Oxidizable PEDOT Derivative via Controlled Polymerization. Intended for Submission.

## **ERKLÄRUNG**

nach der Promotionsordnung für die Bayreuther Graduiertenschule für Mathematik und Naturwissenschaften (BayNAT) vom 15. September 2017 (§ 9)

Hiermit versichere ich eidesstattlich, dass ich die Dissertation selbständig verfasst und keine anderen als die von mir angegebenen Quellen und Hilfsmittel benutzt habe (vgl. Art. 64 Abs. 1 Satz 6 BayHSchG). Ich habe die Dissertation nicht bereits zur Erlangung eines akademischen Grades eingereicht und habe nicht bereits diese oder eine gleichartige Doktorprüfung endgültig nicht bestanden. (§ 9 S. 11 Nr. 3)

Hiermit erkläre ich, dass ich keine Hilfe von gewerblichen Promotionsberatern bzw. -vermittlern oder ähnlichen Dienstleistern weder bisher in Anspruch genommen habe noch künftig in Anspruch nehmen werde. (§ 9 S. 11 Nr. 4)

Hiermit erkläre ich mich damit einverstanden, dass die elektronische Fassung meiner Dissertation unter Wahrung meiner Urheberrechte und des Datenschutzes einer gesonderten Überprüfung unterzogen werden kann. (§ 9 S. 11 Nr. 7)

Hiermit erkläre ich mich damit einverstanden, dass bei Verdacht wissenschaftlichen Fehlverhaltens Ermittlungen durch universitätsinterne Organe der wissenschaftlichen Selbstkontrolle stattfinden können. (§ 9 S. 11 Nr. 8)

Bayreuth, den 14.05.2020

Philip Schmode